Control of light in a disordered medium with gain : wavefront-shaping the pump in fiber amplifiers and fiber lasers

Tom Sperber

Sorbonne Université

Ecole Doctorale Physique en Île-de-France

Laboratoire Kastler Brossel/ Institut Langevin

Control of Light in Disordered Media with Gain

Wavefront-Shaping the Pump in Fiber Amplifiers and Fiber Lasers

Par Tom Sperber

Thèse de doctorat de Physique

Dirigée par Sylvain Gigan et Patrick Sebbah

JURY

M.	Alain Barthelemy	Rapporteur
M.	Yaron Bromberg	Rapporteur
M.	Yannick De Wilde	Examinateur
Mme.	Mélanie Lebental	Examinateur
Mme.	Claire Michel	Examinateur
M.	Jean-Pierre Huignard	Invité
M.	Patrick Sebbah	Co-Directeur de thèse
M.	Sylvain Gigan	Directeur de thèse

Table of Contents

List of Figures

List of Used Acronyms

SM/MM – Single mode/ Multimode

MMF – Multimode Fiber

FMF – Few Mode Fiber

MMFA – Multimode Fiber Amplifier

TM – Transmission Matrix

DOF – Degree of Freedom

LP – Linearly Polarized

SLM – Spatial Light Modulator

WFS – Wavefront Shaping

EDFA/YDFA – Erbium/Ytterbium Doped Fiber Amplifier

ASE – Amplified Spontaneous Emission

GRIN – Graded Index

NA – Numerical Aperture

DM – Dichroic Mirror

BS – Beam Splitter

PBS – Polarizing Beam Splitter

General Introduction

Profound understanding of the major phenomena central to the behavior of light and its interaction with physical media - most notably refraction, scattering, wave interference, and diffraction - has been well established for at least the last two centuries. However, a broad and significant field remained essentially uncharted territory, largely considered too complicated to study: the propagation of light in what is typically called a "random medium", i.e. a medium in which the light is elastically scattered by variations in the refractive index bearing no specific and simple order in their spatial arrangement. This perception endured despite the fact that the underlying physics at play are completely encompassed by classical optical theory and the above-mentioned phenomena.

It was only quite recently that the emergence of a novel and intriguing insight - in a nutshell, that disorder, or randomness of arrangement, does not equate chaos and non-determinism - ushered in a plenitude of research works and applications, not only in the domain of optics [1-2], but also in microwave radiation [3], acoustic waves in biomedicine [4] or seismology [5], and even in matter waves [6]. The fundamental principle shared across these fields – indeed, a principle universal to wave phenomena – is that a particular realization of the disorder, although "drawn" from some random distribution, does not interact with the waves in a random manner. Once the realization of disorder has been fixed, the scattering it induces upon a given incoming wave - albeit very complex - is deterministic and repeatable, producing a fixed result in terms of the outgoing waves. Therefore, the control of, or the extraction of useful information from, the outgoing waves is possible, provided that a sufficiently complex scheme of modulation of the incoming, or outgoing, wavefronts is implemented in order to circumvent or untangle the effects of scattering. Specifically in optics, the advent of technologies fulfilling this requirement – most notably, spatial light modulators providing millions of spatial degrees of freedom for the formation of desired wavefronts – has paved the way for formidable advances [7]. In particular, an important paradigm which facilitates the majority of research works in the wavefront shaping (WFS) field is the study of a medium assumed to be non-dissipative (i.e. with no gain or loss), by the characterization of its transmission as a linear system, aptly dubbed the "transmission matrix" [8-9].

The work presented in this thesis has explored the possibilities offered by WFS techniques, for the manipulation of the emission of a system featuring both disorder and optical gain (we shall refer to this emission that has undergone amplification as the ***signal*** light). More specifically, the work studied two different configurations: an optical amplifier, and a laser - both based upon an amplifying multimode optical fiber (that is to say, a fiber doped by a rare-earth element so as to make it a gain medium). Ultimately, it should be specified that the focus of the thesis was the particular prospect of

applying the wavefront shaping upon the ***pump***, i.e. the light beam which provides the energy necessary for the amplification or lasing processes to occur, by means of exciting the electronic levels of the gain element. We shall see later on, that this framework represents a context quite unique in the landscape of WFS research: from the perspective of the light whose wavefront we shape, that is the pump, the medium is far from linear; indeed, the appearance of the process key to our study depends on efficient absorption of this light. Moreover, for the second configuration studied – namely, a laser – the notion of linear transmission holds limited relevance for the signal, self-generated by the excited medium itself. However, that is not to imply, that the mainstay methods and approaches of the wavefront shaping domain, such as the transmission matrix approach, are of no value in this work; indeed, they provide an essential base, and as such shall be presented and utilized where relevant. But more importantly, the broader conclusion derived from this domain serves as the general inspiration stimulating and directing this work: that **complexity and 'randomness' in a medium do not necessarily preclude the controlled manipulation of light propagating within it**.

The unique aspect of the approach driving this work - wherein a gain process is manipulated by the spatial modulation of the pump light exciting the medium - may be viewed in the following manner: Rather than considering some given, fixed disorder determined by a medium (e.g., the physical arrangement in space of an ensemble of scattering particles), and shaping the signal light propagating in it - we shape the light which, to some extent, determines the disorder. This is due to the fact that the **population inversion** generated by the pump throughout the volume of our system shall exhibit **spatial heterogeneity**, which will act upon the signal light in a manner highly analogous to scattering. Briefly stated, we are therefore interested in the shaping of a lightbeam - not with the purpose of engineering its interaction with a given transmission function - but rather with the purpose of tailoring the transmission function 'seen' by another lightbeam. The essence of this view of the research is loosely illustrated in the following picture:

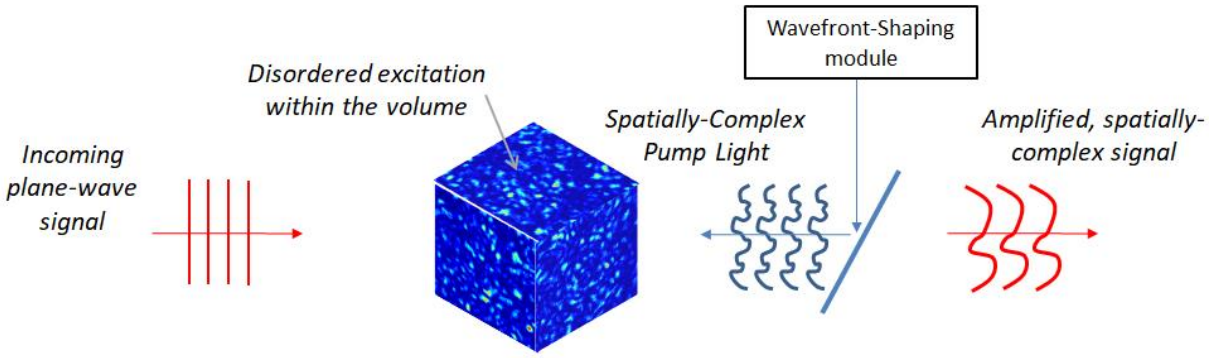

Conceptual illustration of the key elements of the research approach (omitting details such as the gain medium being an optical fiber, i.e. a waveguide); the central characteristic being, that the wavefront shaping is harnessed to excite a gain medium with spatially heterogeneous patterns of population inversion; which in turn acts upon a 'signal' light in a manner analogous to scattering.

It should be noted that similar schemes of pump shaping have already been studied: regarding optical amplifiers - notably in the context of the management of gain in a multimodal amplifier for optical communication links where multiple information channels are multiplexed in the spatial mode domain [10]; and regarding lasers - notably in the context of controlling the emission of so-called "random lasers" [11-12]. These works shall be referenced in detail within the thesis; however, this general framework for exploring disordered media with gain offers a wide and interesting range of research questions, far from having been exhausted yet. The thesis hereby presented has attempted to explore some of these directions.

The thesis is arranged in five main chapters, as follows. Chapter 1 reviews and summarizes the fundamental, ‘textbook-level’ theoretical background in all the concepts and topics pertinent to our work, which are: the scattering of light by disorder and the paradigm of wavefront shaping; light guidance in MM optical fibers, and its analogy to scattering; the gain system enabling optical amplification by interaction with electronic levels; and the working principles of amplifiers and lasers. The next two chapters will lay out in detail the foundations for the main research work. Chapter 2 covers the subject of wavefront shaping in complex media, in particular as applied to passive (non-amplifying) optical fibers, and establishes necessary WFS methods and techniques based on a literature survey, an elementary numerical simulation, and preliminary experimental work. Chapter 3 is where gain enters the picture; the central theoretical model of the work – namely, a model for computing the transmission matrix of a MMFA (multimode fiber amplifier) as a function of the chosen pumping configuration - is constructed and presented, supported by its implementation in numerical simulations tools; results from these simulations are presented and discussed. Finally, the last two chapters cover the main experimental work carried out, and present its results: chapter 4 is dedicated to experiments with an amplifier configuration, while chapter 5 is dedicated to the lasing cavity configuration.

References for the General Introduction

[1] I. M. Vellekoop, A. P. Mosk, Focusing Coherent Light through Opaque Strongly Scattering Media, Opt. Lett., Vol. 32 No. 16, 2309-2312 (2007).

[2] I. M. Vellekoop, A. P. Mosk, Universal Optimal Transmission of Light through Disordered Materials, Phys. Rev. Lett., No. 101, 120601-120604 (2008).

[3] J. Wang, A. Genack, Transport through Modes in Random Media, Nature, No. 471, 345-348 (2011).

[4] C. Prada, M. Fink, Eigenmodes of the Time Reversal Operator: A Solution to Selective Focusing in Multiple-Target Media, Wave Motion, Vol. 20 No. 2, 151-163 (1994).

[5] M. Fink, Time Reversal Acoustics in Complex Environments, Geophysics, Vol. 71 No. 4, 1151-1164 (2006).

[6] Y. V. Nazarov, Limits of Universality in Disordered Conductors, Phys. Rev. Lett., No. 73, 134-137 (1994).

[7] S. Rotter, S. Gigan, Light Fields in Complex Media: Mesoscopic Scattering Meets Wave Control, Rev. of Mod. Phys., Vol. 89, 15005 (2017).

[8] S. M. Popoff, G. Lerosey, R. Carminati, M. Fink, A. C. Boccara, S. Gigan, Measuring the Transmission Matrix in Optics: An Approach to the Study and Control of Light Propagation in Disordered Media, Phys. Rev. Lett., No. 104, 100601-100604 (2010).

[9] S. Popoff, G. Lerosey, M. Fink, A. C. Boccara, S. Gigan, Image Transmission through an Opaque Material, Nat. Comm. 1, No. 81 (2010).

[10] N. Bai, E. Ip, L. Guifang, Multimode fiber amplifier with tunable modal gain using a reconfigurable multimode pump, Opt. Exp., Vol. 19 No. 17, 16601-16611 (2011).

[11] N. Bachelard, J. Andreasen, S. Gigan, P. Sebbah, Taming Random Lasers Through Active Spatial Control of the Pump, Phys. Rev. Lett., No. 109, 33903 (2012).

[12] N. Bachelard, S. Gigan, X. Noblin, P. Sebbah, Adaptive Pumping for Spectral Control of Random Lasers, Nat. Phys., No. 10, 426-431 (2014).

1 Theoretical Background

The purpose of this chapter is to provide the reader with the general knowledge and basic definitions in the fields of research, at whose intersection this thesis was accomplished:

i) The control of light propagation through complex media by wavefront shaping;
ii) Optical fibers (specifically those guiding multiple spatial modes);
iii) The harnessing of optical gain for either amplification of light, or its generation by means of a lasing process.

Each of these topics shall be presented in its separate sub-chapter in a concise manner, aiming only to cover the fundamentals of the field; later chapters of the thesis will then expound upon each subject in its turn, surveying with greater detail both recent developments found in literature, and the methods and principles used in our work.

As a result, the current chapter represents an arrangement of subjects without an immediately-apparent connection to bind them. However, their mutual relevance shall become clear in the following chapters, where at first work on the control of light through optical fibers by means of wavefront shaping techniques shall be presented; then serve as the basis for the work presented on light control in an *amplifying* optical fiber.

1.1 Scattering of Coherent Light by Disorder

Let us consider a medium composed of many dielectric particles whose distribution in space is disordered, i.e. not structured in any specific periodic pattern. Furthermore, we specify that light propagating in the medium interacts with the particles only by elastically scattering upon them; the optical energy is not absorbed. We denote the cross-section for light scattering by a single particle as σ_s , and the density of the particle distribution throughout the medium's volume as ρ. In the case where several approximations may be made, most notably - that the medium is dilute enough to allow us to neglect recurrent scattering, or in other words to treat the particles as independent from each other – we may use the Beer Lambert law to describe the intensity attenuation of a plane wave entering a slab of this medium: $I(z) = I_0 e^{-\rho\sigma_s \cdot z}$ (where z is the direction perpendicular to the slab's surface, and along which the wave propagates). The product of the cross-section and the density, commonly known as the *scattering mean free path*: $l_s = \rho\sigma_s$, then takes on the meaning of the typical depth of penetration into the medium, over which the energy of the *ballistic* component of the light exponentially diminishes; Where by ballistic we designate the component of the field keeping the same direction of propagation and phase as the incident illumination. Intuitively, we can understand

the ballistic part as the photons which have not interacted with the particles; and in a complementary fashion, the 'missing' energy corresponds to those photons which have undergone scattering events. We are interested in a medium with a thickness of a least a few scattering mean free paths: $L \gg l_s$, a situation commonly referred to as the multiple scattering regime [1]. We can expect to find, behind such a medium, a non-negligible population of photons which have interacted with at least a few particles; which means the optical field they produce manifests the combined effects of multiple scattering events, bearing no correlation in phase and directionality to one another, due to the particles' disorder.

The case where such multiple scattering brings about a very interesting phenomenon is when the incident light is monochromatic and coherent. Because the intensity at any given point behind the medium is a coherent sum of many uncorrelated phasors, representing the different paths the light has followed within the medium, the interference effect gives rise to variations of the intensity. The resulting spatial pattern, which exhibits a complex granular-like fluctuation between bright and dark spots (points of constructive and destructive interference, respectively), is called a *speckle* [2]. A typical example of a speckle is shown in figure 1.1; the total intensity at any point is the sum of the variations δI produced by the coherent interference, and a 'DC term', namely the average intensity $\langle I \rangle$ (which may still contain a significant ballistic component).

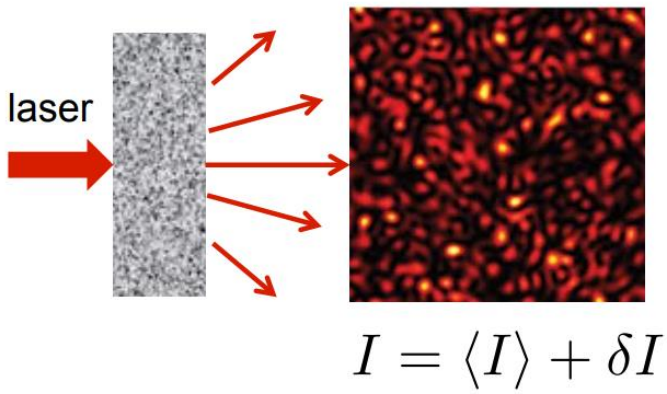

Figure 1.1: Schematic representation of the generation of a speckle pattern by passing coherent light through a layer of disordered scatterers (image courtesy of Prof. R. Carminati, Institut Langevin).

For the sake of accuracy in the applied terminology, the phenomenon of 'speckle' is more general than the scheme discussed here, of propagation *through* a scattering medium; In fact, historically the term was first applied to the pattern observed in the *reflection* of coherent light (in directions other than the specular reflectance) from any surface with roughness on the order of the wavelength or larger (an observation made very shortly after laser sources became available [3]). In both cases, the speckle is a manifestation of the 'scrambling' of the light's wavefront due to the interaction with the disorder; and it comes as no surprise that strong intensity variations are easily observed in scattered

reflection, where the ballistic component is altogether missing. At any rate, since our interest in this work is to make the analogy with light transmission through a multimodal waveguide, we shall limit the analysis of disordered scattering media to the transmission scenario.

In order to complete the discussion, an additional length scale should be introduced: the *transport mean free path,* commonly denoted l^*. It is defined as $l^* = l_s/(1 - g(\omega))$, where $g(\omega)$ is a factor, called the *anisotropy factor,* characterizing the directionality of the scattering process induced by a single particle upon light at an optical frequency ω. The rigorous development may be found in references [1,3]; for our purposes, it shall suffice to say that $0 \leq g \leq 1$, and therefore $l^* \geq l_s$ always, with identity in the last expression (instead of a general inequality) obtained when the particles' scattering is completely isotropic. The physical meaning of the transport mean free path is the distance of propagation over which the scattered (non-ballistic) component of the field becomes, on average, isotropic; and the situation where the medium's thickness is larger than a few such lengths, $L \gg l_s$, is commonly called the *diffusive regime* [4]. In this regime, the probability distribution function of the speckle intensity is a negative exponential function, with a ratio of unity between the mean value of the intensity, and its mean variation (i.e. the contrast is at the maximal possible value of 1). This is referred to as a fully-developed speckle.

A large body of work has treated the nature of the multiple scattering of light in disordered media. It has been realized quite early on that, although the transmitted and back-scattered light fields have been locally randomized by a very intricate process (when the number of scatterers is large, the task of theoretically predicting the amplitude/phase at some given point behind a given layer might pose a difficulty that is practically impossible to overcome), there is nothing non-deterministic about them: for a specific, static realization of the disorder, that is – as long as the scatterers remain in fixed positions - the output pattern is perfectly determined by the initial conditions, that is by the incoming light field. Furthermore, in the absence of absorption, the spatial and angular information contained in the input beam has not been lost, merely re-organized and 'scrambled' together with information about the scattering events the waves have undergone. Hence, despite its random-like appearance, the speckle output is not chaotic – only complex. Starting at about 3 decades ago, early theoretical works have proposed that underlying correlations in the speckle could be observed [5], and moreover, that the spatial information carried by light that has undergone multiple scattering might be "de-coded" for imaging and sensing applications [6]. Freund's visionary work has suggested, that disordered media which are virtually opaque for direct-imaging schemes, might be rendered not only detrimental but even *favorable* (e.g., serve as optical components such as lenses or polarizers) to imaging applications, granted prior knowledge of their transmission is available and may be exploited in a holography-like scheme [7]. Current day methods of light control in disordered media draw significant inspiration from these concepts; the survey and discussion of these practical techniques is left to the following chapter.

1.2 Light Guidance in Ideal Passive Optical Fibers

The previous section dealt with the scattering of light inside an array of disordered scatterers; the transition to multimode fibers may not seem so evident, as their essential trait – that of guiding light in a highly directional and confined channel – may be viewed as somewhat being the opposite of scattering. Indeed, an optical fiber cannot be classified, strictly speaking, as a scattering system. However, we shall see in this section how the multimodal nature of its guidance gives rise to a 'scrambling' or 'randomization' of the wavefront, in a way very much akin to the process occurring in a medium composed of a disordered arrangement of scatterers. Simply stated, the coupling of coherent light into a fiber (granted that no special care is taken to tailor this coupling to very specific conditions) produces a developed speckle at the fiber's output.

1.2.1 The Guided Modes

The theory covered in this section follows the pioneering paper of Gloge [8], and the textbook of Buck [9]. As this subject had been well consolidated 5 decades ago, and has since then been widely covered by many renowned sources, the following section briefly follows the main definitions and results, without repeating all the formal steps of mathematical development and proof.

We begin by considering a step-index fiber with a core of radius a, and an infinite cladding surrounding it. The refractive indices of these two parts are, respectively, n_{core} and n_{clad} . We denote the refractive index difference $\Delta n = n_{core} - n_{clad}$, which is of course positive (otherwise the fiber would not be a waveguide). Furthermore, it is assumed to be much smaller than the indices themselves: $\Delta n \ll n_{clad}$. This is generally known as the assumption of a "weakly guiding fiber", and it is the condition which will allow us to narrow our perspective from the more general case - where the waveguide solutions are vectorial modes (such as TEM, EH, HE, etc.) - to the particular case where the solutions may be expressed as the much simpler Linearly-Polarized (LP) modes.

The guidance of light in the fiber is fundamentally connected with the physical phenomenon of total internal reflection - namely, the perfect reflection of a ray back into a high-index medium, from an interface with a lower-index one, granted the angle of incidence is larger than some critical angle. As could be intuitively expected based on this connection, the light rays which may coupled into a lightfield guided by the fiber core reside within a range of incidence angles – commonly referred to as the *acceptance cone* – and this angular range is fully determined by the refractive indices of the core and the cladding. The convection is to define the half-angle of the acceptance cone as the *numerical aperture* (NA). It can be shown that:

$$NA = \sqrt{n_{core}^2 - n_{clad}^2} \tag{1.1}$$

Then, given a specific optical wavelength λ (vacuum wavelength) that shall be coupled into the fiber, a dimensionless 'V' number is defined:

$$V = \frac{2\pi}{\lambda} a \cdot NA = \frac{2\pi}{\lambda} a \cdot \sqrt{n_{core}^2 - n_{clad}^2} \tag{1.2}$$

Qualitatively speaking, the larger the V number - the larger the number of modes (i.e., discrete solutions of the Maxwell Equations in the fiber's geometry) that may be guided. More quantitatively, in order to precisely find the supported modes and know their exact field forms, one must find all possible solutions for two scaling parameters, u and w (the first will control the electric field residing within the core, the second the field extending in the cladding), that satisfy this defining equation:

$$V^2 = u^2 + w^2 \tag{1.3}$$

As well as the so-called 'Characteristic Equation' (which is derived by imposing the requirement that the electric field at the core-cladding boundary be continuous):

$$\frac{J_{l-1}(u)}{J_l(u)} = \frac{-u}{w} \cdot \frac{K_{l-1}(w)}{K_l(w)} \tag{1.4}$$

Where J, K are, respectively, ordinary and modified Bessel functions of the first kind; and l, appearing as the order of these Bessel functions, is an index running from 0 over the positive integers, up until the maximal integer of cutoff (above which no more solutions may be found for the specific V number considered). As the characteristic equation is transcendental, expressions for the solutions are not available in closed analytic form, and approximate numerical methods must be used. For this reason, it is not immediately apparent why a second index, usually denoted m, is needed in order to represent all possible modes (although this index does not explicitly appear in the characteristic equation). Good insight into this question may be gained by employing the graphical method to find the solutions of the characteristic equation (i.e., plotting the right-hand side and the left-hand side of eq. (1.4) as a function of the parameter u and for all relevant values of the index l, and finding point of intersection). It is then found that m naturally arises because for each value of the l index there are generally multiple distinct intersections (i.e. solutions). Excellent illustrations of the graphical method are found in [9]; instead of reproducing them here, we simply assert that a set $\{u_{lm}\}$ of solutions for the scaling parameters exists, with $l = 0,1,2,3$ ... and $m = 1,2,3$ ..., and that each such solution gives rise to a LP mode, which is necessarily an **eigenmode** of the waveguide. Moreover, this set of modes constitutes an **orthogonal** base for guided lightfields. The exact number of modes found for a given V number depends on the specific behavior of the terms appearing in the characteristic equation, and therefore no precise analytic formula may be derived for it. However, the following approximation holds from V numbers of around ~30, and becomes better as V further increases:

$$Number\ of\ \{u_{lm}\}\ \text{solutions} \approx V^2/8 \tag{1.5}$$

Note that this is the number of *solutions to eq. (1.4)*; the number of *guided LP modes*, as we will shall see later on in this section, is (almost) four times larger, due to mode degeneracy in both polarization and orientation of the intensity pattern.

The transverse electrical field distribution of the LP modes may be expressed in polar coordinates $\{r, \theta\}$ as the following form:

$$\psi_{lm}(r,\theta) = \begin{cases} \cos(l\theta) \cdot J_l\left(u_{lm}\frac{r}{a}\right)/J_l(u_{lm}) & r \le a \\ \cos(l\theta) \cdot K_l\left(w_{lm}\frac{r}{a}\right)/K_l(w_{lm}) & r \ge a \end{cases} \quad (1.6)$$

Note that the field is expressed as a scalar, representing only its magnitude. We may do so because the orientation of the field is constant across the entire plane; this is in fact the meaning of the linearly-polarized approximation. Upon inspection of this expression, it becomes apparent that the l index produces an *angular* modulation of the mode's spatial distribution, while the index m modifies the *radial* dependence of this form. Figure 1.2 demonstrates, for a lightly multimode fiber (with a V number of 15), the spatial distributions of the supported modes, as derived according to eq. (1.6):

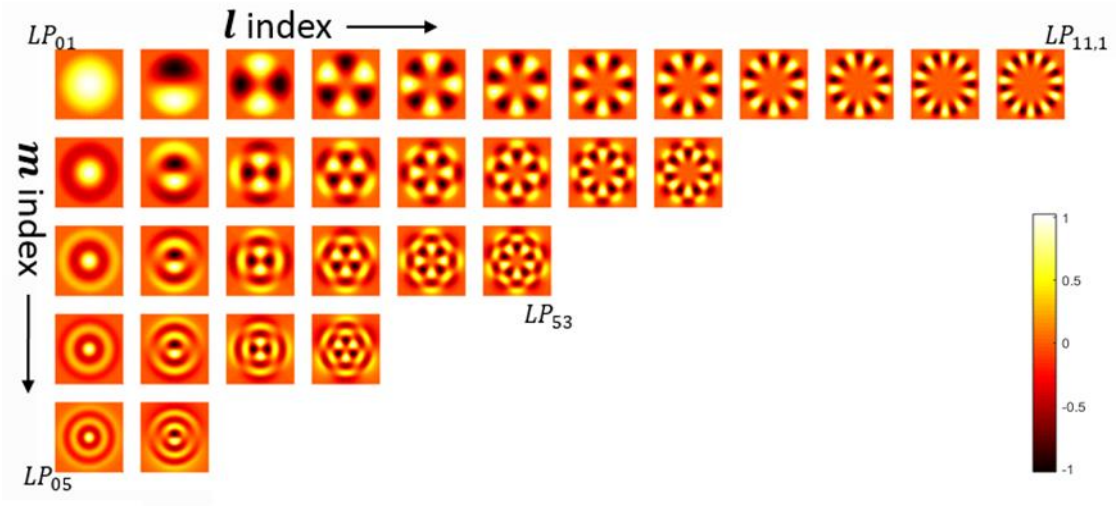

Figure 1.2: Spatial forms of the LP modes, found by numerically solving the characteristic equation (1.4) for a step-index fiber with a V number of 15. The modes are arranged by the angular index (horizontal), and the radial index (vertical).

We mention as well the degeneracy of the LP modes. In principal, every solution u_{lm} has a 4-fold degeneracy, because the angular dependence of the field's *intensity pattern* may be rotated in the transverse plane (the cosine term in eq. (1.6) might be replaced by a sine term, giving 2 orthogonal modes); and then, each such pattern may be realized with a choice for the *orientation of the field itself*, i.e. the polarization adds a further 2-fold degeneracy (either vertical or horizontal). For the former type of degeneracy, i.e. that of the pattern's orientation, the terms 'even' and 'odd' are commonly used, and a sub-index marked either 'o' or 'e' is affixed after the l, m indices. Note that this type applies only to the LP modes where the angular dependence is not void, i.e. those with $l > 0$. Figure 1.3 demonstrates the 4-fold degeneracy for the example of LP21:

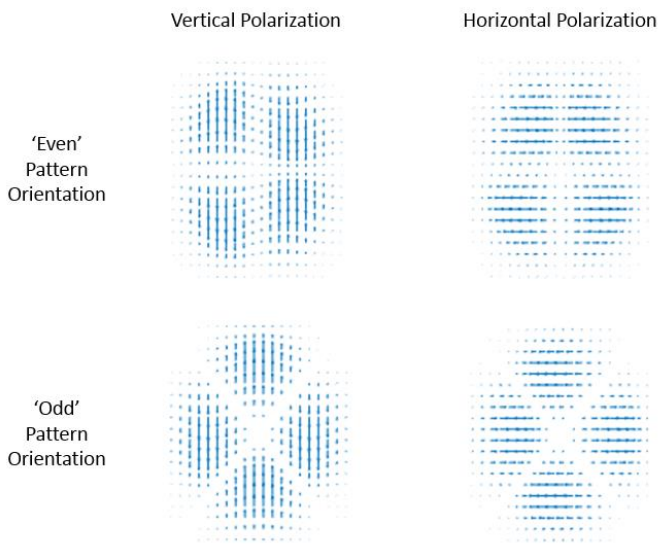

Figure 1.3: The LP21 mode displayed in its four possible degenerate versions (the arrows indicate the electrical field in both their orientation and norm). Top - LP21e, in both polarizations; Bottom – same for LP21o.

Turning now to the subject of the propagation of the modes in the waveguide - each such solution corresponds to a unique propagation constant (phase velocity):

$$\beta_{lm} = \sqrt{\frac{4\pi n_{core}^2}{\lambda^2} - \frac{u_{lm}^2}{a^2}} \tag{1.7}$$

Which means that the transverse field of any LP mode, at a given position z along the axis of propagation, is given as:

$$E_{lm}(r,\theta,z) = E_0 \cdot e^{-\beta_{lm} \cdot z} \cdot \psi_{lm}(r,\theta) \tag{1.8}$$

Where E_0 is a complex amplitude we are free to set.

It is instructive to define a normalized propagation velocity factor b thus:

$$b = \frac{\beta_{lm}/k - n_{clad}}{n_{core} - n_{clad}} \tag{1.9}$$

Where $k = 2\pi/\lambda$ is the wavenumber of our wavelength.

The parameter b is simply a measure of how close a mode's propagation constant is, to the two extremes between which it is always confined: plugging into it the β value which corresponds to light propagation in a bulk medium whose refractive index is n_{core} gives a value of 1; while the β value which corresponds to a bulk medium whose refractive index is n_{clad} will give a value of 0. The modal dispersion arising from eq. (1.7) is illustrated, in terms of this normalized propagation velocity, in figure 1.4. It should be evident from the graph that for a given V number, the set of supported modes will display a range of phase velocities extending between the value for the lowest-order ("fundamental") LP01 mode - which 'almost' corresponds to the core index – and the value for the highest-order mode, which will be almost 0 and therefore close to corresponding to the cladding index.

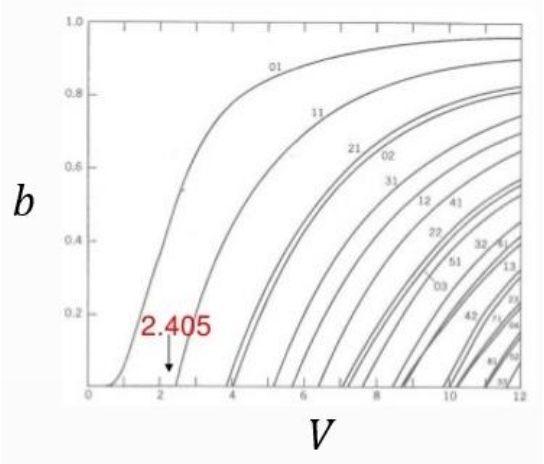

Figure 1.4: Dispersion curves for LP modes, taken from [9]. The y axis is given in units of normalized propagation velocity b as defined in eq. (1.9); the closer a curve is to '1', the more the mode's velocity corresponds to the core index. The V number noted in red is the cutoff value for the second mode LP11, meaning that for V numbers below it the fiber is singlemode, since only the 'fundamental' mode LP01 is guided.

1.2.2 Optical Fibers as Examples of Complex Media

As mentioned earlier, optical fibers may not be formally regarded as scattering media; nevertheless, the coupling of coherent light into a sufficiently multimodal fiber gives rise to a speckle at its output. Similarly to the scattering medium case, where the speckle is the result of a superposition of many contributions (different paths through the disorder) whose phases are uncorrelated, the fiber-generated speckle is the interference sum of many contributions with 'randomized' phases – the various spatial modes. Figure 1.5 demonstrates with a simple numerically-simulated example, how the superposition (with randomly-distributed complex weights) of a sufficient number of LP modes gives rise to a complicated speckle intensity pattern.

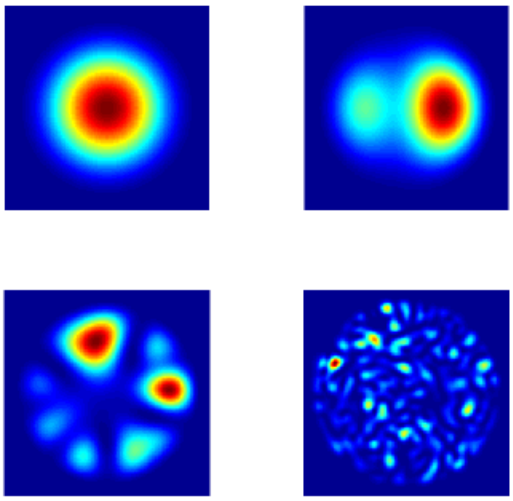

Figure 1.5: Numerical simulation of the coherent summation of LP modes with uncorrelated phases, with the number of superposed modes gradually increasing - from top left to bottom right: 1, 2, 10, and 100 modes.

The complex spatial pattern at the output of a multimode fiber is a manifestation of the fact that the dispersion (i.e., the propagation velocity differences) between the different spatial modes follows no special harmonic relation; therefore, the propagation is necessarily accompanied by a de-phasing of the modes with respect to each other, hence any given lightwave coupled to the waveguide will develop into a speckle.

The analogy with a scattering medium is limited; for example, the transport mean free path cannot be defined. However, one can estimate the typical propagating length over which a lightwave coupled into a fiber will be scrambled, i.e. the distance over which the modes' phases loss correlation: As can be inferred from the modal dispersion curves (see figure 1.4), this length scales as the inverse of the core-cladding refractive index difference. In a typical few-mode or multimode fiber where this difference represents a few percent of the mean refractive index, the propagation of several tens or hundreds of wavelengths (which, for IR light, is on the order of sub- millimeter) suffices to completely de-phase the spatial modes.

1.2.3 Corrections for the Case of Graded-Index Optical Fibers

Closing the section about optical fibers is a brief point about the so-called 'graded-index' fibers (which will be relevant for the experimental work presented in following chapters, where such a fiber was used). The definition and analysis relies on references [10] and [11].

Graded-index (GRIN) fibers are fabricated with a profile of refractive index that gradually changes across the core, as a function of the radial distance from the center. The maximum index, which we shall denote n_0, is found at the center of the guiding core; moving away towards the cladding the refractive index falls according to the following power law, commonly referred to as an 'alpha-power' profile:

$$n(r) = \begin{cases} n_0\sqrt{1 - 2\cdot\Delta\cdot(r/a)^{\alpha}} & r \le a \\ n_0\sqrt{1-2\cdot\Delta} & r \ge a \end{cases} \tag{1.10}$$

Where, as before, a denotes the radius of the core. The parameter α dictates the smoothness of the profile as a function of the radial coordinate r: for $\alpha \to \infty$, the fiber will approach the step-index profile which has been studied so far in this section, while for $\alpha = 2$ the profile will constitute a parabolic one. Usually, graded-index fibers are fabricated with alpha-powers of a little more than 2, depending on the desired modal behaviour. Finally, the parameter Δ scales the index profile in the vertical axis, or in other words determines the total index change between the center and the uniform value found throughout the cladding. Similarly to the relation eq. (1.1) expressed for the step-index case, it may be shown that the GRIN fiber's numerical aperture is $NA = \sqrt{2\Delta\cdot n_0^2}$.

Although the analytic treatment of the modes' behavior (characteristic equation, field distribution, dispersion etc.) is more complicated for the step-index case, it should be understood that the essential features remain the same: a set of discrete LP modes may be found, defined by two parameters l, m (angular and radial, respectively), and it serves as an orthogonal base for all lightfields guided in the fiber. For our purposes in this work, it shall suffice to state that the total number of solutions to the characteristic equation may be approximated by:

$$Number\ of\ \{u_{lm}\}\ \text{solutions}\ \approx \frac{\alpha}{\alpha+2}\cdot\frac{\Delta}{4}\cdot\left(\frac{2\pi a}{\lambda}\right)^2 \tag{1.11}$$

Again, due to the degeneracies of mode and polarization orientation (same as for eq. (1.5)), the number of modes is nearly four times larger than the number of solutions. From eq. (1.11) we can see that as the alpha parameter decreases (i.e. the fiber's profile becomes more graded), less modes are supported; the parabolic GRIN fiber ($\alpha = 2$) guides half the number of modes as the equivalent step-index fiber.

Lastly, we mention that as the alpha parameter decreases and the refractive index profile departs from the step-index form, the modes' field distributions scale in the radial coordinate to become more confined within the core. Generally, exact solutions require numerical approaches. An approximation for the fundamental mode was derived, by a trial and error approach, in reference [11]. A formula (depending on a large number of heuristically-found constants) for the factor by which the waist of the mode is reduced as a function of α may be found there.

1.3 The Gain Medium and the Rate Equation of an Amplifier

The subject of this section is the interaction of light with the electronic states of an atom that is laser-active, i.e. capable of acting as an optical gain system. The practical example kept in mind is that of rare-earth elements incorporated as dopants into an optically transparent environment such as silica, as was the case in our work with doped fibers. Nonetheless, the theory covered is general and may equally describe other types of amplifying media, such as the noble gases found in common gas lasers.

The theory presented follows the fundamental textbook of Davis [17], as well as the papers of Barnard [12] and Paschotta [13]. Again, this is a well-known and established subject, for which many sources may be found; the following section therefore covers it in a concise and abridged manner, so as to quickly arrive at the important definitions and results.

1.3.1 The Two-Level Gain System and the Rate Equations

A photon may interact with a pair of energy levels in the medium by either being absorbed so that an electron is excited from the lower level to the higher one, or by being created (i.e. emitted) when an electron makes the opposite transition. The latter might take place as a spontaneous emission process, or by the stimulated emission interaction, wherein an existing photon induces the electron to decay from the upper level by emitting a new photon, identical in its properties to the first. To each of the three interactions is assigned a probability (the well-known Einstein coefficient), as shown in the following illustration:

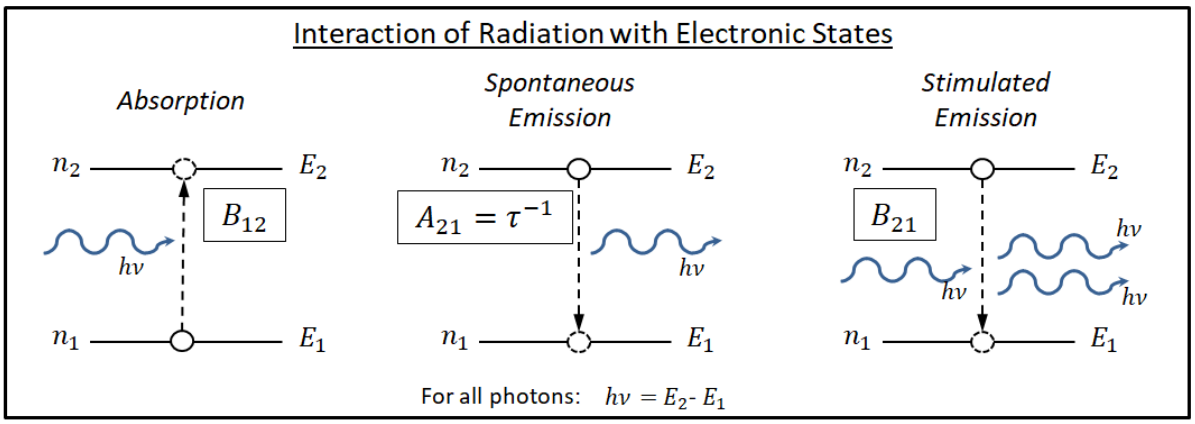

Figure 1.6: Conceptual illustration of the three interactions of photons with a pair of energy levels. The coefficients appearing in boxes are the Einstein coefficients, representing the probabilities of these interactions.

The medium's ability to emit photons raises the prospect of optical gain; however, the important notion of *population inversion* must first be introduced. The third process depicted in figure 1.6 is the basis of optical amplification – an existing photon may be duplicated by the downwards transition of an electron; but it should be understood that the photon's annihilation by the opposite transition

upwards (i.e., the first process depicted in the same figure) – is equally permitted. The physical principle named the Einstein coefficient relation demonstrates from that in fact, for a pair of (non-degenerate) energy levels in thermodynamic equilibrium, the probability of absorption and of stimulated emission must be identical: The result is that if an equal number of electrons is found in the upper level of the relevant transition as in its bottom level – the rate at which signal photons are created (by stimulated emission) and annihilated (by absorption) would be the same, with a zero net gain. Therefore, in order for light amplification to take place, the population at the higher energy level must be larger than the one at the lower level.

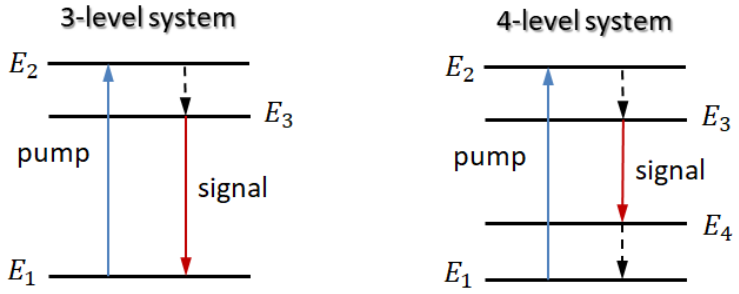

Figure 1.7: Conceptual illustration of the two main types of electronic level structure found in gain media, and their interaction with the two interesting wavelengths, the pump and the signal.

An optical gain medium is a system with at least 3 different electronic levels able to interact with photons: a ground level with energy E_1; a high-energy level E_2 to which electrons may be stimulated (from the first level) through the absorption of a photon at a wavelength which we refer to as the *pump*; and a third level E_3 situated between the two, to which the electrons that have been excited (pumped) to the higher E_2 may decay by some rapid transition (usually, but not always, through the emission of phonons that thermalize the medium). By 'rapid' it is meant, that the decay occurs at a rate high enough to create a significant population at its destination level E_3 (otherwise, competing processes acting upon the electrons at E_2 – such as the further excitation of the electrons to even higher levels, or their decay all the way back down to the ground level - will leave the third level unpopulated). The desirable process which justifies the 'gain medium' title is the emission of a photon at a wavelength we refer to as the signal, due to the decay of electrons from E_3 down to – either back to the ground level, in the case of a 3-level system – or, in the case of a 4-level system, to yet a fourth level E_4 (from which the return to E_1 may occur through another thermalization process). Essentially, the electronic levels have permitted the transfer of energy from the absorbed pump photons (whose frequency corresponds to the energy difference $E_2 - E_1$) to newly created signal photons (whose frequency corresponds to the energy difference $E_3 - E_1$ or $E_3 - E_4$, for a 3-level or 4-level system, respectively).

Although the description given above (and illustrated in figure 1.7) is the correct physical model of a real gain medium, in an analytical treatment of the dynamics of the gain system it is usually more

convenient to simplify the three or four-level structure into an artificial two-level model. The two higher levels E_2 and E_3 are simply lumped together into an *upper level*, and E_4 (if relevant) is lumped together with the ground level and viewed as a single *lower level*. Basically, what we are assuming is that the thermal transitions between the levels bunched together are so rapid that they may be ignored altogether, thus effectively joining the populations of electrons in these levels as one common population.

However, this simplification is permitted as long as we retain as independent parameters, the probabilities of all four true transitions taking place: the absorption and emission of the pump photons, which are represented by the cross-sections $\sigma^a_{pump}, \sigma^e_{pump}$ respectively, and the absorption and emission of the signal photons, which are represented by the cross-sections $\sigma^a_{sig}, \sigma^e_{sig}$ respectively. In a pure two-level system, the two cross-sections per each wavelength would be identical - and no population inversion would be possible, as explained earlier (not to mention that the separation between pump and signal would be meaningless, as both wavelengths would correspond to the same energy difference). But since the actual system does contain separate sub-levels, which we have bunched together for convenience - the fact that these 4 parameters are specified independently reflects the true behavior of the medium, and the possibility of using it as a gain system.

We proceed to give the following definition for either one of the relevant wavelengths, pump or signal: The cross-sections σ^a, σ^e, for absorption and emission respectively, determine the rate at which photons populate and evacuate the upper level population. An incident light beam with optical frequency ν and field E induces the rate equation (for the time derivative of the upper level population), expressed in eq. (1.12). The first term represents a positive contribution by light absorption, and the second term represents the negative contribution by the two emission processes, first- the stimulated, and appearing second- the spontaneous.

$$\frac{dn_2}{dt} = R^{1\to 2}\cdot n_1 - [R^{2\to 1} + A_{21}]\cdot n_2 \;=\; \frac{\sigma^a}{h\nu}|E|^2\cdot n_1 - \left[\;\frac{\sigma^e}{h\nu}|E|^2 \;+\; \frac{1}{\tau}\;\right]\cdot n_2 \qquad (1.12)$$

Where h is Planck's constant, τ is the lifetime of the upper level, and the populations themselves are expressed as dimensionless fractions between 0 and 1 (i.e. they satisfy $n_1 + n_2 = 1$). For this reason, the rate equation for the lower level is simply the same equation with the signs flipped: $n_1' = -n_2'$.

For calculating the steady-state populations of the levels in the presence of both pump and signal lightwaves, generally we would need to consider eq. (1.12) for each of them, then sum all terms together. Consequently, a complicated interplay arises between five driving processes – the four possible transitions due to absorption/emission by either of the wavelengths, and spontaneous emission from the upper level. We greatly simplify the problem, however, by narrowing our view to the case commonly known as the "non-depleted pump" assumption: The signal's intensity is small

enough, compared to the pump's intensity, so that the two transitions induced by it (i.e. the signal) can be altogether neglected in the rate equations.

Thus, the upper level's steady-state population is determined only by the pump's absorption and emission rates, and its lifetime:

$$n_2 = \frac{R_{pump}^{1\to2}}{R_{pump}^{1\to2} + R_{pump}^{2\to1} + R_{spontaneous}^{2\to1}} = \frac{\sigma_{pump}^{a} \cdot I_{pump}}{(\sigma_{pump}^{a} + \sigma_{pump}^{e}) \cdot I_{pump} + h\nu_{pump}/\tau} \tag{1.13}$$

We find, for the relation between the pump intensity and population excitation, a simple saturation curve. It is convenient to define 2 characteristics of the medium, the first one being the upper limit of the population inversion, to which the system asymptotically approaches, as the pump intensity approaches infinity:

$$n_{2max} = \frac{\sigma_{pump}^{a}}{(\sigma_{pump}^{a} + \sigma_{pump}^{e})} \tag{1.14}$$

And the second one being the intensity at which the population inversion is exactly half of the aforesaid upper limit – this is where the curve attains its "knee" point:

$$I_{saturation} = \frac{h\nu_{pump}}{(\sigma_{pump}^{a} + \sigma_{pump}^{e})\tau} \tag{1.15}$$

With these 2 definitions, the excitation is readily expressed as:

$$n_2 = n_{2max} \cdot \frac{I_{pump}}{I_{pump} + I_{saturation}} \tag{1.16}$$

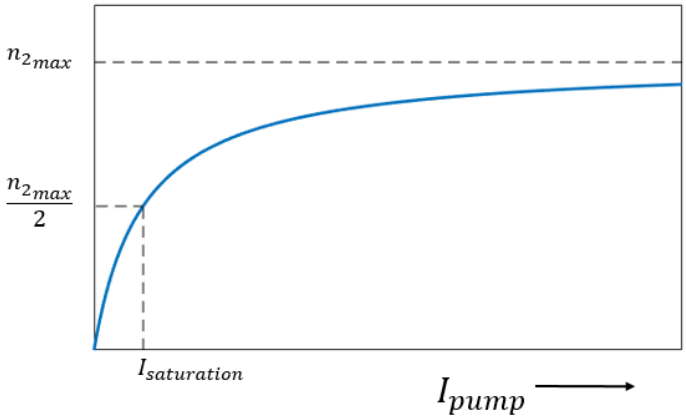

Figure 1.8: the population vs. pumping intensity saturation curve, according to eq. (1.16).

It should be noted that the above curve does not, in general, precisely represent the gain experienced by the signal, since larger-than-zero upper level population does not necessarily imply signal amplification. This would be the case only in a classic 4-level system, where the un-pumped medium is transparent for the signal wavelength. In a 3-level system, however, the transition interacting with the signal photons ends at the ground state (or very close to it, which is referred to as a "quasi 3-level" system); hence a non-zero population exists from which the signal can excite electrons, the same way as the pump does. In these systems, as eq. (1.13) - this time considered for the signal wavelength – would suggest, the amplifier gain begins (for 0 pumping, when n_1 is still close to unity)

at negative values, meaning the signal experiences net absorption. Only after the pumping rate has increased sufficiently, up to the point where the lower-level's absorption and the upper level's amplification cancel out, do we start to have positive gain for the system. This pumping intensity is commonly called the threshold of transparency:

$$I_{transparency} = \frac{h\nu_{pump}}{(\frac{\sigma^e_{sig}\sigma^a_{pump}}{\sigma^a_{sig}} - \sigma^e_{pump})\tau} \tag{1.17}$$

Incidentally, both Erbium and Ytterbium-doped fibers are considered to be "quasi 3-level" systems at least for some of the wavelengths within their signal band.

So far, we have discussed an arbitrary volume of the gain material, interacting with the light as a function of time (appearing in the rate equations) but not as a function of spatial coordinates. We would like now to consider the propagation of a light field through our gain medium (along, say, the z axis). Resulting from the definition of the cross-sections given in eq. (1.12), the attenuation or amplification of the light field traversing some given lower and upper populations n_1, n_2 is:

$$\frac{d|E|}{dz} = \frac{1}{2}(\sigma^e n_2 - \sigma^a n_1)N_d \cdot |E| \tag{1.18}$$

Where N_d is the total concentration of doped gain element, in m^{-3}, and the ½ factor accounts the equation describing amplification in terms of field and not intensity.

For the simple case of a signal propagating through a medium pumped by a very strong pump – enough for us to assume the upper level is everywhere saturated, meaning $n_2(z) = n_{2_{max}}$ as defined in eq. (1.14) – we may define a constant gain coefficient (in units of reciprocal of length):

$$\alpha_{gain} = [\, n_{2_{max}} \cdot (\sigma^e_{signal} + \sigma^a_{signal}) - \sigma^a_{signal}] \cdot N_d \tag{1.19}$$

Thus, for some length z along the propagation axis of the amplifier, the accumulated gain seen by the signal (in terms of power) would be a simple exponential increase: $e^{\alpha_{gain}z}$. In a more complex scenario where the populations vary as a function of the spatial coordinates, a direct integration of eq. (1.18). We shall see in chapter 3 that such an approach was the basis of our model for a multimodal fiber amplifier.

We conclude this section by mentioning that the gain medium acts upon the signal lightwave in 2 ways: First, there is the increase, or decrease, in the amplitude, as was discussed above – in other words, the gain or absorption of energy. Secondly, there is a shift of phase which necessarily accompanies such gain/absorption. Commonly, this is modeled by writing the change caused to the refractive index by the presence of the gain medium as being complex: $n = n' + j \cdot n''$, so that n' determines the change of the wave's phase , and n'' contributes a change in transmission (gain or absorption). Then, by force of the refractive index being a physical, causal quantity, these two contributions must be tied together through the Kramers-Kronig relation, since they are, respectively, its real and imaginary parts (see, for example, the classical textbook of Boyd [12]). As a result, an

increase of the gain at a given signal wavelength (e.g. by pumping the system) entails a proportional increase/decrease in the real part of the refractive index, in other words – a dephasing that is proportional to the amplification. Empirical measurements of the magnitude of this effect, for a given material, may usually be found in the literature under the designation Refractive Index Change (RIC). In this work we denote the factor in this linear relation thus:

$$K_{RIC} = \frac{n'}{n''} \tag{1.20}$$

It should be noted that in a real amplifier, a phase change for the signal in the presence of a pump arises also from additional factors other than the resonant nature of the electronic gain/absorption – mainly from thermal contributions (see, for example, [15- 16]). Still, in a simple model of the system (e.g., where no sharp modulation of the pump power in time exists), all contributions may be lumped together in the proportionality factor K_{RIC} defined above.

1.3.2 Spectral Dependence of the Gain and Line Broadening

All the characteristics discussed above, which determine the behavior of the gain process, are wavelength dependent; Both the pump and the signal wavelengths must lie in regions of the spectrum for which (in the specific gain medium chosen) their absorption and emission cross-sections, respectively, are significant enough to enable efficient population excitation and amplification. Considering the fact that both processes are resonant interactions of a photon with an electronic transition, it is indeed expected that all relevant cross-sections will attain a maximum at a central wavelength which corresponds to the energy difference of said transition through $h\nu = \Delta E$, and fall off away from this frequency with some finite spectral width.

For the gain media discussed in our work, the widths of the spectral curves around the absorption and emission peaks are at least a few nm, and more typically a few tens of nm. This is several orders of magnitude larger than the width one may naively expect to find when viewing these interactions as with a classical electromagnetic resonance, that is - taking the inverse of the lifetime of the upper energy levels (the so-called 'natural linewidth'). This is because significant broadening mechanisms, occurring mainly because of interactions between the gain atoms and their surrounding environment, 'smear' the energy of the electronic levels over a wide range of possible values, thereby enlarging the range of optical frequencies over which a photon may match the transition's energy difference.

An important distinction should now be noted between '*homogenous'* broadening mechanisms and '*inhomogeneous*'ones. It is true, that when considering an amplifier, the details of this distinction are of no crucial importance; Once the specific pump and signal wavelengths are chosen, they remain constant, and each of them "sees", where they happen to fall within the spectral gain curve, some fixed absorption and emission coefficients, which may be either directly measured or taken from tables in

the literature. However, for the case of laser system - as will be discussed further in a later section - the inner details of the line broadening phenomena are of great interest.

When considering the ensemble of all gain atoms incorporated in some gain medium, then: A mechanism of Homogenous Broadening is one that equally affects (broadens the transitions of) all atoms in the ensemble. One example is the thermal exchange all atoms perform with their environment; since the temperature is homogenous over the system, all lines are identically broadened. Another example is the Stark broadening – the fact that the energy levels split into a manifold of sub levels in the presence of an electric field. Conversely, inhomogeneous Broadening mechanisms are perturbations to the transition energy difference, which vary between different sub-groups of atoms within the overall ensemble. An example is local variations within the host material in which the gain atoms are embedded; different sites induce different shifts of the central frequency of the transition, resulting in a total gain curve which is a broadened, 'smeared' overlay of the gain curves of sub-group of atoms (sometimes dubbed spectral packets), corresponding to different sites throughout the gain medium. Each one of these 'packets' will have the same linewidth, namely the one caused by the homogeneous broadening.

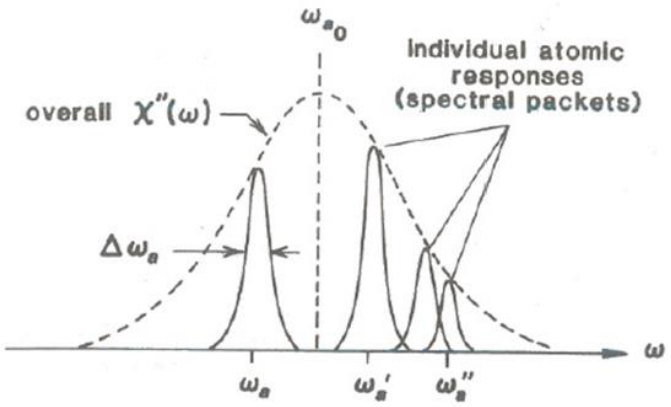

Figure 1.9: Schematic representation of a spectral gain curve composed of both homogenous and inhomogeneous line broadening mechanisms. Taken from [18].

1.4 Lasers

At the heart of the lasing phenomenon – as the acronym '**L**ight **A**mplification by **S**timulated **E**mission of **R**adiation" suggests - is the optical amplification process which was studied in the previous section; therefore the current section, dealing exclusively with lasing cavities, arrives as a natural continuation. It is necessary, however, to first lay down the basic theory of the transmission of a passive (i.e., with no amplification) cavity. Then the gain shall be re-introduced back into the discussion. The theory covered in this section follows the seminal book by Siegman [18].

1.4.1 The Passive Fabry-Perot Cavity

We begin by examining a one-dimensional linear cavity composed of nothing more than 2 reflecting surfaces, with reflectivities R_1, R_2 , and separated by a distance L. No gain mechanism is yet present; the transmission properties of such a passive system (sometimes referred to as a "cold" cavity) are the result of the interferometric effect between some incoming lightwave $e^{j\omega t}$, and the infinite series of reflected and re-reflected waves it gives rise to. In other words, the cavity is a Fabry-Perot interferometer. The transmission function is thus a periodic comb of peaks, each corresponding to a "longitudinal mode" – an optical frequency for which the light wave forms a standing wave within the cavity, because the cavity length exactly matches an integer multiple of its wavelength:

$$\omega_{longitudinal\,mode} = m\frac{\pi \cdot c}{n \cdot L} \tag{1.21}$$

Where m is an integer, and n is the refractive index in the cavity. These maxima of the transmission function are in fact the resonances of the cold cavity.

By considering the frequency difference between the transmission peak 'm' and its nearest neighbor 'm+1', we easily find the important cavity parameter commonly called the *free spectral range* – namely, the *spacing* (separation) between the longitudinal modes:

$$FSR = \Delta\omega_{spacing} = \frac{\pi \cdot c}{n \cdot L} \tag{1.22}$$

An immediate result is that for realistic fiber-based systems, where the length tends to be very large, the typical free spectral ranges are extremely small: as an order-of-magnitude example, a 1 meter-long silica fiber with mirrors on each end will exhibit a cold-cavity longitudinal mode spacing of 200MHz. Translating from the optical frequency domain to wavelength terms (for radiation around 1μm), we may say the modes are separated by less than a picometer!

The second important parameter characterizing the Fabry-Perot cavity is the *width* of the peaks in the transmission comb. As each such peak represents the fulfillment of the condition of constructive superposition of all lightwaves created by the multiple reflections steadily circulating within the cavity, it may be intuitively understood that the stringency of the condition will increase in direct relation to the efficiency with which the reflective surfaces enclose the light within the cavity. Stated otherwise: the higher the number of round-trip passes a photon is expected on average to undergo

before exiting the cavity - the narrower the transmission peaks would be in the frequency domain. Indeed, it may be shown that the full-width at half-maximum of the cavity's resonances relate to the FSR by a single parameter, commonly named the finesse, which depends only on the cavity losses. The definition and consequent relation are:

$$\mathcal{F} = 4\sqrt{R_1 R_2}/(1 - R_1 R_2) \tag{1.23}$$

$$\Delta\omega_{FWHM} = \frac{\Delta\omega_{spacing}}{\mathcal{F}} \tag{1.24}$$

Note that we have here assumed that the only losses experienced in the cavity are due to the finite reflectivities of the mirrors; but the definition of the finesse may easy be generalized by replacing the term $R_1 R_2$ by the term $1 - Loss_{RT}$, where the loss variable stands for the total loss seen by the light beam during a full round-trip inside the cavity.

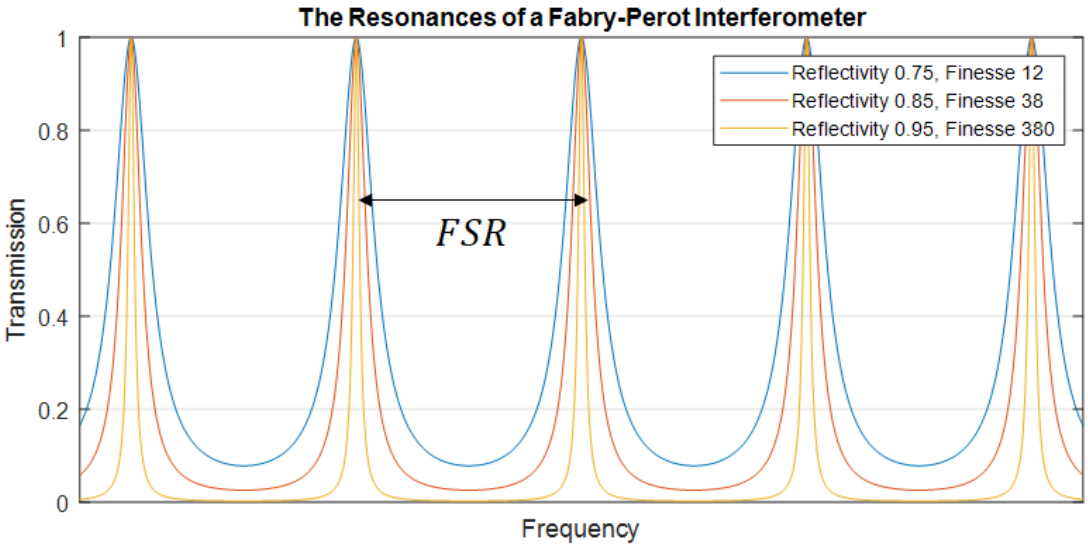

Figure 1.10: The transmission curve of an ideal Fabry-Perot cavity, for 3 different values of the loss (the reflectivities and the resulting values of the finesse are indicated in the legend).

1.4.2 The Cavity with Gain

The path towards a laser starts by taking the cavity of the previous section, and adding a gain mechanism that will amplify the radiation with each pass in between the reflectors. In our case, this shall mean pumping the fiber, thereby raising some rare-earth ions to their excited upper state, and enabling our hypothetical circulating lightwave - namely, our signal - to enjoy amplification through the process of stimulated emission. What shall happen as the gain is slowly raised?

At first, the system is no different from the aforementioned Fabry-Perot cavity, with a modified loss term appearing in the equation defining the finesse – because the amplification process serves only to compensate for a portion of the natural losses. As long as the total round-trip loss remains positive (that is, the term $1 - Loss_{RT}$ remains less than unity), an increase of the pumping is seen still

as an effective ‘cold’ cavity, albeit with improved quality factors for its resonances: these transmission peaks became both narrower and higher.

Eventually, the strengthening of the gain process would result in peak values of the transmission curve reaching unity; the amplification in this case exactly cancels out, for the longitudinal modes, the natural losses of the cavity. Equations (1.23), (1.24) predict that at this point the finesse would be infinite, and the resonances would attain zero width. In fact, the system then stops behaving as a passive cavity, and enters a new regime – that in which a signal lightwave may start oscillating independently within it. The unique point, where the following condition is precisely fulfilled, is therefore the threshold where the onset of lasing occurs:

$$\frac{Gain_{RT}}{R_1 R_2} = 1 \tag{1.25}$$

Once this threshold is crossed and a signal begins to oscillate, or lase, in the cavity, it experiences exponential amplification due to the above-unity gain it experiences with each repetition of the round-trip pass. Why does this signal, then, not shoot upward towards infinite powers? The answer is, of course, that the energy supplied by the pumping process is finite, and as the lasing signal grows the former is saturated because the latter begins depleting it. In terms of the rate equations, this means that the term proportional to I_s and represents the evacuation of the upper level population by stimulated emission, begins decreasing the available gain, which in turns acts back upon it with negative contribution. The feedback loop thus created results in a steady-state solution, in which the signal power is precisely the one for which its depletion of the cavity’s gain maintains the condition stated in eq. (1.25).

In short, gradual increase of the pumping raises the gain-to-loss ratio until it reaches unity, at which value it will remain exactly fixed by the onset of oscillation. The critical mechanism that determines the steady-state regime, therefore, is the saturation of the lasing signal’s gain. For this reason, the saturation process also lies at the heart of the dynamics which determine how many modes may simultaneously lase in the cavity, as we shall see in the next section.

1.4.3 Mode Competition within the Lasing Cavity

So far we have considered only one spectrally-selective feature of our system, namely the periodic oscillation in the transmission of the Fabry-Perot cavity, which is responsible for defining the discrete peaks. It should now be taken into account that, even in the cold cavity, the different peaks do not necessarily all share a uniform maximal transmission value (for instance, in case the mirror reflectivities vary with wavelength). More importantly – in the pumped cavity, the gain process is surely strongly wavelength-dependent; hence we may expect that, with increasing pump powers, the transmission curve featuring the ‘comb’ of longitudinal modes will be modulated by a slow envelope

that reflects the spectral dependence of the amplification (and as such, will have a typical width of at least several nanometers, see section 1.3.2). Figure 1.11 schematically illustrates this behavior.

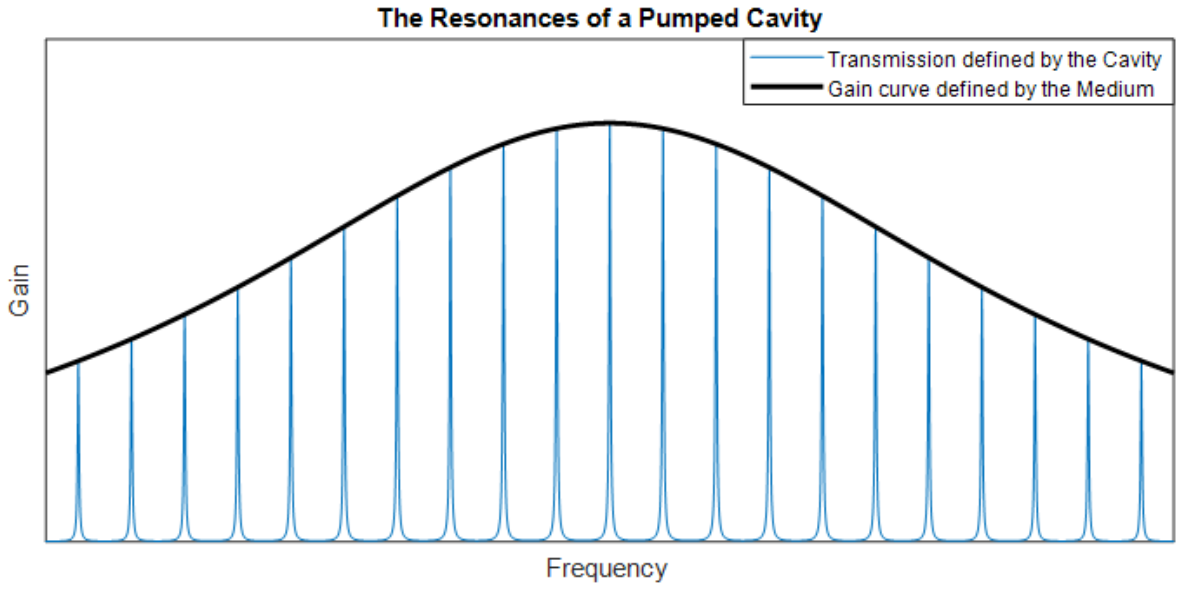

Figure 1.11: Numerical simulation of the transmission peaks of a resonant cavity, multiplied by a slow envelope representing some hypothetical gain spectrum.

Furthermore, we may consider the center-most mode within this envelope, and expect (since it will always, for some given pumping power, enjoy the highest gain-to-loss ratio amongst all modes) it to be the first to reach unity transmission, i.e. arrive at the lasing threshold. As stated earlier, once the oscillation regime is entered, the lasing mode's power exponentially builds up to the steady state balance point where it has saturated the available gain. Consequently, we may anticipate this mode to be the only lasing mode once the threshold condition is reached, in the manner of 'winner takes all'. This, however, may hold true only if said signal mode may truly take 'all', i.e. exploit the total amount of energy deposited in the system by the pumping process. In realistic lasers, this is rarely the case. Two channels may be identified, through which multiple lasing modes may co-exist despite the competition between them over the available gain, and both stem from less-then-complete overlap between the different cavity modes –the first, in the spectral domain, and the second in the spatial domain.

Spectral Hole Burning: In the case where inhomogeneous line broadening is responsible for at least some part of the medium's spectral gain curve, a lasing mode will be found at the center of its 'spectral packet', i.e. some sub group of atoms that share the same gain curve; However, the atoms belonging to other packets (see figure 1.8) will not contribute as much to its amplification, and their population inversion will accordingly be less depleted by it. Hence, the gain these other atoms

represent will be left available to other cavity resonances, which lie at the centers of their respective gain curves, thus leading to a multiplicity of longitudinal modes capable of simultaneous oscillation.

In short, inhomogeneous broadening mechanism serves to isolate different lasing modes in the spectral domain, thus preventing them from fully competing over the same energy quanta and allowing them to co-exist in the system. Since each individual mode will saturate the gain available in its 'own' spectral packet, causing a dip in the gain spectrum confined to the locality of that packet, the lasing in this case is said to be dominated by 'spectral hole burning'.

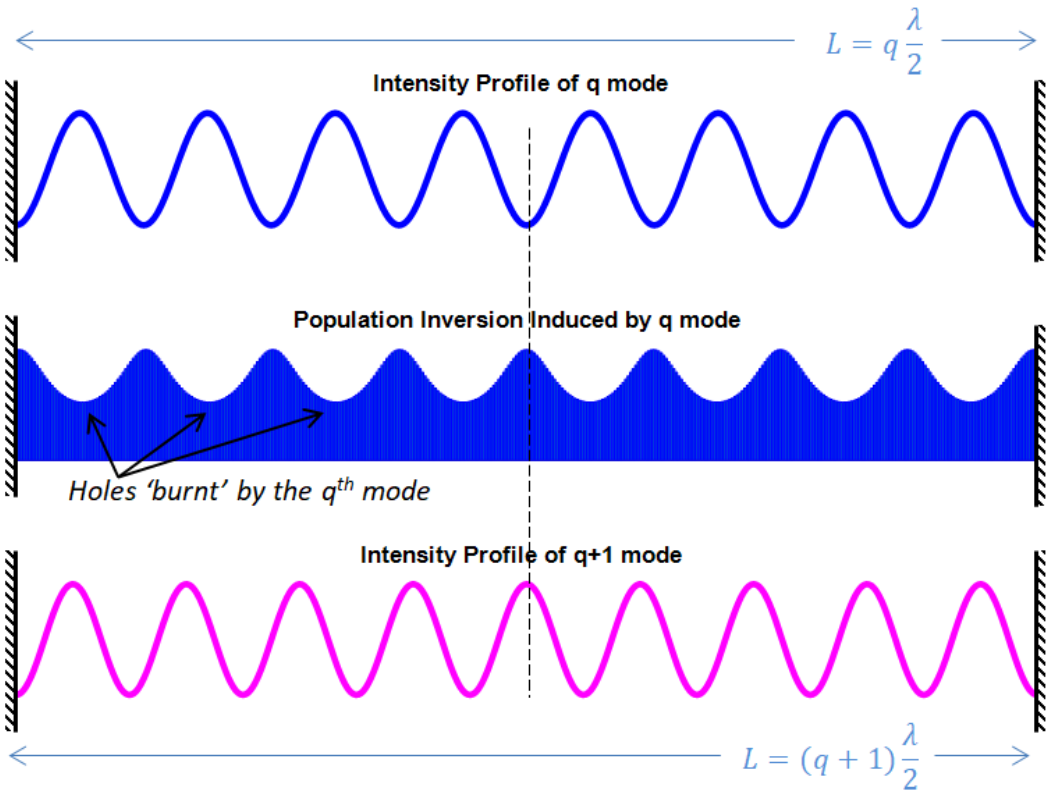

Figure 1.12: Schematic illustration, adapted from [18] pg. 466, of the spatial hole-burning phenomenon: The intensity patterns of two different longitudinal modes will not spatially overlap along the entire length of the resonant cavity, hence the second mode (denoted 'q+1', appearing at the bottom in magenta) may be amplified by locations in the population inversion left non-depleted by the first mode (denoted 'q', in blue).

Spatial Hole Burning: Even if the line broadening present in the medium is completely homogeneous, i.e. all atoms share the same gain spectrum, separation (i.e., non-complete overlap) between different longitudinal modes may be found in the spatial domain, due to the fact that each such mode must be a standing wave of the cavity. Figure 1.12 illustrates this for the simple case where the cavity is single-mode in the transverse axes, and so may be considered as one dimensional: the modes extend across the longitudinal axis as perfect standing waves with a half-wavelength periods. The stationary spatial distribution of such a mode exhibits nodes of vanishing intensity; the gain atoms in these localities cannot contribute to the amplification of that mode and are thus remain undepleted.

Since the wavelengths of other resonances are by definition different (each one is a different integer divisor of the cavity length), their stationary nodes do not coincide throughout the entire length of the cavity, meaning they are able to benefit from the undepleted gain. The end result is that multiple modes may lase simultaneously, as long as the spatial profiles of their standing waves are sufficiently shifted with respect to one another.

Again, and similarly to the previous mechanism of separation in the spectral domain, we speak of hole burning, but rather in the spatial domain (and relying only on the homogeneous line broadening). The first mode to oscillate will saturate the gain, or 'burn holes' in it, in the points where its stationary intensity profile is strong; But other modes may co-lase and compete with it due to their ability to enjoy the non-saturated gain available outside these 'holes'.

References for Chapter 1

[1] G. Maret, P.E. Wolf, Static and Dynamic Multiple Scattering of Light, Physica A, No. 157, 293-300 (1989).

[2] R. V. Langmuir, Scattering of Laser Light, App. Phys. Lett., Vol. 2 No. 2, 29-30 (1963).

[3] A. Ishimaru, Wave Propagation and Scattering in Random Media, IEEE Press, Oxford (1997).

[4] J. W. Goodman, Speckle Phenomena in Optics, 1st Edition, Greenwood Village, CO: Roberts and Company Publishers (2007).

[5] S. Feng, C. Kane, P. A. Lee, A. D. Stone, Correlations and Fluctuations of Coherent Wave Transmission Through Disordered Media, Phys. Rev. Lett., Vol. 61 No. 7, 843-846 (1988).

[6] R. Berkovits, S. Feng, Theory of Speckle-Pattern Tomography in Multiple-Scattering Media, Phys. Rev. Lett., Vol. 65 No. 25, 3120-3123 (1990).

[7] I. Freund, Looking Through Walls and Around Corners, Physica A, No. 168, 49-65 (1990).

[8] D. Gloge, Weakly Guiding Fibers, Applied Optics, Vol. 10 No. 10 pg. 2252, 1971.

[9] J. A. Buck, Fundamentals of Optical Fibers, 2nd Edition, Hoboken, New Jersey: John Wiley & Sons, 2004.

[10] D. Gloge, E. A. J. Marcatili, Multimode Theory of Graded-Core Fibers, The Bell System Tech. J., Vol. 52 No. 9, 1563-1578 (1973).

[11] D. Marcus, Gaussian Approximation of the Fundamental Modes of Graded-Index Fibers, J. Opt. Soc. Am., Vol. 68 No. 1, 103-109 (1978).

[12] C. Barnard *et al*, Analytical Model for Rare-Earth-Doped Fiber Amplifiers and Lasers, IEEE Journal of Quant. Elec., Vol. 30 No. 8 pg. 1817, 1994.

[13] R. Paschotta *et al*, Ytterbium-Doped Fiber Amplifiers, IEEE Journal of Quant. Elec., Vol. 33 No. 7 pg. 1049, 1997.

[14] R.W. Boyd, Nonlinear Optics, 3rd Edition, Academic Press, Elsevier, 2008.

[15] R. Soulard *et al*, Detailed Characterization of Pump-Induced Refractive Index Changes Observed In Nd:YVO4, Nd:GdVO4 and Nd:KGW, Optics Express, Vol. 18 No. 2 pg. 1553, 2010.

[16] M. S. Kuznetsov *et al*, Electronic and Thermal Refractive Index Changes in Ytterbium-Doped Fiber Amplifier, IEEE Journal of Quant. Elec., Vol. 30 No. 8 pg. 1817, 1994.

[17] C. C. Davis, Lasers and Electro-Optics – Fundamentals and Engineering, 1st Edition, Cambridge: Cambridge University Press (1996).

[18] A. E. Siegman, Lasers, 1st Edition, Sausalito, CA: University Science Books (1986).

2 Wavefront Shaping in Non-Amplifying Complex Media and Multimode Fibers

The purpose of this chapter is to provide the practical framework within which this thesis was conducted: the control of light propagation in a multimode fiber (MMF) through the use of wavefront shaping. The chapter is arranged as follows: First, a broad survey of wavefront shaping tools and techniques (in any complex media, scattering layers or MMF alike) will be given as a general background; followed by a narrower survey of the applications and the challenges specific to wavefront shaping in MM fibers. A short numerical model section will provide some necessary background for understanding and quantifying modal control in a MMF (without gain, yet) by means of focusing. Lastly, the architecture and methods that will serve in the main experiments of this thesis (those that will include gain) will be discussed in detail and experimentally demonstrated in a passive system, i.e. a non-amplifying fiber.

2.1 Control of Light Propagation in Complex Media by Wavefront Shaping

Diffractive optical elements (DOE) able to efficiently convert a singlemode beam into one with a spatially-complex wavefront - such as diffractive beam shapers/beam splitters - have been around for a long time, practically since the invention of holography. These elements are traditionally not reconfigurable, meaning the modulation they apply upon the wavefront is fixed. Since the 1990's, with the advent of digitally-programmable diffractive devices - such as deformable mirrors, micro-electro-mechanical (MEMS) mirror arrays, and LCOS (liquid crystal on silicon) spatial light modulators - an intriguing prospect opened up: the use of spatially-complex wavefront shaping for the control of light in disordered media.

It is true that reconfigurable wavefront shaping already existed since the 1970’s as a topic of research, notably in the field of astronomy – where optical devices had been developed for compensating the low-order aberrations created by earth’s atmosphere, resulting in significant improvement of the sharpness of telescope images [1]. However, the aberrated wavefronts found in these applications may be considered as having undergone only weak scattering. The first use of wavefront shaping for the control of light in a truly strongly scattering medium was demonstrated in

2007, in the seminal work of the complex photonic group at Twente [2-3]. Using a liquid-crystal modulator, the local phases across the wavefront of an initially-plane-wave laser beam were optimized so as to create a strong, tight focus point beyond layers of strongly-scattering materials such as TiO2, ZnO, and biological tissue.

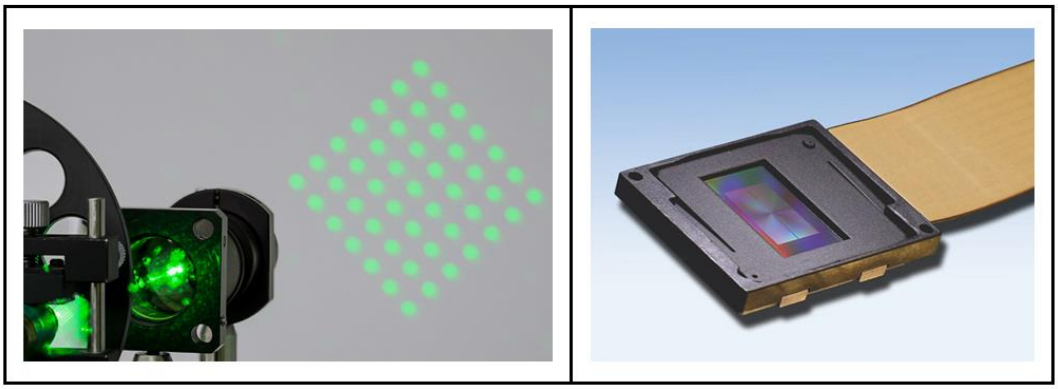

Figure 2.1: Left panel – a diffractive optical element designed to split a singlemode input beam into a fixed pattern of multiple beams arranged in a grid (image copyright – HoloOr Company). Right panel – a 'Pluto' Spatial Light Modulator (image copyright – Holoeye Company). The modulator may be viewed as a programmable extension of the DOE, with millions of degrees of freedom: The phase retardation of each pixel in the LCOS display may be set electronically, allowing the generation of arbitrarily-designed diffraction masks.

2.1.1 Linearity of the Transmission and the Transmission Matrix

The surprising ability of spatial modulation to form well-controlled intensity patterns on the other side of a disordered, non-absorbing but strongly scattering medium (such as was defined in section 1.1), which is essentially opaque to 'traditional' imaging schemes, was explained as follows: The relation between the input optical field E_{in} (specifically, the one impinging upon the modulator) and the field after the scattering medium E_{out} (specifically, the one formed upon the camera sensor) is not only deterministic, but linear in the spatial coordinates. Stated more explicitly - if we segment the modulator plane into N sub-parts (namely, pixels), and likewise identify M pixels of interest at the camera plane, then the field at each of these output pixels (which we shall denote $Eout_m$) is a linear combination of the contributions of each of the input pixels:

$$Eout_m = \sum_n^N t_{mn} Ein_n \tag{2.1}$$

and the particular way the light waves have propagated to, within, and from the medium - including the scattering processes by its disorder - are 'hidden' in the complex coefficients of transmission t_{mn}.

The important point is, that although prediction of these coefficients for a given scattering system is often extremely difficult, due to the very complicated nature of the light propagation through the disorder – they represent a fixed (as long as the medium is not moved) and linear system which completely determines the output field. Therefore, control at the output is possible because the correct modulation of the input field across its N segments - namely one that represents the reciprocal of the given transmission T - would effectively negate, up to a certain point, the effects of scattering. Specifically for focusing at a chosen output pixel, a phasor-diagram of the output field there as the sum of the contributions from all different input pixels is instructive: Initially, the orientations of the different phasors are distributed all over k-space because the scattering process has randomized them, resulting in the total field following speckle statistics. However, the wavefront shaping at the input can change or select the phasors so as to make them constructively interfere. For the case of phase-only modulation, the shaping that should be applied is the shifting of each input pixel's phase by $-\measuredangle(t_{mn})$, i.e. by the phase of its respective transmission coefficient conjugate; This will elegantly align the orientation of all the phasors representing the different contributions superposed at that output pixel, thereby producing a tight spot of constructive interference. The idea is depicted in the illustration on the left-hand side of figure 2.2 (adapted from [4]). For the case of amplitude modulation, a similar logic may be applied by choosing to switch off those pixels which contribute destructively to the desired focus, as was demonstrated in [5]. The right-hand side of the same figure is an excerpt from this reference.

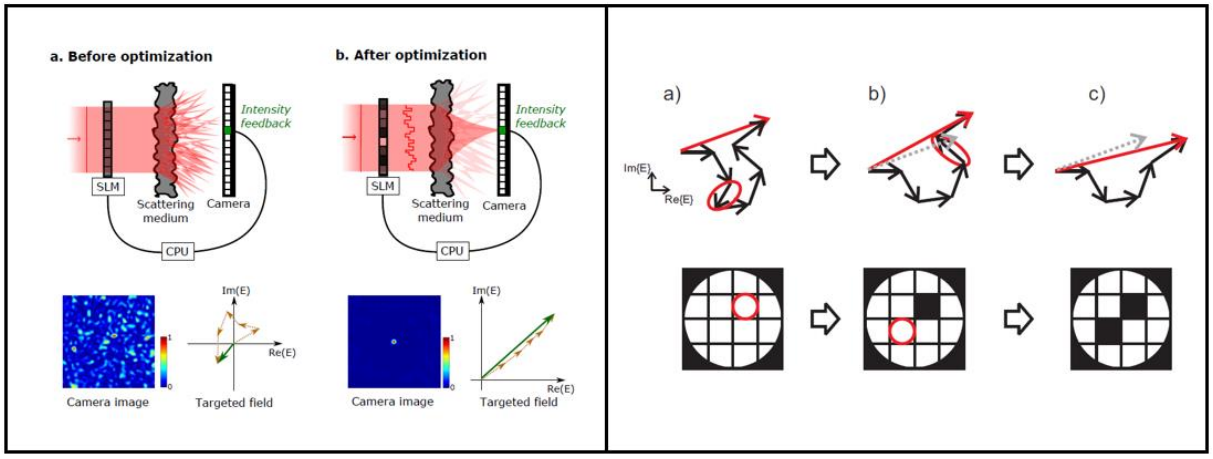

Figure 2.2: Illustration of the optimization of the intensity at a chosen output point by wavefront shaping, with phase-only modulation (left panel, adapted from ref. [4], courtesy of Dr. H. Defienne), and with binary amplitude modulation (right panel, adapted from ref. [5]).

The focusing demonstrated in the above-mentioned experiments was based on an optimization process, in which the intensity at a designated 'target' (a chosen location in the output plane) was maximized by iteratively changing the modulator's degrees of freedom. But one can do better: It should be evident from eq. (2.1) that the entire modulation-imaging system is in fact characterized by

a single linear matrix T of size MxN, where each column corresponds to a specific modulator pixel, and the mth entry in said column represents the amplitude and phase of the field contributed by said input pixel to the mth camera pixel. This entire transmission matrix (TM) can be measured by smartly making use of the linearity of the system [6]: First, the output's response to each of the single spatial components Ein_n is measured *separately* (i.e. by activating the input segments on at a time), allowing the matrix to be constructed column by column. Then, the transmission coefficients in any given row, say the mth row (t_{m1} ... t_{mN}), provide the full information necessary for focusing at any given location at the output plane. Furthermore, under certain conditions the generation of more complex output patterns, up to full images, is possible [7]. Ideally speaking, if the TM is known with good enough accuracy in order to compute its inverse T^{-1}, then the input field that should be formed by the spatial modulator in order to obtain some desired target field at the output, is given by:

$$E_{in} = T^{-1} \cdot E_{target} \tag{2.2}$$

It should be noted that the set of spatial components over which to measure the responses – in other words, the input base – need not necessarily correspond to the physical pixels of the modulator; indeed, the base components need not even avoid overlap as in the 'canonical' pixel base (i.e. the division of the plane by a Cartesian grid). For example, references [6-7] employ the Hadamard base (a set of binary masks, each one of which extends over the entire input plane). Whatever base is used, the definition of the TM remains essentially the same: each column describes the medium's response to a specific member of the input base, meaning the complex field measured at the output when that specific member is activated. However, in our experimental work we shall confine ourselves only to the canonical representation of the modulator plane.

2.1.2 Measurement of the Transmission Matrix

An important issue concerning the measurement of the transmission matrix should be mentioned, and that is the need to measure the output *field*, meaning both the amplitude and the phase of the light. The common method of doing so by using a sensor sensitive only to intensity (as is almost always the case in optics) is based upon the interference effect, which, indeed, is the effect responsible for the appearance of the speckle pattern in the first place. The method requires however that a *constant reference field* – i.e., one that is guaranteed not to be modulated throughout the measurement procedure – be superposed, in the output plane, together with the field we wish to measure. We denote the former E_{ref}, and the latter E_{mod}, because it is the field controlled by our modulator. Then, once these two fields are summed up together at the camera sensor, the intensity detected is the well-known expression that appears in any homodyne detection scheme:

$$I = |E|^2 = \left|E_{ref} + E_{mod}\right|^2 = \left|E_{ref}\right|^2 + |E_{mod}|^2 + 2 \cdot Re\{E_{mod} \cdot E_{ref}^*\} \tag{2.3}$$

The first two terms are the stand-alone intensities of each of the two patterns. The third term is the interesting one, because it is sensitive to the phase of the field we wish to measure; suggesting the possibility of extracting the phase from intensity-only measurements. However, this is not so straightforward – the phase modulates this term only through the interference with the reference field. At this point, the distinction between two different popular techniques of applying and using the reference field should be discussed.

The first possible approach is the off-axis holography method, which employs an external reference field – meaning, one that has not gone through the scattering medium. This field is always split-off from the light source as a separate arm, so that it shares a common phase with the main arm, regardless of the ever-present noise and drift of the source's phase. The reference arm is led around the disordered medium to arrive at the output detection plane (namely, the camera sensor) as a plane wave with a slight misalignment of its beam with respect to the main one (say by some angle φ). Combining the two beams at the sensor gives rise to interference fringes whose spatial frequency is determined by the misalignment angle thus:

$$Re\{E_{mod} \cdot E_{ref}^{*}\} \propto Re\{E_{mod} \cdot e^{-jk \cdot x \cdot \sin\varphi}\} \sim \cos(k \cdot \varphi \cdot x) \cdot E_{mod} \qquad (2.4)$$

A Fourier transform of the image then readily gives access (by looking at the 1st Fourier order) to both the amplitude and the phase of E_{mod}. An example of the use of this method, from ref. [8], is shown in the left panel of figure 2.3.

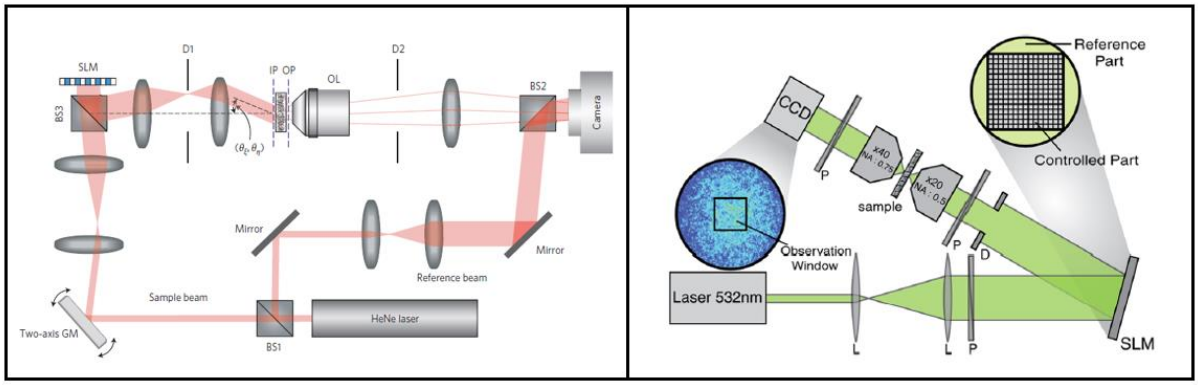

Figure 2.3: The two common methods for measuring the output light field using interference with a reference field. The left panel, taken from ref. [8], is an example of an experiment utilizing an external reference arm for an off-axis holographic detection scheme. The right panel, taken from ref. [6], is an example of an internal-reference setup, with the surfaces around the SLM's controlled area used for supplying the reference.

The advantages of this method are, the ability to extract the full information by a one-shot imaging operation, and that the reference beam may be applied across the output plane as a homogenous, flat-phased beam, thereby facilitating the direct measurement of the 'true' TM – in the sense that all output pixels share the same known reference phase and amplitude. The obvious

disadvantage is the need to supply this reference field by means of an external arm; Firstly, for applications where the entire purpose of measuring the transmission of the complex medium is to 'see beyond it' (i.e., image objects to which there is no access except through the light-scattering layer), this requirement renders the external reference approach irrelevant. Secondly, even for applications where physical access to the 'distal end' of the medium is allowed, the external reference technique presents considerable challenges of noise and measurement drifts, due to the technical difficulty of stabilizing the path-difference between the two arms with the required precision.

The second approach, that of an 'internal' or 'co-propagating' reference, does not employ an actual separation of the reference light from the modulated light. Rather, a portion of the beam coupled into the medium is designated as the reference by leaving it unmodulated, and hence it propagates through the medium together with the modulated part, and likewise generates at the output a field that is a complicated speckle. An example of the use of this method, from ref. [6], is shown in the right panel of figure 2.3.

Obviously, the off-axis holography concept may not be employed in this configuration, because the modulated and the reference fields completely overlap in k-space (so the desired information may not be retrieved by going to the Fourier space). Instead, a different technique involving modulation in time is used. If the input pixel of interest is modulated so as to sweep its phase through a full period (i.e. in the range $0 - 2\pi$), the interference between its corresponding output field and the constant reference field will exhibit a beating effect. It will be pronounced as an intensity modulation, by a full sine wave, of the optical power at any observed output pixel:

$$Re\{E_{mod} \cdot E_{ref}^{*}\} = |E_{ref}| \cdot |E_{mod}| \cdot \sin(\theta_{sweep} + \emptyset) \qquad (2.5)$$

Where $\emptyset$ is the relative phase-difference between the reference and the modulated field. The sweeping of θ through a full period is almost always done by a series of discrete measurements, or phase-steps, from which the sine wave may be fitted in order to extract the desired value $\emptyset$; as an example, reference [9] gives the full analysis 'recipe' for the case of 4 discrete samples, commonly called the 'four-image method'. A schematic illustration of the interference-based method is given in figure 2.4, adapted from [10].

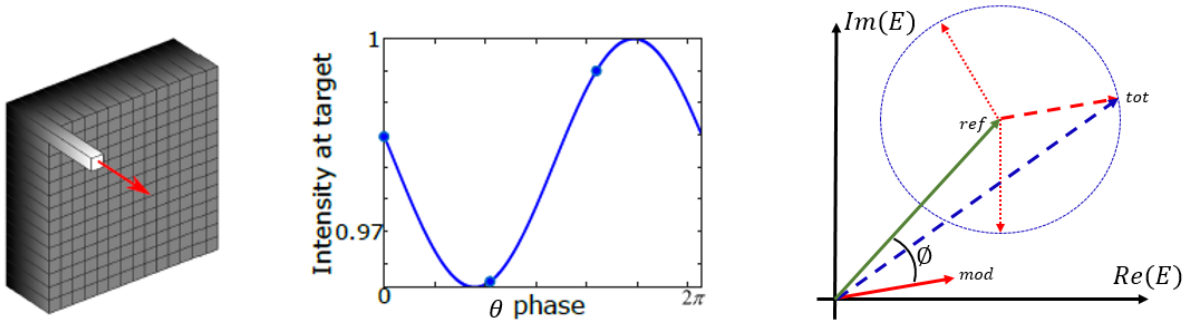

Figure 2.4: A schematic description of the time modulation technique used for retrieving the output field in the internal-reference approach (partly adapted from ref. [10], courtesy of Dr. T. Chaigne). As the phase of each modulator pixel is swept (left), the intensity at the output varies as a sine wave (center). This is explained by the phasor diagram (right), where the solid green arrow represents the constant reference field, the dotted red arrows represent the modulated field at different phases during the sweep, and the dotted blue line represents the resulting magnitude of the total field (their sum, which plots a circle in the complex plane).

The considerable disadvantage of the co-propagating reference method (besides the obvious penalty in measurement time) is the fact that the reference field is itself a speckle, and therefore the different M output pixels do not share the same reference phase and amplitude. This is equivalent to measuring the TM with an unknown, arbitrary complex coefficient multiplying each row. However, for the purpose of focusing the light at any single given output pixel m, this is already sufficient (as long as this arbitrary coefficient does not approaching zero, which indeed will be the case for certain, albeit rare, output pixels – where the reference field's speckle attains a dark spot). This assertion will be now clarified by a brief discussion of the scheme in which a measured TM may be used for performing such focusing.

2.1.3 Focusing Using the Transmission Matrix

The construction of focus at a single output point was interpreted at the beginning of section 2.1.1 as a constructive superposition of the phasors corresponding to the input segments (as graphically visualized, in figure 2.2, by the 'alignment' of the phasors). Recalling also the description of how the medium's TM is constructed column by column as a set of vectors representing the response to the individual input segments (likewise, see section 2.1.1), the procedure for using the TM to focus is readily established. In the ideal case where TM is perfectly measured and known, in order to focus at the mth camera pixel we would: Take the entries of the mth matrix row (t_{m1} ... t_{mN}); configure our modulator so the field sent by each of the input segments is the *conjugate of the corresponding matrix entry*, i.e. set the modulation $Ein_n = t^*_{mn}$; and plugging this into the equation (2.1) which defines the transmission matrix in the first place, we obtain $Eout_m = \sum_n^N t_{mn} \cdot t^*_{mn} = \sum_n^N |t_{mn}|^2$ - which is none other than a constructive superposition of all field components at the mth camera pixel.

The problem with the above is that the assumption of 'perfect' knowledge of the TM is not so easily satisfied, as indeed we have seen in section 2.1.2: the need to measure the field's phase through an interferometric technique necessarily leads to a measured TM where all entries represent the product of the desired field with the reference field (instead of just the desired field itself). This can be readily seen throughout equations (2.3-5); the reference field, whether applied in the 'external' method or the 'internal' one, always remains as a factor multiplying the measured entries of the matrix. In the external reference method, this multiplicative factor is roughly identical across all output pixels (up to the quality with which we can approximate a plane wave reference, i.e. collimate and homogenize the external beam); while in the internal reference method, the multiplicative factors strongly vary between output pixels, because the reference is a speckle. The important point is that - even in the latter method – for a given *single* row of the TM, the factor arising from the reference field is identical for all entries; therefore, focusing at a *single* output pixel can be performed with precisely the same procedure as described above for an 'ideally-measured' matrix, namely – configuring a modulation function where each member of our input base takes on the value of the conjugate of the corresponding measured TM element. This is summarized by the following expression, as well as in figure 2.5:

$$Eout_m|_{focusing} = \sum_n^N t_{mn} \cdot (t_{mn} \cdot Eref_m^*)^* = Eref_m \sum_n^N |t_{mn}|^2 \qquad (2.6)$$

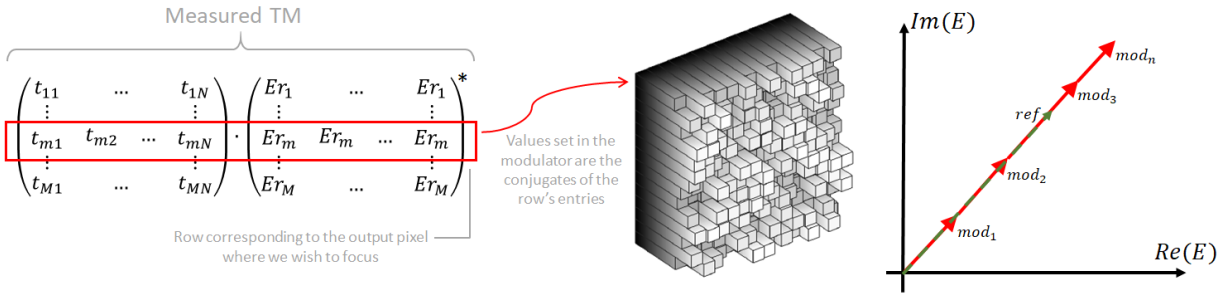

Figure 2.5: A schematic description of focusing at the mth output pixel using a TM measured with a reference field, either external or internal. The illustration is partly adapted from ref. [10], courtesy of Dr. T. Chaigne. On the left, the measured TM is shown as a product (note that the multiplication is element-wise!) of the 'true' TM and a matrix (whose columns are identical) representing the reference field. The entries of the mth row (conjugated) are used as the modulation values for the input base; since the reference field appearing in all products in that row is the same, it does not impede the constructive alignment of the contributions of all inputs that forms a focus (as pictured on the right).

2.2 Wavefront Shaping in Passive Optical Fibers

The strong similarity between the scrambling of light propagating in a disordered, strongly scattering medium such as paint, and within a multimode fiber, has already been discussed in the theory chapter. It is therefore not surprising, that the evolution of the field of optical wavefront-shaping for complex media has included, from very early on, significant work on such fibers. Notable first works were based on a time-reversal scheme (by digital phase conjugation) to obtain the desired output: A steered, nearly-collimated beam in the case of the groups at the Ecole Polytechnique and Thales (see [11]), and a controlled array of focus points in the case of a group in Rome (see [12]). Another subject of immediate interest was the ability to isolate the discrete eigenmodes of a given multimode fiber, inject them into the fiber by design, and measure their transmission. Reference [13] describes an optimization scheme for the selective coupling of a single eigenmode; while later works sought to study the entire base of eigenmodes for applicative purposes of fiber telecommunication, and fiber-based microscopy - see [14-15], and [16-17], respectively. These important papers will be discussed in detail in the next chapter, since their findings serve to establish certain parts of our model of the multimode fiber amplifier.

The remainder of this section will overview, in a more concise manner, the main motivations and characteristics of the research carried out in recent years within the context of the two abovementioned major applicative fields – namely, optical telecommunications, and microscopy. Then, a survey of some established experimental techniques found in the literature will follow, focusing on two essential aspects of a wavefront shaping setup: the configuration of the optical system for constructing the input field; and the configuration of the output field's phase measurement scheme. This survey will serve as a basis for the discussion of our experimental setup, and the essential considerations in its design.

2.2.1 Multimode Fibers in Telecommunication

Currently, telecommunication-oriented research shows immense interest in multi-mode fibers as promising enablers of a much-needed leap of the capacities of long-haul optical links [18]; the idea being to multiplex several independent data channels in a single fiber (and in each single wavelength, and for each polarization) upon the different guided spatial modes – the so-called MDM (Mode Division Multiplexing) approach. Techniques of wavefront-shaping - such as the SLM-based Multi-Plane Light Converter (MLPC) [19] - are of key importance in this effort, so that the desired combination of spatial modes could be launched in a controlled manner into the fiber, and then de-multiplexed at the receiver end. It should be noted however, that due to the complex nature of the mode-coupling in a realistic long-distance optical fiber, the de-multiplexing into the separate channels

needs to be followed by some form of MIMO-type (Multiple Input Multiple Output) signal processing module, which mitigates the channel crosstalk [20]. From the perspective of the wavefront shaping technology, then, the challenge is coupling the beams in the scheme which best exploits the theoretical data capacity of the fiber's mode base, while taking into account the capabilities and constraints of the MIMO processing. For example, the complexity and cost of the latter system grows rapidly with the increase of the temporal dilation a pulse undergoes in the transmission channel; therefore, multiplexing the information stream upon a set of spatial modes with large modal dispersion is undesired.

The number of spatial modes supported in the fibers typically employed in current MDM research ranges from 3-4, to about 15 at most; Additional increase of the total information capacity of the single fiber, up to a hundred-fold in some cases, is often made possible by the use of multiple cores, each core supporting a few spatial modes [21].

2.2.2 Multimode Fibers in Microscopy and Biomedical Applications

Optical fibers have been extensively used in such fields such as medical diagnosis, surgery, and biomedical research, in order to probe and image deep inside biological tissue; their excellent guidance of light has permitted significant improvement upon the original approach for endoscopy, where the camera as a whole was miniaturized and inserted into the body. However, the need to form an image of many pixels that cover the desired field-of-view - either by mechanically scanning the distal tip of a *singlemode* fiber [22], or employing a bundle of many such fibers [23] – prevents further reduction in the size of the scope that must be brought to close proximity with the imaged tissue. Similarly, the need to efficiently focus the collected light into the fibers and control the imaging distance necessitates the placement of optics at the distal tip, unless clever computational techniques are used to 'decrypt' the optical information [24].

Compared to such mechanical devices or bundles, which typically have a width of no less than a millimeter, a single *multimode* fiber is typically about x10 thinner in diameter (and hence x100 smaller in footprint); Yet it still has the potential of gathering and transmitting a full image containing the same spatial information – granted only that this information be mapped to its modes, and then correctly reconstructed at the proximal end by some form of 'de-scrambling' the propagation effects. Therefore, enormous interest for wavefront-shaping in MMFs as tools for various endoscopic applications has been showed in recent years [25]. A non-exhaustive survey includes achievements in fiber-based confocal microscopy for direct imaging [26] and fluorescence imaging [27], Optogenetics [28], and in-vivo micromanipulation by the implementation of optical tweezers at the fiber's end for the purpose of trapping and moving cell-size objects [29], and even for micro-fabrication by polymerization [30].

Unlike the fibers found in the telecommunication applications, which tend to be few-mode, the fibers typically used in the imaging-oriented applications are highly multimode, in order to enable high-resolution and wide field-of-view imaging. For example, reference [27] employs a fiber with a 62.5μm core, which supports several hundred modes, while the fiber utilized in [28] has a core diameter of 365μm and guides an estimated number of modes exceeding 10^5.

2.2.3 Approaches for Shaping the Input Wavefront and Coupling into the Multimode Fiber

The optical path, through which the light reflected off the SLM screen passes until it reaches the fiber entry point, is of critical influence upon our ability to efficiently couple this light into the fiber and control its modal content. The first important choice to be considered in the design of this optical relay is the imaging relation - namely, whether to conjugate the SLM plane to the fiber facet plane, or to place the two so that they are in each other's Fourier plane.

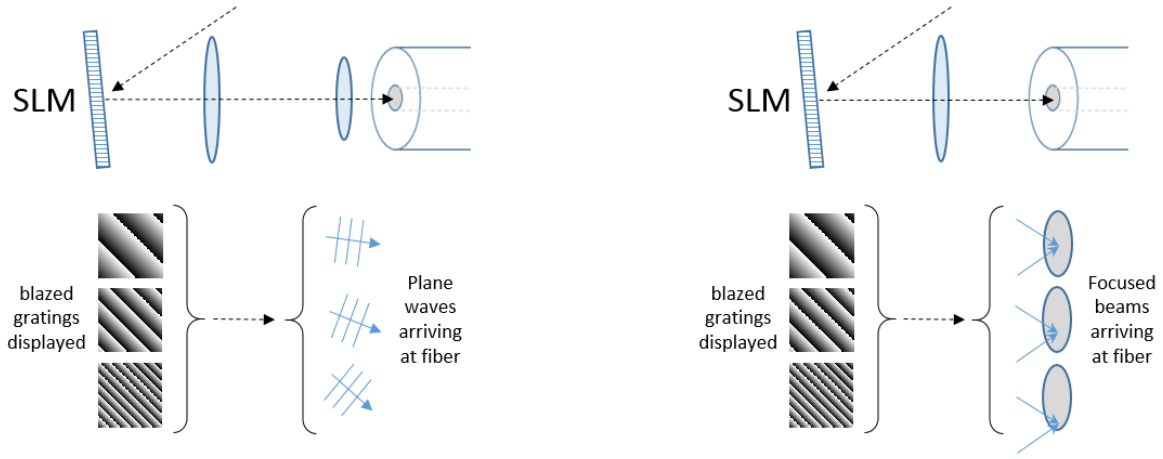

Figure 2.6: The two common architectures for the optical relay from the spatial modulator to the input facet of the fiber. Left-hand side – imaging conjugation; Right-hand side – Fourier conjugation.

A seemingly straightforward way of setting up a system for shaping the wavefront at a fiber's input is that of image-conjugating the SLM and the fiber planes to each other, for example as was done in [31] and [32], which demonstrated confocal microscopy through a multimode fiber (by means of digital phase conjugation in the former, and by a transmission-matrix approach in the latter). The left-hand side of figure 2.6 schematically shows this type of configuration, in its simplest possible implementation - using a 4F system (only 2 lenses). As this constructs an imaging system in which the modulator surface is de-magnified and reproduced at the medium's entrance, the modulator pixels will correspond to spatial locations across the fiber facet. Evidently, the size of the usable modulator area will simply be the size of the fiber core's image upon the SLM surface (any pixels outside this area will always be imaged to a point in the cladding). Furthermore, the display of gratings upon the SLM

would produce, at the entrance to the fiber, plane waves whose k-vector (i.e., angle of incidence upon the facet) correspond to the grating period. Therefore, the acceptance cone of the waveguide may be accessed by sending a set of gratings, with the maximal spatial frequency (i.e. minimal period) calculable by this simple relation:

$$P_{min} = M_{4f} \frac{\lambda}{NA} \tag{2.7}$$

Where M_{4f} is the demagnification factor of the imaging relation from SLM to fiber.

It is worthwhile to note that typical SLM surface sizes are on the order of a centimeter, making the image-conjugation SLM relay configuration well-suited for fibers with relatively large core diameters; Indeed, in both references quoted above for this method, the fiber under study has a core size of 105μm. For work with fibers with medium or small cores (say, 50μm and below) the de-magnification values needed would be rather large, in the vicinity of a 100 or higher. Thus a practical optical relay for a few-mode fiber would probably consist of more than one 4F system, i.e. demagnification in stages.

Another option for configuring the wavefront-shaping setup is to Fourier-conjugate the modulator plane to that of the fiber; this means that the SLM pixels are mapped in the k-space of the guided light in the fiber, and hence correspond to different ray angles within the acceptance cone of the waveguide. The simplest possible way to implement this configuration, as schematically depicted in the right-hand side of figure 2.6 would with a single lens that forms a 2F system between the spatial modulator and the fiber. Such a setup was implemented, for example, in [33]. Some technical difficulty arises in a true 2F relay because of the need to place the SLM rather close (one focal distance) to the lens/objective. This is usually overcome by relaying the SLM with an additional 4F system to an image plane, which coincides with the back-focal plane of the lens/objective that focuses the light into the fiber; an example is given in [34] and [35]. Such a relay allows the placing of the SLM at a comfortable physical distance (also, the introduction of some demagnification, if convenient), but it does not change the essential Fourier relation between modulator and medium.

In this configuration, a uniform illumination impinging upon the SLM would produce a focus point lying on the fiber facet plane, because the Fourier-transform of a plane wave leaving the modulator is a focused spot. For this reason, the Fourier-conjugation method lends itself easily to work with fibers of relatively small core sizes. Considering again the display of different blazed gratings on the SLM, we see that this would readily allow us to access the entire acceptance width of the waveguide, by spatially displacing the focus spot across the fiber facet - because a linear modulation is transformed to a translation in the Fourier space coordinates. In particular, the minimal grating period that could be coupled into the fiber would then be:

$$P_{min} = 2 \frac{f \cdot \lambda}{D_{core}} \tag{2.8}$$

Where f is the focal length of the single lens, and D_{core} is the diameter of the fiber core.

We conclude the discussion of the input side of the setup by mentioning another important consideration for the input side, that of **"on/off axis":** Meaning, whether to place the fiber so that its core receives all light reflected from the modulator, including the 0th order of diffraction; or rather, to place it "off-axis", meaning **intentionally misaligning** the fiber core with respect to the center of the 0th order, in which case only higher orders of diffraction intentionally directed at the core will be coupled to the fiber.

In the configuration where the SLM is placed in the Fourier plane of the fiber, the misalignment may be performed by displacing the fiber in the transverse XY coordinates, whereas in the configuration of the SLM imaged to the fiber plane, the misalignment is performed by tilting the fiber facet in its yaw/pitch angles. The desired wavefront modulation should then be encoded upon a blazed grating whose 1st diffraction order corresponds (either in real space or in k-space, respectively to the two configurations) to the new location/orientation of the fiber core. In practice, it might in fact be easier to tilt the SLM itself, rather than translating/tilting the fiber; from the perspective of the wavefront shaping, this is equivalent.

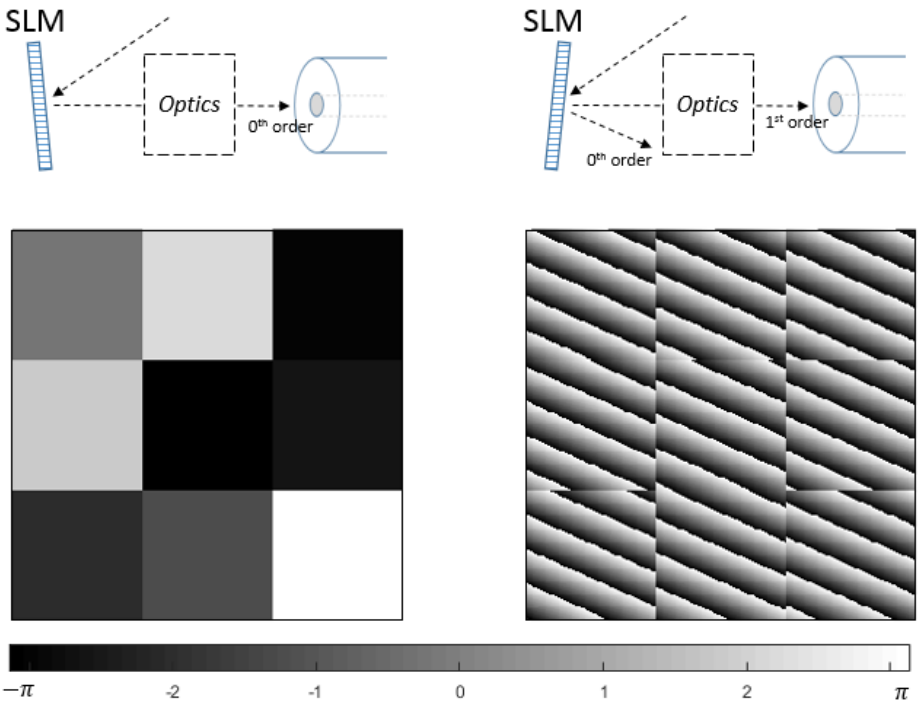

Figure 2.7: The two options for setting up the alignment of the fiber with respect to the spatial modulator's diffraction orders, and the phase mask that would be displayed on the modulator to implement an example of a 3x3 phase modulation function. Left-hand side – 'on axis', the 0th order is coupled into the fiber core, hence each super-pixel of the SLM simply takes on the uniform value of the assigned phase. Right-hand side – 'off axis', the 0th order is directed away. Now the same 3x3 phase modulation is performed by displaying on each super-pixel of the SLM a blazed grating whose 1st order is coupled into the fiber core, and the assigned phase value is encoded as the phase shift of the grating. The 'optics' module designates either image or Fourier conjugation.

Regardless of the chosen conjugation relation (whether Fourier-conjugation, or imaging), the scheme of implementing a desired wavefront-modulation function in "off-axis" remains the same: convolution of the desired function with the higher-frequency grating, which corresponds to the offset between the modulator and the fiber core. An example is illustrated in figure 2.7. An additional benefit of this technique is the ability to easily implement *amplitude modulation* in parallel to the *phase modulation*, simply by reducing the amplitude of the grating. For example: a blazed grating which spans only a $[-\pi/2\,,+\pi/2]$ phase range diffracts ½ (in field amplitude) of the light that a grating with a full $[-\pi,+\pi]$ range would.

Naturally, the off-axis method requires higher spatial resolution for the modulator; every degree of freedom of the modulation function is represented by a 'super pixel', i.e. a tile containing a sufficient number of actual modulator pixels for displaying a diffraction grating.

The "on/off axis" consideration is a significant one, as the diffraction efficiency of our spatial modulator is finite – typically between 80% and 50%, depending on the diffraction angle. The rest of the optical power, which remains undiffracted on the 0th order, is unmodulated by our shaping. Therefore, working on-axis means that some component of the field coupled into the fiber is 'static', and may not be changed by the phase mask displayed. Consequently, an on-axis alignment has the obvious advantage of minimizing the loss of optical power, but it inevitably limits our control of the light's propagation in the fiber. *Only by employing off-axis injection may we fully shape the field coupled into the waveguide.*

In summary: in order to completely eliminate any 'static' (i.e., non-modulated) light fields in our fiber, as well as to facilitate the encoding of both phase and amplitude information in the modulation of each SLM tile, the alignment of the SLM in our setup was always off-axis. The chosen relay method was a variant of the Fourier-conjugation method (with a different setup that used the image-conjugation architecture, serving in a preliminary phase as a benchmark). Section 2.4 will describe the specific implementation of these approaches in our experiment with greater detail.

2.2.4 Approaches for Measurement of the Output Field of the Multimode Fiber

The discussion of this topic that has already been carried out in the more general section overviewing any type of disordered media (i.e., the presentation and comparison of the 'external' and 'internal' reference approaches), holds true as well for the specific case of multimode fibers; Indeed, the design considerations and analysis methods relevant for the *output side* of the experimental system hardly change whether the medium of interest is a layer of truly disordered scattering material, or a multimode waveguide. For this reason, the description of these two methods need not be repeated here for the specific case of wavefront shaping in fibers. It is worth noting though, that in almost all the works found in the literature about light control in multimode fibers, the detection of the output field

was based upon the external reference field approach. This is due mainly to the need to capture the field distribution across the full output plane, in order to study the relation of the speckle pattern to the fiber's spatial modes. However, the stability issues (already alluded to above) entailed by the use of an interferometric architecture (i.e., two separate arms) are considerable; an example of this, taken from [36] and shown in figure 2.8, demonstrates – for a MMF control setup – the sizeable noise and drift in the phase measurements.

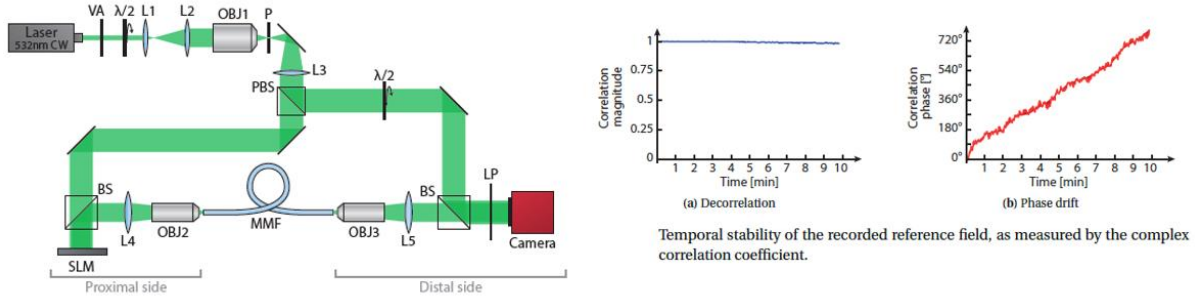

Figure 2.8: Example of the measurement problem brought about by the use of the holography method with an external reference, taken from ref [36]. Left-hand side – the experimental setup, including the external reference arm that recombines with the output of the main arm just before the camera. Right-hand side – the significant phase noise and drift (in red) observed, even when the intensity pattern of the speckle exhibits good stability (as is evident form the intensity correlation measurement, in blue).

In order to avoid these complications inherent to the external reference method, and the additional correction systems typically needed to overcome the noise (such as phase tracking and interpolation modules), the chosen detection method for our work was based on an internal (co-propagating) reference. Section 2.4 will describe the specific implementation of this approach in our experiment with greater detail.

2.3 Focusing Light through a Passive Multimode Fiber – Numerical Simulations

As mentioned in the theory chapter, the LP modes constitute an orthogonal base for any lightfield guided in our fiber. Specifically for the goal of concentrating as much of the energy as possible into a single speckle grain, i.e. forming a focus spot, the optimal shaping one can achieve is by linearly combining the modes each with an amplitude equal to the value its field attains at the desired spatial point (because this is what one would get by decomposing a perfect focus, namely a diffraction limited spot situated at the desired point, over the mode basis). Explicitly stated, the field constructed when one optimally focuses at some point (x_0, y_0) is given by:

$$E_{best\ possible\ focus}(x,y) = \sum_j^n B_j \cdot \psi_j(x,y) \quad \text{, where} \quad B_j = \psi_j(x_0,y_0) \tag{2.9}$$

Since the set of functions $\{\psi_{l,m}(x,y)\}$ are field distributions all with uniform phase (only variation is in the field's local strength), the 'best achievable' focus described above by Eq. (2.8) represents a combination of the LP modes with varying absolute amplitudes, all aligned to the same phase; and the particular weighting between the absolute amplitudes determines the spatial location of the focus point.

The significant difference between wavefront shaping in a truly disordered scattering medium, such as a layer of paint or biological tissue, and in an optical fiber, is that while for the former the number of propagation modes into which light may be coupled is so large as to be virtually infinite (at any rate, much larger than the number of degrees of freedom controlled by the modulator), the number of modes for the latter is finite and often (in the case of few mode fibers) even quite small. This difference has important implications for the prospect of focusing the light at the output of the system; In particular, the spatial characteristics and the achievable contrast of a focus spot formed at the output of a MMF are dictated by the limited number of supported modes.

2.3.1 Focus Spot Size

Behind a layer of a disordered, strongly scattering medium, the smallest achievable focus point has an Airy disk with a full width at half maximum of $w = 1.03 \cdot \lambda \cdot f/D$, where f is the distance from the scattering layer to the focal plane, and D is the diameter of the illuminated area on that layer [37]. Considering the ratio f/D as, essentially, the reciprocal of the numerical aperture at the system's output, we see that this width is none other than the diffraction limit for the set of all free-space plane waves contained in the k-space seen from that plane (and is therefore also the minimal size of the speckle grains).

Quite similarly, at the output of a multimode fiber, a focus spot's width will be dictated by the diffraction limit, but this time the set of modes from which the spot may be constructed is not the free-space plane waves, but the spatial modes guided in the fiber. Therefore, the numerical aperture is not the sole criterion that determines the width of the focus – as demonstrated in figure 2.9, in which are shown numerical constructions of a 'best possible focus' (as per eq. (2.9)) in 3 different fibers, all with NA=0.1 but with increasing core diameters. It is evident that the more modes are guided by the fiber, the tighter the focus that may be formed. Intuitively, it should indeed be expected that since the spot is a constructive interference of the fiber's spatial modes, its Airy disk may only be as small as the smallest lobe of the highest-order mode supported.

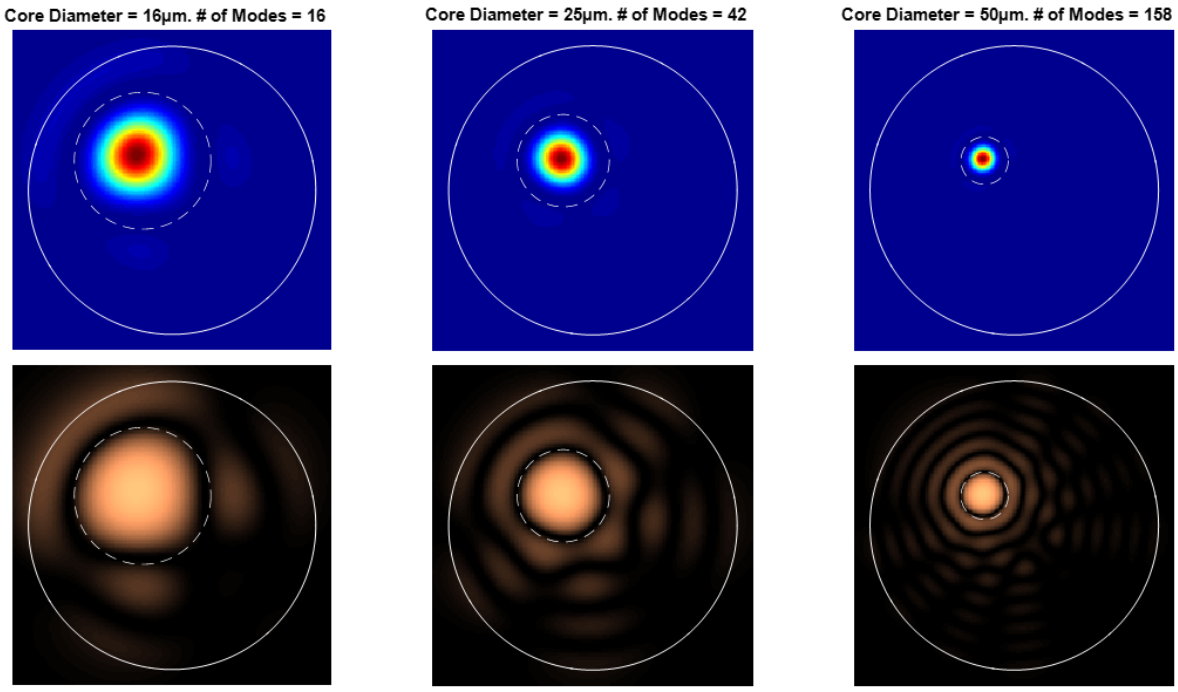

Figure 2.9: Numerical simulations of 'best possible' foci for 3 different step-index fibers with increasing, from left to right, core diameters (and therefore increasing number of modes – as indicated in the titles). Top row, in colormap – Intensity images of the foci, in linear scale; Bottom row, in grayscale – the same intensity images, but plotted in logarithmic scale. Solid white lines designate the core boundary; Dashed white lines designate the Airy disk of the focus.

The distinction made above becomes less pronounced when the number of modes is very high, e.g. several hundreds and above; However, in a few-mode fiber, an explicit expression for the smallest achievable spot size is not readily available (also, a small dependence on the position of the focus point with respect to the core center is found [38]). Generally speaking, however, it should be understood that for a wavefront shaping experiment in a given fiber that supports some finite number of modes, full control of the excitation of this mode set should permit the generation of focus spots with dimensions closely comparable to those of the (non-shaped) output speckle patterns.

2.3.2 Focus Spot Contrast and the Confinement Metric

Behind a layer of a disordered, strongly scattering medium, the enhancement factor for a focus point created by wavefront shaping (defined as the ratio between the shaped intensity, and the average intensity of the speckle before shaping), is $\eta = 1 + (N-1)\cdot\pi/4$, where N is the number of degrees of freedom controlled by the spatial modulator [2]. Evidently, the contrasts achievable with a sufficiently large number of modulator segments are very high, for example enhancement factors of over 100,000 have been demonstrated for focusing through holographic diffusers [39].

Focusing light through a multimode fiber is quite a different story, because the contrast achievable is determined by the nature of the spatial modes rather than by the resolution of the wavefront shaping system: It should be evident that with a finite number of spatial modes available - beyond some point, no further increase in the number of modulator segments would be able to improve upon the limit dictated by the 'best achievable focus' described above. Therefore, a numerical simulation study of this theoretical limit is instructive.

Before presenting the results of these simulations, it should be remarked that the enhancement factor, as a metric, is not well suited for assessing the quality of a focus in a fiber system, especially when the total number of modes is low, because the definition of the average intensity before shaping becomes imprecise (there are not enough speckle grains). Furthermore, this factor would depend directly on the number of modes guided by the specific fiber under study, which is inconvenient as a global measure of focusing quality. Therefore, a more useful metric was used in this work, that of the intensity confinement.

As is evident from the bottom panel of figure 2.9, the intensity distribution of a focus constructed from LP modes strongly resembles a sinc function - a strong peak, surrounded by weak lower-order rings. Hence, a useful metric to define for judging the quality of such foci is how much of the total guided optical power is contained within the main peak (the 0^{th} order lobe). Numerically, we may easily evaluate this ratio by defining a disk, the diameter of which is the distance between the 'zeros' bordering the central lobe (this is in fact the Airy disk of the focus spot), and applying it over the intensity image as a binary mask.

$$Confinement = \frac{I_{inside\ central\ lobe}}{I_{total}} \tag{2.10}$$

For the same 3 example fibers mentioned above in figure 2.9, "best achievable" foci were numerically realized in all points across one quadrant of the fiber facet (in any other quadrant, the results would of course repeat, due to the circular symmetry), and the confinement quality metric was calculated for each point. Figure 2.10 shows the results; it can be seen that for all points within the core, a focus spot may be formed with a confinement of between **85% - 90%**, approximately (as mentioned previously, a slight dependence on the radial distance of the focus point from the center is present). Quite interestingly, the maximum possible confinement scores are found far from the center, adjacent to the core's edge, where the highest-order modes participate significantly in the construction of the focus. We assert, that this limit holds regardless of the number of modes supported by the fiber; The fewer modes are guided, the less tight (i.e., of larger Airy disk) the focus spot becomes, but it is always possible to confine at least 0.8 of the guided intensity within that disk.

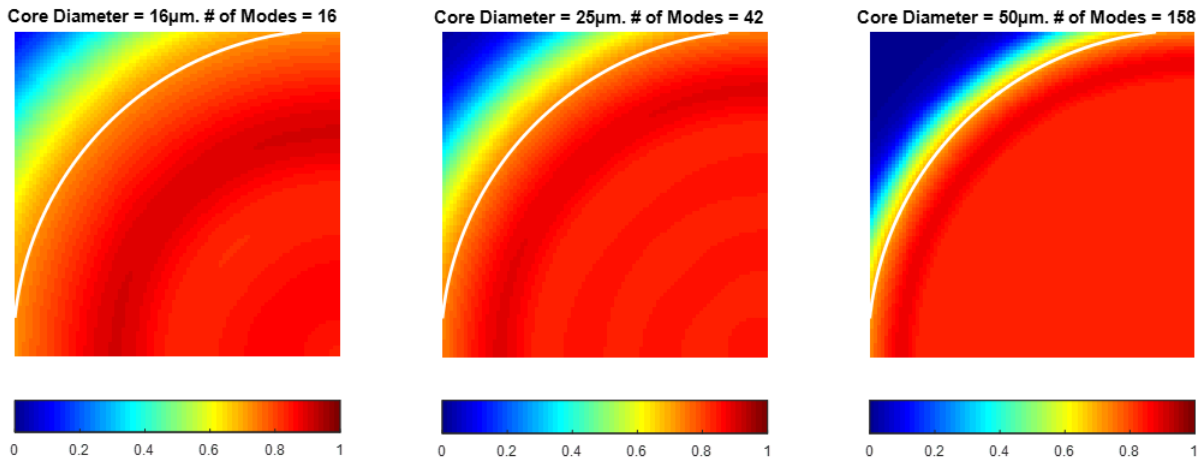

Figure 2.10: The confinement metric of a 'best possible' focus, as a function of spatial location across the fiber facet, for 3 different step-index fibers with different core diameters (and therefore different number of modes – as indicated in the titles). The solid white lines designate the core boundary.

2.4 Focusing Light through a Passive Multimode Fiber – Experimental Results

2.4.1 Motivation and Constraints

This sub-chapter describes an experimental setup of wavefront-shaping light in a passive fiber that was planned and implemented as an intermediary step towards the more complex experiment of shaping the pump in an amplifying fiber. The main motivation was to verify and prove, that the design and methods – later to be copied in the gain system – would enable, to the fullest extent possible, the exploration of the space of possibilities available for pump shaping. This means we'd like to maximize, in our modulation scheme, the access to (hopefully all) degrees of freedom in the spatial-mode space.

It should be stressed that we are not interested in the modulated beam's output pattern, per se (indeed, in an efficient gain-medium scheme, the modulated beam in our case - the pump - should not appear as an output speckle of the waveguide, but be completely absorbed within it). Rather, the observation of the output patterns served as an indication to the degree of control our modulation method has over the modal content of the beam as it is propagating through the fiber. In this spirit, and based upon the previous section's discussion of the construction of focus spots from the LP modes, it should be evident that demonstration of efficient focusing across the fiber output facet is a convenient way to validate the desired degree of control: The ability to focus anywhere at the fiber's output is equivalent to having access to the full set of degrees of freedom in the modal space. In other words, the base of spatial modes and the base of non-overlapping foci covering the fiber's cross-section are

interchangeable; therefore demonstrating control in terms of the latter is sufficient proof for being able to shape the former.

In light of this role of the passive setup, as a building block for the 'full-fledged' system, its design sought to address the main issues which would later be relevant features in the gain-medium experiment. These were:

1) Work with a few-mode fiber, due to the requirement of keeping the amplifier's core size relatively small. For the passive experiment, a step-index fiber with NA= 0.1 and a core diameter of 25μm (Thorlabs FG025LJA) was used. For the visible wavelength of our source, the number of modes guided per polarization was calculated to be 42.

2) The need to minimize, as much as possible, the amount of optical power lost at all stages of beam control and shaping placed between the source and the fiber. This is due to the severe limitation of total deliverable power in the pump sources available to us.

3) The requirement of leaving sufficient physical space between the spatial modulator and the optics coupling light in and out of the fiber, in order to place - in the amplifier configuration - a dichroic filter element that separates the signal output beam from the pump input beam (or, in the case of the lasing cavity configuration, the same dichroic element serves as the mirror closing the cavity).

The rest of this section covers:

- A technique used in our setup in order to maximize the control of the modal content of the beam coupled into the fiber, by addressing the problem of the non-participation of the modulator segments supplying the reference beam, in the wavefront shaping.
- Two experiments performed with different architectures for the SLM-fiber optical relay, with the goal of validating our chosen approach for addressing the last two above-mentioned requirements (namely, allowing a distance between the modulator and the fiber input, while at the same time simplifying the optical relay and minimizing losses). As a preliminary phase, a setup with the conventional image-conjugation architecture was built, serving as a benchmark. Then, a setup with the 'final' relay method (that would later be implemented for the amplifying fiber experiment) was built and its results were compared to this benchmark.

2.4.2 Ensuring Full Control in the Modal Space: The Reference Beam Problem

As was mentioned in the previous section, the few-mode fiber system presents the unique characteristic of supporting only a quite limited number of modes, all of which must be controlled by the wavefront shaping scheme at the input in order to exercise complete control of the output pattern. Specifically considering the circle of acceptance defined across the plane of the spatial modulator – all locations within it must participate in the modulation scheme, or else certain guided modes will remain inaccessible, or at least only partially accessible, to the control setup. Equivalently, locations that are outside the circle of acceptance cannot compensate for any unused segments within; no matter what modulation function is displayed upon them, the light emanating from such points will always be

imaged to the cladding and therefore to unguided modes. In short, this means that the ‘usual’ technique of using the area around the SLM (as used for example in ref [6], see also figure 2.3) as the source of a co-propagating reference beam is inapplicable for a FMF experiment. If the co-propagating reference method is to be used in our system, a non-negligible portion of the modulator's pixels which are mapped to guided fiber modes must be ‘sacrificed’ for the generation of the constant reference field - thereby forfeiting some of the degrees of freedom in the finite space offered to our control of light. At best, the reference pixels may only be 'switched off' while focusing, so as to eliminate their contribution - which would only add an undesired static background upon the shaped output pattern.

A possible way to evade this problem would be to detach the reference light from the spatial modulation optical path, while still have it co-propagating in the fiber. This may be accomplished by splitting the beam prior to the SLM and leading the second arm directly (i.e. while circumventing the modulator) to a point just prior to the coupling into the medium, where it could be recombined with the main (shaped) beam. This solution requires, however, adding several optical components, including in the path of the modulated light itself (at the recombination point), and was therefore not chosen for our experimental setup.

In our work, a different scheme was devised (no examples of a similar method were found in the literature) in order to eliminate the problem of the non-participation of the 'reference' degrees of freedom. This scheme involves paying a penalty in measurement time, rather than in setup complexity and/or optical power. The key lies in the fact, that the reason the segments devoted to reference-supplying are prevented from participation in the application of the measured matrix, is because they remained non-modulated during its *measurement process (*so of course, their transmission values remain unknown); however, there is no real essential obstacle to their exploitation for the control of light, granted only these ‘missing’ values are measured separately.

The basic principle of our scheme, therefore, is to repeat the TM measurement process twice, with the role of the 'reference pixels' alternating between two completely different subsets of the SLM's segments. It is evident, that if these 2 subsets are mutually exclusive, the combination of the 2 matrices will include transmission measurements for the entire set of all SLM segments; The only snag being, that the transmission values for each of the 2 matrices were measured with respect to some arbitrary reference phase, which was not in any way shared between them. Therefore, an additional step is required in order to "stitch together" the two data sets. The two measured matrices are numerically combined into one unified matrix with a single variable $e^{j\theta}$ multiplying the values corresponding to one of the sets; this represents the unknown relative phase between the two sets, and θ may be scanned to find the value of maximal constructive interference for some desired focus point (similarly to the procedure with which a TM column is measured, by scanning the phase of the SLM segment it corresponds to).

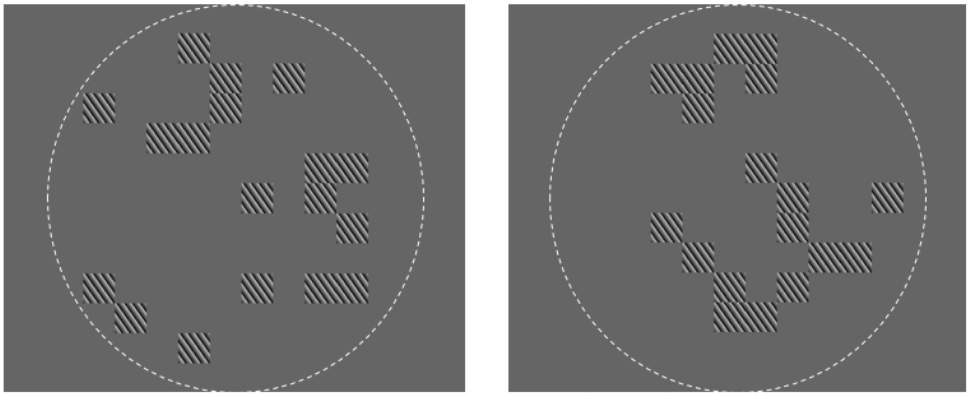

Figure 2.11: An example of the setting up of co-propagating reference beams in our experiment. The images are of the SLM display (grayscale corresponds to the $0-2\pi$ phase modulation). The dashed white line represents the border of the effective control area of the SLM (i.e., the image of the fiber's acceptance cone upon the modulator surface). Several tiles are randomly selected to supply the reference beam, hence the blazed grating corresponding to the fiber's misalignment is statically displayed upon them. After the transmission for all other tiles are measured with the first set of reference tiles (left hand side), the second measurement stage begins by selecting a new (and mutually exclusive) set of tiles as reference suppliers.

2.4.3 Benchmark Experiment with SLM image-conjugated to the Fiber Facet

The setup is schematically depicted in figure 2.12. Two concatenated 4f systems imaged the SLM display to the fiber's input facet, providing two stages of demagnification. The total demagnification was x220, and the alignment of this relay system was fine-tuned with the help of the back-reflection camera, which provided an image of the fiber facet through the injection lens. A chessboard pattern presented on the SLM appeared in-focus and well-centered upon the fiber's core only when these two 4f systems were reasonably aligned in both z and the transverse coordinates.

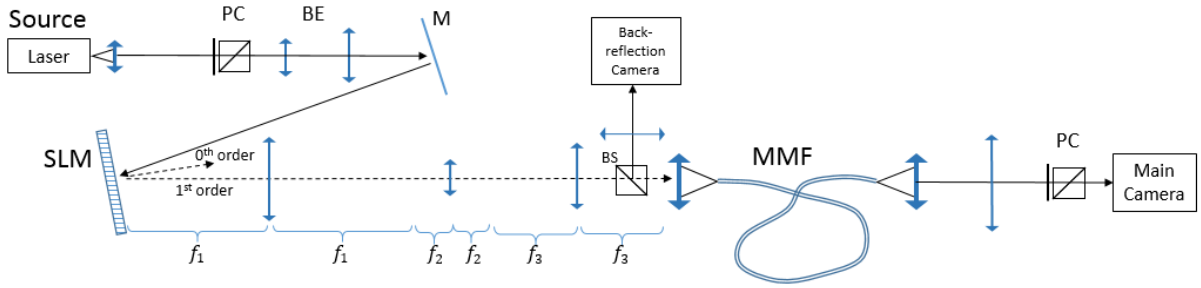

Figure 2.12: The first passive-fiber experimental setup implemented, with image-conjugation between the SLM and the fiber input facet.

Results of the focusing experiment demonstrated the ability of the wavefront shaping system to create tight and highly-contrasted focus spots, anywhere within the core, at the fiber's output facet. All the foci created attained **confinement scores in the range 60% - 75%**, which is close to the

theoretical limit of 85% - 90% for focusing in a MMF (see previous section). The (small) variation of the confinement scores exhibited no correlation to the radial location of the focus point (i.e., focusing at the center was not necessarily less efficient than close to the core edge, nor vice versa). Six typical examples of the intensity images obtained with the setup of figure 2.12 are shown in figure 2.13.

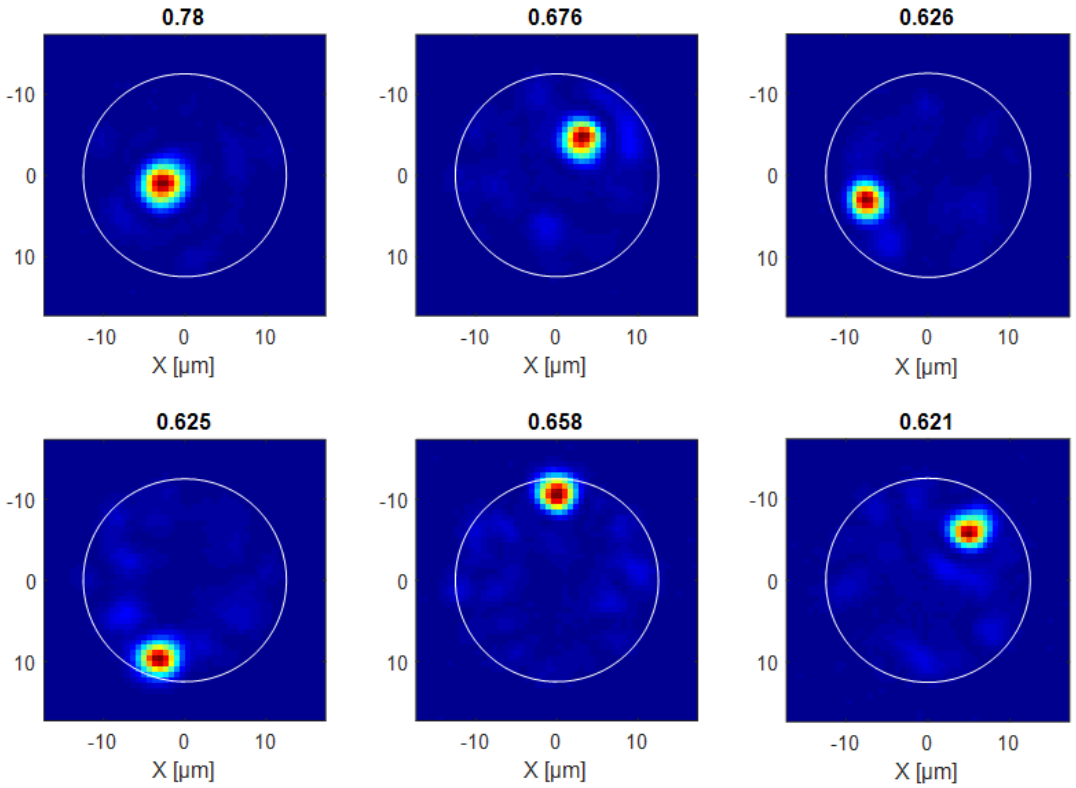

Figure 2.13: Experimental results from the passive-fiber setup where the SLM was image-conjugated to the fiber facet; six examples of focus spots formed at different locations in the output facet of the fiber. The confinement score for each image is specified above it.

As previously explained, the goal of this first experiment was to serve as a benchmark for the final configuration, where the imaging relation between the SLM and the fiber was not of a conventional type found in the literature (i.e. did not match a 'perfect' conjugation neither in image nor in Fourier space). The confinement scores obtained in the benchmark setup (where the optical relay did correspond to a conventional imaging relation) were considered as a reference point for the typical best confinement scores attainable in a realistic setup; the difference between them and the theoretical limit is explained by the various imperfections of any experimental system. Amongst these imperfections one may count:

- The finite resolution of the modulator, both in the spatial coordinates (i.e. the pixelization in XY), and in the phase axis (i.e. the finite dynamic range of the displayable phase levels). These two quantization effects limit the SLM's ability to perfectly represent, by means of a diffraction grating, any given phase or amplitude modulation.

- The measurement noise affecting the process of TM measurement, arising mostly from the sensitivity of the interferometric method for measuring the optical field's phase.
- The slow drifts affecting the final focusing results, due to the duration of the TM measurement process (typically taking between a few, and a few tens, of minutes).

2.4.4 Ensuring Full Control in the Modal Space: The SLM Physical Positioning Problem

As previously mentioned, the preferred design for the amplifying-fiber setup included placing the SLM and the coupling optics which focus the beam into the fiber, at a certain physical distance that does not allow the optical conjugation relation conventionally found in the literature of wavefront shaping in fibers. Generally speaking, this should not pose a fundamental problem to the control scheme: As long as our approach to the control of light in the system consists only of the study of the *total* transfer function relating the modulator plane to the medium's output, this medium need not necessarily be optically relayed to the spatial modulator by a specific "known" analytical transformation, such as imaging or focusing. Indeed, in the 'classical' experiment of controlling the light's propagation in a disordered scattering layer, any arbitrary placement of the medium's entrance plane, with respect to the modulator plane, will do. This is because the unknown optical transform between the two, which we may denote as a transmission matrix TM_{relay} will anyhow be followed by the complex transfer function describing the propagation within the medium, TM_{medium}, which cannot be known a priori; The total transmission, which is the concatenation of the two, $TM_{total} = TM_{relay} * TM_{medium}$, is measured as one entire matrix, without the need to separate the two contributions. However, for the case of a well-defined waveguide such as an optical fiber, the medium also behaves as a strong spatial filter, because wavefronts arriving at its input plane do not necessarily couple well to the finite set of guided modes. Consequently, the control offered by the total TM may be degraded in case the optical relay leading to that intermediate input plane does not permit efficient coupling into the fiber's modes.

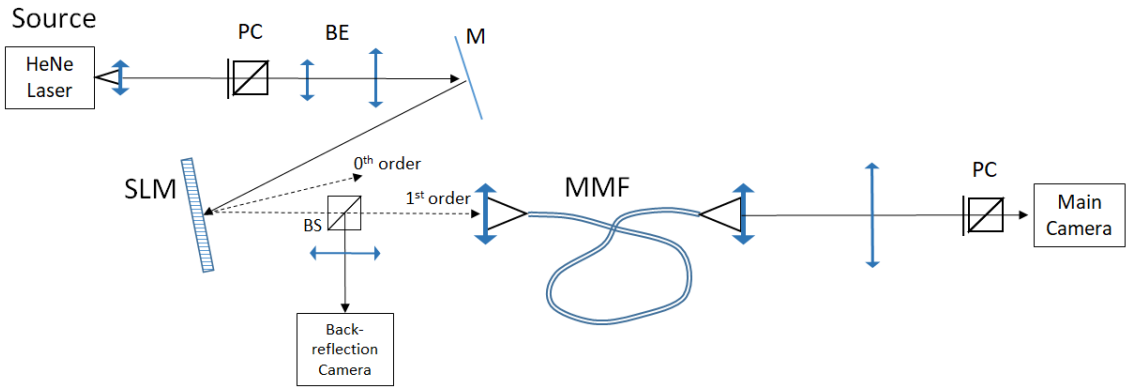

Figure 2.14: The passive-fiber experimental setup implemented so as to resemble as closely as possible the setup later on used for active (amplifying) fiber experiments.

The goal of this experiment was therefore, validation that all guiding modes in the fiber were accessible to our wavefront modulation scheme, under the condition of the non-traditional positioning of the modulator. The setup is schematically depicted in figure 2.14. As can be observed, the only difference with respect to the first setup is the simplification of the optical relay between the SLM and the lens coupling the beam into the fiber; the physical distance between the two was approximately 20cm, with no additional optics to provide a conjugation relation.

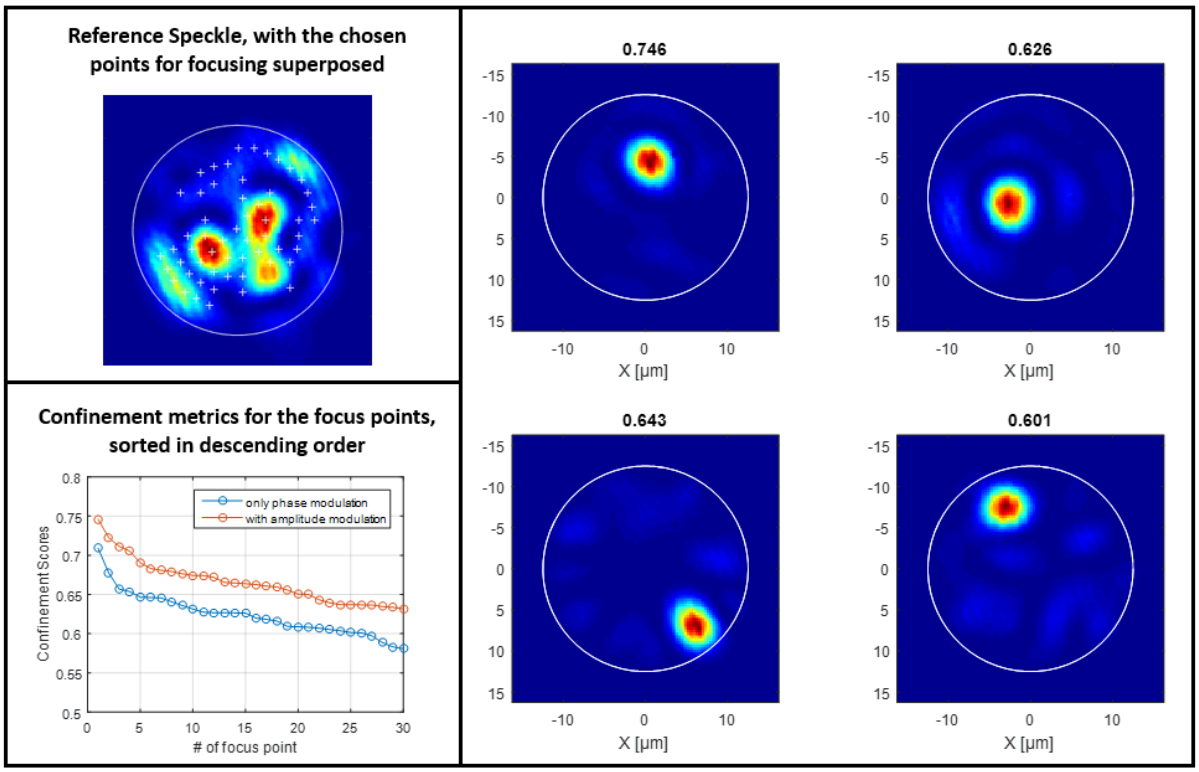

Figure 2.15: Experimental results from the passive-fiber setup simulating as closely as possible the amplifying-fiber implemented later on in this work. Top left panel – the speckle of the reference light, with the 30 locations at which the focusing quality was measured marked by white plus signs. Bottom left panel – the confinement scores obtained at these pointed, arranged in descending order. Right panel - Four examples, out of the total 30 focus spots, shown formed at different locations in the output facet of the fiber (the confinement score for each image is specified above it).

Results of the focusing experiment, as shown in figure 2.15, demonstrated the ability of the wavefront shaping system to create tight and highly-contrasted focus spots anywhere within the core at the fiber's output facet. The distribution of the confinement scores was virtually identical to the benchmark setup: All the foci created attained **scores in the range 60% - 75%**. This excellent result validated the assumption, that the physical distance constraint imposed upon the input side of the setup does not degrade the extent of our control upon the modal content of the beam coupled into the fiber.

2.5 Summary and Discussion

The chapter began with a general review of the control of the propagation of the light inside (non-amplifying) complex or disordered media by means of wavefront shaping. Then followed a more detailed review of the research, within this broad domain, focused on the control of light in multimode fibers; a literature survey covered the major methods and techniques used in this field for shaping the light coupled into the fiber and for measuring the fiber's transmission. Lastly, the work performed on the subject of focusing light at the output of a few-mode fiber was presented:

- Numerical simulations of the creation of focus spots as a constructive superposition of the LP modes guided in a few-mode or multimode fiber, and the best possible figures of merit for such foci.
- Experimental implementation of a wavefront shaping system, employing both phase and amplitude modulation of the beam injected into the fiber core, through the use of off-axis diffraction. The measurement of the Transmission Matrix of the fiber was performed based on the co-propagating reference approach; The issue of incomplete coverage of all the degrees of freedom potentially available in the modal space was addressed and solved by a unique technique of using two separate reference beams and "stitching" together the resultant two sets of measurements. Additionally, the potential penalty of an 'imperfect' conjugation relation between the modulator and the fiber input facet was studied.

The purpose of the work presented in this chapter was to lay the ground for the control of the pump beam in the central (amplifying-fiber) experiments of the thesis. The experiment carried out using a passive fiber, where the measured TM was used for focusing at different points across the output facet, served as a demonstration and verification of the ability of our wavefront shaping scheme to exert full control over the modal content of the light beam propagating in a fiber. The results obtained, with a setup whose design was as close as possible to that used later in the gain-medium experiments, were excellent in terms of control: Efficient focusing, with at least 60% of the total guided optical power confined within the foci at all radial positions within the fiber's core, was demonstrated. The conclusion, therefore, is the validation of our chosen spatial modulation architecture and methods as a good platform upon which to carry out the wavefront shaping in our next experiments.

References for Chapter 2

[1] F. Roddier, Adaptive Optics in Astronomy, Cambridge University Press (1999).
[2] I. M. Vellekoop, A. P. Mosk, Focusing Coherent Light through Opaque Strongly Scattering Media, Opt. Lett., Vol. 32 No. 16, 2309-2312 (2007).
[3] I. M. Vellekoop, A. P. Mosk, Universal Optimal Transmission of Light through Disordered Materials, Phys. Rev. Lett., No. 101, 120601-120604 (2008).
[4] H. Defienne, Quantum Walks of Photons in Disordered Media, PhD Thesis of University Pierre and Marie Curie (2015).
[5] D. Akbulut, T. J. Huisman, E. G. Van Putten, W. L. Vos, A. P. Mosk, Focusing Light through Random Photonic Media by Binary Amplitude Modulation, Opt. Exp., Vol 19 No. 5, 4017-4030 (2011).
[6] S. M. Popoff, G. Lerosey, R. Carminati, M. Fink, A. C. Boccara, S. Gigan, Measuring the Transmission Matrix in Optics: An Approach to the Study and Control of Light Propagation in Disordered Media, Phys. Rev. Lett., No. 104, 100601-100604 (2010).
[7] S. Popoff, G. Lerosey, M. Fink, A. C. Boccara, S. Gigan, Image Transmission through an Opaque Material, Nat. Comm. 1, No. 81 (2010).
[8] M. Kim, Y. Choi, C. Yoon, W. Choi, J. Kim, Q. Park, W. Choi, Maximal Energy Transport through Disordered Media with the Implementation of Transmission Eigenchannels, Nat. Phot., Vol. 6, 581-585 (2012).
[9] A. Dubois, L. Vabre, A. C. Boccara, E. Beaurepaire, High-Resolution Full-Field Optical Coherence Tomography with a Linnik Microscope, App. Opt., Vol. 41 No. 4, 805-812 (2002).
[10] T. Chaigne, Control of Scattered Coherent Light and Photoacoustic Imaging, Thèse de Doctorat de l'Université Paris 6 (2016).
[11] M. Paurisse, M. Hanna, F. Druon, P. Georges, C. Bellanger, A. Brignon, and J. P. Huignard, Phase and Amplitude Control of a Multimode LMA fiber Beam by Use of Digital Holography, Opt. Exp., Vol 17. No. 15, 13000–13008 (2009).
[12] R. Di Leonardo, S. Bianchi, Hologram Transmission Through Multi-mode Optical Fibers, Opt. Exp., Vol. 19 No. 1, 247-252 (2011).
[13] G. Stepniak, L. Maksymiuk, J. Siuzdak, Binary-Phase Spatial Light Filters for Mode-Selective Excitation of Multimode Fibers, J. of Light. Tech., Vol. 29 No. 13, 1980-1987 (2011).
[14] J. Carpenter, T. D. Wilkinson, Characterization of Multimode Fiber by Selective Mode Excitation, J. of Light. Tech., Vol. 30 No. 10, 1386-1392 (2012).
[15] J. Carpenter, B. J. Eggleton, J. Schröder, 110x110 Optical Mode Transfer Matrix Inversion, Opt. Exp., Vol. 22 No. 1, 96-101 (2014).

[16] T. Cizmar, K. Dholakia, Exploiting Multimode Waveguides for Pure Fibre-Based Imaging, Nat. Comm., 3 No. 1027 (2012).
[17] M. Plöschner, T. Tyc, T. Cizmar, Seeing Through Chaos in Multimode Fibres, Nat. Phot., 9, 529-535 (2015).
[18] D. J. Richardson, J. M. Fini, L. E. Nelson, Space-Division Multiplexing in Optical Fibres, Nat. Phot., No. 7, 354-362 (2013).
[19] G. Labroille, B. Denolle, P. Jian, P. Genevaux, N. Treps, J. F. Morizur, Efficient and Mode Selective Spatial Mode Multiplexer Based on Multi-Plane Light Conversion, Opt. Exp., Vol. 22 No. 13, 15599-15607 (2014).
[20] H. Huang, G. Milione, M. P. J. Lavery, G. Xie, N. Ahmed, T. A. Nguyen, M. J. Li, M. Tur, R. R. Alfano, A. E. Willner, Mode Division Multiplexing Using an Orbital Angular Momentum Mode Sorter and MIMO-DSP Over a Graded-Index Few-Mode Optical Fibre, Nat. Sci. Reports, 5 No. 14931 (2015).
[21] T. Mizuno, H. Takara, K. Shibahara, A. Sano, Y. Miyamoto, Dense Space Division Multiplexed Transmission Over Multicore and Multimode Fiber for Long-Haul Transport Systems, J. Light. Tech., Vol. 34 No. 6, 1484-1493 (2016).
[22] G. Oh, E. Chung, S. H. Yun, Optical Fibers for High-Resolution in vivo Microendoscopic Fluorescence Imaging, Opt. Fiber Tech., No. 19, 760-771 (2013).
[23] W. Gobel, J.N. Kerr, A. Nimmerjahn, F. Helmchen, *Miniaturized Two-Photon Microscope Based on a Flexible Coherent Fiber Bundle and a Gradient-Index Lens Objective*. Opt. Lett. 29, 2521–2523 (2004).
[24] A. Porat, E. R. Andresen, H. Rigneault, D. Oron, S. Gigan, O. Katz, Widefield Lensless Imaging through a Fiber Bundle Via Speckle Correlations, Opt. Exp., Vol. 24 No. 15, 16835-16855 (2016).
[25] S. Gigan, Viewpoint: Endoscopy Slims Down, Physics 5, No. 127 (2012).
[26] D. Loterie, S. A. Goorden, D. Psaltis, C. Moser, Confocal Microscopy Through a Multimode Fiber Using Optical Correlation, Opt. Lett., Vol. 40 No. 24, 5754-5757 (2015).
[27] S. Sivankutty, E. R. Andresen, R. Cossart, G. Bouwmans, S. Monneret, H. Rigneault, Ultra-Thin Rigid Endoscope: Two-Photon Imaging Through a Graded-Index Multimode Fiber, Opt. Exp., Vol. 24 No. 2, 825-841 (2016).
[28] S. Ohayon, A. Caravaca-Aguirre, R. Piestun, J. J. Dicarlo, Minimally Invasive Multimode Optical Fiber Microendoscope for Deep Brain Fluorescence Imaging, Biomed. Opt. Exp., Vol. 9 No. 4, 1492-1509 (2018).
[29] I. T. Leite, S. Turtaev, X. Jiang, M. Siler, A. Cuschieri, P. S. J. Russell, T. Cizmar, Three-Dimensional Holographic Optical Manipulation Through a High-Numerical-Aperature Soft-Glass Multimode Fiber, Nat. Phot., No. 12, 33-39 (2017).
[30] P. Delrot, D. Loterie, D. Psaltis, C. Moser, Single-Photon Three-Dimensional Microfabrication through a Multimode Optical Fiber, Opt. Exp., Vol. 26 No. 2, 1766-1778 (2018).

[31] I. N. Papadopoulos, S. Farahi, C. Moser, D. Psaltis, Focusing and Scanning Light Through a Multimode Optical Fiber Using Digital Phase Conjugation, Opt. Exp., Vol. 20 No. 10, 10583-10590 (2012).

[32] D. Loterie, S. Farahi, I. N. Papadopoulos, A. Goy, D. Psaltis, C. Moser, Digital Confocal Microscopy Through a Multimode Fiber, Opt. Exp., Vol. 23 No. 18, 23846-23859 (2015).

[33] J. Carpenter, B. C. Thomsen, T. D. Wilkinson, Degenerate Mode-Group Division Multiplexing, J. of Light. Tech., Vol. 30 No. 24, 3946-3952 (2012).

[34] A. M. Caravaca-Aguirre, E. Niv, D. B. Conkey, R. Piestun, Real-Time Resilient Focusing Through a Bending Multimode Fiber, Opt. Exp., Vol. 21 No. 10, 12881-12887 (2013).

[35] T. Cizmar, K. Dholakia, Shaping the Light Transmission through a Multimode Optical Fibre: Complex Transformation Analysis and Applications in Biophotonics, Opt. Exp., Vol. 19 No. 20, 18871-18883 (2011).

[36] D. Loterie, Microscopy and Digital Light Shaping through Optical Fibers, Thèse No. 7799 Ecole Polytechnique Fédérale de Lausanne (2017).

[37] I. M. Vellekoop, A. Lagendijk, A. P. Mosk, Exploiting Disorder for Perfect Focusing, Nat. Phot., No. 4, 320-322 (2010).

[38] R. N. Mahalati, D. Askarov, J. P. Wilde, J. M. Kahn, Adaptive Control of Input Field to Achieve Desired Output Intensity Profile in Multimode Fiber with Random Mode Coupling, Opt. Exp., vol. 20 No. 13, 14321-14337 (2012).

[39] H. Yu, K. Lee, Y. Park, Ultrahigh Enhancement of Light Focusing through Disordered Media Controlled by Mage-Pixel Modes, Opt. Exp., Vol. 25 No. 7, 8036-8047 (2017).

3 Model and Numerical Simulations of a Multimode Fiber Amplifier with Configurable Pumping

So far, the propagation of light in a multimode fiber was discussed solely in the context of control of the fiber's output by means of wavefront shaping at the input. It was understood that since the LP modes constitute a complete basis for light fields guided in the core, any possible output field must be constructed from these modes; but the inner dynamics of the modes' propagation was not considered in detail (except to say that randomization of the modes' amplitudes and phases causes their superposition pattern to behave like a speckle). We shall now enter with more detail into the propagation process; which essentially amounts to the transmission matrix (TM), in the modal basis, of a MMF. This will lay out the necessary foundation for the purpose of this chapter, which is to present **a model for the TM of a multimode fiber that is also an amplifier (MMFA),** pumped by a coherent pump whose modal content we are able to choose. We shall refer to this as the gain-dependent TM, for as we shall see, the transmission of a signal amplified by such a pump may be modified by selection of different pumping configurations.

The chapter is arranged as follows: First, literature studying the general subject of fiber amplifiers, and in particular multimodal amplifiers where the pump beam may be spatially shaped, is surveyed in detail to provide background and general motivations. Then, a simplified model of the TM of a *passive* MMF shall be discussed – furnishing a basis to be applied for both the *signal* beam and the *pump* traveling in our amplifier; the model for the gain-dependent TM will then be developed by adding the effects of the amplification as a perturbation upon the passive model. Lastly, the results of numerical simulations based upon this model, and performed towards the goal of studying the 'flexibility' of the TM as a function of the pump configuration, shall be presented and discussed.

3.1 Fiber Amplifiers – Background and Major Developments

3.1.1 General Background

Almost immediately after the invention of the laser, the demonstration of the first optical fiber amplifier quickly followed, in 1964. The MIT group that was the first to implement a glass fiber-based laser showed that amplification of an external signal could also be performed in their system, provided simply that the fiber ends were "beveled" (i.e., angle polished) in order to eliminate the optical feedback which allows lasing [1]. This amplifier was, for the signal, a single mode fiber, but the pump was not guided within it at all (the fiber was pumped through the means of illuminating its entire length with a flash tube). The development of a laser-pumped fiber amplifier had to wait until the emergence of optical-fiber communication technology, where the first Erbium-doped fibers (EDFA) [2-3], proved to be extremely efficient in-line repeaters (meaning, the signal could be amplified without first being converted to the electronic domain, then regenerated back as an optical one) in long-distance channels. In this type of amplifier, the pump is single mode: it is injected into the same core which guides the signal. The confinement of the pump within the small cross-section lowers the typical power needed for achieving good population inversion, as well as rendering the overlap between the signal and the pump fields nearly perfect. Accordingly, the common core-pumped fiber amplifiers - which serve as the backbone of the high-speed global telecommunication network - typically supply to WDM (Wavelength Division Multiplexed) signals gains in excess of 30dB, using pump powers of a few hundred milliwatts [4]. In parallel to communication-oriented research, huge interest was also shown in fiber lasers and amplifiers as devices for high-power industrial and sensing applications, such as laser marking, laser machining, and LIDAR. In these applications, fiber architectures (as opposed, for example, to gas lasers) offer excellent brightness, power efficiency, ease of beam delivery to the target, and low maintenance overheads. We shall now continue to survey the major technologies and design-concepts in the field of fiber amplification without particular attention to the specific application.

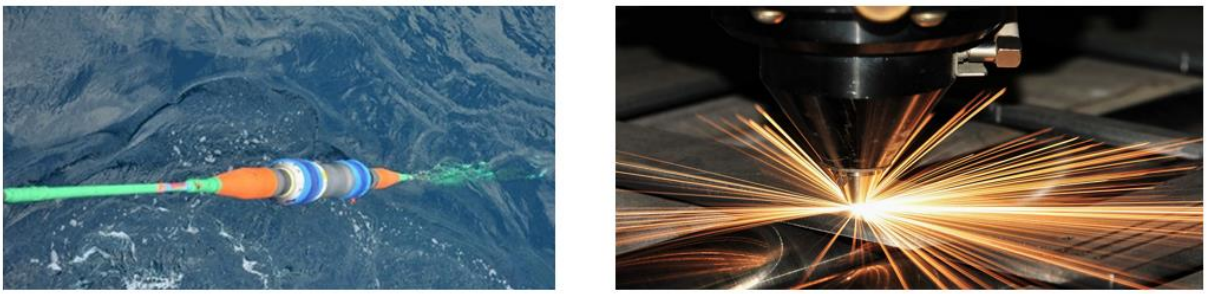

Figure 3.1: Two major application domains where fiber-based optical amplification has found abundant use are long-distance optical telecommunications, and industrial laser devices. Left – an EDFA repeater in an optical communication submarine cable (image copyright – Huawei Corporation). Right – a high-power fiber-laser metal cutting device (image copyright – Atcore Group).

Alongside the core-pumped architecture, another type of optical amplifier has been widely used since the early 90's - the double-cladding fiber [5]. It consists of not one waveguide structure, but two: The first, a small core which guides the signal and is also doped with the gain atoms, is contained within the second larger 'core', which guides the pump light. As the latter surrounded the signal core, it is commonly called the inner cladding; in itself it is surrounded by a second, external cladding. The main advantage of this configuration is that the inner cladding may be designed with both a large-enough diameter and a high-enough N.A. to allow efficient coupling of very powerful pump sources into it, despite the tendency of such sources to have low brightness. Meanwhile, the signal is confined to a core which may be both small and of low aperture, quite often so much as to allow only single-mode guidance. Essentially, this system transfers optical power from the pump to a beam with a much higher brightness. An impressive example is given in [6] (albeit, in a fiber laser scheme rather than an amplifier) where the dual-core fiber is pumped by stacked laser-diodes with a total power of 1.8kW.

An additional feature of the distinction between the pump-guiding volume and the signal-guiding core is the ability to couple the pump from the side of the fiber, by disrupting the inner cladding structure with grooves that act as injection mirrors [7]; Thus the insertion of the pump through the end facets - which always requires some pump\signal separation module (such as a dichroic mirror) to be employed - may be avoided. The major trade-off of the double-clad geometry is that the pump contributes to amplification only when it is traverses the small core, where it may be absorbed by the gain medium. This results in two interesting outcomes, both described neatly in [8]:

1) Unless the circular symmetry of the inner cladding is broken, the higher-order spatial modes of the pump will represent lost energy that will never participate in the gain process; Therefore the typical double-clad fiber amplifier is designed with an irregular shape, such as a 'D' figure, a rectangle, or a hexagon [9], for the cross-section of the inner cladding.

2) Even with a non-symmetrical waveguide shape, which allows nearly all the pump's energy to eventually overlap with the doped core and be absorbed, this is achieved only after a sufficiently long propagation distance. In fact, it is shown that the typical absorption length of the pump scales in proportion to the ratio of areas of the inner-cladding and the core, so that a very large waveguide for the pump (with respect to the core) would necessitate a very long amplifier in order to fully utilize the input power. This is sometimes undesired, due to the fact that the threshold of detrimental non-linear processes such as Brillouin scattering becomes lower with growing total fiber length [10].

3.1.2 Motivation for Multimode or Potentially-Multimode Fiber Amplifiers

From the perspective of fiber-based communication applications, the desire to move from the singlemode regime to the multimodal is obvious – the amplifier simply following the link itself in the attempt to increase the information capacity (see chapter 2). As for the high-power applications, the motivation is slightly more subtle: In fact, the challenge in this domain is to move towards fiber which potentially support many guided modes, but nevertheless to operate them in the singlemode regime.

As the interest in further scaling of output powers grew, it quickly became apparent that the most serious limitation was the onset - when the signal intensity guided within the small core becomes too large - of detrimental non-linear effects such as SPM (Self-Phase Modulation) and SBS (Stimulated Brillouin Scattering) [11]. The approach which previously permitted the increase of pumping powers - namely, the double-clad design - could not be so easily adapted to this problem, because if the propagating signal was simply allowed to spread over a wide cross-section, it would be highly multi-modal and therefore of low spatial coherence. In other words, the requirement of maintaining a high-brightness (ideally diffraction-limited) output beam necessitated the confinement of the signal within a tight core (so as to assure single-mode operation), which in turn limited the power due to the appearance of non-linear processes at high optical intensities.

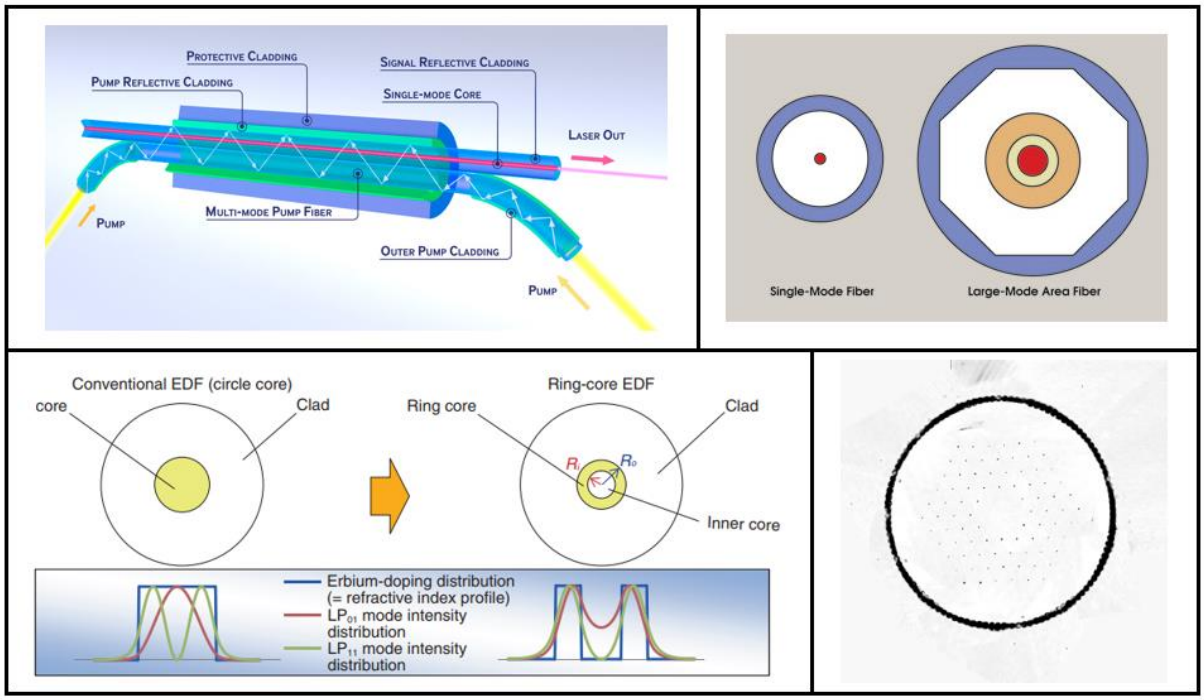

Figure 3.2: Different approaches and architectures used in the field of fiber amplifiers. Top left – Cladding-pumping amplifier (image copyright – IPG Photonics). Top Right – LMA fiber amplifier cross-section (image copyright – nLIGHT Photonics). Bottom Left – Radially-dependent doping profile in an EDFA (taken from ref. [23]). Bottom right – Microscope image of a photonic crystal fiber, where the signal is guided, as a single mode, by the lack of air holes at the center (taken from ref. [21]).

At first, the power limit was improved upon by stretching the core diameter while at the same reducing the numerical aperture, so as to keep the V-number of the fiber low enough to ensure single-mode guidance at the signal wavelength [12]. This approach became known as Large-Mode-Area (LMA) fibers, and successfully allowed a roughly ten-fold increase of the core area (from the typical 4-5um diameter to around ~20um), with the NA being minimized to almost 0.05. However, it could only go a certain way, as further reduction of the NA is impractical both from the aspect of fabrication

tolerances, and that of guiding efficiency [13]. Further progress was made by exploiting the sensitivity of high-order modes to bends in the waveguide; By taking a fiber amplifier with optical properties that would normally support a few tens of modes and tightly coiling it, the loss for all spatial modes except the fundamental were heightened to the point where an output signal with nearly perfect beam-quality (M^2= 1.1) was attained [14]. Obviously, the advantage offered by this method, too, is limited by trade-offs such as loss penalties for the low-order modes as well [15]; Furthermore, coiling the fiber beyond some optimal bend radius result in dramatic shrinking of the effective mode-field area, which defeats the purpose for which multimodal guidance conditions were allowed in the first place [16].

The next steps in this field saw the development of more complicated profiles of the refractive index and the doping distribution along the fiber's radius. Again, notable work was carried out aiming at high-power applications [13, 17-18] but not exclusively, for example [19] is an example of tailoring the doping profile for a telecommunication-link amplifier. For the former type of applications, preferential amplification of the fundamental mode over higher-order ones was induced by concentrating the rare-earth ions in a central area smaller in diameter than the core itself. Coupled to this, slight modulation of the refractive index profile (addition of ring-like zones of slightly elevated index around the center) altered the mode field distributions so as to further help suppress higher-order content. By careful tailoring of these radial profiles, fiber amplifiers with core diameters of almost 100um, but still operating stably in the single transverse mode regime, could be implemented [20]. For the later type of applications, the same concept was used for the opposite goal: By concentrating more ions in radial rings, thereby equalizing gain between the modes, which represent the different data-carrying channels.

Lastly, interesting advancements were made by harnessing the growing field of photonic crystal fibers (PCF). By embedding the right micro-structure of air holes in the glass fiber, a waveguide characterized by a large mode field diameter, but nevertheless displaying a truly single-mode guidance, may be obtained [21-22].

3.1.3 Wavefront Shaping in Multimode Fiber Amplifiers – Literature Survey

Recent works that have sought to exploit the fact that the ***pump*** is multimodal in a MMFA, and may therefore be spatially shaped in order to improve the amplifier performance, have been carried out within the context of optical telecommunications. The interest in this field has been limited to the requirement of minimizing the 'modal dependent gain' (MDG), also commonly referred to as "gain equalization" (between the multiplexed spatial channels). The natural tendency of lower-order spatial modes to enjoy higher gain in a uniformly-doped fiber amplifier (as well as their tendency to suffer less loss in the long-distance fiber link preceding the amplifier) was compensated by modifying the modal content of the pump (increasing the weight of high-order modes) so as to flatten the gain curve across the channels, i.e. the signal's modes. Early works modified the pump modal configuration by simply offsetting its injection with respect to the core center [24], or by generating different pump

modes using phase plates, for equalizing 2 signal modes [25] and later 6 signal modes [26]. Later work demonstrated control of the pump by wavefront shaping using an SLM, for equalizing the amplifier gain across 12 signal modes (in 2 polarizations) [27]. The theoretical treatment of the problem, in this context (namely minimization of MDG in optical communication amplifiers), e.g. ref [28-29], treated the different spatial modes as independent (no interaction between them through the gain medium is taken into account). Since the framework considered was the multiplexing of data channels over the spatial modes, only the intensities of the different modes were studied (aspects relevant to the spatial-domain observation of the amplifier output, such as dephasing effects, were naturally not examined).

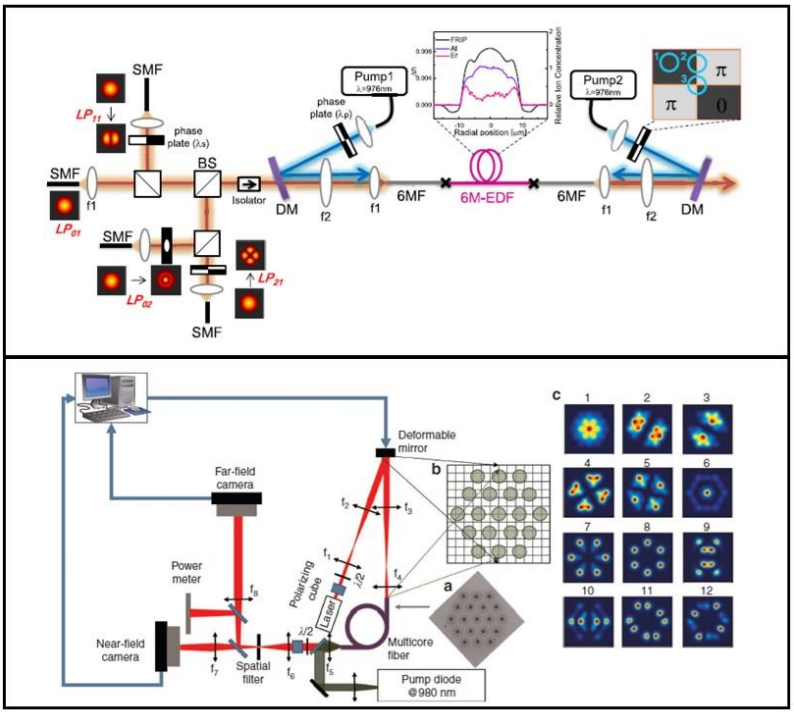

*Figure 3.3: Two examples of recent research utilizing wavefront shaping techniques for control of multimode fiber amplifiers. Top – gain equalization in a six-mode EDFA through the shaping of the **pump** beam, using a mode combiner based on a 'tree' of beam-splitters with a different phase plate at each branch - taken from ref. [26]. Bottom – control of the output of multimodal multi-core fiber amplifier, by wavefront shaping the input **signal** beam using a deformable mirror - taken from ref. [32].*

Recent works in which the prospect of wavefront shaping the ***signal*** beam, on the other hand, were found primarily in research oriented towards high-power sources for industrial applications or imaging. One example is an experiment where the modal composition of the input of an LMA fiber amplifier was controlled by injecting it through a 3-port photonic lantern [30]. A notable example where a full wavefront shaping scheme, based on a spatial modulator with over 100 degrees of freedom (i.e. controllable elements), was implemented at the input of a high-power multimode fiber amplifier, demonstrated full control of the amplified output [30-31].

3.2 Proposed Model for the Gain-Dependent TM of a Multimode Fiber Amplifier

3.2.1 Transmission Matrix for Realistic Passive Optical Fibers

In chapter 1, the propagation of light in a perfectly symmetrical and straight cylindrical waveguide was treated by presenting the solutions to the Maxwell equations is such an idealized system. Since each solution (i.e., each LP mode) constitutes an eigenmode, and would therefore propagate in the guide with no alteration except that of its phase. Next, the question of how this model fares in a real fiber should be posed. For several years, it had been assumed that realistic imperfections – particularly, core ellipticity, core boundary roughness, and fiber curvature – give rise to mode coupling and mixing processes along the fiber length, and thus significantly randomize and complicate the propagation. Interestingly, a certain robustness to imperfections and even bending (i.e. low coupling), was observed over 20 years ago [33], but only for the fundamental mode. The proposition of studying the necessary corrections (with respect to the idealized mode guidance theory) to the transmission coefficients of all the modes, in order to permit direct transmission of images through a MMF, was put forth about a decade ago [34]; and the recent advent and maturation in the field of optical wavefront shaping has greatly facilitated the study of this question. The formidable research presented in references [35-38] has established a striking insight - namely, that the propagation of light in real multimode fibers is not only more deterministic than previously suspected, but even – at least for lengths of fiber in the cm to several meters range – *fully predictable by theoretical models.* Moreover, for lengths in the order of about 0.1 meters, considering the LP modes as a basis of eigenmode remains a surprisingly good approximation. Mode-coupling was shown to be negligible; the dephasing due to the (predictable) modal dispersion was revealed to be the only significant mechanism of the scrambling of the field into speckle patterns. Beyond this distance, the LP modes begin to exhibit a slow splitting into groups of more complicated, vectorial (i.e. with non-linear polarization) modes, whose slight non-degeneracy is the manifestation of the fact that the famous "weak guidance" approximation is, well, an approximation. However, this behavior, as well, remains deterministic, and a new basis of true eigenmodes – named circular polarization (CP) eigenmodes, [38] - may be constructed from the vectorial modes; more importantly, it only couples the 4 degeneracies (in polarization and in field pattern orientation) of a certain l, m mode to each other, without causing mixing between higher and lower order modes. Consequently, the CP correction is indeed of interest for imaging applications – where precise 'unwrapping' of the phases accumulated by each of the propagating modes, with sub-micron accuracy, is required; however, for more general models, such as the one we wish to develop for the amplifying system, using the LP modes as an eigenmode basis is a sufficiently accurate framework.

To summarize these recent findings, for our purposes - the Transmission Matrix of a MMF, written in the LP mode basis, is nearly perfectly diagonal, and the fact that each diagonal element acquires a different phase over the fiber's total length is what accounts for almost all the difference observed between the fields at the input and output facets.

Thus, if a lightwave has been coupled into a fiber such that it excites the set of N supported LP modes each with an amplitude $C\_injected_i$, we may quite easily predict the electric field at each point along the length – it will merely be the superposition of the same modes (i.e. with the same absolute weights), but with different relative phases:

$$E(z) = \sum_i^N C\_injected_i * e^{j\beta_i z} * \psi_i(r,\theta) \tag{3.1}$$

Where ψ_i are the field distributions of the LP modes, as described in chapter 1, eq. (1.6).

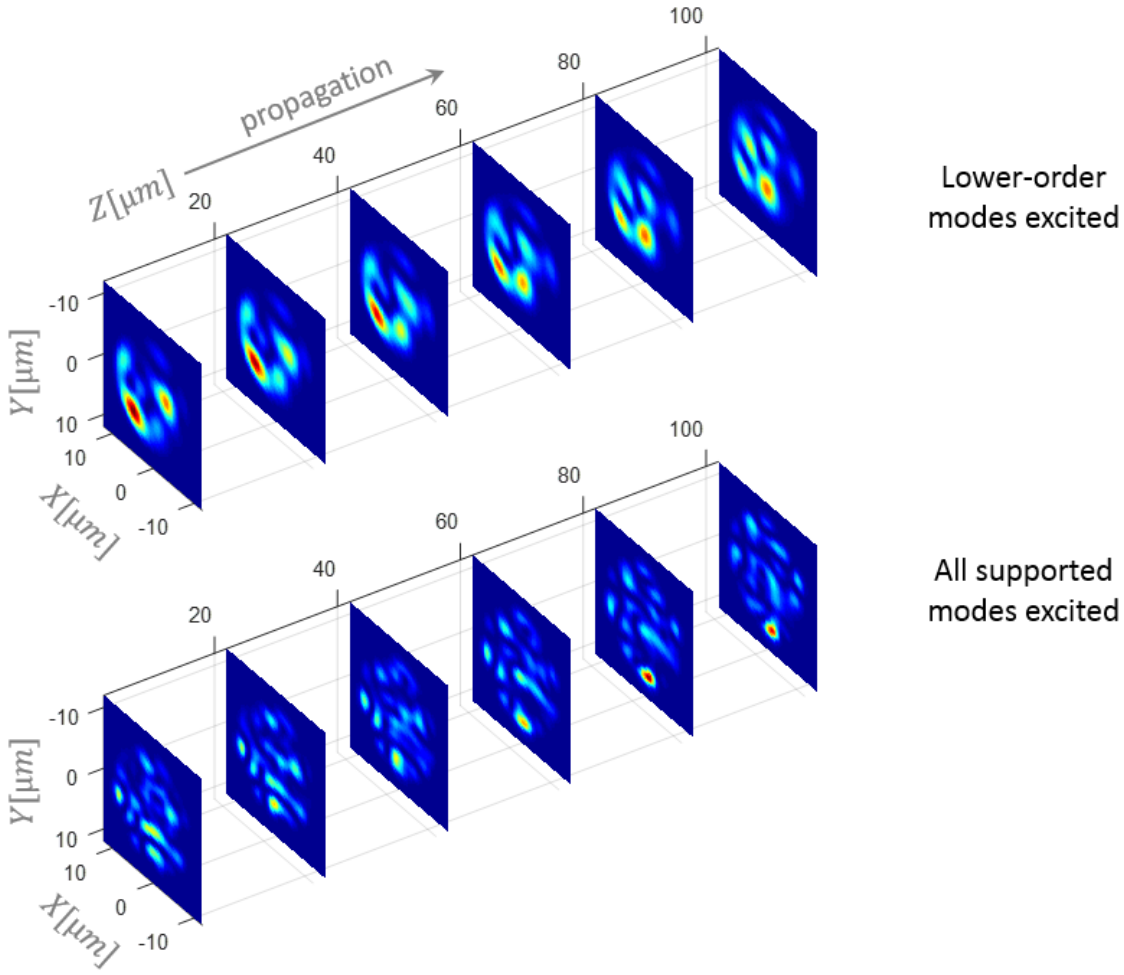

Figure 3.4: Numerical simulation of the intensity profiles occurring at consecutive cross-sections of a step-index multimode fiber, due to the predictable evolution over z of the lightwave. The cross-sections and the distance between them are shown in scale, so as to give a rough sense of the typical distances over which the speckle pattern changes due to the de-phasing. Note that the evolution in the top panel example, where only a few low-order modes participate in the propagating field, is slower than in the bottom panel - where all the fiber's supported modes (about 30 LP modes) are excited. This is due to the fact that the more modes are introduced within the field, the larger the range of phase velocities represented within it, so the typical length of decorrelation grows shorter.

For a standard multimode fiber, where the typical refractive index difference is on the order of $\Delta n \approx 10^{-2}$, propagation over a distance of several tens to hundreds of microns is sufficient to open up, between the low-order modes and the high-order ones, phase differences that are comparable to π. Hence, if we would follow the intensity pattern created by a multimode light beam as it propagates in such a fiber, we would see a rather rapid and complicate, albeit deterministic, speckle evolution along z. An example is demonstrated in figure 3.4.

3.2.2 Incorporation of Gain into the MMFA Model

Our model relies on the following basic premise: since the effect of the gain per unit length is much smaller than the effect of the passive guiding (more rigorously stated, this means that the change in the refractive index caused by the gain medium is much smaller than the core-cladding index difference), we can still treat all lightwaves as composed of the same LP modes described in the first section. The gain does not alter the nature of the modes, but merely adds a small perturbation to their propagation. Moreover, this perturbation may be locally approximated using the first-order Taylor expansion of the exponential function: $e^{gain \cdot \Delta z} \approx 1 + gain \cdot \Delta z$. Most importantly, the result of this perturbation must be re-coupled into the fiber by decomposing it on the LP mode basis; any part of it falling outside this decomposition (due to the complex, 'speckly' nature of the medium's excitation) is not guided and may be ignored (just as any lightfield that impinges upon the input facet of a fiber but does not couple into one of the supported LP modes is lost in the cladding).

The idea is illustrated in figure 3.5, where the fiber is conceptually seen as a series of infinitesimal sections, and the light propagating through them undergoes a repeating pattern of perturbation (by the spatially non-uniform gain profile), then re-coupling into guided light again.

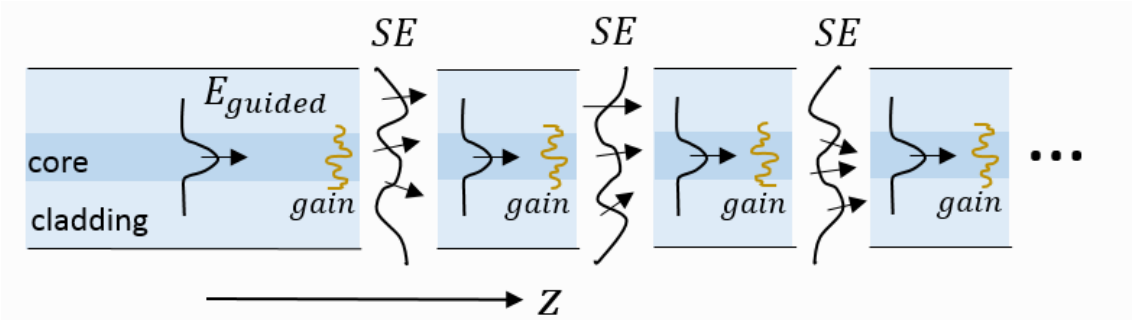

Figure 3.5: Conceptual illustration of the MMFA model. SE stands for stimulated emission; depicting it as if it were a complex wavefront impinging upon a fiber facet at every 'slice' represents the need to perform, at each calculation step, its decomposition upon the set of signal guided modes.

Decomposition is defined as follows, that if at some point z a certain electrical field E has been generated by the interaction of an incoming lightwave (either the pump or the signal) with the gain

medium over a small distance Δz, then the lightwave that will be found propagating in the fiber at the point $z + \Delta z$ will be composed of the LP modes each with an amplitude C_i that equals:

$$for\ i = 1,2,\dots,N:\quad C_i|_{z+\Delta z} = \iint E(x,y,z)\cdot\psi_i(x,y)dxdy \tag{3.2}$$

Considering this first for the pump lightbeam, we propagate it through the amplifier in the manner described as follows. The length of the fiber is divided into 'slices' of length Δz each, short enough so that the effect of the modal dispersion over it may be neglected – i.e., so that any speckle pattern created by a multimode lightwave passing through the slice may be considered to remain constant (not de-phase) throughout it. As explained in section 3.2.1, a typical Δz should be taken to be less than a few tens of microns. Then, the following procedure is iterated over the total length, slice by slice:

- The total pump field arriving at a point z is calculated as a superposition of the modes with their known amplitudes: $E_p(x,y,z) = \sum C_i(z)\,\psi_i^{pump}(x,y)$.
- The absolute value of the field is squared to yield the intensity profile: $I_p = E_p * E_p^*$.
- Using the saturation relation of eq. (1.15), the profile of the upper level population $n_2(x,y,z)$ is calculated. This is a subtle but crucial step, since the saturation curve (reminder: $n_2 \sim I/I + I_{sat}$) may yield a quite homogeneous excitation profile, in the case I is strong enough.
- The modified field is constructed according to eq. (1.18), which describes how a field propagates itself over some unit length Δz in the presence of the two-level gain system. Then, the 'Taylor expansion' argument established above serves to replace the exponent by a sum:

$$E_{modified} = \sum_i^N C_i(z)\cdot e^{-j\beta_i\Delta z}\left\{1+\frac{1}{2}\left[\sigma_{sig}^e n_2(x,y,z) - \sigma_{sig}^a n_1(x,y,z)\right]N_d\right\}\psi_i^{pump}(x,y) \tag{3.3}$$

- The modified field is decomposed over all pump modes, as per eq. (3.2), to yield the modal content of the pump field that has successfully coupled into the next slice – in other words, to yield the set of mode amplitudes $C_j(z+\Delta z)$ for $j = 1,2,\dots,N$.
- The process is repeated, with the amplitudes obtained through the last step serving as the new amplitudes for the next step.

Evaluation of the signal's propagation through the pumped amplifier is very similar, extended to the form of a complete Transmission Matrix (written in the modal base) – we would like to take advantage of the fact that in our model, the system is linear in the signal (thanks to the assumption of non-depletion). In other words, we would like to have a TM, for a given pump configuration, that enables us to know what amplified output would result from the injection, at the input, of any possible signal field (any combination of the signal's LP modes). Following the same reasoning as above, we see that any single mode of the signal ψ_i^{sig} passing through a section of the fiber where the pump has

induced some spatially-varying n_2 profile, generates a perturbed field (including effects of both propagation and interaction with the 2-level system), which in turn may couple into any member of the signal mode base. Therefore, a TM for the specific fiber 'slice' considered may be constructed thus, with each element [r,c] (signifying row, column) being computed as:

$$TM_{[r,c]}^{z\to z+\Delta z} = e^{-j\beta_c\Delta z}\{\,\delta_{rc} + (1+jK_{RIC})\iint \frac{1}{2}\left[\sigma_{sig}^{e} n_2(x,y,z) - \sigma_{sig}^{a} n_1(x,y,z)\right]N_d \cdot \psi_r^{sig}(x,y)\cdot\psi_c^{sig*}(x,y)\,dxdy\,\} \qquad (3.4)$$

Where the Kronecker Delta represents the fact that only when $r = c$ (i.e., when the two interacting signal modes are one and the same, or in other words we are considering the coupling of the mode to itself) do we have the '1' term which is the 0^{th} term of the Taylor expansion (i.e., the '1' term represents passive propagation). This perfectly agrees with the expectation, that if all gain effects in the medium vanish (the expression containing the level populations is nullified), we remain with a perfectly diagonal matrix, in which all on-diagonal elements are simply the propagation phase acquired by the relevant mode over the length of the slice, precisely as described in eq. (3.1) for a passive fiber. Conversely, all elements where $r \neq c$ – namely, the off-diagonal entries of the TM – represent coupling between the signal modes that has been induced by the gain. Again, it should be stressed that in a passive fiber, the modes are orthogonal and do not couple (the TM is diagonal); the appearance of the gain-mediated coupling terms is a manifestation of the fact that if the term appearing in the overlap integral (the one containing the level populations) is not spatially uniform – it disrupts the orthogonally of the modes.

Finally, the total gain-dependent Transmission Matrix is then arrived at by concatenating the effects of all slices, i.e. multiplying all the 'local' TMs:

$$TM_{Total}(L,\ Pump) = \prod_{z'=0}^{z'=L} TM^{z'} \qquad (3.5)$$

3.2.3 Qualitative Analysis of Controllability Based on the Model

The important insight one may derive from the last two equations, viewed from the perspective of our interest in exploiting the multimodality of the pump for controlling the signal, is that such control requires that the population inversion profiles excited by the pump should have high-as-possible contrast, and moreover, that this quality be extended over as much as possible of the fiber's length. Otherwise, the crucial population-difference term inside the overlap integral of eq. (3.4) becomes homogenous in the transverse coordinates, and the signal's TM converges towards a result that is constant regardless of the modal content of the pump. In other words, a very strong pump – one which saturates a large part of the gain profile – contributes to the signal's gain, but not to its dependence on the shaping we perform upon the pump's wavefront. This dependence will begin to emerge only after the pump has propagated a sufficient distance within the fiber, so that enough of its power has been

absorbed by the media to allow significant parts of its speckly intensity patterns to be comparable to the saturation intensity, rendering the excitation profiles non-uniform.

Consequently, one sees that the length of the fiber in which the effects we are interested in occur, is inherently limited by the characteristics of the gain system; one can only 'enjoy' gain that exhibits dependence upon the pumping configuration, within a finite section where the pump progresses between intense (but saturated) powers, and very weak powers. Figure 3.6 visualizes these three situations.

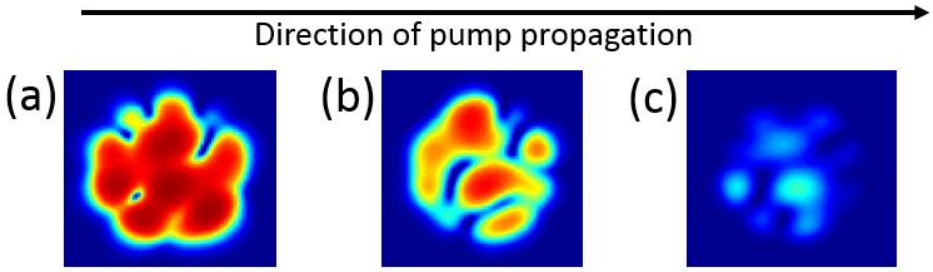

Figure 3.6: Illustration of typical excitation profiles induced by a high-power multimodal pump beam as it propagates through a fiber amplifier, and evolves (due to the system's absorption) from a strongly-saturated regime (a), to the highly-contrasted regime we are interested in (b), up to where it has been almost completely absorbed, and no longer produces meaningful gain (c).

In an informal, qualitative manner, we denote this limited length, along which the population inversion profiles retain a high degree of spatial non-uniformity, $L_{control}$. This quantity shall be discussed more thoroughly in the next chapter; for now, we only illustrate the idea with an example of a 5cm long section of an Ytterbium-doped MMFA, as depicted in figure 3.7. Each color in the graphs corresponds to a different pumping configuration that has been randomly chosen, and numerically propagated through the simulated fiber as per the procedure described above. As we see, the precise rate of pump absorption slightly changes with its modal content (as may be expected, due to the nonlinear, saturable nature of the absorption); nevertheless, the population inversion (middle graph) always follows the same slow evolution, from saturation, through moderate excitation, until lastly a rapid drop indicates the non-saturated exponential absorption of the pump, up to its practical extinction. Therefore, the spatial contrast of the population inversion (bottom graph) at first rises, reaches a maximum (around which our so-called $L_{control}$ length will lie), and finally declines to zero.

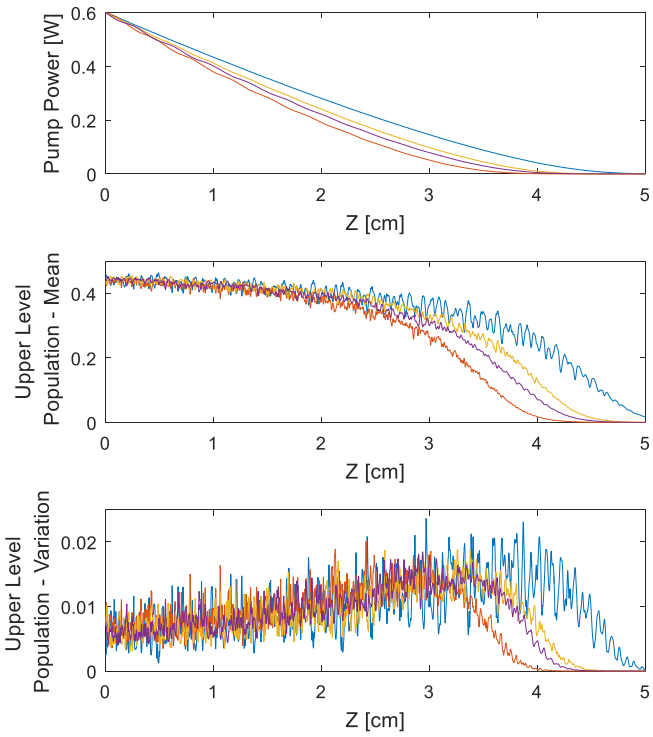

Figure 3.7: Numerical results of propagating different pump configuration in an Yb-doped MMFA. Each color corresponds to a different pump configuration. Pump propagates from left to right. Upper panel – the profile of the pump power, gradually declining as the pump is absorbed by the system. Middle and bottom panels – the spatial mean and the spatial variance, respectively, of the upper level populations excited by each of the pump configurations. Spatial means and variances are defined as averages, over the fiber cross-section, of the population and of its variance, respectively.

To summarize, we shall now assert two exceedingly important statements, which may be derived from the MMFA model purely by qualitative reasoning, i.e. without the explicit numerical solution for a specific set of system parameters. These are:

1. Sensitivity of the amplifier's TM to the modal composition of the pump, and high gain, are (beyond some minimal pump power) at odds with each other; ***there is a trade-off between increasing the gain by injecting more pump power, and the dependence of the overall transmission on the modal configuration of that pump***. This is because, as more length segments exhibiting saturated gain are added to the product represented in eq. (3.5), the relative weight of the non-saturated (and therefore sensitive to the modal shaping) length is diminished.

2. For a given pumping power, the 'amount' (qualitatively speaking) of system controllability obtainable is ***directly dictated by the choice of the gain medium*** - specifically, the rare-earth element chosen as doping - and cannot be improved upon by the tuning of other parameters, such as the doping's concentration or the fiber's guidance parameters. This is due to the fact that, once the cross-

sections for pump absorption and signal emission, σ^a_{pump} and σ^e_{signal} are set in our system - all other parameters merely change the way the configuration-dependent (i.e., spatially non-uniform) gain is spread over the volume; its total amount stays the same.

$$Control \sim \frac{\sigma^e_{signal}}{\sigma^a_{pump}} \tag{3.6}$$

For example, decreasing the doping concentration will slow down the rate of pump absorption, $\alpha_{absorption} = -\sigma^a_{pump} \cdot N_{doping}$, thereby stretching $L_{control}$ (the non-saturated segment). However, the signal's gain per unit length will decrease by exactly the same proportion, $\alpha_{amplification} = \sigma^e_{signal} \cdot N_{doping}$ and the two will cancel (since the effect upon the signal TM is of course proportional to the gain). In short, changing the concentration will merely scale the behavior in the z coordinates, to which the total accumulated gain effects are invariant.

3.3 Numerical Simulations of a Multimode Fiber Amplifier

This section of the chapter is organized as follows: First, the specific values used for all important amplifier parameters in our numerical simulations are presented and justified, by referencing typical values found in the literature. Next, some implications arising from these parameters, such as typical upper bounds on the signal's amplification and its variance, are evaluated by considering the statistics over many ***random*** pump configurations. Then, results of ***optimizing*** the pump configuration towards a specific target of signal control – in particular, enhancing the weight of chosen modes, or enhancing the intensity confined in chosen speckle grains - are presented and discussed. For further details on the numerical implementation of our model as a simulation tool, see Apendix A.

3.3.1 Specific Values for the Physical Parameters Determining Amplifier Performance

Regarding all parameters related to the levels' rate equations: For Ytterbium-doped media, the seminal papers of Pask [39], and Paschotta [40], have served for obtaining exact values. For Erbium-doped media, the papers of Giles and Desurvire [41], Barnes [42], and others [43-45], were used. Excerpts from these papers/textbooks showing the absorption and emission spectra of the two media are displayed in figure 3.8; the precise parameter values taken for the numerical simulation are tabulated in Table 1.

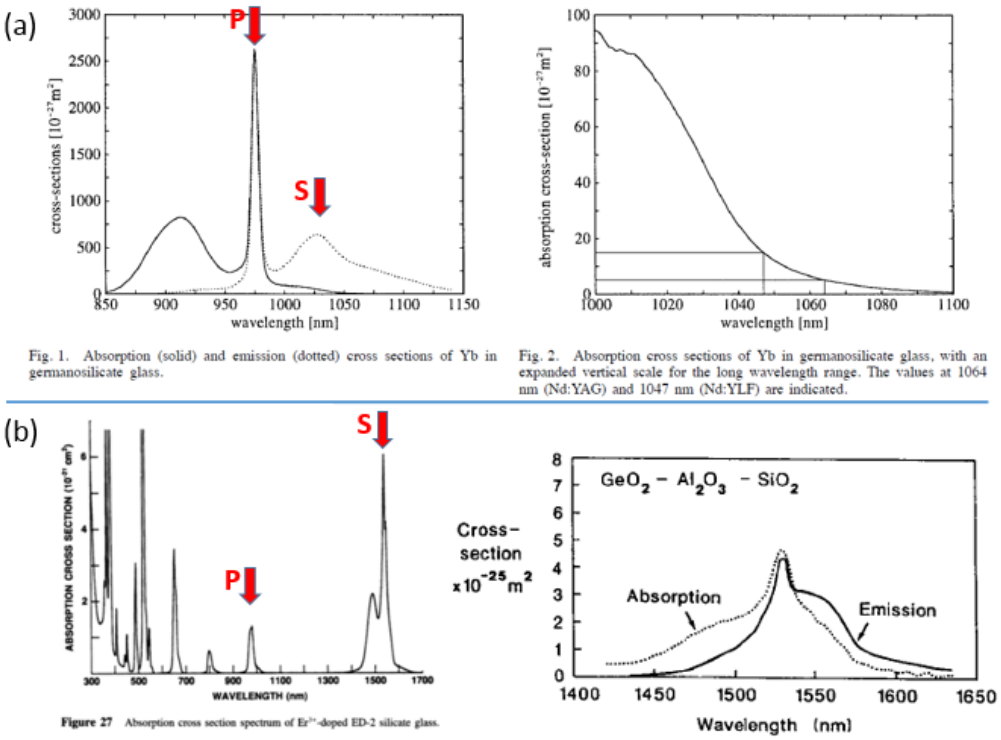

Fig. 1. Absorption (solid) and emission (dotted) cross sections of Yb in germanosilicate glass.

Fig. 2. Absorption cross sections of Yb in germanosilicate glass, with an expanded vertical scale for the long wavelength range. The values at 1064 nm (Nd:YAG) and 1047 nm (Nd:YLF) are indicated.

Figure 27 Absorption cross section spectrum of Er^{3+}-doped ED-2 silicate glass.

Figure 3.8: Absorption and Emission Spectra. Top is for Ytterbium and taken from Ref [40]; Bottom is for Erbium and is taken from Ref [45] and [42]. Red Arrows denoted 'p' and 's' mark the wavelengths of pump and signal, respectively. Right inserts zoom in on the signal wavelength's area for more detail.

	Yb	Er
λ_{pump} $[nm]$	976	976
λ_{signal} $[nm]$	1030	1550
$\sigma_{absorption}$ at λ_{pump} $[m^2]$	$2.6 \cdot 10^{-24}$	$1.7 \cdot 10^{-25}$
$\sigma_{emission}$ at λ_{pump} $[m^2]$	$2.6 \cdot 10^{-24}$	0
$\sigma_{absorption}$ at λ_{signal} $[m^2]$	$6.3 \cdot 10^{-25}$	$2.25 \cdot 10^{-25}$
$\sigma_{emission}$ at λ_{signal} $[m^2]$	$4.5 \cdot 10^{-26}$	$4 \cdot 10^{-25}$
$\tau_{upper\ level}$ $[msec]$	0.8	10

Table 1: Values used in our simulation for parameters controlling the level's rate equations.

The above parameters, which depend only on the specific rare-earth element chosen, already allow calculation of the possible population inversion achievable for the upper level, and the pump intensity required for saturating it.

Conversely - the strength of the gain/absorption experienced by the lightbeams per unit length, depends upon an additional parameter we need to set - the concentration with which the element is doped throughout the amplifier volume. Generally, we are interested in achieving maximal effect upon the signal in minimal fiber length (for several reasons, such as the finite coherence length of our pump

source, and the desire to avoid as much as possible the mode-coupling effects discussed in section 3.2.1). Hence, we would naturally be inclined to choose the highest concentration values possible; however a realistic model should take into account the phenomenon of 'quenching' - the suppression of the gain through ion-to-ion interactions which either reduce the upper level lifetime, or deplete its population through upconversion. For both elements considered, quenching places an upper limit on the range of viable doping concentrations, however the limitation is much stronger for Erbium doping than for Ytterbium. We find in the literature ([46-48] for the former, [49]-[51] for the latter) values representative of the largest doping concentrations typically used. These values are presented in Table 2, along with the effective absorption lengths of the pump wavelength resulting from them (calculated through eq. (1.18)):

	Yb	Er
Typical uppermost doping concentration $[m^{-3}]$	$2.5 \cdot 10^{26}$	$2.5 \cdot 10^{25}$
Resulting typical pump absorption length	1.5mm	23.5cm

Table 2: Values used in our simulation for doping concentrations.

Having chosen the values of doping concentration which will be assumed in our simulations, we now turn our attention to the question of the lengths of fiber modeled.

Presumably, we would like to set the MMFA length equal to the $L_{control}$ (as defined in the previous section) which is dictated by the pump's interaction with the gain media – i.e., the length over which the upper level's excitation is still appreciable, but not yet highly saturated. However, providing an exact formula for this overall length is not straightforward, as it depends upon a rather arbitrary definition of where precisely the speckly excitation profiles become "highly saturated". In fact, by the very nature of the 2-level system's saturation curve, the emergence of strong contrast as the pump power drops with the propagation along z, is a smooth and gradual change, not a sharp transition around some specific point. Another difficulty in deriving a concrete value for this length based only on considerations of spatial contrast, arises from the fact that in our numerical simulation, some contrast will (somewhat unrealistically) exist even for gain profiles excited by extremely strong pumps. This is due to the fact that our pump's speckle is considered to be the interference of perfectly monochromatic modes, and thus always contains singular points of perfect nulls of intensity.

Adopting a simple, more practical approach to the question of choosing a fixed length for our amplifier, we considered the following two additional limiting aspects of our proposed scheme:

1) Reliance on a pump source which is highly coherent, both spatially and spectrally. Reasonable values for the maximal power found today for such laser diode sources are in the area of several hundred milliwatts.

2) Necessity of keeping the total signal gain at reasonable values. Although theoretically, the initial signal injected into the amplifier's input could be assumed infinitely small, so that it might undergo huge gains - realistically this means the signal would at some point become negligible compared to the spontaneous emission arising from the pumping of the medium (essentially, the fiber would no longer be an effective amplifier, but rather a source of noisy broadband emission). Typically for fiber amplifiers, reasonable values of gain should not exceed the area of 50-60 dB.

For Yb-doped fiber amplifiers, it turns out that the first consideration is already enough for placing a limit on the total length: Using the chosen doping concentration (see Table 2), we find that roughly 7 cm of fiber are sufficient for completely absorbing a pump power of 1 Watt. In order to see this, we repeat the simulation presented in the previous section, this time taking 100 different pump configurations and averaging the obtained profiles of evolution along z. The results are shown in figure 3.9; the uppermost graph justifies the assertion that using more than 7 cm of fiber would require going to pump powers exceeding 1 Watt. The bottommost graph, in which the spatial variation (over the fiber's cross section) of the upper level's population is plotted, demonstrates that over this overall length, the excitation profiles undergo the full transition from saturated (the low variance values around z=0), through contrasted (peaking at maximal variance around z=5cm), to complete disappearance of contrast due to the pump's extinction. This suggests, that even if we would have permitted higher initial pump powers, the added contribution to the control of the signal would have been small. Therefore, we may conclude that the choice of $L_{Yb-MMFA} = 7cm$ is reasonable, and that the combination of this length with this given pump power is good in terms of exploiting the potential for high spatial contrast of the gain throughout the volume.

For Er-doped fiber amplifiers, it turns out that due to the slow absorption of the pump, reasonable pump powers of several hundred milliwatts would be able to excite highly-contrasted gain profiles throughout lengths of several meters of fiber. In this case, it is rather the second consideration (namely, that of reasonable total amplifier gain) which places a limit on the length; we find that for 2m of fiber, injection of less than 500mW of pump is already sufficient for obtaining >50 dB gain for some signal modes. Therefore, we set $L_{Er-MMFA} = 2m$, and repeat the same simulation as in figure 3.9, that of averaging the pump's evolution over a 100 random modal configurations. We find that for a fixed pump power of 400mW, the spatial contrast of the excitation profiles (bottommost graph) progresses from low values, through a maximum, and back down to low variances. This indicates that with the choice of this pump power, the fiber's length is being efficiently utilized for our purposes.

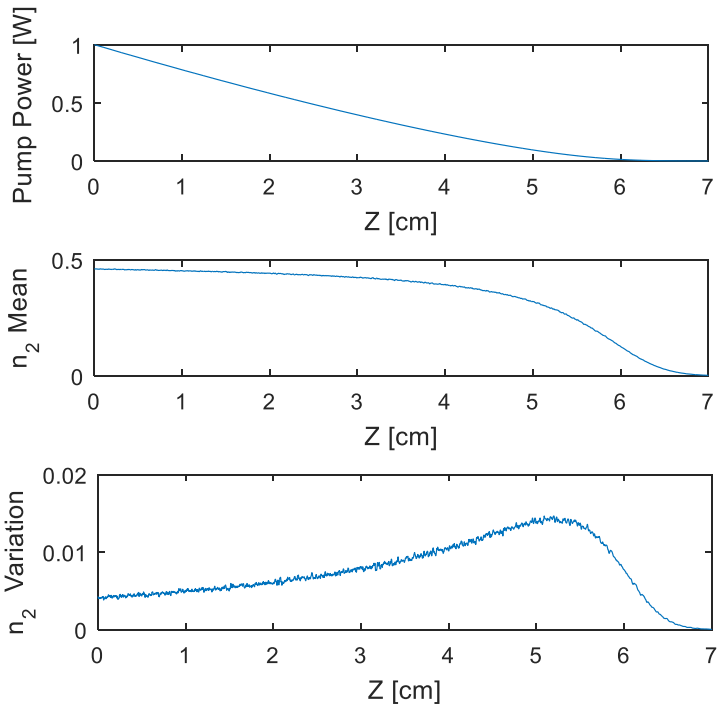

Figure 3.9: For an Yb-doped amplifier, the evolution, along the fiber length, of the pump power, and the resulting n_2 (the upper level population) mean and variation (in the sense of spatial average and spatial average of variance, taken over the fiber cross section), averaged over 100 random pump configurations.

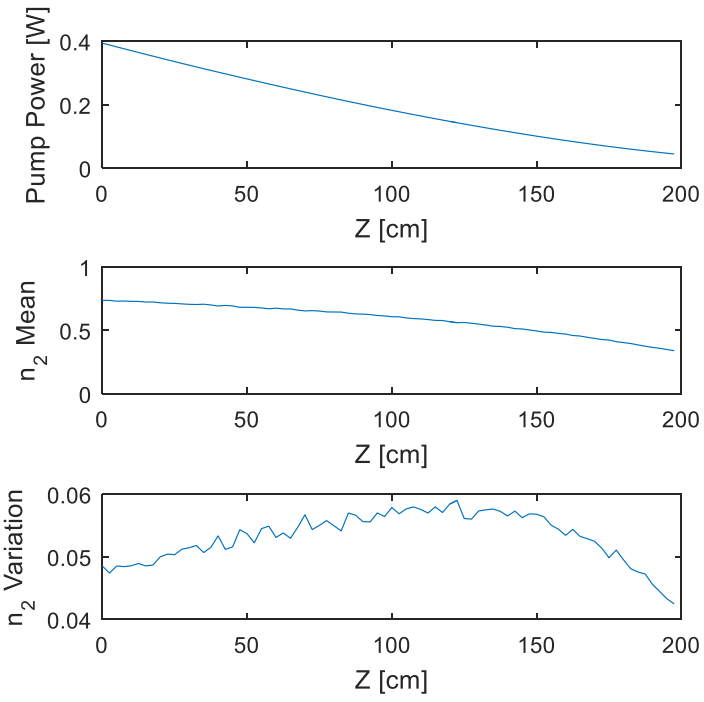

Figure 3.10: For an Er-doped amplifier, the evolution, along the fiber length, of the pump power, and the resulting n_2 (the upper level population) mean and variation (in the sense of spatial average and spatial average of variance, taken over the fiber cross section), averaged over 100 random pump configurations.

Lastly, we fix the important amplifier parameter which we defined in eq. (1.20) as K_{RIC} , the factor relating the phase shift induced upon the signal to the absorption/gain it sees.

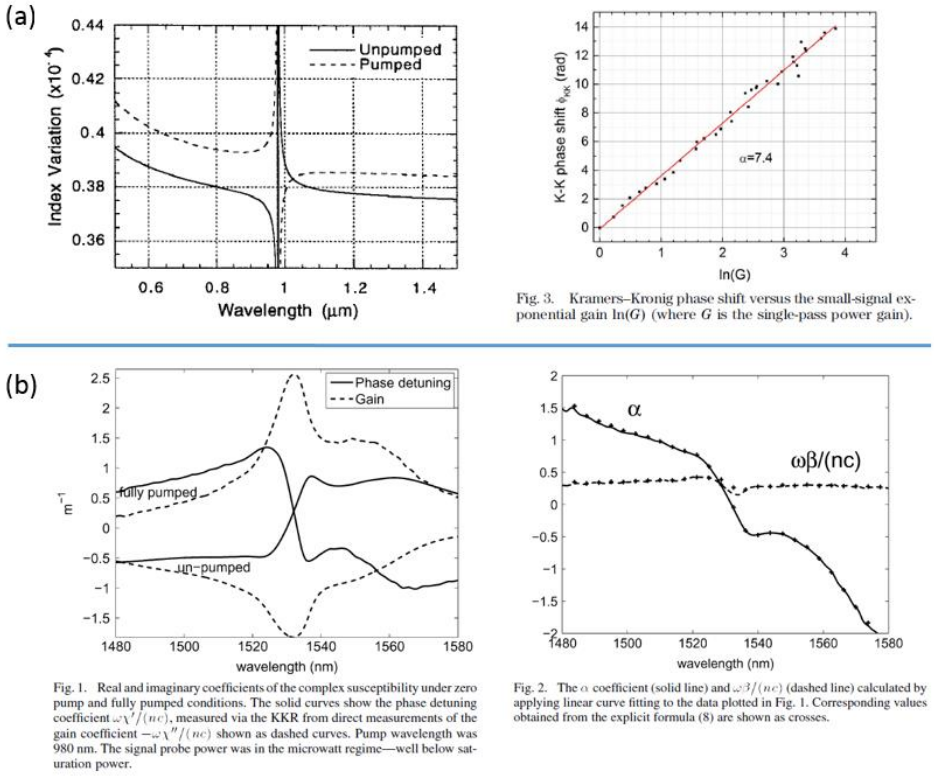

Fig. 3. Kramers–Kronig phase shift versus the small-signal exponential gain ln(G) (where G is the single-pass power gain).

Fig. 1. Real and imaginary coefficients of the complex susceptibility under zero pump and fully pumped conditions. The solid curves show the phase detuning coefficient $\omega\chi'/(nc)$, measured via the KKR from direct measurements of the gain coefficient $-\omega\chi''/(nc)$ shown as dashed curves. Pump wavelength was 980 nm. The signal probe power was in the microwatt regime—well below saturation power.

Fig. 2. The α coefficient (solid line) and $\omega\beta/(nc)$ (dashed line) calculated by applying linear curve fitting to the data plotted in Fig. 1. Corresponding values obtained from the explicit formula (8) are shown as crosses.

Figure 3.11: Top - Complex susceptibility for Yb-doped fibers, left is taken from [53], right is from [54]. Bottom – same for Er-doped fibers, both graphs taken from [57].

For Ytterbium-doped media, papers [52-54] has served for obtaining exact values. For Erbium-doped media, the papers [55-57] were used. Excerpts from these sources showing measurements of the refractive-index change in the two media are displayed in figure 3.11; the precise parameter values taken for the numerical simulation are tabulated in Table 3.

	Yb	Er
K_{RIC}	7.4	-0.5

Table 3: Values used in our simulation for the parameter controlling the signal's pumping-induced phase shift.

3.3.2 Effect of multimodal pumping on the Signal – Statistics

In order to first get some general insights regarding the influence of the pump's configuration (i.e. the pump's modal content) on the transmission of the signal, we begin by running the MMFA simulation for an ensemble of randomly-drawn pump configurations, and study the statistics of the resulting TMs. The randomization is carried out, each iteration, by assigning completely random values to both the amplitudes and the phases of all pump modes, then normalizing all amplitudes so

that the total pump power is constant (and equal to the value mentioned, in the previous section, as being optimal for maximizing the 'control' over the signal in the given fiber).

The most striking feature of the matrices is that they are all nearly diagonal, which means that the self-amplification of each signal mode tends to be significantly stronger than its coupling to other modes. This may be expected from the nature of the multimode pump's 'speckly' intensity profiles, which evolve in a complex, disordered manner over the amplifier's length and therefore tend to average the coupling terms (which alternate between positive and negative values) to 0. Figure 3.12 demonstrates this for an ensemble of 3000 random pump configurations in an Yb-doped amplifier. On the left, one example of a typical TM obtained is displayed, and on the right, 2 histograms calculated over the entire ensemble are displayed: the blue distribution includes only the diagonal elements, and is centered around the mean amplification (in amplitude), while the red includes all off-diagonal elements, whose population remains chiefly at near-zero values. The histograms display the relative frequency (prevalence) of the amplitude values in logarithmic scale. It is evident that, although sometimes specific pump configurations may produce some off-diagonal terms with strengths comparable to the average amplitude of the diagonal elements, this is rarely the case.

The off-diagonal terms will be revisited in section 3.5, where the ability to tailor pump configurations specifically optimized to enhance these coupling terms shall be discussed. For the remainder of this section, these terms shall be neglected, and only the on-diagonal matrix elements will be considered, in order to simplify the analysis of the statistics.

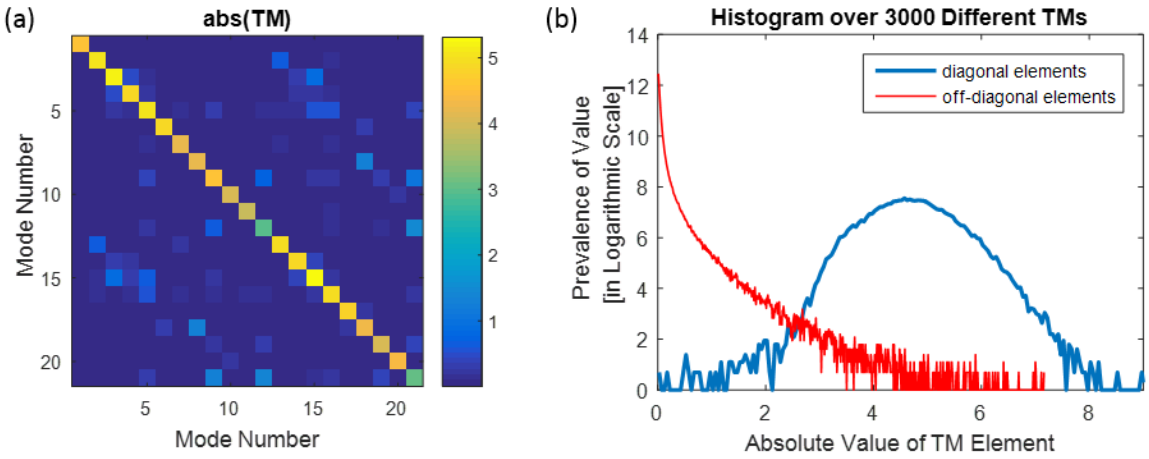

Figure 3.12: Left - A typical transmission matrix for an Ytterbium MMFA, drawn out arbitrarily from the ensemble of 3000 such TMs (corresponding each to a different pump configuration) shown in absolute values. Right - The distribution, over the entire ensemble, of the absolute values of TM elements; in blue is the on-diagonal population, in red is the off-diagonal population.

We now consider the effect of the pumping on the amplitude and phase of each of the signal modes. If we are to fully control the signal by shaping the pump's modal content, we should hope to find an ability to shift the phase of any given signal mode by at least 2π, and – independently - to tune its amplitude between values of strong amplification, and those of extinction. As described in the theory chapter, eq. (1.20) - for an optical amplifier, locally, any gain is accompanied by a linearly-proportional local phase change. This implies that for a *single-mode* amplifier, where the local gain and dephasing are described by scalars, and no modal complexity unties their simple linear relation, the total dephasing and the total gain accumulated remain mutually-determined. Figure 3.13 shows this connection, for the single-mode case - the signal's phase shift is proportional to the logarithm (because the gain is accumulated exponentially) of the gain in amplitude, with the slope of this relation being the Kramers-Kroning factor:

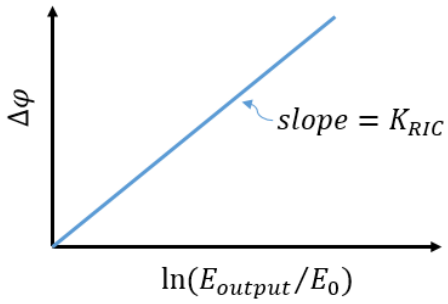

Figure 3.13: The relation, for a single-mode fiber amplifier, between gain-induced dephasing and amplification

In our case of interest, a multimode amplifier, we may raise the question, to what degree can the multimodal complexity detach the phase-shift from the gain; also, more simply, we wish to know, for each of these quantities, the range of values it is possible to obtain by manipulating the pump. It is therefore instructive to study scatter plots of the modes' phase-shifts vs. gain, collected over the ensemble of many random pump configurations.

Since the phase-shift factor in Erbium is significantly smaller than that in Ytterbium, we examine it first, expecting more limited "control". Figure 3.14 displays the scatter plots for the first 4 low-order modes, obtained for several hundreds of pump randomizations (with total pump power kept constant at 400mW), in a 2m-long Er-doped fiber (as per the optimization of length and power explained in the previous section). Evidently, we observe that the multimodal complexity of the pumping has an overall poor ability of altering the behavior of each signal mode from that it exhibits in a single-mode amplifier: the dephasing and the gain retain an almost perfect linear relation (points deviating from a linear regression do occur, but very rarely, and with small divergence). Thus, and in combination with the fact that the slope of this relation is low (the absolute value is 0.5 – see Table 3), the range of achievable phase modulation is very limited: at best, the peak-to-peak spread over the y axis is less

than π. This, despite the fact that the spread over the x axis (i.e., the range of signal gains coverable by choosing different pump configurations) is rather large: translated to terms of power gain, we find peak-to-peak variation of roughly 30 dB.

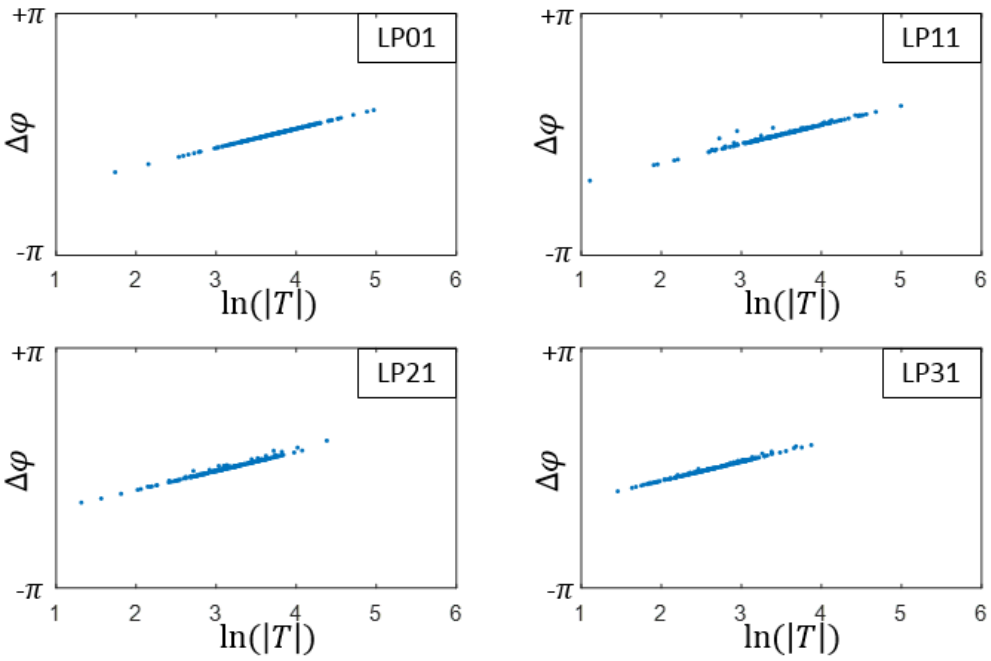

Figure 3.14: Scatter plot of dephasing vs. amplitude gain, collected over 200 random pumps, in an Er-doped MMFA. |T| is the absolute value of the on-diagonal element corresponding to the relevant signal mode in the pump-induced TM. Δφ is the difference between the phase of said element, and the average of this phase over the ensemble (so that all scatter plots are artificially centered over 0 in the y axis).

In summary, we may conclude that in an Er-doped MMFA, shaping the pump in order to spatially control the output signal speckle is not a promising prospect; contrarily, the possibility of modal gain discrimination (selection of modes to be strongly amplified, while others are hopefully suppressed) seems more viable. Such an optimization is presented in section 3.3.

Turning now to Ytterbium media, we similarly run many random pump configurations on an amplifier whose length and fixed pump power are, again, those set in the previous section so as to efficiently exploit the potential for high-contrast excitation (in this case, 7cm and 1W). As before, the scatter plots of each mode resemble quite closely the linear relation of single-mode amplifier; however, because the slope is much larger than it was for Erbium (by a factor of ~15, see Table 3), the variation ranges of the phase-shifts nearly wrap around 2π. As for the variation of the amplitude of each mode, we find that the control is quite limited – at best, the choice of the pump configuration can change the output power by roughly 7 dB. In conclusion, it seems that for Yb-doped MMFA the prospects of control are somewhat opposed to those for Er-doped: The potential for discriminating

between modes in terms of gain appears unpromising, but the ability of the dephasing to reach almost every value in a full period raises the hope of appreciable spatial control of the output speckle (at least in cases where the injected signal at the fiber's input contains, to begin with, the desired modes with amplitudes not too far from the desired values). Such an optimization is presented in the next section.

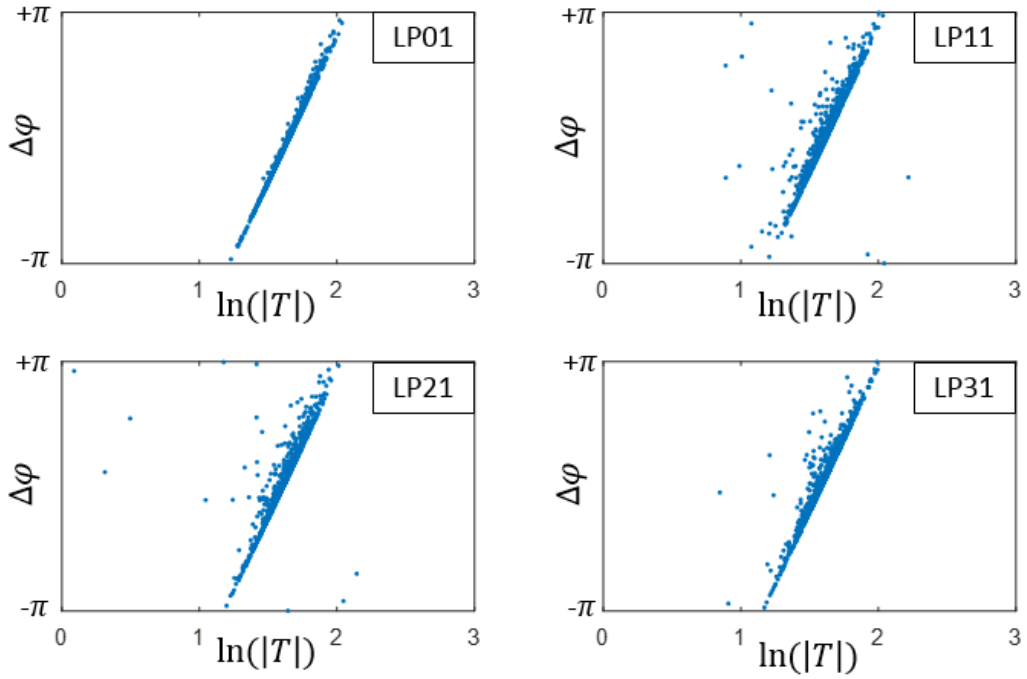

Figure 3.15: Scatter plot of dephasing vs. amplitude gain, collected over 1000 random pumps, in an Yb-doped MMFA. |T| is the absolute value of the on-diagonal element corresponding to the relevant signal mode in the pump-induced TM. Δφ is the difference between the phase of said element, and the average of this phase over the ensemble (so that all scatter plots are artificially centered over 0 in the y axis).

We conclude this section with an important caveat: in the above discussion we have considered each mode separately, as a stand-alone control problem. In the full picture, we would like to determine the phase and/or amplitude of all the modes simultaneously and using the same excitation**.** Stated in terms of the above scatter plots, it is not sufficient that we find for each signal mode a point (i.e., a pump configuration) which brings its amplitude and phase to a desired value; it also must be the same configuration across all the plots. The ability to find a pump configuration that combines the desired effects for, if not for all - then at least for a meaningful sub-group of the signal modes - is best evaluated by optimization processes where a specific control goal is defined in terms of the system's entire output, and searched for. Such optimizations shall be the subject of section 3.3.4.

3.3.3 Effect of multimodal pumping on the Signal – Optimization in the Modal Domain

As an instructive example of control in the modal domain, we consider the goal of selecting a single LP mode and maximizing its amplification, while minimizing all other modes.

As can be easily discerned from eq. (3.3), such a goal would be best served by a pumping configuration where the pump's intensity profile has the best possible spatial correlation with the desired mode's field distribution, during most of the distance traveled along the fiber. Intuitively, we could expect that the best choice would be to inject a pump consisting itself of just a single mode, with the identical indices l, m of the signal mode we would like to maximize (even though the spatial correlation between the modes, the signal's and pump's, would not be perfect due to the difference of wavelengths, it would still be a better overlap than for any other mode with different radial/angular indices). Moreover, such a pump would display a good spatial overlap all throughout the amplifier length (as opposed to a more complex combination of several modes), since the pump's intensity profile would not 'beat' and evolve along z (apart from the slow change of power diminution due to the absorption).

Indeed, optimizations carried out for several test-cases show that this expectation is correct. The metric to be maximized was defined as a "mode discrimination ratio", that is, the ratio between the TM's diagonal element corresponding to the specific mode chosen, e.g. mode j, and the sum total of all diagonal elements:

$$mode\ discrimination\ ratio_{for\ mode\ \#j} = \frac{|TM(j,j)|}{\sum_{i=1}^{N}|TM(i,i)|} \tag{3.7}$$

All multimode pump configurations found by the genetic search algorithm in such optimizations failed to outperform the simple, single-mode pump configuration described above (namely, injecting the pump mode most resembling the signal's mode j).

Figure 3.16 shows the results for an example in a Er-doped MMFA of length 2m, where the mode LP21o (which appears as mode #8 out of the total 10 signal modes supported) was maximized. Fixing the pump's modal content as singlemode - containing nothing but the mode LP21o - the pump power was swept in the range 150-650mW, to find the value where the existence of gain profiles, which are neither over-saturated nor under-pumped, is optimally "spread" over the fiber's entire length (and thus as much as possible of the gain contributes towards modal discrimination). At this optimal pump power, the amplification of the chosen mode is 51.5 dB, significantly higher than all other modes. However, those of the other modes which also happen to have good spatial overlap with the pump's profile, likewise experience strong gain –notably, LP11e and LP11o (#2 and #7), which both reach 32.4 dB.

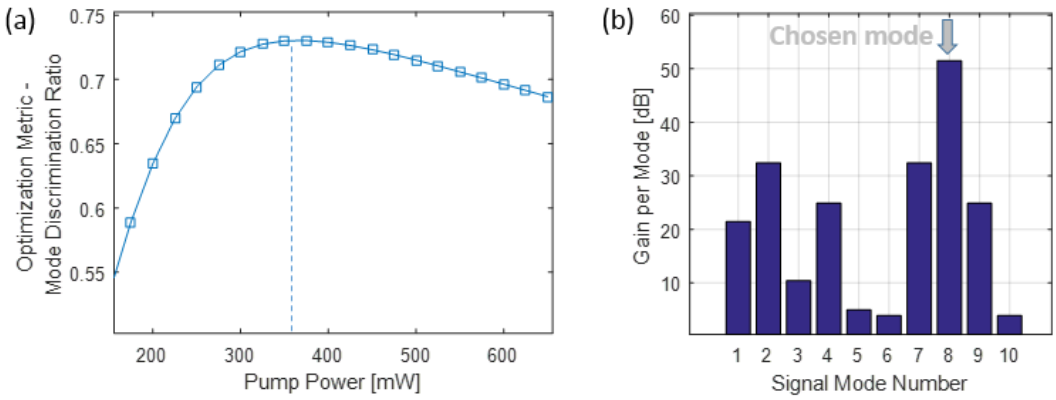

Figure 3.16: Er-doped amplifier: (a) Scan of the pump power used for finding the optimal power, for the fixed amplifier length of 2m, where the gain discrimination between the chosen mode and all others reaches a maximum. This power was found to be 366mW. (b) For said optimal pump power, the different modal gains are compared. The chosen mode, no. 8, gains almost 20 dB more than the nearest (the second-best) competitor.

It is worthwhile, at this point, to come back to the definition given in the previous chapter, that of a gain medium's typical coefficient of signal gain per unit length - α_T (eq. (1.16)). The above results, obtained for an Erbium MMFA, display a fair gain gap of almost 20dB between the desired mode and the nearest competing mode; this reflects the fact that the determining factor for successful mode discrimination is having a large product: $\alpha_T \cdot L_{control}$. This is easy to understand, considering the fact that since we maintain an (almost) identical excitation profile throughout the amplifier, the difference between the different signal modes, in their gain per unit length, is fixed: it is the factor of spatial overlap between this profile, and the field distribution of each mode. Naming this factor η_i, we may approximate the total gain of mode i as $e^{\eta_i \alpha_T L}$. In other words, the total gain gap between the modes will simply grow exponentially along the amplifier's length, with the difference in growth rates dictated by the (difference in) unchangeable geometry of the modes' profiles. It is therefore evident that our only possibility for obtaining high modal gain differences is choosing a gain medium where the aforesaid product is large.

In an Ytterbium MMFA, the overall length $L_{control}$ over which contrasted excitation may be maintained is much smaller than in Erbium, while the typical signal amplification cross-sections in both media are closely comparable (see table 1). Hence, it should come as no surprise that modal control of this form delivers, in an Yb-doped fiber amplifier, poor discrimination ratios, as demonstrated in the following simulation. The important characteristics of total number of signal modes, and the chosen mode for maximization, were kept identical as in the Er-doped example of figure 3.16; also, the process of optimizing the pump power was similarly repeated. The final results are shown in figure 3.17; the gain of the chosen mode, #8, is 21 dB, and the nearest competitors attain 17.4 dB gain.

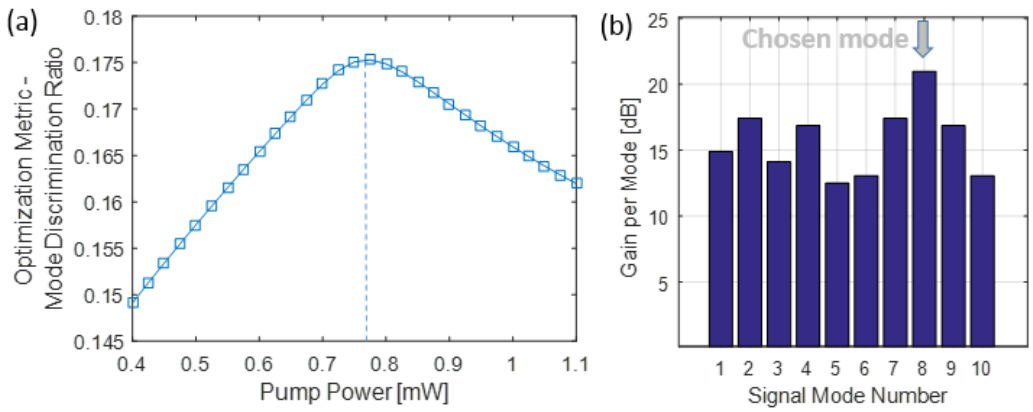

Figure 3.17: Yb-doped amplifier: (a) Scan of the pump power used for finding the optimal power, for the fixed amplifier length of 7cm, where the gain discrimination between the chosen mode and all others reaches a maximum. This power was found to be 770mW. (b) For said optimal pump power, the different modal gains are compared. The chosen mode, no. 8, gains about 3.6 dB more than the nearest (the second-best) competitor.

Another type of control that should be considered directly in the modal domain is the 'encouragement' of gain-induced coupling between signal modes, e.g. the maximization of a specific off-diagonal TM element. We have already seen in section 3.3.2, by looking at the statistics of many random pumps, that these elements tend to be very small; the following 'optimization' serves, in fact, more as an instructive example giving insight into why this is the case - rather than as a realistically useful procedure of performance optimization.

We turn our attention again to eq. (3.3), this time considering not the spatial overlap at some fixed cross-section, but rather the evolution of the integral term over the propagation axis z (and only for $i \neq j$, meaning only the off-diagonal elements). It should be evident that had it not been for the spatially non-uniform population inversion, all integrals would yield nil (orthogonality of the signal modes); but in the presence of multimodal pumping the integral gives some coupling coefficient with real and imaginary parts which have equal probability of being either positive or negative (the result of overlapping the complicated gain 'speckle' with the fields of the modes). Moreover, as we propagate in z and let the pump intensity profile evolve, the real and imaginary parts of this coefficient will fluctuate around zero; and the accumulation of the gain over the length by the multiplication of all matrices will necessarily exhibit strong averaging. In other words, the 'seemingly-random' nature of the evolution of the pump's speckle causes the off-diagonal terms to behave like phasors with an even distribution over the entire complex plane, and the product of many such phasors will tend to remain close to zero.

The only way in which we may avoid the averaging effect is by ensuring that the pump evolution has a periodic behavior, and then satisfying a phase-matching condition between signal and pump. To simplify the problem, we consider the pump contains only two LP modes, so that its evolution is a periodic beating. Then, our 'optimization' is allowed to sweep the optical frequency of the signal, and

the propagation constants of the signal modes are shifted with it. If a frequency is found for which the beating period of the signal pair happens to be equal to that of the pump pair, then the accumulation of the coupling terms (by multiplication of the matrices along z) will be constructive, instead of averaging to very small values as is otherwise the case. We may formulate this by defining the 'detuning' between the pump modal dispersion and the signal's:

$$detuning \equiv \left(\beta_{l1,m1}^{pump} - \beta_{l2,m2}^{pump}\right) - \left(\beta_{l3,m3}^{signal} - \beta_{l4,m4}^{signal}\right)$$

And asserting that if the detuning is brought close to zero, a 'resonance' of sorts would be reached, meaning strong coupling would be induced by the gain between that specific pair of modes. Ostensibly, the scenario of wavelength tuning for an amplifier pumped by only two LP modes is quite artificial; as was mentioned above, the simulation of this optimization serves as an illustrative case which sheds light on the averaging mechanism that comes into the play in more realistic configurations. Results of a simulation carried out for an EDFA are presented in figure 18.

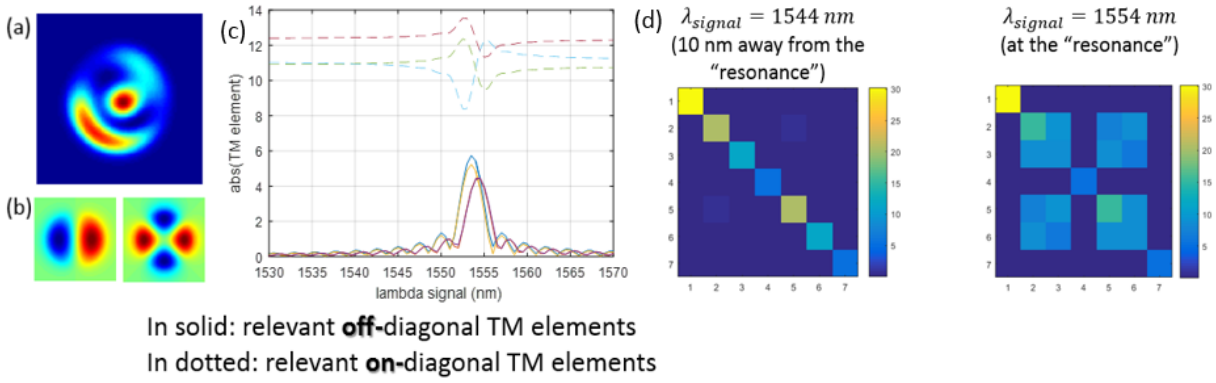

Figure 3.18: Enhancement of the cross talk between 2 signal modes by pumping with a relevant pair of pump modes, and tuning the propagation velocities of the signal so as to equalize the beating length of the signal pair to that of the pump pair. (a) – Example of the intensity profile of the pump, which consists of only 2 modes, at some arbitrary cross-section. (b) – the field distributions of the 2 signal modes being coupled, LP11 and LP21. (c) – results of the tuning of the propagation velocities by sweeping the signal wavelength. (d) – the signal TMs obtained when the phase-matching condition is not satisfied (left), and when the matching is optimal, so that the mode coupling attains its maximum (right).

3.3.4 Control of the Signal in the Spatial Domain by Optimization

In the previous sections, two kinds of analyses (namely, statistics over an ensemble of randomly-selected pump configurations, and optimization in the modal domain), gave important insight into the nature of the controllability of the system, as well as the factors that come into play as limitations. Chiefly, we have seen that:

1. Individual modes may be modulated, with a discernible - but not a totally deterministic - correlation between amplitude and phase. This means that separately manipulating the mode's 2 degrees of freedom (DOF) is possible, albeit 'difficult' (the farther the desired change is from the single DOF correlation, the lower the probability of finding a pump configuration to induce it).
2. Coupling terms between different modes (off-diagonal elements in the TM) are small compared to the self-amplifications terms (on-diagonal), but not totally negligible.

However, these insights apply to the statistics of single elements in the transmission (one mode, or one coupling coefficient). The natural question to be studied next is - to what degree may we manipulate the complete TM, given that it constitutes one complex system where all individual elements are interdependent, and simultaneously modulated by the same single pump configuration. Therefore, the next step was the implementation of a numerical optimization scheme, where a desired goal was set in terms of the entire transmission of the amplifier, and an optimization algorithm sought the pumping configuration best suited to achieve this goal.

Viewed as an optimization problem, the modulation of our signal output by the selection of the pump composition is conspicuously difficult, with several tens of DOFs (twice the number of guided pump modes) interacting together in a highly non-linear and non-separable manner to produce the signal TM. In order to facilitate the exploration of this complex space, a genetic optimization (GA) algorithm was implemented over a cluster of computers, able to run the MMFA model for multiple choices of the pump in parallel. The group of different configurations computed simultaneously in a given single run, or calculation cycle, was in fact a 'generation' of the GA; once this run was completed, the results from the members of this generation (i.e. the different pump configurations) could be collected and compared, then a sub-set representing the best results among them was picked and 'bred' to produce a new generation, and so on. The repetition of the cycles was terminated when the GA seemed to converge to a solution, i.e. when the best result found at the end of each generation was no longer improving by increments over a certain threshold. Additionally to the (roughly) order-of-magnitude speeding-up of the computation afforded by parallelizing the GA over the cluster, the implementation of the numeric model in C++ drastically reduced the calculation time. A schematic illustration of the implemented optimization system, along with two exemplary results, are presented in figure 3.19.

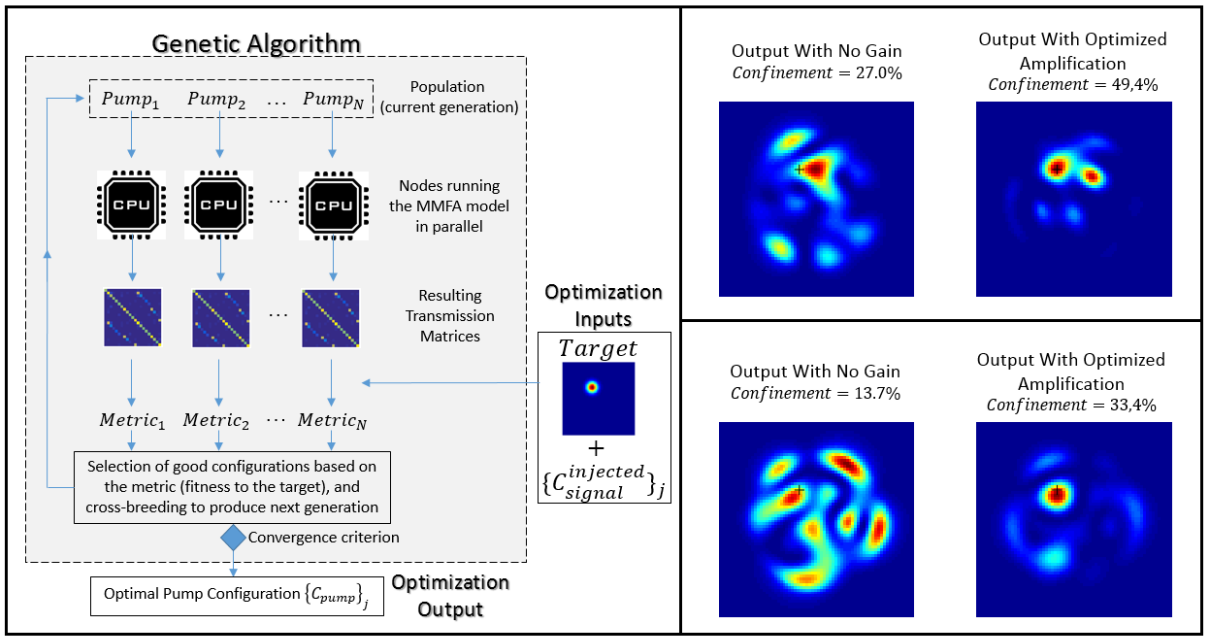

Figure 3.19: the GA optimization function built around the numerical MMFA model for studying the possibility of focusing the output signal by optimal choice of the pumping configuration, in an Yb-doped fiber with the parameters and power set to maximize controllability as per section 3.3.1. Left – block diagram of the optimization system and procedure. Right – results obtained in successful optimization runs, for two different cases of input signal. In each panel (each optimization case), the speckle output with no pumping is displayed on the left, and the output for the best result found (the optimized pump) displayed on the right.

Evidently, the actual improvement in the output's similarity to the desired target (in terms of the confinement, or any other metric) that may be achieved strongly depends both on the initial input signal injected into the amplifier, and on the target itself. Due to the vast extent of possibilities for these input variables, coupled with the highly complex nature of the optimization itself (in the pump DOF space), thorough numerical characterization of the achievable results everywhere in the problem space remained beyond the scope of this work. Nonetheless, the specific examples presented give some meaningful reading of achievable optimizations: in both test-cases of figure 3.19, the confinement of the output power to a desired speckle grain was approximately doubled. As a general conclusion, therefore, we may affirm that the results successfully demonstrated that – despite the various detrimental mechanisms analyzed and discussed throughout this chapter - by careful tailoring of the pump's modal content, significant control may be exercised over the amplified signal in the spatial domain.

3.3.5 Towards the Experimental System

The last section presents the results of numerical simulations carried out as quantitative predictions for the specific experimental MMFA that was built and studied in our work. Full details of this setup and of the specific Yb-doped fiber used will be specified in chapter 4; Without repeating them here, it suffices to state that the parameters of our numerical model were set to the values resembling as close as possible the actual fiber and source in our experiment. A certain limitation of our model, in that respect, should be noted: While the true fiber amplifier's core featured a graded-index profile, our model accounts solely for a step-index fiber (for which explicit solutions for the LP modes' characteristic values may be calculated). This discrepancy was judged to be acceptable, because (once the fiber parameters were tweaked in order to have the correct *total number* of LP modes as in reality) the only significant difference between model and experiment was a correction to the propagation constants (i.e. the β_{lm} values). Had we been interested in predicting the actual speckle at the output of a precisely-defined length of fiber with a precisely-defined pumping configuration, the step-index simplification would have represented a fatal flaw in the model; However, we are only interested in quantifying, in an 'absolute difference' sense, the change to the signal's output one may observe over the ensemble of possible pump configurations. Over this ensemble, as long as the model reflects:

- The right spatial statistics of the pump's speckle patterns (by correctly simulating the 'shape' of the modes, that is their field distributions);
- The right rate at which this speckle evolves and decorrelates as it propagates (by calculating the modal phase velocities with the correct end-to-end spread);

Then the numerical result should represent with reasonable accuracy the overall statistics of the signal TM (note that each TM is obtained by multiplying the gain of many pump 'speckle realizations'). Based on this reasoning, we expected our model to realistically predict the degree of signal variation obtainable by spatially modulating the pump.

First, the numerical simulation was run many times with different pumping configurations, chosen at random, and the resulting signal TMs were collected. Then, pairs were selected – say TM1 and TM2 – and two different measures of variation were calculated: Degradation of a focused signal (i.e. a perfect focus spot was numerically 'created' at the output of TM1, then TM2 was applied to the same input and the loss of confinement due to the change in TM was measured), and the Decorrelation of a speckly signal (same procedure, but with the input signal creating a random speckle at the output rather than a focus). The results are summarized in figure 3.20. Going forward towards the experimental stage, a useful take-away prediction would be that a speckle decorrelation (between a pair of pump configurations) of about 35%-40% should be rare but possible to find.

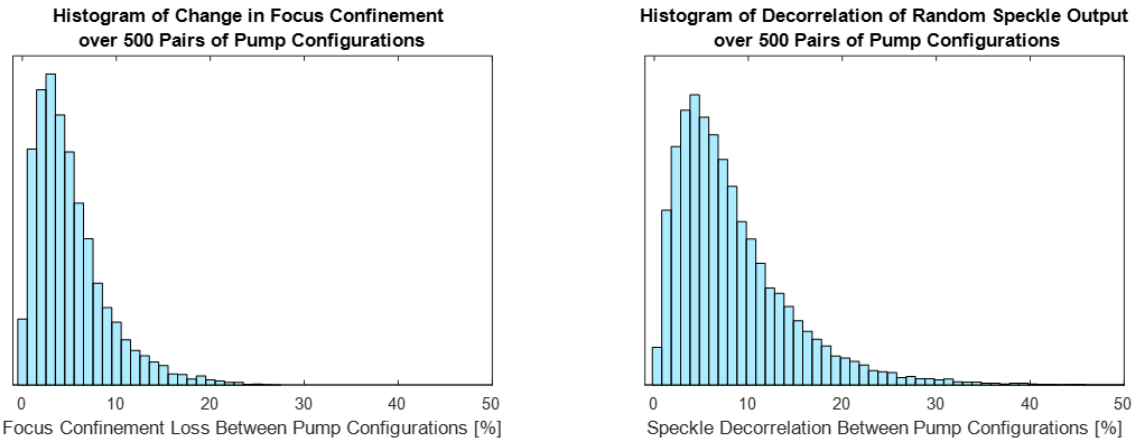

Figure 3.20: Histograms for quantifying the probability of changing the spatial pattern at the output of a MMFA (simulating our experimental setup of chapter 4), by randomizing the pump's modal content. Left – the initial patterns are focused signals, and the change caused by the modification of the pumping configuration is measured as the loss of confinement (in %). Right – the initial patterns are random speckles, and the change (likewise, due to the pump modification) is measured as decorrelation (in %).

3.4 Summary and Discussion

The model presented in this chapter treats a rare-earth doped multimode fiber amplifier pumped by a coherent pump, and enables the numerical evaluation of the amplified signal's TM as a function of the input pumping configuration - meaning, the modal composition of the pump beam exciting the medium. For a given configuration, the population inversion excited throughout the volume is first computed; due to the modal dispersion of the pump's modes, this excitation is formed as a series of 'speckly', i.e. spatially heterogeneous in complex patterns, profiles of inversion. Then, relying on the assumption of non-depletion of the pump, and on the fact that the amplification seen by the signal per unit length is small compared to the fiber's guidance, the TM of each such slice is calculated by numerically evaluating the triple overlap integral between the local gain profile and each possible pair of signal modes. Lastly, the total TM of the MMFA system is readily found as the matricial product of all slices.

On a qualitative level, the model leads us to the conclusion that the amplifier TM may indeed be appreciably modified by the shaping of the pump, while at the same time revealing 3 main system characteristics that set limits on this form of control:

I - The non-linearity, in the pump power, of the population inversion limits the spatial non-uniformity of the gain profiles outside some finite length of fiber where its saturation is low; this limitation is fully determined by the absorption and emission cross-sections of the gain medium (i.e. by the choice of the rare-earth element) and does not depend on doping concentration or other fiber parameters.

II - The scalar nature of the population inversion, namely the fact it does not retain the phase of the pump field that excited it, dictates a limit upon the control's selectiveness between the different signal modes. Simply put - a given composition of pump modes may favor the amplification of a certain signal mode over others, by having good spatial overlap with its intensity pattern; but they as well will always have a non-zero overlap, and therefore will be somewhat amplified.

III - The complicated nature of the evolution of the pump's intensity patterns, over the length of fiber needed for meaningful absorption and amplification, restricts the ability to shape a desired transmission function using solely the modal composition at the input (the injection facet) as the set of controllable degrees of freedom.

In order to quantitatively assess the extent of the influence these limitations would have upon the controllability of a realistic MMFA system, numerical simulations were performed adopting two different approaches: First, statistics were collected over a large ensemble of possible TMs which were the result of generating many pump configurations at random. Then, an optimization function based on cluster computing and a genetic algorithm was implemented and fed specific targets for the modification of the TM (mostly - attempting to focus the output signal into a single speckle grain).

Furthermore, numerical simulations were carried out - in light of the crucial role the choice of the gain medium element plays in the MMFA performance due to both upper level saturation and signal gain-dependent dephasing - for two different types of doping: Ytterbium and Erbium.

It was seen that in an YDFA, due to the rapid absorption of the pump with respect to the signal amplification length, the saturation mechanism inhibits the degree of control much more strongly than in the EDFA case (where the 'inefficient' pump absorption serves our purposes well, by allowing non-saturated gain profiles to be maintained over a long segment of the amplifier). However, the EDFA suffers from a different serious limitation, which is its low real component of electronic susceptibility around the signal wavelength; this renders the gain-dependent phase-shifting rather small, hence the amount of change one may apply to a spatial pattern at the amplifier output is minor. It was shown that at the bottom line, these differences amount to the YDFA system featuring a strong sensitivity to our pump shaping in the spatial domain (e.g. focusing the amplified signal in the near field), and a rather weak receptivity to control in the modal domain (e.g. selective amplification of a selected signal mode); while for the EDFA system, the situation was the opposite.

Lastly, in support of the experimental part of our work, which dealt uniquely with a Yb-doped amplifier, the numerical simulation was run using the characteristic parameters that best simulated the actual setup. Figures of merit for the degree of spatial control we may expect to exercise over the output signal were thus derived and presented as predictions for the following chapter.

References for Chapter 3

[1] C. J. Koester, E. Snitzer, Amplification in a Fiber Laser, Appl. Opt., Vol. 3 No. 10, 1182-1186 (1964).

[2] R. J. Mears, L. Reekie, I.M. Jauncey, D. N. Payne, Low-Noise Erbium-Doped Fibre Amplifier Operating at 1.54um, Elec. Lett., Vol. 23 No. 19, 1026-1028 (1987).

[3] E. Desurvire, J. R. Simpson, P. C. Becker, High-gain erbium-doped traveling-wave fiber amplifier, Opt. Lett., Vol. 12 No. 1, 888-890 (1987).

[4] H.S. Chung, M.S. Lee, D. Lee, N. Park, D.J. DiGiovanni, Low Noise High Efficiency L-Band EDFA With 980 nm Pumping, Elec. Lett., Vol. 35 No. 13, 1099-1100 (1999).

[5] J.D. Minelly, W.L. Barnes, R.I. Laming, P.R. Morkel, J.E. Townsend, Diode-Array Pumping of Er3+/Yb3+ Co-Doped Fiber Lasers and Amplifiers, IEEE Phot. Tech. Lett., Vol. 5 No. 3, 301-303 (1993).

[6] Y. Jeong, J.K. Sahu, D.N. Payne, J. Nilsson, Ytterbium-doped Large-Core Fiber Laser With 1.36kW Continuous-Wave Output Power, Optics Exp., Vol. 12 No. 25, 6088-6092 (2004).

[7] D.J. Ripin, L. Goldberg, High Efficiency Side-Coupling of Light Into Optical Fibres Using Imbedded V-Grooves, Elec. Lett., Vol. 31 No. 25, 2204-2205 (1995).

[8] V. Doya, O. Legrand, F. Mortessagne, Optimized Absorption in a Chaotic Double-Clad Fiber Amplifier, Opt. Lett., Vol. 26 No. 12, 872-874 (2001).

[9] P. Leproux, S. Fevrier, V. Doya, P. Roy, D. Pagnoux, Modeling and Optimization of Double-Clad Fiber Amplifiers Using Chaotic Propagation of the Pump, Opt. Fiber Tech., Vol. 6, 324-339 (2001).

[10] G. Canat, Y. Jaouen, J-C Mollier, Performance and Limitations of High Brightness Er3+/Yb3+ Fiber Sources, C. R. Physique 7, 177-189 (2006).

[11] A.S. Kurkov, E.M. Dianov, Moderate-power CW Fibre lasers, Quant. Elect. Vol. 34 No. 10, 881-900 (2004).

[12] D. Taverner, D. J. Richardson, L. Dong, and J. E. Caplen, 158-mJ pulses from a single-transverse-mode Large-Mode-Area Erbium-Doped Fiber Amplifier, Opt. Lett., Vol. 22 No. 6, 378-380 (1997).

[13] H. L. Offerhaus, N. G. R. Broderick, R. S. Sammut, L.Dong, J. E. Caplen, and D. J. Richardson, High-energy single-transverse-mode Q-switched fiber laser based on a multimode large-mode-area erbium-doped fiber, Opt. Lett., Vol. 23 No. 21, 1683-1685 (1998).

[14] J. P. Koplow, D. A. V. Kliner, L. Goldberg, Single-mode operation of a coiled multimode fiber amplifier, Opt. Lett., Vol. 25 No. 7, 442-444 (2000).

[15] M. Y. Cheng, A. Galvanauskas, P. Mamidipudi, R. Changkakoti, P. Gatchell, High Energy and High Peak Power Nanosecond Pulse Generation With Beam Quality Control in 200um Core Highly Multimode Yb-Doped Fiber Amplifiers, Opt. Lett., Vol. 30 No. 4, 358-360 (2005).

[16] J. M. Fini, Bend-resistant design of conventional and microstructure fibers with very large mode area, Opt. Exp., Vol. 14 No. 1, 69-81 (2006).
[17] J. A. Alvarez-Chavez, H. L. Offerhaus, J. Nilsson, P. W. Turner, W. A. Clarkson, D. J. Richardson, High-Energy High-Power Ytterbium-Doped Q-Switched Fiber Laser, Opt. Lett., Vol. 25 No. 1, 37-39 (2000).
[18] J. M. Sousaa, O. G. Okhotnikov, Multimode Er-doped Fiber for Single-Transverse-Mode Amplification, Appl. Phys. Lett., Vol. 74 No. 11, 1528-1530 (1999).
[19] G. Le Cocq, L. Bigot, A. Le Rouge,M. Bigot-Astruc, P. Sillard, C. Koebele, M. Salsi, Y. Quiquempois, Modeling and characterization of a few-mode EDFA supporting four mode groups for mode division multiplexing, Opt. Exp., Vol. 20 No. 24, 27051-27061 (2012).
[20] J. Limpert, H. Zellmer, A. Tunnermann, T. Pertsch, F. Lederer, Suppression of Higher Order Modes In a Multimode Fiber Amplifier Using Efficient Gain-Loss-Management (GLM), Advanced Solid-State Lasers Conf., 2002 Tech. Digest, 112-114 (2002).
[21] J. Limpert, A. Liem, M. Reich, T. Schreiber, S. Nolte, H. Zellmer, A. Tunnermann, Low-Nonlinearity Single-Transverse-Mode Ytterbium-Doped Photonic Crystal Fiber Amplifier, Opt. Exp., Vol. 12 No. 7, 1313-1319 (2004).
[22] W. S. Wong, X. Peng, J. M. McLaughlin, L. Dong, Breaking the Limit Of Maximum Effective Area For Robust Single-Mode Propagation in Optical Fibers, Opt. Lett., Vol. 30 No. 21, 2855-2857 (2005).
[23] H. Ono, Optical Amplification Technologies for Space Division Multiplexing, NTT Tech. Rev., Vol. 15 No. 6 (2017).
[24] M. Salsi et al., "In-line Few-Mode Optical Amplifier with Erbium Profile Tuned to Support LP01, LP11, and LP21 Mode Groups," Proc. ECOC'12, Tu.3.F.1 (2012).
[25] N. Bai, E. Ip, L. Guifang, Multimode fiber amplifier with tunable modal gain using a reconfigurable multimode pump, Opt. Exp., Vol. 19 No. 17, 16601-16611 (2011).
[26] Y. Jung, Q. Kang, J. K. Sahu, B. Corbett, J. O'Callagham, F. Poletti, S. Alam, D. J. Richarson, Reconfigurable Modal Gain Control of a Few-Mode EDFA Supporting Six Spatial Modes, IEEE Phot. Tech. Lett., Vol. 26 No. 11, 1100-1105 (2014).
[27] R. N. Mahalati, D. Askarov, and J. M. Kahn, Adaptive modal gain equalization techniques in multi-mode erbium-doped fiber amplifiers, J. Lightw. Tech., Vol. 32, No. 11, 2133–2143 (2014).
[28] E. Ip, Gain Equalization for Few-Mode Fiber Amplifiers Beyond Two Propagating Mode Groups, IEEE Phot. Tech. Lett., Vol. 24, No. 21, 1933-1936 (2012).
[29] Z. Qin *et al*, Azimuthal Dependence of Modal Gain and its Impact on Gain Equalization in Multimode Erbium-Doped Fiber Amplifiers, Optik 126, 3538-3543 (2015).
[30] J. Montoya, C. Aleshire, C. Hwang, N.K. Fontaine, A. Velázquez-Benítez, D. H. Martz, T.Y. Fan, D. Ripin, Photonic Lantern Adaptive Spatial Mode Control in LMA Fiber Amplifiers, Opt. Exp., Vol. 24 No. 4, 3405-3413 (2016).

[31] R. Florentin, V. Kermene, J. Benoist, A. Desfarges-Berthelemot, D. Pagnoux, A. Barthélémy, J. P. Huignard, Shaping the Light in a Multimode Fiber, Nat. Ligh & Sci. App., No. 6 (2017).
[32] R. Florentin, V. Kermene, A. Desfarges-Berthelemot, A. Barthélémy, Space-time Adaptive Control of Femtosecond Pulses Amplified in a Multimode Fiber, Opt. Exp., Vol. 26 No. 8, 10682-10690 (2018).
[33] M. E. Fermann, Single-Mode Excitation of Multimode Fibers With Ultrashort Pulses, Opt. Lett., Vol. 23, No. 1, 52-54 (1998).
[34] A. Lucesoli, T. Rozzi, Image Transmission and Radiation by Truncated Linearly Polarized Multimode Fiber, Applied Opt., Vol. 46 No. 15, 3031-3036 (2007).
[35] J. Carpenter, T. D. Wilkinson, Characterization of Multimode Fiber by Selective Mode Excitation, J. of Light. Tech., Vol. 30 No. 10, 1386-1392 (2012).
[36] J. Carpenter, B. J. Eggleton, J. Schröder, 110x110 Optical Mode Transfer Matrix Inversion, Opt. Exp., Vol. 22 No. 1, 96-101 (2014).
Imaging interest:
[37] T. Cizmar, K. Dholakia, Exploiting Multimode Waveguides for Pure Fibre-Based Imaging, Nat. Comm., 3 No. 1027 (2012).
[38] M. Plöschner, T. Tyc, T. Cizmar, Seeing Through Chaos in Multimode Fibres, Nat. Phot., 9, 529-535 (2015).
[39] H.M. Pask *et al*, Ytterbium-Doped Silica Fiber Lasers: Versatile Sources for the 1-1.2 μm Region, IEEE Journal of Selected Topics in Quant. Elec., Vol. 1 No. 1 pg. 453 (1995).
[40] R. Paschotta *et al*, Ytterbium-Doped Fiber Amplifiers, IEEE Journal of Quant. Elec., Vol. 33 No. 7 pg. 1049 (1997).
[41] C. R. Giles, E. Desurvire, Modeling Erbium-Doped Fiber Amplifiers, Journal of Light. Tech., Vol. 9 No. 2 pg. 271 (1991).
[42] A. L. Barnes *et al*, Absorption and Emission Cross Section of Er3+ Doped Silica Fibers, IEEE Journal of Quant. Elec., Vol. 27 No. 4 pg. 1004 (1991).
[43] C. Barnard *et al*, Analytical Model for Rare-Earth-Doped Fiber Amplifiers and Lasers, IEEE Journal of Quant. Elec., Vol. 30 No. 8 pg. 1817 (1994).
[44] S. Shimida, H. Ishio, Optical Amplifiers and Their Applications, Chichester, England: John Wiley & Sons, (1994).
[45] N. K. Dutta, Fiber Amplifiers and Fiber Lasers, Singapore: World Scientific Publishing Co., (2015).
[46] P. Blixt, J. Nilsson *et al*, Concentration-Dependent Upconversion in Er3+-Doped Fiber Amplifiers: Experiments and Modeling, IEEE Trans. Photonics Tech. Letters, Vol. 3 No. 11 pg. 996 (1991).
[47] J. L. Wagener *et al*, Effects of Concentration and Clusters in Erbium-Doped Fiber Lasers, Optics Letters, Vol. 18 No. 23 pg. 2014 (1993).

[48] P. Myslinski *et al*, Effects of Concentration on the Performance of Erbium-Doped Fiber Amplifiers, Journal of Light. Tech., Vol. 15 No. 1 pg. 112 (1997).
[49] R. Paschotta, J. Nilsson *et al*, Lifetime Quenching in Yb-Doped Fibres, Optics Comm., No. 136 pg. 375 (1997).
[50] A. V. Kiryanov *et al*, Cooperative Luminescence and Absorption in Ytterbium-Doped Silica Fiber and the Fiber Nonlinear Transmission Coefficient at $\lambda = 980nm$ With a Regard to the Ytterbium Ion-Pairs' Effect, Optics Express, Vol. 14 No. 9 pg. 3981 (2006).
[51] L. De La Cruz-May *et al*, Transparency Power Calculation in Yb3+-Doped Fiber Due to Temperature Variations, Proc. Of SPIE Vol. 7839,WSOF-2 (2010).
[52] M. J. F. Digonnet *et al*, Experimental Evidence for Strong UV Transition Contribution in the Resonant Nonlinearity of Doped Fibers, Journal of Light. Tech., Vol. 15 No. 2 pg. 299 (1997).
[53] J. W. Arkwright *et al*, Experimental and Theoretical Analysis of the Resonant Nonlinearity in Ytterbium-Doped Fiber, Journal of Light. Tech., Vol. 16 No. 5 pg. 798 (1998).
[54] H. S. Chiang, J. Nilsson *et al*, Experimental Measurements of the Origin of Self-Phasing in Passively Coupled Fiber Lasers, Optics Letters, Vol. 40 No. 6 pg. 962 (2015).
[55] E. Desurvire, Study of the Complex Atomic Susceptibility of Erbium-Doped Fiber Amplifiers, Journal of Light. Tech., Vol. 8 No. 10 pg. 1517 (1990).
[56] S. C. Fleming, T. J. Whitley, Measurement of Pump Induced Refractive Index Change in Erbium Doped Fiber Amplifier, Electronics Letters, Vol. 27 No. 21 pg. 1959 (1991).
[57] S. Foster, Complex Susceptibility of Saturated Erbium-Doped Fiber Lasers and Amplifiers, IEEE Photonics Tech. Letters, Vol. 19 No. 12 pg. 895 (2007).

4 Experimental Results for Pump Shaping in Amplifier Configuration

In the previous chapters, we have seen how wavefront shaping techniques allow the control of the modal composition of a lightbeam propagating in a multimode (MM) fiber – but hitherto, only for a passive fiber (chapter 2); and how the modal composition of a lightbeam pumping a MM fiber amplifier (MMFA) affects the amplified signal – but only through theoretical modeling and simulation (chapter 3). In the following chapter, these two worlds come together: the experimental implementation of a wavefront shaping scheme modulating the pump beam injected into a MMFA will be presented. The purpose of this chapter is the experimental investigation of the dependence of the amplifier's transmission (for the signal) upon the pump shaping, and the comparison of these results to the predictions given by the numerical model of chapter 3.

4.1 Set-up Configuration

At the center of the setup is the fiber sample, held at its two ends by two XYZ translation stages (Thorlabs 'NanoMax 300' model), which enable the placement and alignment, with about 1μm precision, of each fiber end with respect to its corresponding coupling lens. Both lenses are N-BK7 aspherics with focal length f = 25mm and a clear aperture D = 10mm, serving as objectives - i.e., each lens focuses an incoming beam into the fiber facet placed precisely at its back focal plane.

The rest of the setup may be broadly divided into two branches, namely the pump and the signal branches, corresponding to each of the fiber ends (so that these two lightwaves always counter-propagate in the amplifier). Their detailed description follows below.

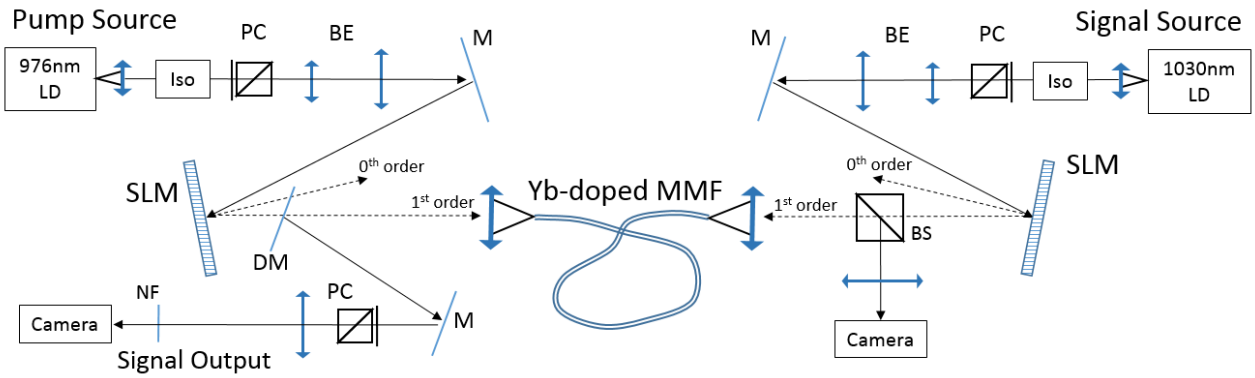

Figure 4.1: Schematic description of the amplifier experiment. Iso – Isolator, PC – Polarization Control, BE – Beam Expansion, BS – Beam Splitter, M – Mirror, DM – Dichroic Mirror, NF – Notch Filter.

4.1.1 Signal Branch

The signal source is a DFB (distributed feedback) diode laser at 1030nm with 50mW output, manufactured by Innolume Gmbh. Single frequency operation with high coherence (the spectral width is specified at <5Mhz) is ensured by the DFB selectivity. The diode is fiber coupled by a single mode Panda PM fiber with NA = 0.12. We collect the beam emerging from the SM fiber using an aspheric collimation lens with f = 15.29mm; then the collimated beam is passed through an isolator based on a Faraday rotator, and a polarization control module (serving also as a variable attenuator) consisting of a half-lambda waveplate and a PBS (polarizing beam splitter) Next, the signal beam is expanded by means of 2 achromatic lenses (f = 60mm and f = 250mm) arranged in a Keplerian telescope configuration, so that a sufficiently-large area of the LCOS (liquid crystal on silicon) display of the spatial light modulator ('Pluto' Phase Only SLM, supplied by Holoeye Photonics) may be illuminated. The light reflected off the SLM was passed through a non-polarizing BS (beam splitter), with a 90:10 R:T ratio, and then coupled into the fiber by means of the aforementioned coupling lens. The addition of the BS in this path made possible the imaging of the fiber facet; this imaging branch is essential for system monitoring and alignment, since it permits seeing the signal focus spot being injected into the fiber (thanks to the Fresnel back-reflection from the facet).

4.1.2 Pump Branch

The pump source initially used was a 'BL976-PAG900' FBG-stabilized (fiber Bragg grating) laser diode, supplied by Thorlabs, capable of delivering 900mW at 976nm. The motivation for choosing this source was its relatively high output power; however, we found out that its coherence was insufficient for generating, throughout the fiber length, the kind of excitation profiles desired. Specifically, the speckle patterns observed at the output of a short fiber sample injected with this pump were well-contrasted but not stable in time: the patterns displayed sharply visible grains, but with a shape that randomly drifted and decorrelated over time spans of few seconds. This was explained by the existence of several (few) longitudinal modes in the diode, which apparently do not maintain stable phase relations (the FBG stabilization serves to precisely fix the central lasing wavelength, but not the relative phases between the different spectral modes).

Subsequently, a different pump source of strictly single-frequency operation was searched for. The available commercial options dictated a compromise in total output power: The highest-power laser diode to be found with emission at 976nm was a 500mW diode, manufactured by Innovative Photonic Solutions. Its output is single frequency (specified linewidth <100kHz) and spatially single mode (fiber-coupled).

Departing the source, the rest of the pump branch resembled very much that of the signal, as described in the previous paragraph. The only differences between the 2 branches are listed as follows:

- The pump was collimated by an ashperic lens of focal length f = 13.86mm, in order to make sure that the collimated beam's diameter was small enough so as not to lose any power while passing through the isolator (due to its 4.5mm aperture).

- The pump's beam expander was built with the same configuration as in the signal branch, but with a magnification factor of only x2 (the achromatic lenses were f = 75mm and f = 150mm), in order to minimize power loss due to the finite size of the LCOS display of the SLM (which was, as for the signal, also a 'Pluto' supplied by Holoeye).

- A dichroic mirror which passes the pump wavelength and reflects the signal's (i.e. a shortpass filter), was placed between the SLM and the pump coupling lens; Its role was to allow the imaging of the amplifier output while still allowing the wavefront-shaping and injection of the pump beam (since the side that serves as input for the pump is the output for the signal). This filter, manufactured by Semrock, features a very sharp transmission edge around 1μm, so that the transmission at the pump wavelength is >97%, while an optical density >3 is seen at the signal wavelength. The signal reflecting off the dichroic mirror is passed through the following imaging path:

4.1.3 Imaging of the Output

A half-lambda waveplate and a PBS provide polarization control of the imaged radiation, and an additional Semrock spectral filter, with a narrow transmission band (a "notch") around 1030nm rejects both the broad ASE emitted by the amplifier, and any residual of the pump which survived the first dichroic filter. Then, a long focal-length lens, f = 1000mm, forms the image of the fiber facet upon the camera placed at its focal plane. Together with f = 25mm coupling lens which also serves for injection, the imaging system formed is a 4f relay with a magnification of 1000/25 = 40. The camera (supplied by Thorlabs) sensor is a CMOS (complementary metal oxide semiconductor) array of size 1280x1024 pixels, with a pixel pitch of 5.3μm.

4.2 Yb-doped Fiber Characterization

4.2.1 Fiber Specifications

The fiber used in this work was fabricated specifically for our purposes by the ‘Fiber optics and applications’ group at the InPhyNi research institute in Nice. If consists of a simple single-cladding, single-core structure, whose respective diameters are 125μm and 18μm. Due to the constraints of the specific fabrication process used, the refractive index profile is a graded-index one (GRIN), rather than the step-index form assumed in our numerical model. The fiber is doped with Ytterbium, with the doping profile identical to that of the refractive index (so the entire core area serves for gain).

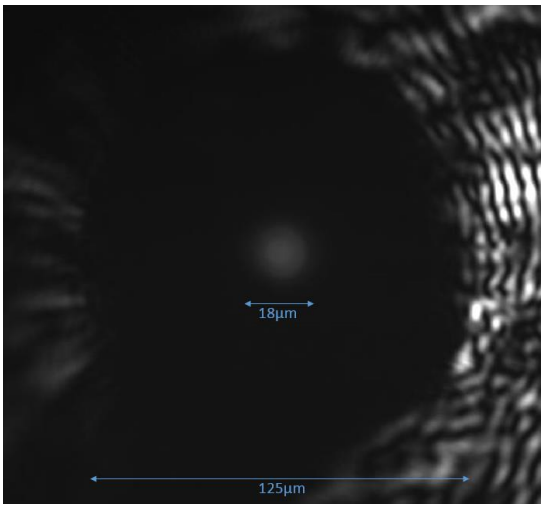

Figure 4.2: Image of the output facet (with respect to the pump injection) of the fiber used in the amplifier experiment. In the center, the core is visible due to the emission of incoherent ASE as a result of the pumping. The cladding is dark, but its borders are visible due to the contrast with stray light in the background (the stray light was introduced behind the fiber for the purpose of outlining its edges).

Using the data specified by the fabricator (displayed in figure 4.3), the core's refractive index was fitted to the parabolic form which is customarily used to describe GRIN fibers [1] (commonly called an "alpha-power" profile). The fit yielded the following results for the fiber parameters:

$$\propto \approx 3.3 \quad , \Delta \approx 0.0105 \rightarrow \quad NA \approx 0.21$$

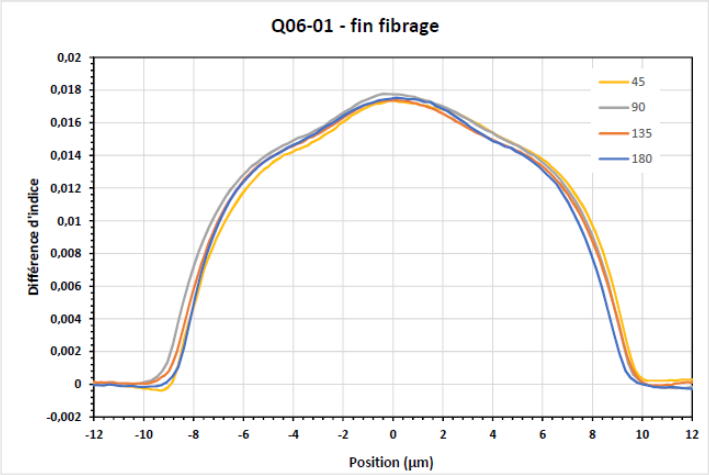

Figure 4.3: Measured refractive-index profile of the Yb-doped fiber, courtesy of the fabricator at the Nice Institute of Physics. The 4 colors represent the 4 different orientations of the cross-sections measured.

Based on these fitted parameters (the index difference and the alpha power-coefficient), the V-number of the fiber was found to be ~9. Accordingly, and based on the approximation discussed in section 1.2.3 (for GRIN fibers), the number of spatial modes supported by the fiber at the signal wavelength may be estimated to be ~18 modes per polarization.

4.2.2 Signal Coupling and Propagation

The typical speckle patterns observed at the output of the fiber when the signal was coupled into it, as well as the focused spots that were obtained by applying the TM-based focusing method, were consistent with the above estimate of the number of modes. An example is displayed in figure 4.4:

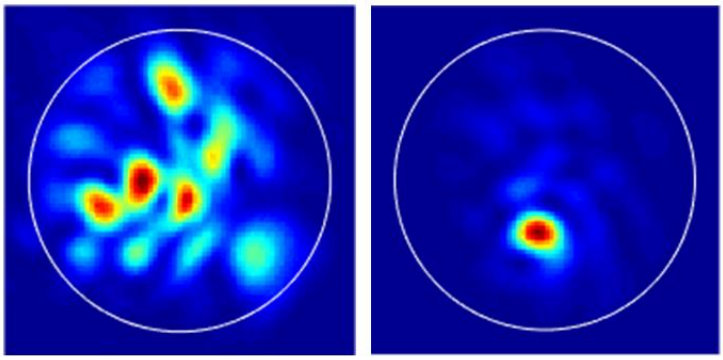

Figure 4.4: Typical images of the output facet of the fiber when the signal light is coupled into it; left – a random speckle, right – spot obtained by focusing using the signal SLM. The white circle is superposed on the image to mark the core-cladding boundary.

4.2.3 Absorption and Saturation Measurements

Before carrying out the desired experimental work with our Yb-doped fiber, a preliminary verification of the following characteristics was carried out:

1) The doping concentration N_{Yb}

2) The pumping saturation power $Ppump_{sat}$

Both these parameters might vary with respect to the values expected theoretically; the concentration, because of inevitable tolerances in the fabrication process; and the saturation power[1], due to the considerable sensitivity of the electronic level structure upon the specific glass host [3].
As a result, empirical validation of the true values of these important parameters is necessary.

Supposedly, evaluation of the doping concentration should be straightforward, because it dictates an easily-observed quantity - the typical absorption length $\alpha_{abs} = \sigma^{a}_{signal} \cdot N_d$ (while having no effect at all on the saturation power). So a naive approach would be to simply compare the output power vs. the input power into a known length of fiber L, and use the relation derived from eq. (1.18) - namely that the optical power decreases exponentially with length, $P_{output}/P_{input} = e^{-\alpha_{abs} \cdot L}$.

[1] It should also be noted that even in the hypothetical case all relevant rates and lifetimes of the electronic level structure were known, and the saturation intensity could be precisely calculated, the saturation power would still remain an approximate estimate, due to the complex way the intensity spreads out over the fiber cross-section to yield some given total power. Indeed, our definition of a saturation power is valid only in the sense of an effective average over the ensemble of intensity distributions supported by the waveguide.

However, closer consideration reveals that two major facts complicate the practical measurement of these characteristics:

I) The two parameters are inextricably connected in any measurement of output vs. input power; the saturation will reduce (at least in the beginning of the fiber, close to the pump injection point) the medium's capacity to absorb power. In turn, the weight of the saturation effect will gradually diminish along the fiber length with a rate that is governed by the typical absorption length. As a result, a single measurement of the overall absorption of a single sample cannot alleviate the ambiguity between concentration and saturation power.

II) The true amount of optical power coupled into the fiber waveguide is difficult to know, due to the finite efficiency of coupling any free-space optical field to the supported spatial modes. Unlike the measurement of the output power, where one requires no more than to place a power-meter after the fiber's end facet, the same type of measurement performed at the input yields a value which may be a significant over-estimate of the actual power injected.

A common technique used to resolve these complications is the cut-back method [4], where a series of absorption measurements is made, each for a different length of the same medium (by gradually shortening it from the output end, while care is taken to change nothing at the input side). However, the process is cumbersome, and requires repeating a cycle of cleaving, measurement of resultant length, and realignment, several times. Therefore, an alternative approach was designed: Similarly to the cut-back method, a series of absorption measurements was taken, but the parameter varied was not the medium's length, but rather the pump power. The data points of absorption vs. input power were then fed into a numerical solver which fitted for 3 free variables: the two desired characteristics N_{Yb} , $Ppump_{sat}$, and a third coupling efficiency variable $0 < \eta_{coupling} < 1$ which scaled the pump power measured at the fiber input so as to represent the power loss at the air-to-fiber interface.

The underlying idea of sweeping the pump power was to allow the collection of data points for the same sample, but over two opposing regimes - one where saturation plays the dominant role (i.e. the pump is strong enough to saturate most of the fiber and hence be absorbed along it mostly following a linear law), and the regime where saturation is almost negligible (i.e. the pump is weak enough to follow the exponential curve of absorption throughout most of the fiber). The wider the range of relative weight between saturated and non-saturated behavior, covered by the measurement set - the better the fitting function is able to evade the inherent mutual dependence between the 3 unknown parameters, in order to evaluate them without minimal ambiguity. For this reason, the method was based on injecting the pump into a relatively short fiber sample. The length chosen was 33cm. The results obtained are presented in figure 4.5. The fit yielded the following fiber parameters:

$$N_{Yb} \approx 1.4 \cdot 10^{25}\ m^{-3} \quad , \qquad Ppump_{sat} \approx 5.7mW$$

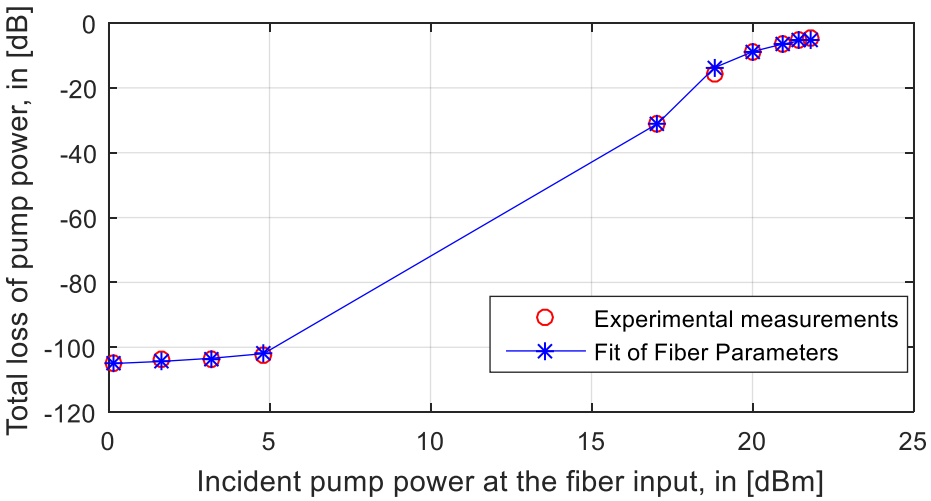

Figure 4.5: the series of absorption measurements carried out by varying the pump power injected into a fiber sample short enough to be almost completely saturated by the maximal available power.

4.2.4 Pump Coupling and Propagation

A validation of the similarity of the fundamental behavior of the pump light in the fiber to that of the signal light (most notably, the ability to wavefront-shape it) was carried out by using the same short fiber sample on which the absorption measurements described above were performed. The injected pump power was raised to a high-enough level so as to allow significant power to survive the absorption and come out of the other end, where it was imaged (with the help of a spectral notch filter at 976nm, which rejected the ASE emitted by the fiber around 1030nm).

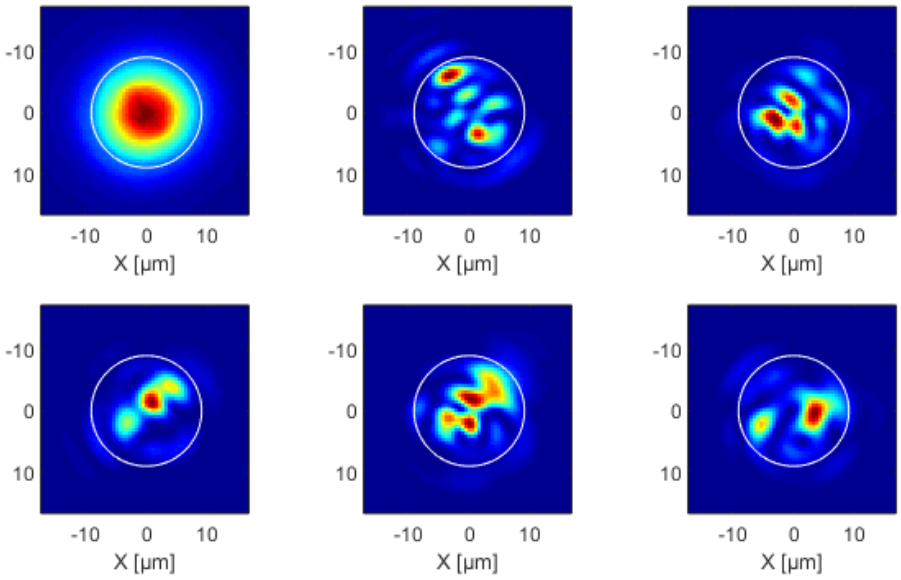

Figure 4.6: Typical images of the facet of a very short fiber into which pump light is coupled from the other end. Top left – the broad ASE emission observed when the injected pump power is small enough so that the residual (non-absorbed) pump light is negligible; other 5 panels – typical random speckles of residual pump radiation that manages to survive the fiber when the injected pump power is high.

Examples of the pump speckles obtained at the pump-output end are shown in figure 4.6; the variation (the different speckle patterns) represents different pumping "configurations", i.e. different modulations of the pump's SLM. These images serve to demonstrate that our pump source was of sufficient coherence to induce well-contrasted excitation patterns within the fiber, and their dependence on the wavefront shaping.

4.2.5 Design Considerations – Choice of Fiber Length

An important provision that must be made in the implementation of a fiber amplifier is the elimination of parasitic lasing, which could arise for sufficiently-strong pumping as an oscillation between the fiber facets. Commonly in such experiments and in commercial applications, this is done by preparing at least one facet with an angled cleave, so that the Fresnel reflection from it do not couple back into the guiding core. Since the apparatus for performing such cleaves was not available in our lab, a different method was improvised: By considerably lengthening the fiber sample, to well beyond the length over which the available pump power is absorbed, large absorption losses were added to the round-trip gain budget of the signal. Of course, for a real application this would represent an unacceptable penalty which defeats the purpose of the amplifier itself; However, for the purpose of studying the signal behaviour in the spatial/modal domain, this addition of a constant loss factor is of no harm, since it only attenuates the signal power before it arrives at its interaction with the pump-induced excitation.

A length of L = 310cm was taken, which (based on the doping characterization of the previous sub-section), for a signal at 1030nm and a nonpumped system, represents a total absorption of approx. 17dB. Coupled with the loss caused by the silica-air Fresnel reflection of the facet, which is at least about 13dB, the total round-trip loss was too high for our available pump power to compensate so as to achieve the oscillation threshold.

This estimate was empirically verified by observing the fiber's output with our spectrum analyser, under the condition of maximal pumping ('flat phase' for the SLM). Indeed, no parasitic lasing was seen, only the broader emission of ASE – as displayed in figure 4.7.

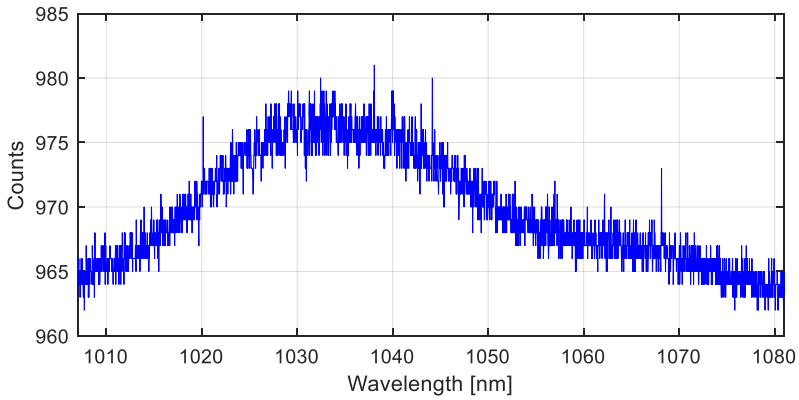

Figure 4.7: Measured Spectrum at the output of the pumped amplifier, showing broad ASE (but no lasing).

4.2.6 Benchmark for Effects of Gain – Passive Fiber 'Benchmark' Experiment

In order to better understand our experimental observations and to avoid the interpretation of non-related artifacts – most notably, thermal effects – as the results of our wavefront shaping, a comparison to a gain-less system was carried out by replacing the amplifier fiber with a passive (non-doped) one. The importance of this for the separation of the shaping-dependent effects, from the 'baseline' observed changes, will be discussed in the next section. The fiber sample taken for this benchmark experiment was as similar as possible to the Yb-doped one: a bare (jacket-less and non-connectorized) fiber, with a cladding diameter of 125μm and graded-index guiding. The mechanical mounting of the passive fiber, using clamps, was also identical to the active case. Only the core diameter, D = 50μm, was larger than that of the amplifier fiber, due to the difficulty of finding a commercial fiber with non-standard core size.

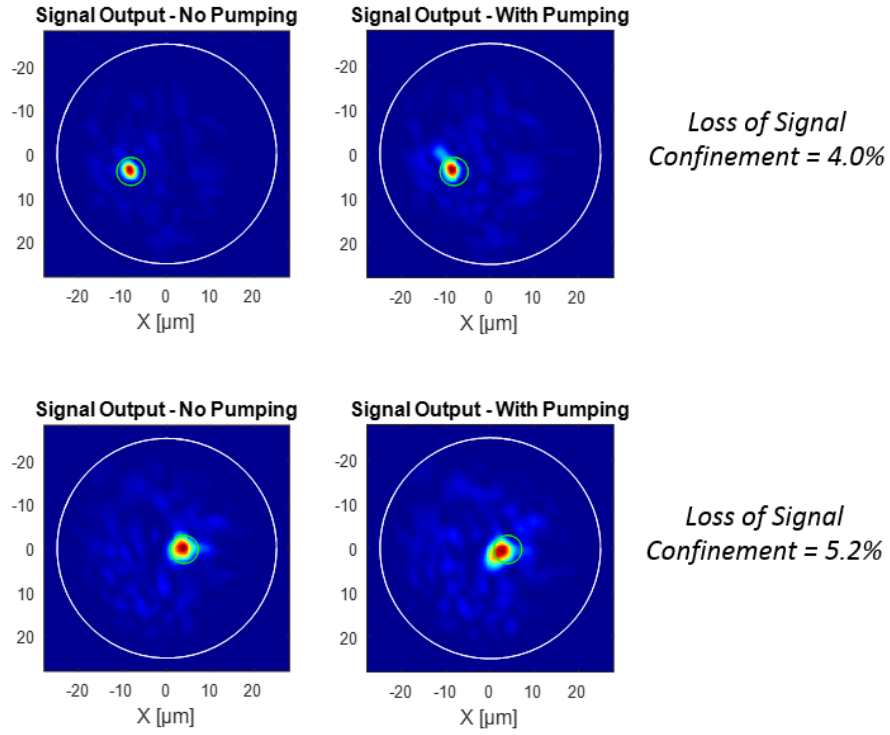

Figure 4.8: Decorrelation of a signal focused at the output of a passive *MM fiber when the pump beam is introduced into the core, due to thermal effects. The white circles denote the fiber core; the green circles represent the area over which the confinement of the signal power was calculated.*

An observable change of the signal's output speckle pattern occurred when the pump was coupled into the fiber, although no gain was present in the system. The output was first focused, using the SLM on the signal branch, while the pump beam was shut down. Then, the pump power was turned on, and the effect on the signal was measured as the change in the confinement metric (as defined in eq. (2.10)). Results for 2 different focused points are shown in figure 4.8.

The passive fiber 'benchmark' experiment demonstrates that the presence of a pump induces non-negligible effects which we will need to separate from the effects of the pump *shaping*.

4.3 Results of Pump Wavefront Shaping Experiments

4.3.1 Gain Effects on the signal speckle - baseline vs. variations by pump shaping

The effect we wish to study in this chapter is the possible manipulation of the amplified signal's speckle pattern by the choice of the modal composition of the pump. A crucial pitfall we must avoid is that the modulation of the pump unavoidably comes with some penalty on the coupled power, resulting in varying values of the total gain; this in itself causes the signal's speckle to undergo changes.

In order to see why this is so, we may look at the decorrelation (as a function of the gain value) that the signal speckle coming out of a non-pumped fiber would exhibit, were a completely spatially homogenous population inversion to appear and produce said gain. This amplification state is described as the one where all the active ions throughout the fiber are uniformly excited; In our work, this remains a hypothetical definition, but it is by no means unrealistic - for example, it could be achieved by pumping the system with a source of sufficiently low coherence. It should be understood that such gain would significantly alter the signal speckle (with respect to the non-pumped case) due to two main reasons:

1) The distribution of the doping ions is not uniform throughout the entire waveguide structure - it is limited to the core. Therefore, differential gain would develop between the signal modes, with the higher-order ones (which extend more into the cladding) undergoing less amplification. Even with relatively small gain differences that would not considerably alter the distribution of power between the signal modes, significant decorrelation of the speckle may arise due to differential phase-shifts. This was numerically demonstrated in our simulation, as was described in the previous chapter.

2) Pumping the fiber always incurs some transfer of thermal energy to the fiber, and the heating of the waveguide may alter the signal speckle because the refractive index varies slightly with temperature. For the case of an amplifying fiber, the thermal effect is understood to arise notably due to the fact that most transitions of the electrons within the upper and lower manifolds are non-radiative, i.e. the electron relaxations release phonons within the glass host [5,6]. However, even in a passive fiber, pump injection will induce some modifications of the output speckle of a signal beam, although no gain is present. This was experimentally demonstrated in our setup, as was described in the previous section (the 'benchmark' experiment).

Considering these effects of a spatially homogenous pump, it is evident why such pumping should be defined as the 'baseline' from which our observations will be isolated, in order to faithfully measure the effect of our shaping. Although this case represents a (spatially) fully-determined pumping configuration, with zero degrees of freedom allowed for choosing the pump's modes, it already produces a net change of our output speckle. Therefore, it stands as a 'DC' level of signal

decorrelation, and the amount of decorrelation brought about only due to our shaping of the pump has to be measured as a variation with respect to it.

The following experiment was conducted in order to demonstrate the difference between the baseline, and the desired variations attributed to the pump shaping: At first, a reference image was taken with the pump fully turned on but with no shaping ('flat' phase mask on the SLM). Then, several hundred random masks were displayed, representing randomized pump shapings, inevitably having different coupling efficiencies. The spatial modulation of the pump followed the scheme presented and used in section 2.4, namely - phase and amplitude modulation of a grid of SLM gratings in an off-axis scheme. This was done in order to explore the space of possible modal configurations as fully as possible. For each mask, the image of the signal output was correlated with the initial reference image, and the relation between the found decorrelation (Y axis) and the measured gain (X axis) was plotted as a scatter plot, displayed in figure 4.9.

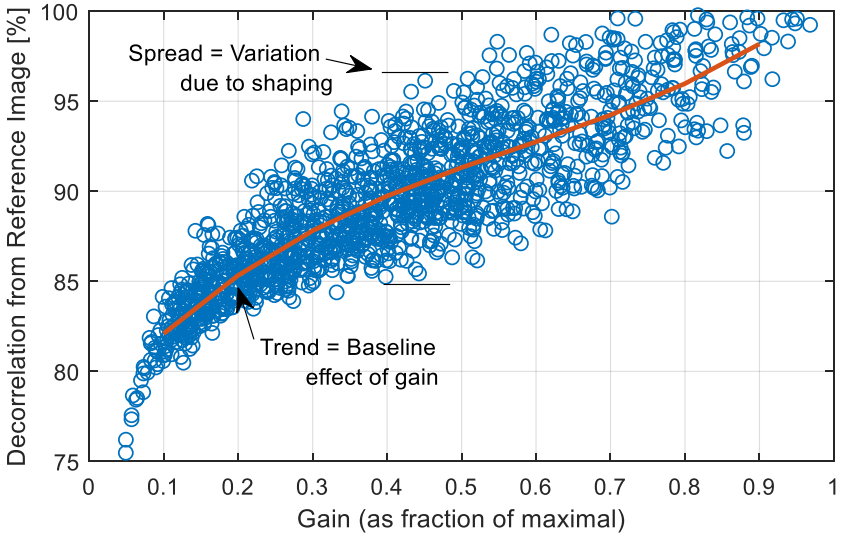

Figure 4.9: Scatter plot of measured signal speckle decorrelation, for 1500 random pump configurations

As can be seen by the dominant overall trend, there is strong correlation between a drop in gain and decorrelation of the signal with respect to the 'maximal-amplification' speckle (i.e., the one obtained at the 'flat phase' pump shaping). This trend represents the **baseline** - the modulation of the speckle inevitably contributed by the overall presence of gain, regardless of pump spatial distribution. Note that the total amplitude of this baseline – i.e., the overall decorrelation between maximal amplification, and no gain at all – is, in our case, not much more than 25% decorrelation. Based on the theoretical model, it should not necessarily be expected that this total decorrelation be very large (e.g. close to 100%), because it represents only the *differential* gain experienced by the signal modes (although there is also a small component of thermal decorrelation, as the measurements is section 4.2.6 indicate).

More importantly -the effect we wish to demonstrate is represented by the **spread (in Y) around this baseline** at some given gain value - meaning, the decorrelation of the speckle one may induce by choosing different pump configurations that share the same amplification.

4.3.2 Results of Pump Shaping – Maximizing Signal Decorrelation

Having described the observable expression of the effect at the center of our interest – namely, the dependence of the amplified signal's speckle pattern upon the modal composition of the pump - we are now ready to directly measure it. Moreover, our purpose is to see the maximal extent of this dependence, or in other words – to what degree may the signal's transmission be modified by the choice of the pumping configuration. For this purpose, an optimization process which searched for the *highest possible difference* (spatial decorrelation) between equal-gain signal outputs was implemented. For a given signal injection, the optimization function randomized the phase and amplitude across the pump SLM and compared the resultant amplified signal speckles in pairs; The equal-gain constraint enforced (in order to isolate, as was discussed above, the difference attributed solely to the spatial distribution of the pump speckle, from the gain-dependent baseline) was that two configurations were allowed to be compared only if their gains differed by less than 5%.

As discussed in section 2.4.2, our chosen spatial modulation scheme was based on the 'off-axis' misalignment of the SLM (so as to eliminate the constant, non-modulated contribution), and on the modulation of both the phase and the amplitude of the gratings displayed across the SLM area. These choices were meant to ensure the fullest possible access to the space of possible pump modal compositions. At first, the shaping scheme was taken as a 3x3 grid across the pump SLM, representing 9 independent modulation points (18 degrees of freedom, since both phase and amplitude were controlled).

The optimization was run on several tens of different signal injections; five cases which converged successfully to an appreciable change in the output speckle are presented in figure 4.10. Each row in the figure represents one case (i.e. one specific injection of the *signal* input); the pair of output speckles corresponds to the two most-distant *pump* configurations that were found by our optimization process. The SLM masks which correspond to all found pump configurations are presented in appendix B.

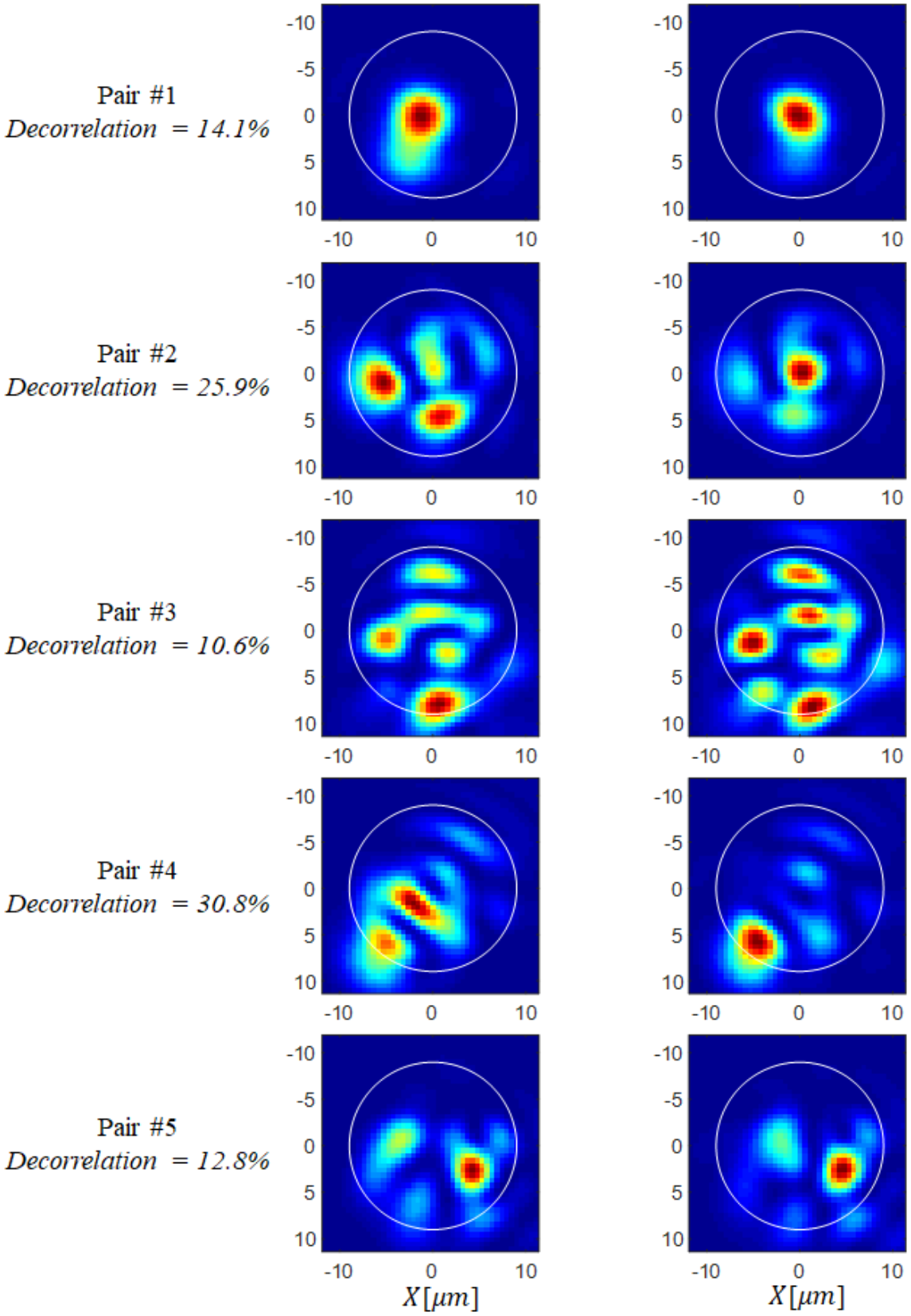

Figure 4.10: Results of the signal decorrelation optimization performed with the pump shaping controlled by a 3x3 point grid. Each row represents a different case of initial injection of the signal into the amplifier; the 2 images represent the found pair of equal-gain output speckles with maximal spatial difference.

It is apparent from these results that a clearly discernible, non-negligible dependence of the amplified signal's modal composition on the pumping configuration was demonstrated. The degree of maximal change that could be obtained was significantly different for different initial signal injections; however, it can be generally observed that whatever the signal injection was, the degree of decorrelation achievable through pump shaping was, as expected based on the arguments presented in sections 3.3.2-3.3.5, limited: The output speckle for a given case always remained more or less composed of the same sub-set of speckle grains, with the total decorrelation almost entirely explained by a change in their relative power ratios, rather than the appearance of new grains/the complete disappearance of existing grains.

Next, the same optimization procedure was attempted with 4x4 grid of modulation points on the pump SLM. This elevated number of degrees of freedom should, theoretically, permit fuller control of the pump's modal composition, as the total number (16 points) is nearly equal to the estimated number of modes supported by the fiber. On the other hand, the nearly two-fold rise in the number of variables to control presented a sizeable increase of complexity of the optimization function's task. It should be stressed again that the non-linear nature of our problem (stemming from the fact that we control the pump's modes, i.e. the light field, while the effect on the signal is dictated by the modes' combined intensity profile) prevents the reduction of its complexity by separately treating each modulation point – as done, for example, in the TM-based focusing method 'classically' performed on the input field of the same lightwave being observed.

The optimization was run on several different signal injections, three of which converged successfully to an appreciable change. The results are shown in figure 4.11, in the exact same convention as previously explained for the experiments presented in figure 4.10.

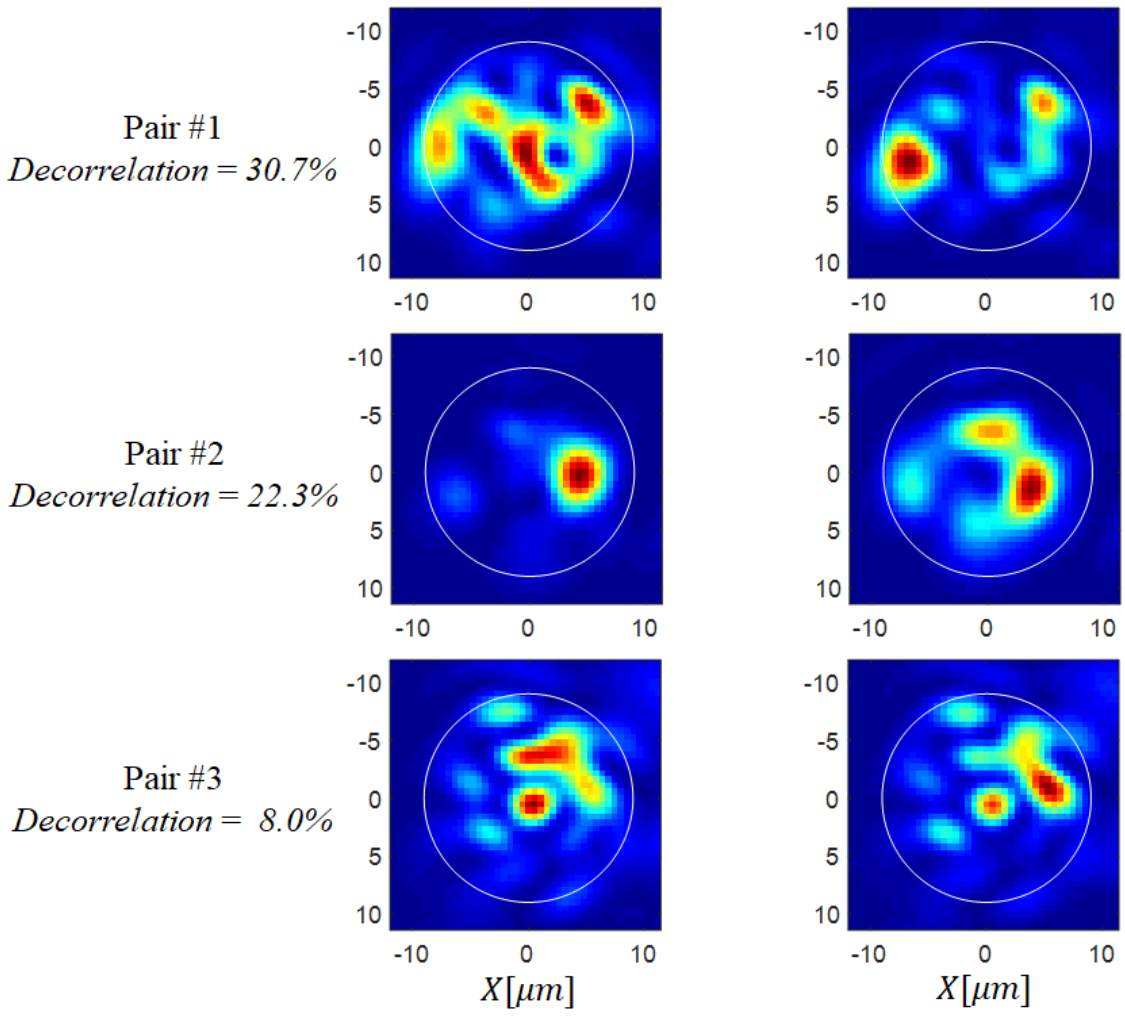

Figure 4.11: Results of the signal decorrelation optimization performed with the pump shaping controlled by a 4x4 point grid. Each row represents a different case of initial injection of the signal into the amplifier; the 2 images represent the found pair of equal-gain output speckles with maximal spatial difference.

4.4 Discussion and Summary

The experimental implementation of a multimode fiber amplifier system with wavefront shaping of the pump was presented. Based on the theoretical predictions for such a system, given by our model and numerical simulations (covered in chapter 3), we expected to see an ability to manipulate - but not fully control - the signal's output speckle. However, the expectation of observing non-negligible ability of manipulation was not trivial, due to the characteristics inherent to the pump-medium and medium-signal interactions: the absorption saturation restricting the spatial contrast of the excitation contrast, the scalar nature of the excitation restricting the selectivity in terms of the signal modes, and the self-averaging brought about by the complicated evolution of the intensity patterns along the fiber length, due to the modal dispersion.

The experiment fully supported the theoretical predictions: discernible decorrelation of the output speckle could be clearly achieved by selecting different modulation masks for the pump beam. The measures taken to separate the results of this selection (that is, the choice of the pump's modal composition in the waveguide) from the overall effects of the gain, served to demonstrate that indeed, the signal's TM of the MMFA has a significant component dependent on the pump's modal content.

In view of the limitations discussed above, the system's flexibility – which remained quite far from the prospect of forming any arbitrary desired speckle pattern at the output – generally agreed with our expectations. In particular, the different amplified speckles that could be obtained by varying the pump's shaping for a specific initial signal injection, seemed to be largely composed of the same speckle grains, with the attained decorrelation being mostly the result of changes in the relative intensity and phase of these grains. This behavior naturally stems from the system's function as an amplifier (in particular, one where the complete suppression of an injected mode, or the significant excitation of a mode not present in the injection, is essentially prohibited). In short, the system's output strongly depends on the 'initial-conditions' factor – namely, the choice of the input signal injected into it. Superposed upon this factor are the effects of our choice of pumping configuration – namely, some control of the relative weights (and phases) between the gains seen by each signal mode.

Going forward, it might be speculated that further investigation of the flexibility of this system could be promoted by improving the multi-variable optimization procedure, more specifically its ability to handle a higher number of degrees of freedom; for example, one limiting factor experienced in this work was the long durations of time needed in order to explore the vast space of possibilities offered by an optimization problem depending non-linearly on several tens of independent variables. Eventually, when these time durations increased so as to be comparable to the typical times (on the order of an hour) over which the set-up's alignment remains tolerably stable, this issue presented itself

as the major limit for assessing the achievable degree of manipulation of the signal. Therefore, a feasible direction for further research could be either the speeding-up of the modulation-to-measurement cycle (which is the basic building block of the optimization process), or the implementation of better search algorithms.

References for Chapter 4

[1] K. Okamoto, T. Okoshi, Analysis of Wave Propagation in Optical Fibers Having Core with Alpha-Power Refractive-Index Distribution and Uniform Cladding, IEEE Trans. On Microwave Theory and Techniques, Vol. MIT-24 No. 7, 416-421 (1976).

[2] D. Gloge, E. A. J. Marcatili, Multimode Theory of Graded-Core Fibers, Bell Sys. Tech. J., Vol. 52 No. 9, 1563-1578 (1973).

[3] H. Tünnermann, J. Neumann, D. Kracht, P. Weßels, Frequency resolved analysis of thermally induced refractive index changes in fiber amplifiers, Opt. Lett., Vol. 37, No. 17, 3597-3599 (2012).

[4] D. C. Hanna, I. R. Perry, R. G. Smart, P. J. Suni, J. E. Towsend, A.C. Tropper, Efficient Superfluorescent Emission at 974nm and 1040nm From an Yb-Doped Fiber, Opt. Comm., Vol. 72 No. 3,4, 230-234 (1989).

[5] H. Takebe, T. Murata, K. Morinaga, Compositional Dependence of Absorption and Fluorescence of Yb+3 in Oxide Glasses, J. Am. Ceram. Soc., Vol. 79 No. 3, 681-687 (1996).

[6] A.A. Fotiadi, O. L. Antipov, P. Mégret, Dynamics of Pump-Induced Refractive Index Changes in Single-Mode Yb-doped Optical Fibers, Opt. Exp., Vol. 16 No. 17, 12658-12663 (2008).

5 Wavefront Shaping of the Pump in a Lasing Cavity Configuration

The work presented so far has dealt with a system in which a multimodal signal, provided by an external source, enters our gain medium, and the particular way in which the heterogeneous excitation is arranged within the volume affects, through the amplification process, its final state at the output. In this chapter, we study a system that is fundamentally different: There is no external injection of the signal. Rather, it is generated within our gain medium by a lasing process, which means that the specific signal observed at the output has emerged out of a hypothetical space of many different possible outputs, by crossing the oscillation threshold. The existence of a threshold where a dramatic selection takes place between the modes precisely reaching it, and those failing to do so (even by a small difference), leads to the expectation of strong sensitivity to changes in the system, including the type of spatial modulation (of the pumping) we employ in our study. This is interesting from the viewpoint of applications where the ability to manipulate and control the output of a fiber-based laser is desired. Furthermore, a lasing system has the intriguing property of functioning as a sort of "self-organizing" solver, in the sense of the system's geometry being viewed as a "problem", and the lasing mode appearing is the solution which the cavity "found by itself".

The chapter will begin by discussing these motivations; then the theoretical modelling and the experimental work carried out on our fiber-based system shall be presented. In contrast to the organization of previous chapters - where first a detailed theoretical model was put forth, to be then followed by the description of the experimental work and the comparison of its results to the predictions of the former - the current chapter is organized differently, with a slightly more empiricism-driven outlook: We began by describing the experimental setup of a fiber-based lasing cavity (in its several different variations) and some preliminary results observed in them. We continue with a theoretical discussion of these observations and illuminate the major phenomena behind them; And having establishing a toy model of the system, we return to the experimental domain, this time performing spatial modulation of the pump, with the control of the laser emission as the goal in mind. Hopefully, this organization of the chapter will prove more instructive and readable, by avoiding a lengthy and abstract theoretical discussion of the many intricate aspects which drive the system behavior, before any tangible observations are presented.

5.1 Background and Motivations

Complex lasers featuring scattering due to disorder within their cavities - typically referred to as "random lasers" - have been the subject of lively research in recent years. Specifically, the control of the emission of such lasers by the tailoring of the spatial structure of their pump has been studied and published in two main types of systems: An optofluidic random laser, where the pump was modulated in a one-dimensional scheme along the lasing channel [1-3], and a semiconductor microdisk cavity over which a two-dimensional modulation scheme is applied [4-7]. Illustrations extracted from the references are displayed at the top panels of figure 5.1. It should be stressed that the "randomness" of these lasers does not immediately arise from the complexity and multimodality of the cavity, but rather from the presence of scatterers arranged in a disordered pattern within the cavity (dielectric pillars with random positions along the channel in the first type of random laser; the roughness of the microdisk edges in the case of the second type).
Although several critical differences exist between these works and ours, such as:

- The fact that our system cannot be considered as a random laser;
- The presence of an optical waveguide with well-known modes in our system;
- The fact that the pump does not transverse our system perpendicularly, but rather propagates within it along with the signal and hence must be considered in no less than three dimensions;

To name a few – still, the successful control of lasing by pump shaping demonstrated in these references, encourages the study of a similar scheme in our fiber-based cavity. A fundamental conclusion derived in these previous works (in particular, see [2] and [7]) is that, although the different lasing modes strongly overlap within the medium, selection between them by adaptive pumping may be exercised – not by perfectly 'matching' the pump to some desired mode – but rather by the tailoring of the pump so as to target the terms of cross-saturation in order to 'throw' the competition between the modes in favour of the desired mode.

An altogether different context in which the study of complex lasers has recently flourished is the consideration of such lasers as "self-organizing" solvers. In this approach, we wish to find - out of all possible paths for propagation in the complex cavity - the one characterized by the highest metric of some kind (this is the 'problem to solve'); and the engineering of some loss mechanism corresponding to said metric facilitates an "all-optical solution" of the problem, meaning that the lasing mode appearing in the cavity may be readily identified as the desired path. In this sense, the lasing phenomenon is interpreted as the "computation" of the optimal solution of some optical problem. The idea of lasers as self-solving systems has motivated several works based on a free-space cavity that is highly multimodal in the spatial domain, with notable examples of the problems optically-computed being focusing behind a layer of scatterers [8], the retrieval of the phase after scattering by an arbitrary

transparency [9], and the shaping of propagation invariant beams with complex transverse profiles [10]. Illustrations extracted from these references are displayed at the bottom panel of figure 5.1.

In the spirit of such an approach, we may also view our study of the effects of pump shaping in a fiber-based laser as having the interesting potential of setting-up problems related to propagation in multimode fibers, for similar optically self-solving schemes.

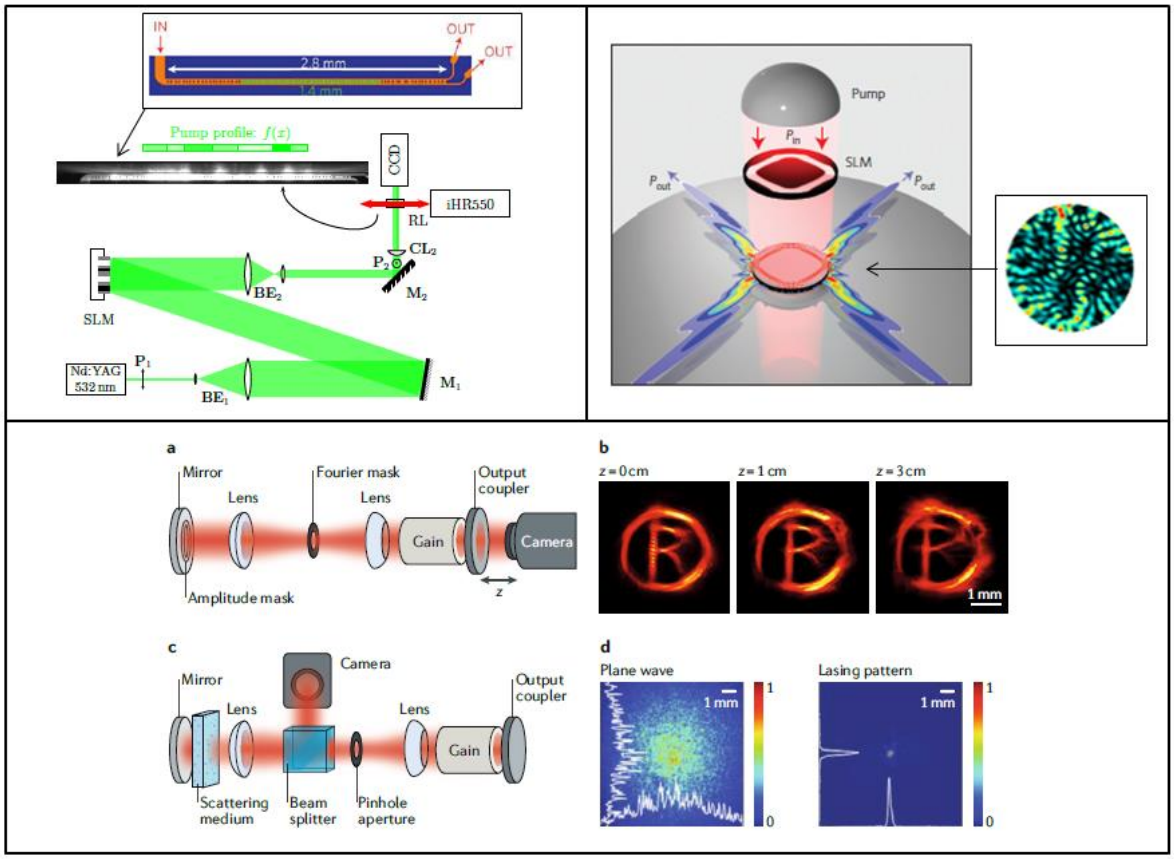

Figure 5.1: Examples of disordered and complex lasers studied within the context of wavefront shaping. Top left – a setup for the control of a lasing optofluidic channel with random scatterers, with a 1D pump-modulation scheme, taken from [3]. Top right – a setup for the control of a lasing semiconductor microdisk, with a 2D pump-modulation scheme, taken from [4]. Bottom panel – an excerpt from [11] reviewing two experiments based on a "self-solving" lasing cavity: (a) and (b) illustrate a cavity for shaping propagation invariant beams (see [10]); (c) and (d) illustrate a cavity for focusing behind a scattering layer (see [8]).

The oscillation dynamics of a cavity that is multimodal both in the longitudinal (i.e. frequency) domain and the transverse (i.e. spatial) domain, may potentially be extremely complex and difficult to predict. For some cavity mode to stand as a 'candidate' for oscillation, a single relation must be fulfilled: that of the standing wave, namely - that its propagation through a full round-trip of the system be the identity operation. In a cavity such as ours, the number of possibilities to construct a mode satisfying this single condition are vast: Any of the spatial modes may 'find' many frequencies in which its effective wavelength is an integer multiple of the round-trip length. Furthermore, a *combination* of several spatial modes (of the waveguide) may also be a legitimate cavity mode, if

some frequency is found for which each of the effective wavelengths happens to be an integer multiple of the length. In the presence of broadening mechanisms (see discussion in the theoretical background section 1.4.3), the richness of the mode space naturally leads to an abundance of possibilities of competition between coexisting lasing modes. It should also be noted, that in Yb-doped silica fibers, the homogeneous linewidth broadening and the inhomogeneous broadening are of comparable magnitude [12-13]; this further compounds the complexity of the mode competition, since both spectral and spatial hole burning effects play a role.

Consequently, the complete and precise modelling of such a system (that is, a model encompassing the entire space of modes over the frequency and the spatial domains) remained beyond the scope of this work (even for the below-threshold regime). The approach adopted for studying the system was that of comparison between different architectures. By implementing different variations of the cavity's design, some separation of the different mechanisms coming into play was obtained.

5.2 Experimental Setup and Some Elementary Results

5.2.1 Experimental Setup and Typed of Fiber-Based Cavities Implemented

The setup for studying lasing in a multimodal amplifying fiber was based on the same pump source and scheme for its spatial shaping, as well as the same Yb-doped fiber, used for the amplifier configuration experiments of the previous chapter. Therefore their description, which may be found in sections 4.1-4.2, shall not be repeated. The two main differences with respect to the amplifier configuration were the removal of the external signal source (the 1030nm source), and the assurance of lasing conditions in the pumped fiber, by implementing a cavity in two different designs:

(I) Cavity consisting of nothing but the fiber itself, where the two ends function as the cavity mirrors, thanks to the Fresnel reflections from the silica-air interface. In this case, no optical components are added to the setup, and the condition of oscillation is ensured by setting the length of fiber long enough so as to enable sufficient gain due to good absorption of the *pump* power, but not long enough to add too much loss (by absorption of the *signal* in a segment that will remain unpumped - see discussion in section 4.2 where this was done intentionally). Furthermore, the fiber ends must of course be cleaved without an angle that supresses back reflections, i.e. cleaved perpendicularly to the fiber axis. For silica's refractive index of ~1.45, the well-known Fresnel equation $R = ((n_1 - n_2)/(n_1 + n_2))^2$ gives a reflection coefficient of 3.4%.

(II) Cavity consisting of the fiber and external optics which form, at each of the two ends, a 2f imaging system folded upon itself that reproduces the fiber outgoing light field as a re-entering one. On the side from which the system is pumped, the mirror used was a dichroic mirror (short-pass with edge at 1μm, supplied by Semrock) so that the pump beam could be injected through it. On the other

side, a partial-reflectivity mirror (with 96% reflectivity at the signal wavelength range, supplied by Layertec) was used to act as the cavity coupler. It should be noted that the addition of the external mirrors does not eliminate the reflections from the fiber facets; however, since the reflectivity of the latter are significantly weaker than those of the former, they shall be neglected in our analysis.

These two implementations are schematically illustrated in panels (a) and (b), respectively, of figure 5.2. Not shown in these schemes is the output measurement side, which consisted of 2 parts – spatial imaging (again, identical to the one in the amplifier configuration setup), and measurement of the output's spectrum by a grating-based spectrometer (Horiba, model iH550, featuring a resolution of ~50 pm).

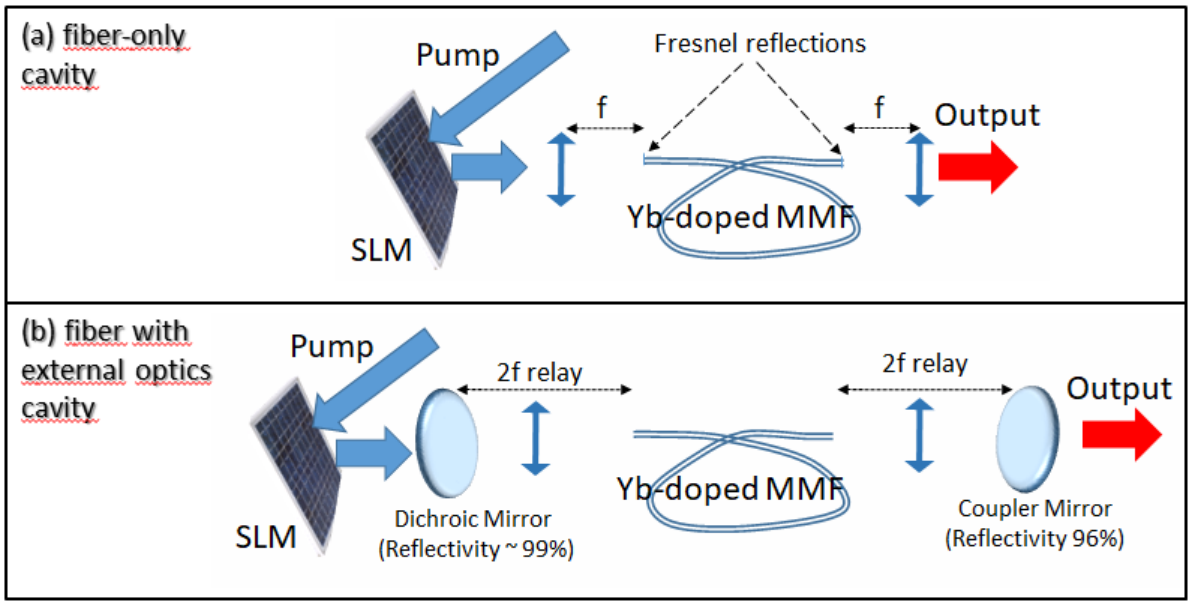

Figure 5.2: Schematic description of the two versions of a lasing cavity implemented; Top – the amplifying fiber itself serves as the cavity; Bottom – the fiber is surrounded by external optics which reflect the outgoing light at each end back into the core with by means of a self-imaging 2f system.

5.2.2 Lasing in the fiber-only cavity

The essential observations of lasing in the MMF fiber-only cavity are summed in figure 5.2: On the left side, four examples of the spectrum measured at the output, representing four 'snapshots' during a gradual increase of the pumping, show the transition from a broad ASE source operating below threshold (the first two spectra), to a lasing system – first (as seen in the third spectrum, right after the threshold has been crossed) onset of oscillation of a single mode, and later (fourth spectrum, representing maximal pumping) the rise of another oscillating mode co-existing with the first.

On the right side, two images of the fiber's output facet are displayed: The first is the incoherent ASE emitted in the below-threshold regime, and the second is the emission seen in the lasing regime. The ASE fills, as could be expected, the entire core; conversely, once lasing sets in, the pattern which appears is more much confined, because it is in fact none other than the fundamental mode of the

fiber. Its spatial profile and waist width fits well the theoretical prediction for the LP01 mode of our graded-index fiber (see section 1.2.3 in the background chapter for the relevant relation between the core's refractive index profile and the resulting shape of the fundamental mode). It should be remarked that this observed intensity pattern remained the same for different levels of pumping (from the threshold and upwards, of course), and for different coiling or positioning on the table of the fiber (although such physical perturbations shifted and changed quite easily the positions of the lasing modes in the spectrum). This indicates a persistence of the fundamental mode as the only spatial mode to participate in the lasing, even while a few different longitudinal modes are involved, or while the cavity geometry is modified.

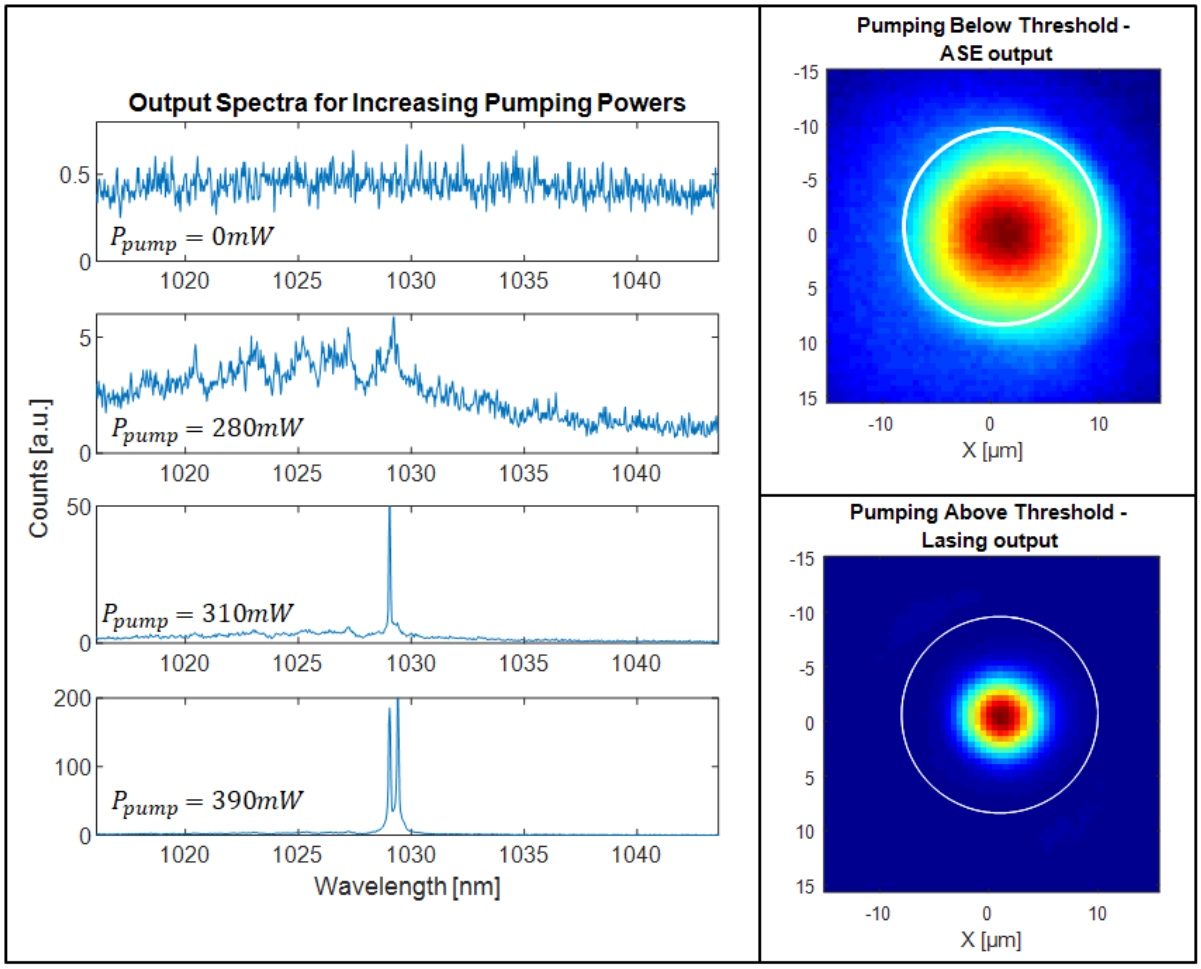

Figure 5.3: Elementary results for the fiber-only cavity. Left – four spectra representing the output for increasing (from top to bottom) pumping power, in order to demonstrate the clear observation of lasing beyond a certain threshold. Right, top and bottom – the image of the fiber output facet, below and above the lasing threshold, respectively. The white lines indicate the fiber core.

5.2.3 Lasing in the cavity based on external optics

The primary goal of the introduction of external optics is improvement of the cavity's quality (in the sense of reducing its losses), so that the oscillation condition may be reached earlier (i.e. at lower

pump powers); as the Fresnel reflectivities which define the fiber-only cavity are quite low, it comes as no surprise that the addition of the two mirrors as illustrated in panel (b) of figure 5.2 significantly lowered the lasing threshold. In the spatial domain, as well, the introduction of the external optics brings about discernible changes. The lasing emission is no longer the pure fundamental mode. However, it does not resemble a fully developed speckle either; rather it is appears to be the fundamental mode with low-order aberrations and distortions, meaning it is a superposition a few low-order modes of the fiber.

Furthermore, and contrary to the previous 'fiber-only' case, where the spatial image of the output was independent of perturbations to the fiber, the lasing was now exhibiting a certain sensitivity to such changes. This is demonstrates in figure 5.4: the four examples of intensity patterns seen at the fiber's output facet were obtained by gently moving and curving the fiber on the optical table (without disturbing the optics which define the cavity

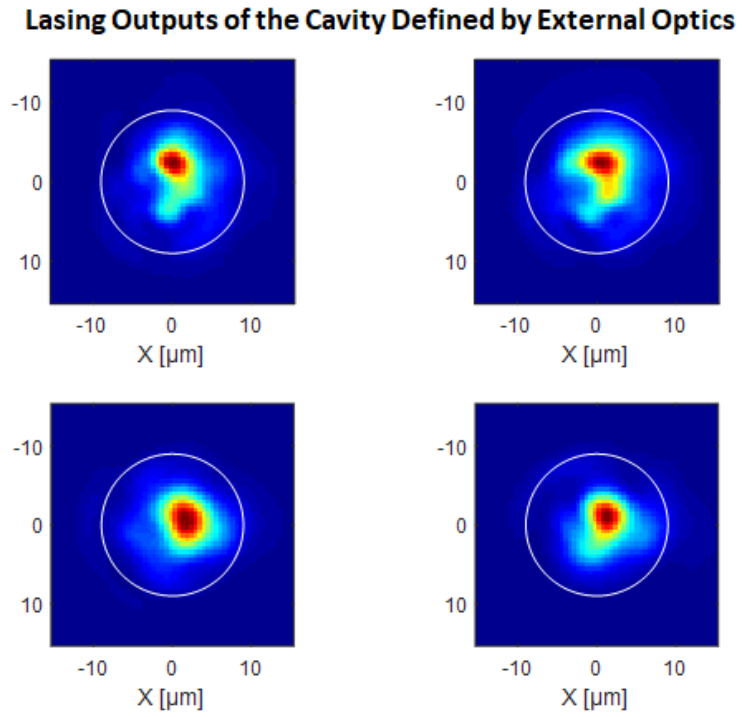

Figure 5.4: Elementary results (intensity patterns above threshold) for the external-optics cavity, showing several low-order spatial modes (not just the fundamental) are oscillating. The four patterns represent different stable positions in which the fiber was placed on the optical table (i.e; the fiber was perturbed between images, but each represents a stable lasing output taken at a static configuration). The white lines indicate the fiber core.

5.2.4 Range of Lasing Wavelengths in Both Cavity Types

The introduction of the external optics affected the spectral domain as well. In order to examine the difference, many spectra were taken in each of the two cavity types; a side by side comparison of examples chosen to represent the variance over the wavelength axis are displayed in figure 5.5. For each cavity, the variation among spectra represents different positioning or coiling of the fiber, in the

same way that was described above where the sensitivity of the spatial patterns to small cavity perturbations was tested. The purpose here was not to assess the sensitivity itself (which was high for both types), but rather to explore the spectral range over which each cavity may oscillate. As can be seen, the range of potential lasing modes is smaller for the fiber-only cavity; all modes are found in a band of roughly 8-9nm width. Conversely, for the cavity with external optics, modes may be excited from about 1026nm to about 1048, representing a range of over 20nm width.

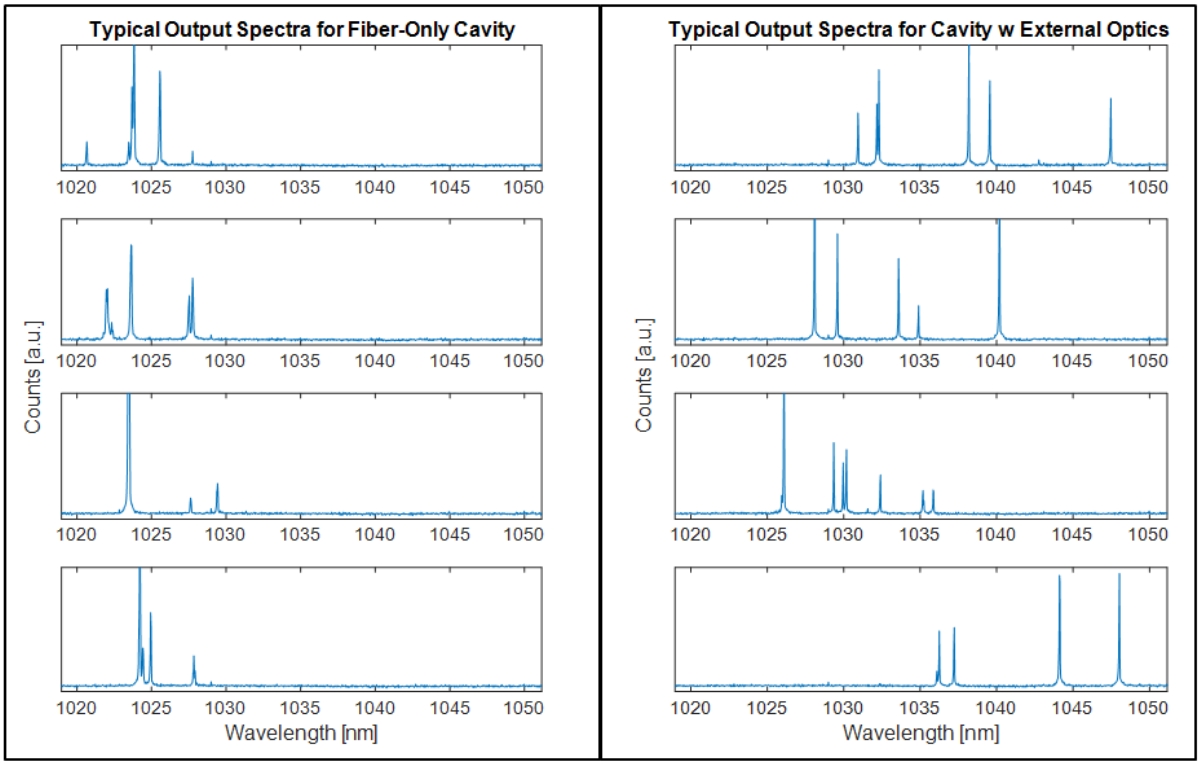

Figure 5.5: Comparison of the typical lasing spectra of the fiber-only cavity (left panel) and the cavity with external optics (right panel). In each panel, the four spectra represent different stable positions of the cavity (i.e, the placement of the fiber on the optical table and the external optics were perturbed between measurements, but each represents a stable lasing output taken at a static configuration). The range of wavelengths over which the external-optics cavity can potentially lase is significantly larger.

The immediate questions that arose were, what determines the spatial forms the lasing emission takes on, and can a correlation between the spatial and the frequency domains be found. More concretely - whether or not specific intensity patterns showing up on the camera correspond to specific lasing modes detected at the spectrometer. Already for the elementary results presented above, the comparison between the types of cavity hints that a strong connection exists between the two domains. This subject will be studied in the following theoretical discussion, as well as in the pump-shaping experiments.

5.3 Theoretical Discussion of Lasing In Fiber-Based Cavities

In the general discussion of lasing in the background chapter (section 1.4) we saw how first of all, the 'cold' Fabry-Perot cavity defines discrete resonances solely by virtue of its geometry, then the addition of gain to the system may drive some of these resonances to oscillation. Our fiber-based laser is fundamentally no different: our discussion of it should begin by first considering the passive geometry, then the gain process. Its particular richness and interest (with respect to the one-dimensional model presented in chapter 1) will emerge from the fact that the propagation between the boundaries is supported by a waveguide that is multimodal in the transverse coordinates; and further unique traits, as we shall see later, will arise due to the ability to pump the medium in a spatially-varying scheme.

We begin the discussion by examining the fiber-only cavity. If the fiber is singlemode, then the case is essentially that of the 1D Fabry-Perot system analysed in the general theory chapter: the system's resonances are described by a single 'comb', as represented in figure 1.10, extending along the frequency axis because each discrete peak corresponds to a different longitudinal mode. If, however, the fiber is multimode, another axis is added to this picture, representing the fact that each spatial mode may propagate inside the cavity, at any of the frequencies which happen to correspond to a standing wave with the particular effective refractive index that this spatial mode sees in the fiber. Implicit in this analysis is the assumption, that each LP modes is an eigenmode of the fiber cavity, meaning that it remains unchanged while circulating within it. This assumption is a very reasonable one, since an LP mode has only transverse components of the electrical field (see eq. 1.4), and therefore would be reflected from a perpendicular facet with a uniform reflection coefficient, i.e. with no change to its field except the reversal of the propagation direction. As for the propagation itself within the fiber, the validity of treating the LP modes as good approximations of the pure eigenmodes of MM fibers of lengths in the cm/meter range is discussed in section 3.2.1.

In other words, each LP mode identified by some l, m indices will retain its own 'comb' of resonances, with peaks at optical frequencies at integer multiples of the term $\pi c/L \cdot n_{l,m}$ (same as in eq. 1.18, but with the light's phase velocity dependent upon the specific spatial mode concerned). . Panel (a) and (b) of figure 5.6 (found in pg. 132) illustrate, in the spirit of the above descriptions, the cavity resonances for a SM and MM fiber, respectively.

Note: Of course, if one is interested only in the frequency domain, one could "collapse" the dimension of the different spatial modes and represent all resonances together on the frequency axis – the result will be a superposition of N combs shifted with respect to one another, and also featuring slightly different FSR spacings, due to the modal dispersion relation. We will, however, continue to use the two-dimensional depiction of figure 5.6, where the combs of different LP modes remain separated and identified, because we are interested not only in their frequencies but also in the spatial distribution of their optical fields.

A point should be noted to conclude our discussion of fiber-only cavities (before moving on to cavities containing additional external optics), concerning the relative height of different cavity resonances (i.e. their peak values of transmission) in the presence of gain. In the SM case, we expect to find the comb modulated by an envelope embodying the spectral gain curve of the amplifying medium, as was explained and illustrated in section 1.4.3 (indeed, panel (a) of figure 5.6 in this current chapter is essentially identical to figure 1.11). In the MM case, as is illustrated in panel (b), the same spectral modulation along the frequency axis holds true for all spatial modes; and in addition, the entire comb of each individual spatial mode would potentially be multiplied by its own gain coefficient, reflecting the fact that different LP modes might experience varying amplification strengths, depending on their spatial overlaps with the excitation of the gain medium. In short, the two-dimensional 'field' of potential cavity modes is modulated by two different trends, the first representing the gain medium's response in the optical wavelength axis, and the other representing the variation in gain efficiencies among the fiber's spatial modes.

The other panels of figure 5.6 (c-d) illustrate cases of cavities defined by external optics, as already described above in section 5.2; we now turn our attention to this architecture. Two new aspects which will act upon the transmission in an interesting way may be summarily pointed out:

1) By necessarily adding some slight aberrations and misalignments in the optical relay (the collimation, reflection and re-focusing into the fiber), the external optics may serve as mode 'mixers'. Unless their transmission is a perfect self-imaging operation, which reproduces as input to the fiber the exact same beam that appeared as its output - they will alter the modal content by coupling each of the outgoing spatial modes to others.

2) Reflection and re-injection into the fiber that are different from perfect self-imaging will, in addition, also be non-unitary, since coupling into a fiber's core represents a spatial filter. This may serve to strongly attenuate some of the modes by efficiently coupling them into non-guided modes, which represents net loss, while keeping the efficiency of re-coupling back into the core high for others.

A more thorough discussion justifying the above analysis, including some numerical modelling of the system's transmission, is given in Appendix C. Within the chapter, for the sake of brevity, we shall move ahead and arrive directly at the important conclusions. The combination of external optics and the fiber waveguide induces upon the system eigenmodes which are *combinations* of the fiber's LP modes. First of all, this shall be evident in the spatial domain, where the lasing modes (which must be eigenmodes of the cavity) will take on forms resembling speckles, since they will be superpositions of several LP modes. Note that in this case, the spatial shape of a lasing mode is expected to evolve as it propagates along the fiber length, as the different waveguide modes de-phase with respect to each other; of course the condition of repeating the exact same field distribution after a full round-trip is

fulfilled (it is the very definition of a cavity eigenmode), but throughout this propagation quite complex evolution of the intensity pattern may occur.

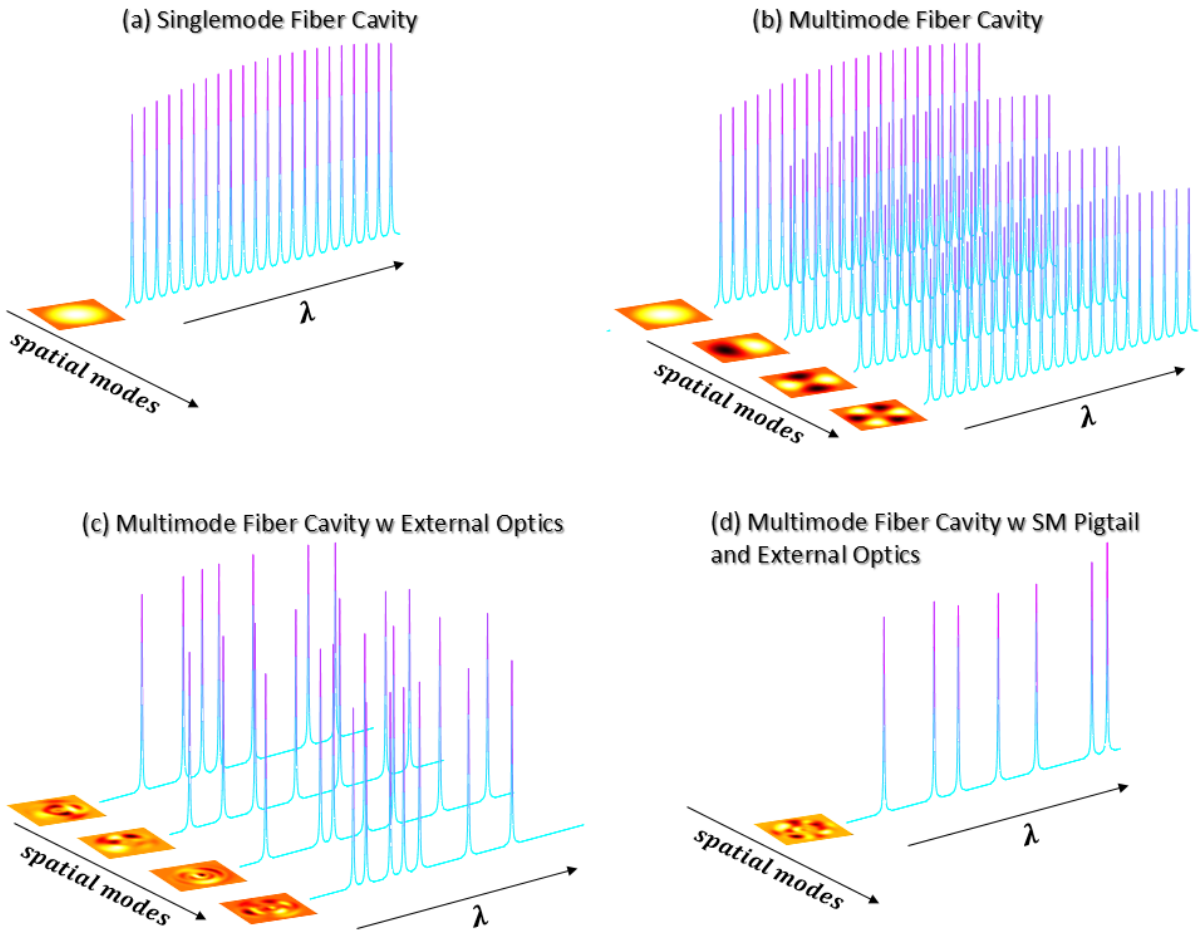

Figure 5.6: Conceptual illustration of the space of potential lasing modes, for the four different fiber-based lasing cavities treated in our work. The space is depicted as a 2D plane defined by the wavelength axis and the axis of the waveguide's spatial modes.

Secondly, considering the frequency domain: the condition for a standing wave shall now involve multiple requirements on the different modal phase velocities associated with any given wavelength (corresponding to the different LP modes "forced" by the free-space optics to participate in some new eigenmode). The interesting result will be the "thinning out" of the spectrum of longitudinal modes supported by the cavity, since the fulfilment of the multiple conditions of resonance in the given cavity length, imposed upon the wavelength, will take place more rarely. Again, a more detailed discussion is given in the appendix (where it is shown the effect of larger spacing between lasing modes is equivalent to the slow beating appearing when several similar frequencies are superposed). Lastly, the longitudinal modes will not only be 'thinned out', but also their peak transmission values will vary as a function of the complex way the spatial filtering at the fiber facets and the multiple standing-wave

conditions combine to find a resonance. Therefore, we may say the cavity's passive geometry already contains an element able to superpose a non-uniform 'envelope' of efficiency upon the field of potential modes (contrary to the simpler fiber-only cavity, where resonances began exhibiting different peak transmissions only after the gain was added to the picture).

All of these effects are schematically visualized in panel (c) of figure 5.6: along the spatial modes dimension, the discrete 'coordinates' are no longer the pure modes of the fiber, but rather more complex superpositions of the LP modes, determined by the mixing added at the external optics. The space of potential cavity resonances is more sparse, due to the "thinning out" of the comb of valid standing waves per each spatial mode; moreover, the 'envelope' modulating the peaks of the resonances is more complex than the gain curve of the gain medium.

In the last panel (d) of figure 5.6 a further variation upon the cavity's architecture is presented: the addition of yet more spatial filtering by splicing a single-mode fiber to the amplifying multimode fiber as a pigtail. A schematic illustration of this arrangement is shown in figure 5.6. The SM pigtail is passive and does not contribute to the gain; its role is to function as a pinhole small enough to permit the passage of only one transverse mode. This imposes a condition upon any lasing mode travelling in the cavity, which will essentially reduce the degrees of freedom previously available to the cavity in the spatial-mode dimension, to a single option (due to the fact that the SM-MM interface uniquely dictates what combination of LP modes is guided in the MM fiber). Hence, the space of potential modes in our depiction "collapses" back to a 1D axis, as was the case for an entirely SM cavity in panel (a). However, the important difference is that the mode still constitutes a superposition of several LP modes of the active MM fiber, and therefore exhibits the spectral features established above in the discussion of panel (c). For the same reason, it also develops and changes as it propagates along the MM part of the cavity – with different longitudinal modes experiencing slightly different lengths of evolution. The significance to our work lies in the fact that different lasing modes, although all conforming to the constraint of the SM part, would still have non-overlapping intensity patterns throughout the MM part. This is in fact a generalization of the standing-wave 'shifting' mechanism at the root of spatial-hole burning phenomena (see discussion in section 1.4.3), from the case of a SM (one-dimensional) cavity, to our configuration where the intensity patterns exist in the 3D volume of the MM waveguide.

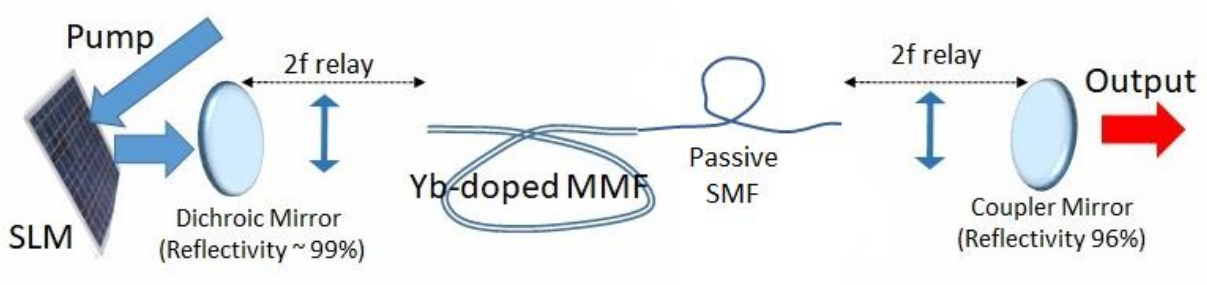

Figure 5.7: Schematic description of the external optics-based cavity with the addition of a single mode fiber pigtail – the configuration corresponding to panel (d) of figure 5.6.

The introduction of the SM pigtail as a spatial filter draws inspiration from previous works, that have studied – by employing a SM-MM splice - the self-imaging effect of MMF (i.e. the tendency of a multimode fiber to exhibit the Talbot effect, reproducing the initial field after a certain distance of propagation) [14]; and have harnessed this effect in a cavity with an active MMF in order to tune or control the lasing output [15-16]. By adding the constraint of the single spatial mode at one certain point in the system, the cavity is confined to solutions with a pre-determined modal composition, yet it can find such solutions at wavelengths whose multimodal interference (MMI) fulfils a self-imaging condition. From our perspective, this is instructive to the investigation of the effect of our pump shaping, since it reduces the a-priori vast space of potential lasing modes to a smaller sub-set with less ambiguity.

5.4 Main Experimental Results

5.4.1 Evidence of Modal Discrimination through the Pump Shaping

Our toy model suggested that the geometry of the cavity, particularly the fidelity of the imaging performed by the external (free-space) optics, is the primary factor influencing the selection of both the *spatial* modes participating in the lasing mode, and the particular *longitudinal* modes which will lase first. This leads to the expectation that if the free-space components were to be deliberately misaligned, the cavity would produce lasing emission containing more LP modes, and of higher order, and hence be characterized by more spatially-complex, 'speckly' patterns. Furthermore, different combinations of LP modes, corresponding to rather far-apart frequencies but having more or less similar lasing thresholds, could be expected to appear. Lastly and most importantly - since these different combinations represent potential oscillating modes, not vastly different in terms of possibility to excite, and yet clearly distinguishable (both in the spatial and frequency domains) - we may hope that the spatial modulation of gain distributed in the cavity, namely the shaping of our pump, would allow us to selectively favour or disfavour them.

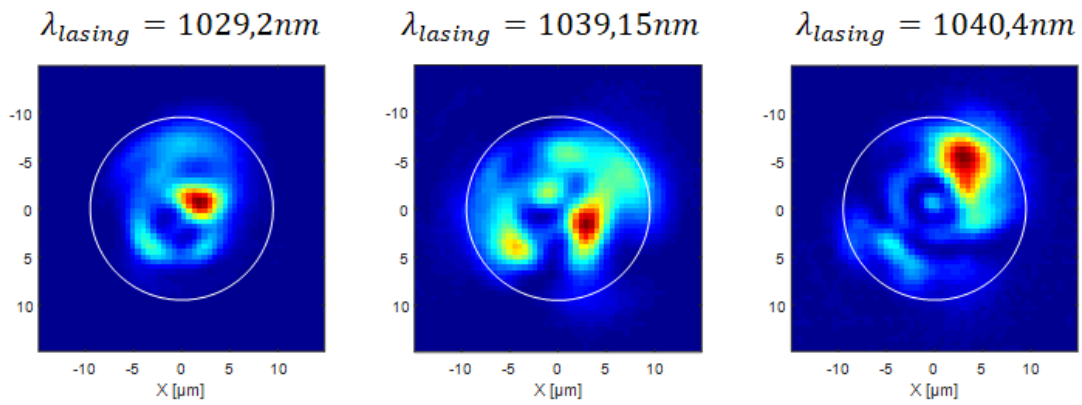

Figure 5.8: The speckle output (and wavelengths, displayed in the titles) of three different lasing modes, that have been isolated by optimizing the pump spatial modulation so as to select each one as the first-lasing mode, then attenuating the pump power to ensure single spectral-mode operation. As can be seen, different wavelengths correspond to different speckle patterns.

Indeed, this was found to be the case, as demonstrated in figure 5.8. The external mirrors providing the reflections back into the cavity were intentionally misaligned once (meaning they were not perturbed again for the entire duration of the experiment). The immediate result of misalignment was the development of higher-order speckle grains in the output intensity pattern; the degree of misalignment was fixed at a 'sweet spot' large enough to make this spatial effect clearly visible, but small enough to still guarantee oscillation. In fact, the cavity was kept at a sufficient margin above threshold so as to ensure the pump could be spatially modulated (i.e., so that the loss of pump power inevitably brought about by the wavefront shaping would not cause the loss of the lasing). Next, the distinct lasing modes shown in the figure were found by trying many random phase masks as pump modulation functions, identifying three configurations which happened to favour three different modes. Finally, the pump power was attenuated (while displaying each of the found masks) until only a single mode managed to oscillate. It should be made clear, that the choice of the pump shaping could not completely isolate each of modes, i.e. it could not ensure single longitudinal-mode operation at maximal pumping; but the results prove that the choice of pump shaping definitely succeeded in discriminating enough between the modes, so as to change the order in which they lase. In other words, the pump modulation was able to modify the thresholds of the various wavelengths sufficiently to switch their places.

Before moving on to the next section, where the ability to favour or disfavour certain modes will be further explored by looking not just at thresholds but also at slopes, a note should be made about the spectral distribution of the lasing modes. In fact, the following is a revisit of the observation

previously made about the range over which the lasing modes appear (see figure 5.5), supported by the toy model presented in the theoretical section 5.3.

The three modes displayed in figure 5.8 represent a large spectral range of over 10 nm; this might seem a bit surprising, considering the width of the Ytterbium gain spectrum at these wavelengths (a deviation of 5nm from wherever the central, highest-gain wavelength is, would signify a drop of roughly 10% in the gain). However, as argued in the theoretical discussion above, this reasoning holds true only within the model of a simple spatially-monomode lasing cavity. In a cavity featuring multiple transverse modes that are coupled to each other through a lossy mixing mechanism, the comb of potential longitudinal modes is modulated both by the spectral curve of the response of the gain ions, and by the complex efficiency function induced by said mechanism. It therefore seems highly fitting to interpret the large spread over the spectrum of our found lasing modes, as the direct result of the mode-mixing and spatial filtering constraints brought into the cavity by the external optics.

5.4.2 Measurement of Slopes in a Cavity With Fully Multimodal Guiding (no SM Filter)

In order to fully observe the effect of the spatial shaping of the pump, upon the competition between the different laser modes, the measurement of the power contained in each of the discrete longitudinal modes (within limits of the spectral resolution of our spectrometer) as a function of the injected pump power[1] was carried out; this shall be referred to (for the sake of brevity) as 'slope measurement'. The cavity was defined by the external optics, slightly misaligned but not perturbed during the entire experiment (same as explained in section 5.4.1 above), and the waveguide consisted only of the amplifying MM fiber. The experiment was conducted in two parts: first, an optimization stage was run in order to find a pair of pump configurations (i.e. SLM modulation functions, implemented in the same manner as described in chapter 4 for the amplifier decorrelation experiments) with the highest possible differentiation between their respective output spectra. In the second stage, slope measurements were performed for each of the two pump configurations found. The results are displayed in figure 5.9, along with the camera images captured at maximal pumping for each configuration.

[1] The swept pump power shall be measured throughout the chapter in dimensionless units, as a fraction of the maximal pump power available in our setup; this allows for convenient comparison between the modes' thresholds and slopes. For conversion to real units of power – the maximal power was 400mW.

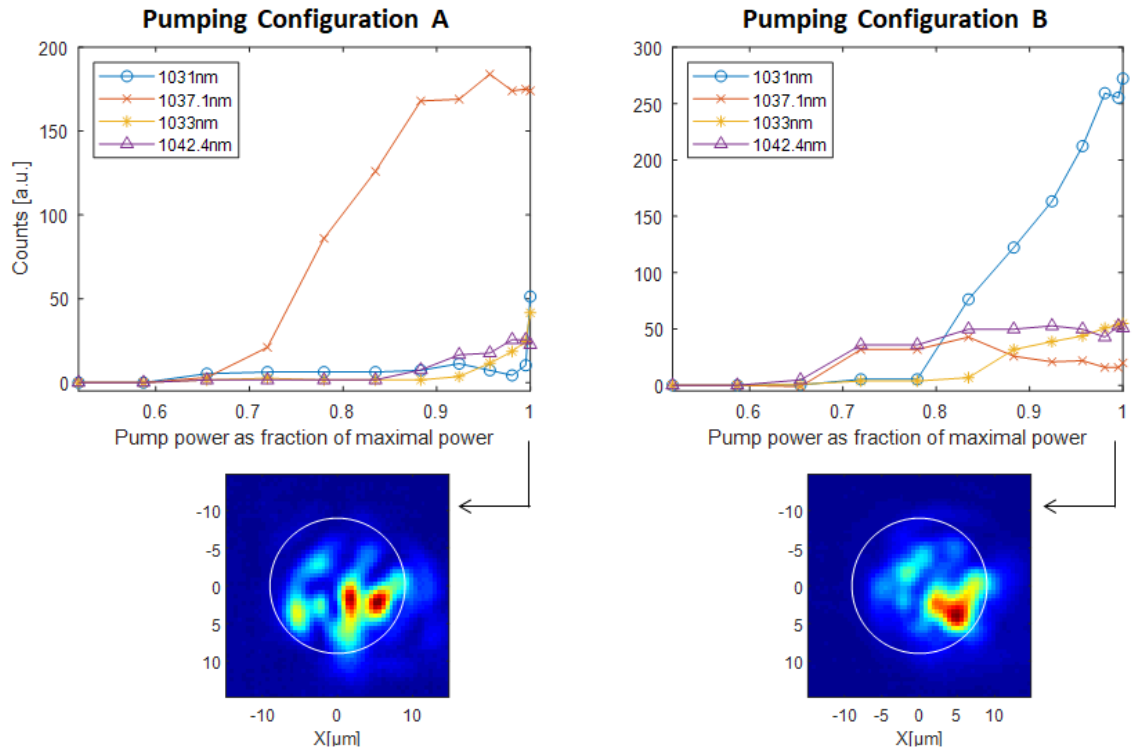

Figure 5.9: Experimental results of the optimization of the pump spatial modulation, for the case of four competing lasing modes. Two pump configurations are presented: Left - the mode at 1037nm (denoted by 'x' markers in red) is favoured; Right - the mode at 1031nm (denoted by 'o' markers in blue) is favoured, although it is still not the first to lase. The images of the fiber output facet displayed in the bottom correspond to the state, for each pump configuration, at maximal pump power.

The mode competition is clearly visible in the system – for example, in the left panel, the mode denoted by 'x' markers in red is the only one increasing as a result of the pump power rising from 0.7 to about 0.88, while the other three modes gain nothing along this segment; Then there is a distinct and simultaneous change of all slopes, and in the segment beyond 0.88 the stronger (red) mode stalls and ceases to grow while the three weak modes begin to profit from the gain. Moreover, the modification of the pump shaping strongly influences this competition: in the right panel, the interrelations between the modes are entirely different – the strongest mode is now the one denoted by 'o' markers in blue, and its appearance does not seem to interfere as much with the other modes. Similarly, the mode denoted by triangle markers in magenta, which was previously supressed by the strongest (in red), now co-evolves together with it and the two share almost identical slopes (at least until the fourth mode begins rising).

As the competition between even a limited number of lasing modes is quite complicated and difficult to interpret, the same experiment was repeated for cavity arrangements characterized by the appearance of 2 strong longitudinal modes. It should be reiterated that generally in all our lasing

experiments, the particular geometry in which the ‘cold’ cavity was positioned and aligned was the dominant factor in the selection of a certain sub-set of lasing modes, out of the entire range of possible wavelengths and spatial patterns; the pump shaping was then capable of manipulating the laser output by selecting modes among this sub-set, to be discriminated or promoted. In light of the theoretical analysis conducted above, this precedence of the geometry is not surprising: both the effective length of the fiber and the spatial filtering at its interfaces serve as extremely efficient and sensitive mode selectors due to their interference-based nature.

Typical results of the optimization and slope measurement experiment for a cavity with two main lasing modes are presented in figure 5.10. This time, 3 pump configurations are shown: the pair of configurations representing the two most dissimilar results (i.e., found by the optimization as favoring each one of the modes) are plotted center and right, while the configuration plotted on the left represents a typical middle-ground situation. It should be noted, that the spatial images shown have all been normalized (by tuning the camera exposure time), and therefore do not represent the true relative intensities of the different lasing outputs. In order to correctly compare the output powers, the counts of the spectrometer measurements (i.e. the y axis of each slope measurement graph) may be used. As can be seen, the different pumping configurations produce lasing outputs with very different total powers, or in other words, the pump optimization comes with a penalty of laser efficiency. However, it should be stressed that the dominant factor in this variation in power is not some trait inherent to the lasing modes – but rather stems from the limitations of our wavefront shaping scheme (varying loss of pump power, as a function of the SLM mask required for exciting some given modal configuration). In other words, the dominant factor behind the loss of power is not related to the dynamics within the cavity, but to technical details of the transmission relation between our SLM and the entry point to the cavity (which may be improved upon using more sophisticated WFS schemes, approaching unitary shaping).

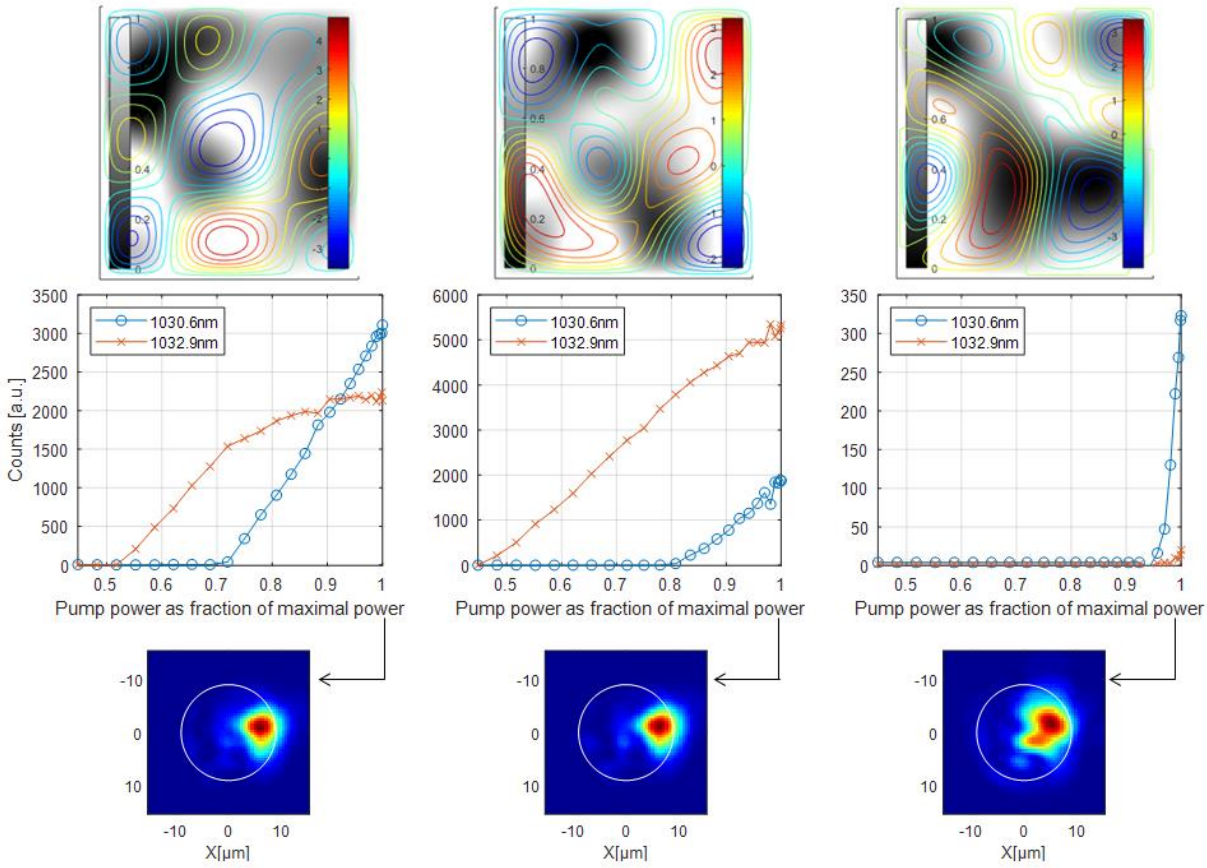

Figure 5.10: Experimental results of the optimization of the pump spatial modulation, for the case of two competing lasing modes. The evolution of the modes' power as a function of the pumping strength is given in the graphs in the middle row. Three pump configurations are presented, from left to right: (1) the 'first' mode (denoted by 'x' markers in red) is in strong competition with the 'second' mode (denoted by 'o' markers in blue), which eventually surpasses it in power; (2) the red mode is significantly favoured over the blue; (3) the blue mode is favoured over the red and becomes the first one to lase. At the top row, the SLM masks producing each configuration are displayed as a superposition of 2 images: Amplitude modulation is shown in grayscale (scale bars on the left inset); Phase modulation is shown by the contour maps in color-scale (scale bars, in radian, on the right inset). The images of the fiber output facet displayed in the bottom row correspond to the state, for each pump configuration, at maximal pump power.

Starting from the configuration on the left, we observe the clear competition between the mode (denoted by 'x' markers in red) which lases first, and the one arriving second (in blue 'o' markers) but eventually surpassing the first in power. While the appearance of the second mode (at 0.7 of the pump power, a threshold approximately 33% larger than that of the first mode) does not completely halt the growth of the first, it significantly hinders it (reduces its slope) – meaning the modes strongly compete. Considering now the configuration at the center, we see not only repression of the blue mode (its threshold now is higher than the red mode threshold by more than 75%), but also removal of the competition between the two: the slope of the stronger red mode does not discernibly change after the weaker blue mode makes its appearance. Conversely, the last configuration (shown on the right)

causes a complete reversal of the relation of between the modes; the blue one is now the first to appear. Since this configuration is characterized by a low efficiency of the pump injection (both modes appear very late in the scan of the pump power), it is difficult to gauge the competition between them. However, it should be stressed again that the weak gain is not an inherent quality of this specific interesting configuration (or of any other, for that matter); rather, the particular transmission relation between our SLM and the fiber facet where the pump is injected dictated that in order to excite that specific modal composition for the pump, the required wavefront modulation mask featured large loss of power. A different wavefront shaping scheme (or, quite simply, a stronger pump source) could inject the same modal configuration with more power delivered to the lasing modes.

5.4.3 Measurement of Mode Slopes in a Cavity With a Spatial Filter – a Spliced SM Pigtail

The last experiment was carried out in a setup as depicted in figure 5.7, with a short section of a passive, single-mode (SM) fiber, spliced on at the end of the active, multimode (MM) fiber, serving as a spatial filter. The purpose of the insertion of the SMF pigtail was to investigate whether the effects of our pump shaping would be significantly changed by the reduction of the space of possible oscillating modes to one specific combination of LP modes (the one determined by the SM-MM interface; see the discussion in section 5.3). The cavity was defined by the same external optics as in the experiments presented above in this section. However, an inevitable outcome of the introduction of the SMF pigtail was the increase of cavity losses (both at the spliced interface and at the SMF-air interface, where the reinjection back into the fiber by the coupler mirror was less efficient due to smaller core size). The result was a higher lasing threshold, and hence a more severe limitation, in terms of pump power lost due to diffraction effects and intentional amplitude modulation) on the wavefront shaping masks that could be employed. The results of the slope measurement for a pair of pump configurations found by optimization (for favouring each of the modes) are presented in figure 5.11. Camera images are not displayed since the intensity pattern on the output side (i.e. at the coupler end) were always the same single-mode emission.

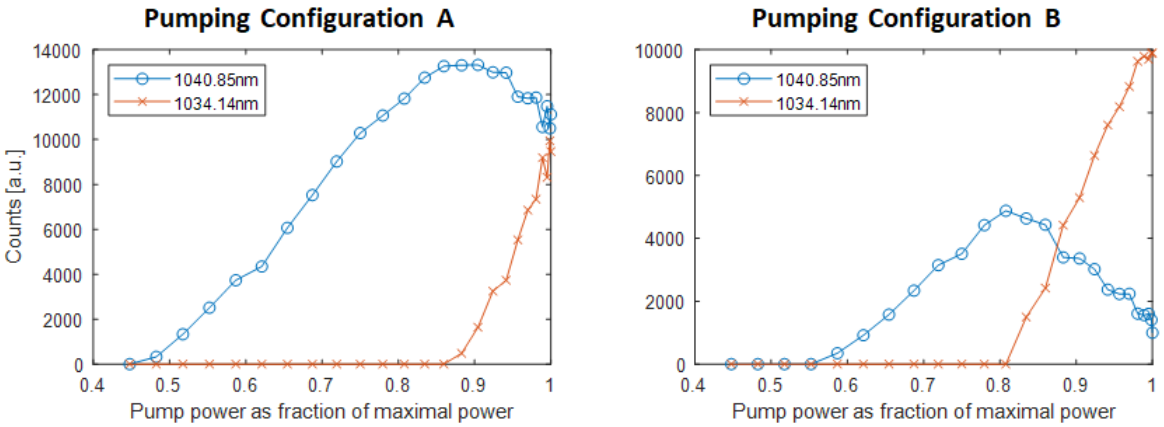

Figure 5.11: Experimental results of the optimization of the pump spatial modulation, in a cavity with a passive SMF pigtail. The evolution of the modes' power as a function of the pumping strength is given for the two configurations, on the left and on the right, found as the most favourable to the 'first' mode (denoted by 'o' markers in blue), and to the 'second' mode (denoted by 'x' markers in red), respectively. The ratio between the thresholds of the two modes is modified, but not enough to flip their order.

Starting from the configuration on the left, we observe once more the modal competition: the mode which lases first (denoted by 'o' markers in blue), not only changes its slope when the other mode (in red 'x' markers) appears and starts oscillating – the slope becomes in fact negative, meaning the second mode takes gain away from the first. Note that the threshold of the first mode is at 0.45 of the total available pump power, while the second threshold is at 0.86, which is roughly 90% higher. Turning now to the configuration on the right, we see the competition has been tipped in favor of the red mode – which still lases second, but the ratio of thresholds has been brought down to about 44%. Although the results are not as dramatic as those presented in figure 5.10 - the order of appearance of the modes has not been flipped – there is still clear evidence that a change of the pump modal composition modifies the interrelation between the cavity's lasing modes, even with the presence of the SM spatial filter. We may therefore infer, that although the lasing modes share the same modal composition, and differ only in wavelength – meaning that their intensity patterns are similar, differing only in the slow evolution along the fiber length as a result of the dephasing of the LP modes with respect to one another – the shaping of the pump is still able to demonstrate selectivity in their excitation. These results demonstrate that indeed, the manner in which the spatial heterogeneous of the pump-induced gain propagates and evolves throughout the entire volume of the fiber is a crucial factor in the composition of the resultant lasing.

5.5 Summary and Conclusions

In previous chapters, our treatment for a multimodal fiber amplifier pumped by a coherent pump lightfield demonstrated why the amplified output could be modified by applying wavefront shaping techniques to his pump. The key for the dependence was that a given modal composition of the injected pump produced a complicated, yet deterministic, distribution of gain within the volume of the fiber core – in short, a 3D 'speckle' of population inversion; and the signal modes experienced differential amplification, as a function of their spatial overlap with this distribution of gain. In this chapter, a different system was studied – that of a laser, based upon the same fiber, in a cavity configuration. Due to the enormous complexity of such a system, arising first of all from rich multimodality in both the spatial and frequency domains, and more notably from its non-linear dynamics above the lasing threshold, development of a predictive numerical model was not attempted; it was however expected, on a qualitative level, that the same fundamental mechanism explored in the amplifier configuration – namely, that different lasing modes would have different spatial overlaps with the 'speckly' excitation – would enable a scheme of wavefront shaping the pump to modify the output of the laser.

The work reviewed in the chapter consisted of experiments with three variations of the architecture of the fiber-based cavity: lasing in a fiber-only cavity, where the fiber ends themselves serve as mirrors; a cavity with external optics, in which the light coming out at each fiber end propagates in free space through a self-imaging 2f system that re-injects it back into the core; and the same cavity with external optics, with the addition of a passive SMF pigtail acting as a spatial filter. Wavefront shaping of the pump was implemented, and positive results – meaning, successful demonstration of the modification of the laser output by the choice of certain pumping configurations – was observed in all three variations. Most notably in the 2nd architecture of the cavity, and to a somewhat lesser extent, also in the 3rd architecture - it was demonstrated that optimization of the pump modulation function allowed selective favouring and disfavouring of specific lasing modes.

Comparison of the three variations of the architecture was instrumental in the study of the system and the development of basic insights into the nature of the lasing modes, because it helped somewhat separate the effects of different factors and mechanisms. In particular, the comparison of the fiber-only cavity to the external optics architecture, yielded important observations in both the spatial and wavelength domain (respectively, appearance of higher-order spatial modes, and a widening of the spectral range supporting lasing, for the 2nd type of architecture). Furthermore, some deliberate misalignment of the external optics proved to be beneficial, as it exposed a clear correlation between different longitudinal modes (i.e. wavelengths) and different intensity patterns (i.e. spatial modes). Lastly, the introduction of the single-mode fiber pigtail seemed to provide further confirmation of our fundamental insight (although it could not provide a direct and conclusive 'proof'

of the control mechanism), that is - that the mode selection observed was indeed the result of the re-arrangement of the excitation speckle within the active fiber's volume. This is because the effect of modal discrimination (by optimization of the spatial modulation of the pump) survived in the simplified, reduced space of lasing modes created by the SMF filtering; although the ambiguity in one dimension was lifted, leaving modes which differed only by the evolution of their intensity patterns along the fiber length.

To concisely summarize the qualitative theoretical description developed to explain the behaviour of our system, we may depict the following picture: The geometry of the cavity, containing both the multimode fiber and the free-space segments (if present), offers a large space (extending over a wavelength dimension and a dimension of different LP modes) of hypothetical lasing modes; but the combination of the imperfection of the imaging relation in the free-space parts, and of the strong spatial filtering at the fiber interface, adds a constraint upon the oscillation conditions, permitting only combinations of LP modes to lase. This may be understood as a quite straightforward result of the re-coupling into the fiber acting as a mode mixer: the induction of new eigenmodes upon the cavity transmission. However, a subtle interplay between spatial (transverse) modes and longitudinal modes occurs, because an eigenmode of the *cavity* is no longer a single eigenmode of the *waveguide*; and any lasing mode arising needs to fulfil a more complex set of conditions in order to constitute a standing wave in the cavity. Consequently, this large space (of hypothetical modes) is modulated by a complicated gain/loss envelope (albeit, rendered more sparse as well). These circumstances are the key which permits our 'control' mechanism, namely the shaping of the pump, to exercise selectivity over a (small) set of lasing modes which significantly differ from one another in both their wavelengths and their spatial patterns.

References for Chapter 5

[1] N. Bachelard, J. Andreasen, S. Gigan, P. Sebbah, Taming Random Lasers Through Active Spatial Control of the Pump, Phys. Rev. Lett., No. 109, 33903 (2012).
[2] N. Bachelard, S. Gigan, X. Noblin, P. Sebbah, Adaptive Pumping for Spectral Control of Random Lasers, Nat. Phys., No. 10, 426-431 (2014).
[3] N. Bachelard, Control of Passive and Active Open Random Media: Theoretical and Experimental Investigations, Thèse de Doctorat de l'Université Paris 6 (2014).
[4] L. Ge, O. Malik, H. E. Tureci, Enhancement of Laser Power-Efficiency by Control of Spatial Hole Burning Interactions, Nat. Phot., No. 8, 871-875 (2014).
[5] S. F. Liew, L. Ge, B. Redding, G. S. Solomon, H. Cao, Pump-Controlled Modal Interactions in Microdisk Lasers, Phys. Rev. A, No. 91, 43828 (2015).
[6] A. Cerjan, B. Redding, L. Ge, S. F. Liew, H. Cao, A. D. Stone, Controlling Mode Competition by Tailoring the Spatial Pump Distribution in a Laser: A Resonance-Based Approach, Opt. Exp., Vol. 26 No. 23, 26006-26015 (2016).
[7] L. Ge, Selective Excitation of Lasing Modes by Controlling Modal Interactions, Opt. Exp., Vol. 23 No. 23, 30049-30057 (2017).
[8] M. Nixon, O. Katz, E. Small, Y. Bromberg, A. A. Friesem, Y. Silberberg, N. Davidson, Real-Time Wavefront Shaping through Scattering Media by All-Optical Feedback, Nat. Phot., No. 7, 919-924 (2013).
[9] C. Tradonsky, R. Chriki, V. Pal, G. Barach, A. A. Friesem, N. Davidson, Teaching an Old Laser New Tricks: Solving the Inverse Scattering Problem Rapidly, Proc. Of CLEO/Europe-EQEC (2017).
[10] R. Chriki, G. Barach, C. Tradonsky, S. Smartsev, V. Pal, A. A. Friesem, N. Davidson, Rapid and Efficient Formation of Propagation Invariant Shaped Laser Beams, Opt. Exp., Vol. 26 No. 4, 4431-4440 (2018).
[11] H. Cao, R. Chriki, S. Bittner, A. A. Friesem, N. Davidson, Complex Lasers with Controllable Coherence, Nat. Rev. Phys., No. 1, 156-168 (2019).
[12] R.T. Brundage, W. M. Yen, Low-Temperature Homogeneous Linewidths of Yb+3 in Inorganic Glasses, Phys. Rev. B, Vol. 33 No. 6, 4436-4438 (1986).
[13] G. Lei, J. E. Anderson, M. I. Buchwald, B. C. Edwards, R. I. Epstein, Determination of Spectral Linewidths by Voigt Profiles in Yb+3 Doped Fluorozirconate Glasses, Phys. Rev. B , Vol. 57 No. 13, 7673-7678 (1998).
[14] X. Zhu, A. Schulzgen, H. Li, L. Li, L. Han, J. V. Moloney, N. Peyghambarain, Detailed Investigation of Self-Imaging in Large-Core Multimode Optical Fibers for Application in Fiber Lasers and Amplifiers, Opt. Exp., Vol. 16 No. 21, 16633-16645 (2008).

[15] R. Selvas, I. Torres-Gomez, A. Martinez-Rios, J.A. Alvarez-Chavez, Wavelength Tuning of Fiber Lasers Using Multimode Interference Effects, Opt. Exp., Vol. 13 No. 23, 9439-9445 (2005).
[16] B. M. Shalaby, V. Kermene, D. Pagnoux, A. Barthelemy, Transverse Mode Control by a Self-Imaging Process in a Multimode Fibre Laser Using a Single-Mode Feedback Loop, J. Opt. A: Pure Appl. Opt., No. 10, 115303 (2008).

General Conclusion and Prospects

The work presented in this thesis explored the propagation of light in a complex medium with gain – specifically, a multimode amplifying fiber – and the outlooks offered by the ability to employ wavefront shaping techniques upon coherent pump light injected into the system, so as to tailor the modal composition of the pumping excitation propagating in the fiber.

The main part of the thesis consisted of an investigation - both by means of theoretical and numerical modeling, and by experimental implementation - of the dependence of the *transmission function* of a MMFA (multimode fiber amplifier) upon the *pumping modal composition*. As a concrete framework for approaching this fundamental study, the research question largely focused on quantifying *the degree of control* one may exercise upon the amplified output signal of the MMFA in the spatial domain, through the choice of the pump shaping. The theoretical model exposed several interesting mechanisms, which rendered this question of control non-trivial: due to the particular characteristics of both the pump-medium interaction, and the medium-signal interaction, the a-priori expectation might be justified - that the effects of the choice of the pump shaping would be effectively "averaged out", yielding only negligible results upon the signal. Briefly summarized, these characteristics were: the saturation of the pump absorption which restricts the spatial contrast of the excitation contrast; the scalar nature of the excitation which limits the selectivity in terms of the signal modes; and the self-averaging brought about by the complicated evolution of the pump intensity patterns along the fiber length, due to the modal dispersion. In view of these mechanisms, the results obtained a posteriori by conducting numerical simulations were meaningful; they indicated that by selecting the pump composition, one is able to significantly manipulate - albeit not fully control - the signal transmission. Stating the major conclusions in a qualitative manner, and in terms of the signal TM expressed in the modal basis - it was found that the major contribution to control arises from the ability to introduce significant differential gain along the diagonal (i.e. increase or decrease the self-amplification of a mode, if it is injected as input); that this differential gain typically entails relative de-phasing between the modes as well; that, by contrast, the ability to induce mode coupling in the fiber (off-diagonal elements of the TM) is small; and that a fundamental challenge characterizing the problem – resulting inevitably in the need to approach it only through optimization processes – is that the effect some chosen pump composition has on the different TM elements is highly non-linear and 'entangled', meaning no separation of the control between the different elements is possible. Furthermore, a comparison between two types of doping elements – Ytterbium and Erbium – served to illuminate an important conclusion about the two fundamental parameters of the gain medium most dominant in determining the system's sensitivity to the pump shaping: $\sigma^{e}_{signal}/\sigma^{a}_{pump}$, i.e. the ratio between the emission cross-section and the absorption cross-section, at the signal and pump wavelengths, respectively; and the coefficient of the gain-dependent phase-shift denoted is this work

as K_{RIC} (signifying refractive index change). It was shown that dependence upon the pump shaping improves with decreasing efficiency for the pump absorption, and with increasing efficiency of the signal amplification; as well as with increasing magnitude of the phase-shift coefficient.

The general predictions given by the model were validated in our experimental setup, where appreciable modification of the speckle patterns at the output of an Yb-doped MMFA was achieved by the optimization of the pump beam's spatial modulation. In the context of fundamental understanding of the effects of disordered (spatially heterogeneous) gain, these results serve as a qualitative demonstration of the persistence, despite complicated "randomization" mechanisms, of deterministic impacts of wavefront shaping. More quantitative results could be obtained using the same model and simulation tools, in case one were to pursue for a specific application of interest, the improvement of some concrete metric of performance (such as, for example, cross-talk in an amplifier in a spatially-multiplexed optical communication channel, or beam quality in an amplifier for free-space laser applications).

In a second phase of the experimental work, the same scheme of pump shaping was applied in a lasing cavity based upon the amplifying fiber. Although full theoretical modeling of such a system remained outside the scope of the this work, the implementation of a laser was stimulated by the general insight obtained from the work on the amplifier configuration – namely, that WFS of the pump is able to modify the spatial arrangement of the excitation profiles within the fiber volume with sufficient distinction to considerably favour or disfavour certain modes. Indeed, the experiments successfully demonstrated discernible influence of the pump's spatial modulation upon the competition between the lasing modes in the cavity, resulting in large changes in the ratios between the modes' thresholds, at times even flipping their order of appearance. The lasing configuration represents a topic of remarkable complexity and richness, and the work carried out in this thesis has not explored the full range of control potentially offered by the wavefront shaping paradigm. In particular, an intriguing idea that could guide further work is the setting up of the lasing cavity as an all-optical solver, with the spatial modulation of the pump serving as the mechanism for programming the details of a specific computation problem, for which the lasing mode represents the optimal solution (similarly to the manner in which the placement of a complicated aperture in a free-space lasing cavity has been used in this field to define the specific conditions of a problem).

As broader prospects for continued research of this topic, or of adjacent topics, two interesting direction are proposed, relevant for both amplifier and laser configurations.

The first is the extension of the work presented to fibers guiding a larger number of modes; this could be considered for the signal light, but also exclusively for the pump beam (by relying on a double-cladding scheme, where the core guiding the signal remains as before, while the pump is guided in a more multimodal inner cladding). Such a scheme would increase the number of degrees of freedom controllable by our shaping, while keeping the same number of degrees of freedom in the

addressed system (i.e. the number of signal modes). Among the significant difficulties that would however arise, one could mention the drastic rise in the complexity of the optimization algorithm that would be needed in order to meaningfully explore the modal space of the pump; and the reduction in the efficiency of the pump absorption caused by the small spatial overlap between the pump's propagation volume and the gain medium.

The second prospect is suggested with the purpose of circumventing a crucial limitation posed by one of the inherent properties of the gain medium - that its excitation does not preserve the phase of the pump light. Although the amplification by stimulated emission is coherent with respect to the signal beam, it is not coherent with the respect to the pump (the population inversion depends solely on the local pump intensity). As discussed and demonstrated in this work, this represents a restriction upon the degree of discrimination between signal modes attainable by the shaping of the gain profiles. Therefore, an interesting direction to pursue could perhaps be the extension of the framework presented in this thesis, to other gain processes which preserve the phase of the pump beam, such as SRS or SBS (Stimulated Raman or Brillouin Scattering, respectively). If the pump-signal interaction were mediated by such a gain mechanism, the spatial heterogeneity formed by the shaping of the pump could contain both amplitude and phase terms, making for a richer (and possibly more selective) scheme of control.

Appendix A: Numerical Simulation Tool for the Computing the MMFA Transmission Matrix

In this appendix, a brief description of the main numerical simulation tool used in our work is given. The full procedure for calculation of the TM of the MMFA is detailed in section 3.2.2; specifically, equations 3.3-3.5 sum up the mathematical formulas upon which the simulation is based. The numerical simulator was implemented in Matlab; a screenshot of the user-interface is presented in this figure:

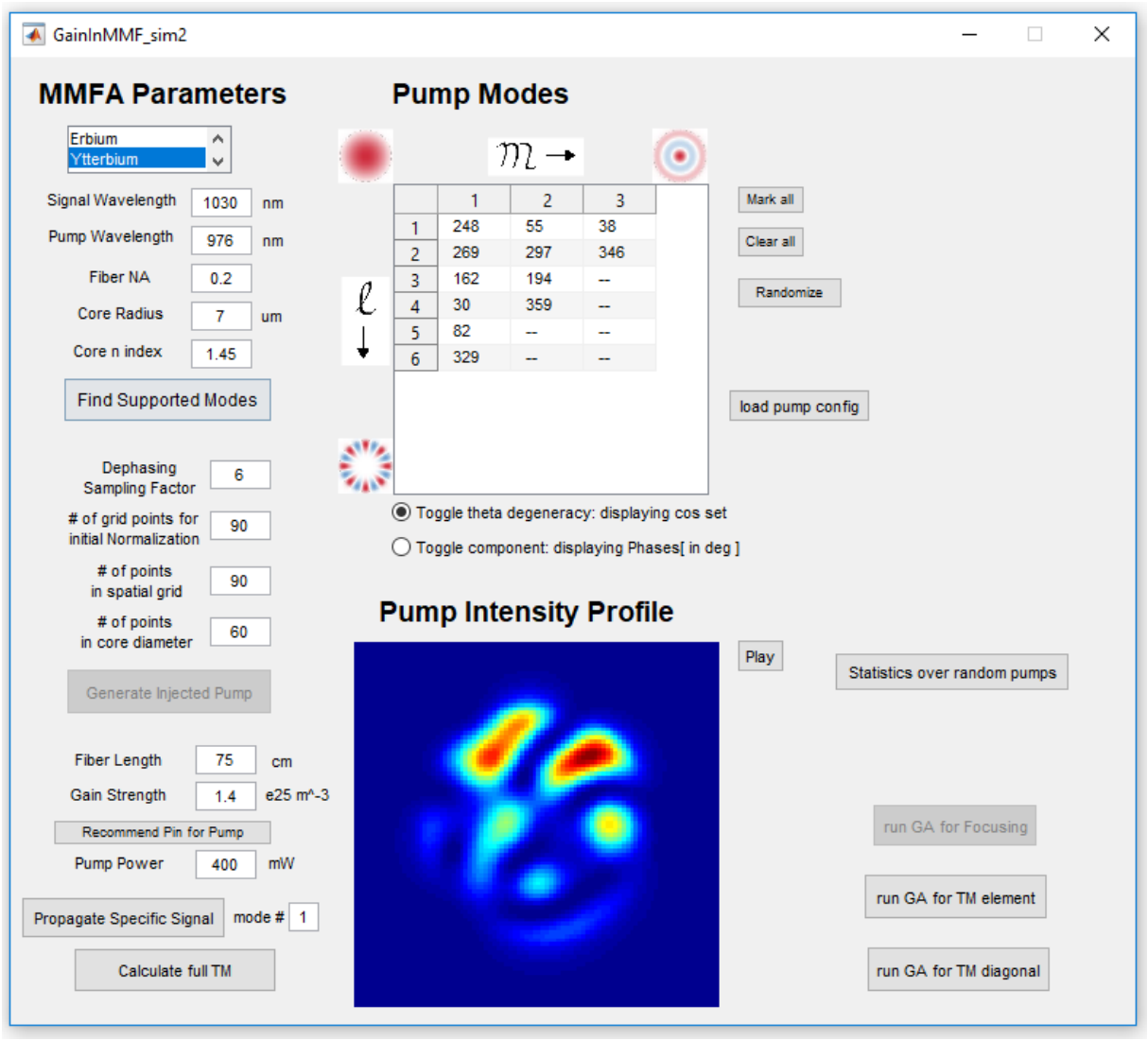

Screenshot of the user interface of our Matlab-based numerical simulator for a MMFA system

For a given fiber geometry, the solver finds the supported modes in both relevant wavelengths (pump and signal), and calculates their fields distributions. Then, a specific pump configuration (i.e. injected modal composition) may be either randomly chosen or directly inputted, and a calculation of the TM (for the specified fiber parameters, as can be seen in the screenshot) may be carried out. The

calculation proceeds in 2 main steps: Firstly, the pump is propagated through the length of the fiber (based on the 'thin slices' approximation as discussed in section 3.2), yielding a 'cube' of data representing the population inversion in the entire volume of the core, $n_2(x,y,z)$. This step is relatively short in computation time, because the computation performed in each slice scales only linearly with the number of pump modes N_{pump}. This is because , as recalled, the pump is propagated by taking into account the saturated and spatially non-uniform absorption that has been induced at the 'current' slice, and decomposing the field that has not been absorbed upon all guided pump modes (meaning, computing N_{pump} spatial integrals); the results of this decomposition are the pump modes arriving at the 'next' slice. The second step now proceeds to receive as input said population inversion 'cube', and uses it to calculate for each slice the 'local TM', whose elements are determined by eq. (3.4), which we reproduce here:

$$TM_{[r,c]}^{z\to z+\Delta z} = e^{-j\beta_c\Delta z}\{\,\delta_{rc} + (1+jK_{RIC})\iint \frac{1}{2}\left[\sigma_{sig}^{e}n_2(x,y,z) - \sigma_{sig}^{a}n_1(x,y,z)\right]N_d \cdot \psi_r^{sig}(x,y)\cdot\psi_c^{sig*}(x,y)\,dxdy\,\}$$

It should be evident that the number of overlap integrals that must now be computed in each slice is equal to the number of elements in the TM (actually, a little more than half that number, since $TM_{[r,c]} = TM_{[c,r]}^{*}$, so if the number of signal modes is N_{sig}, then the number of independent elements is $(N_{sig}+1)\cdot N_{sig}/2$). However, this still means that the computation time scales as $\sim N_{sig}^2$, and evidently, the second step is heavier is terms of computation needs. The final step for arriving at the total TM, which is the concatenation of all 'local' transmission matrices, is negligible in terms of computation time, since no integrals in the spatial domain are necessary (all data is already expressed in the modal domain).

To give a rough estimate of the total computation time required for a typical MMFA system, we take a fiber as the one used in our actual experiment, that is one guiding about ~20 signal modes, and a length of 1m; the evaluation of the total TM in such a case is approximately half an hour, varying with the particular capabilities of the PC running the solver. Scaling this time with the MMFA length is simply linear (directly proportional to the number of slices taken). The scaling with the fiber's diameter or NA is a slightly trickier relation: a simple answer would be the quadratic scaling with the number of modes, $\sim N_{sig}^2$, as discussed above. A more complete answer would be, that as the number of modes is increased, at some point the resolution of the spatial grid used to sample the core cross-section would need to be raised in order to faithfully represent the higher spatial frequencies of the supported modes. The scaling of the computation time with the resolution in x,y is of course quadratic as well, as the overall integrals are calculated over area.

Appendix B: Spatial Light Modulation Masks Corresponding to the Experimental Results in the Amplifier Configuration

In this appendix, data complementary to the results of section 4.3.2 are presented; specifically, the wavefront shaping masks found by the optimization process and displayed upon the pump SLM, yielding the signal speckle outputs which have been presented in the chapter itself. The presentation of a two-dimensional mask containing both amplitude and phase information is not entirely straightforward; however, simply showing the actual phase mask written to the SLM display would be almost meaningless, because the modulation data is encoded into the high-frequency grating corresponding to the off-axis modulation scheme (for details, see section 2.2.3) and thus hard to observe. Therefore, the adopted scheme was that of presenting the grid of modulation values as 2 superposed images – a color-scale contour map representing the phase modulation, and a grayscale image (the bright/dark shading across the mask) represents the amplitude modulation. Figures B.1 and B.2 (split due to the difficulty of fitting all results in a single page) correspond to the experiment where the SLM modulation function was a 3x3 grid. Figure B.3 corresponds to the experiment where the SLM modulation function was a 4x4 grid.

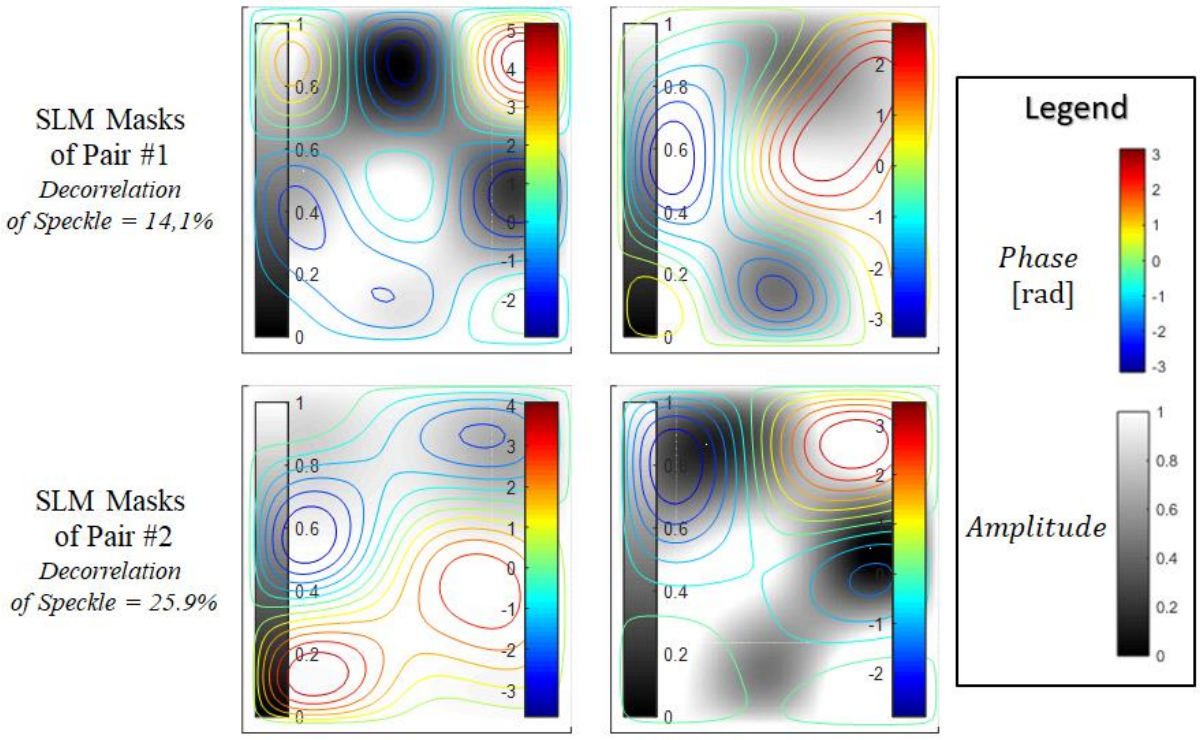

Figure B.1: The SLM masks corresponding to the found signal outputs displayed in figure 2.10 (MMFA signal decorrelation experiment with the SLM modulation defined as a 3x3 grid).

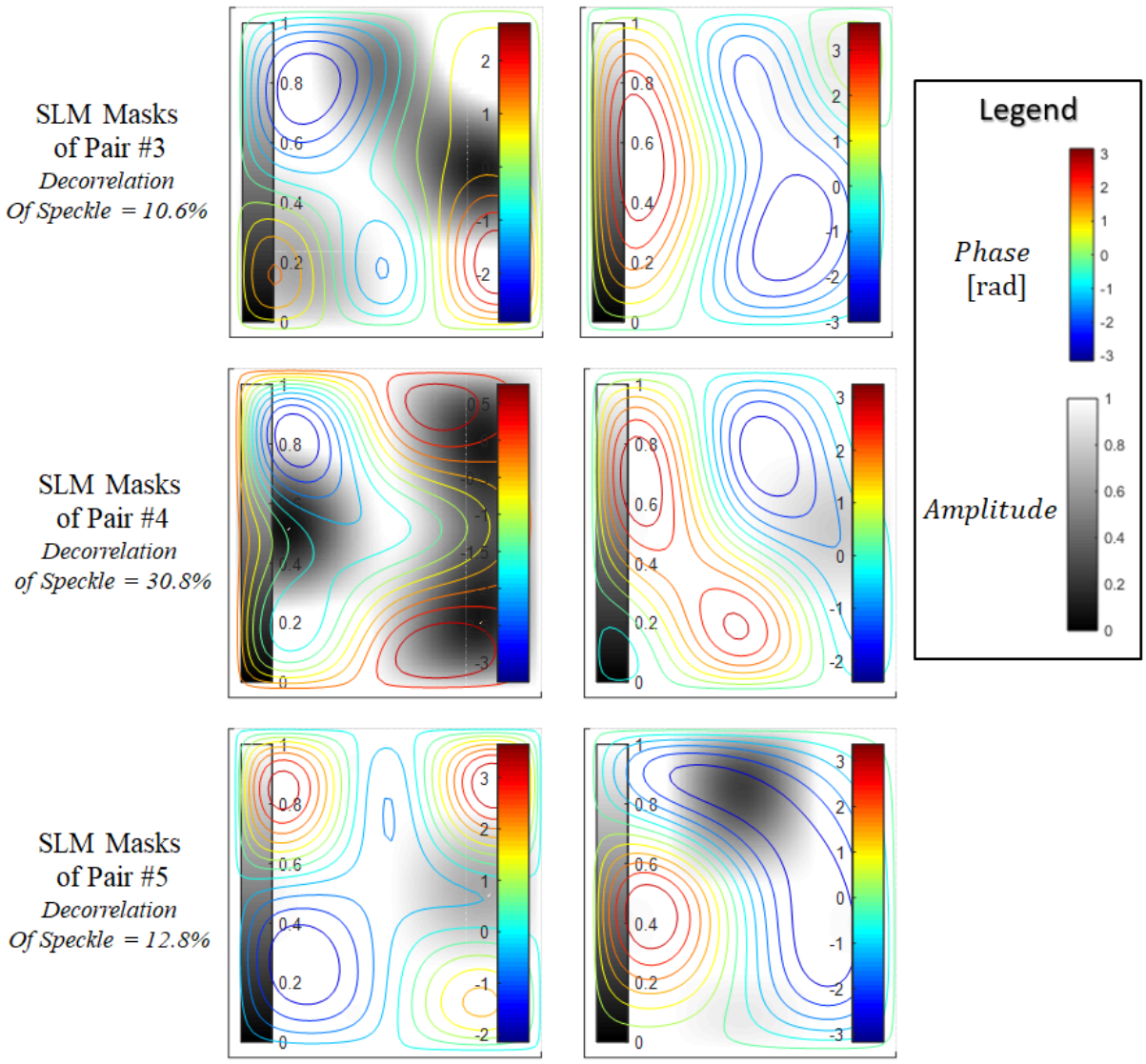

Figure B.2: Continued - The SLM masks corresponding to the found signal outputs displayed in figure 2.10 (MMFA signal decorrelation experiment with the SLM modulation defined as a 3x3 grid).

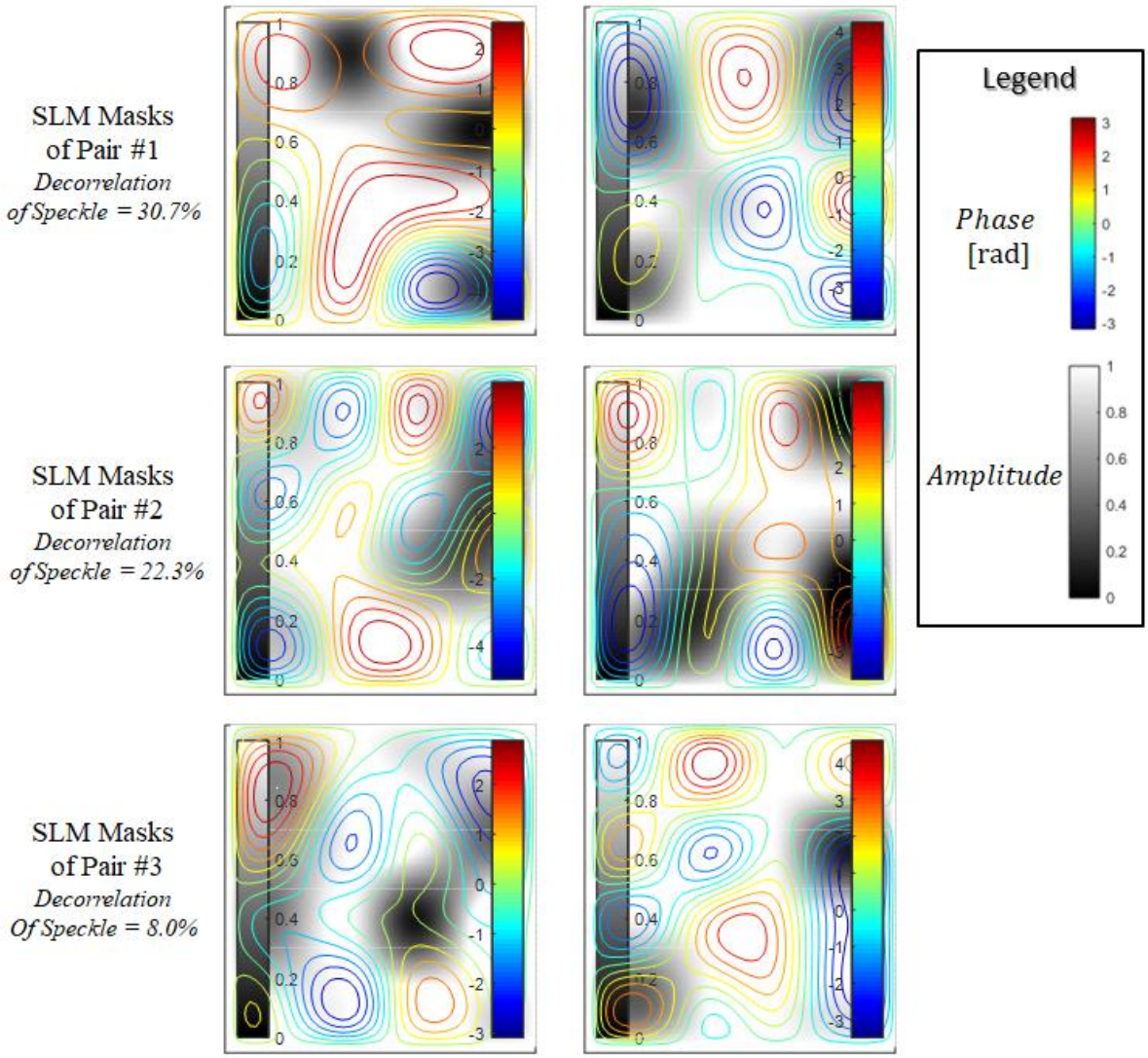

Figure B.3: The SLM masks corresponding to the found signal outputs displayed in figure 2.11 (MMFA signal decorrelation experiment with the SLM modulation defined as a 4x4 grid).

Appendix C: Spatial Mode-Mixing in a Fiber-Based Cavity Defined By Free-Space Optics

The purpose of this appendix is to supplement the theoretical discussion given in chapter 5 (section 5.3) regarding the effects of combining, in a lasing system, both a multimode waveguide (namely, the amplifying fiber) and free-space optics which define a cavity (namely, mirrors external to the fiber, and lenses which collimate the light upon the mirrors/focus the light back into the fiber in the outward and inward directions, respectively). More specifically, the appendix aims to show that the free-space components impose a requirement upon the *waveguide* modes to join each other and form new *cavity* eigenmodes; and that these superpositions of fiber modes are evident not only in the spatial domain (i.e. the intensity patterns of the laser emission), but also in the frequency domain (i.e. the allowed wavelengths of the laser emission)

The demonstration of these effects was simulated with a simplistic numerical model, in which the transmission matrix of the cavity (meaning, a TM representing one complete round-trip of a light field within it) was constructed by the following concatenation of matrices (illustrated in figure C.1): The TM representing the propagation in the fiber, multiplied by a transmission matrix representing the propagation, in free space, to the mirror and back, followed again by the fiber TM (with opposite directionality) and a second free-space matrix with aberrations, thereby completing a full round-trip. The fiber TM was constructed using the LP mode model covered in detail in chapter 3: the known forms of the modes were arranged as a matrix $TM_{pixel\_to\_mode}$ which essentially decomposes a free-space input field (in the pixel basis) upon the modal basis; then a modal-basis matrix reflecting the idealized coupling-free model, as in section 3.2.1, carried these modes (with the right dephasing) to the other end of the fiber, where the field was translated back to the free space with the same pixel-to-mode matrix, transposed. As for the free-space matrices on both sides of the fiber: the 2f relay was simulated with a Fourier transform followed by an inverse Fourier transform, with the following aberrations introduced in-between (as phase modulations across the field): Decentering (in the 2 transverse coordinates x, y), Tilts (same, in x and y), and a global defocus (quadratic phase term). Setting the 5 aberration parameters to 0 reduced the free-space transmission matrix to the identity, as should be for a perfect self-imaging system. Lastly, once the entire TM of the cavity was thus constructed, its eigenmodes were computed; two examples (for a cavity with minor aberrations and for a cavity with stronger ones) of the intensity pattern of the first eigenmode (i.e. the eigenvector with the highest transmission value) are presented in the right panel of figure C.1.As can be seen, the imperfection of the self-imaging outside the fiber modifies the system's eigenmodes from those of the

fiber, to more spatially complex combinations of them. To summarize - this simple numerical model demonstrates the argument of the mode-mixing induced by the external optics.

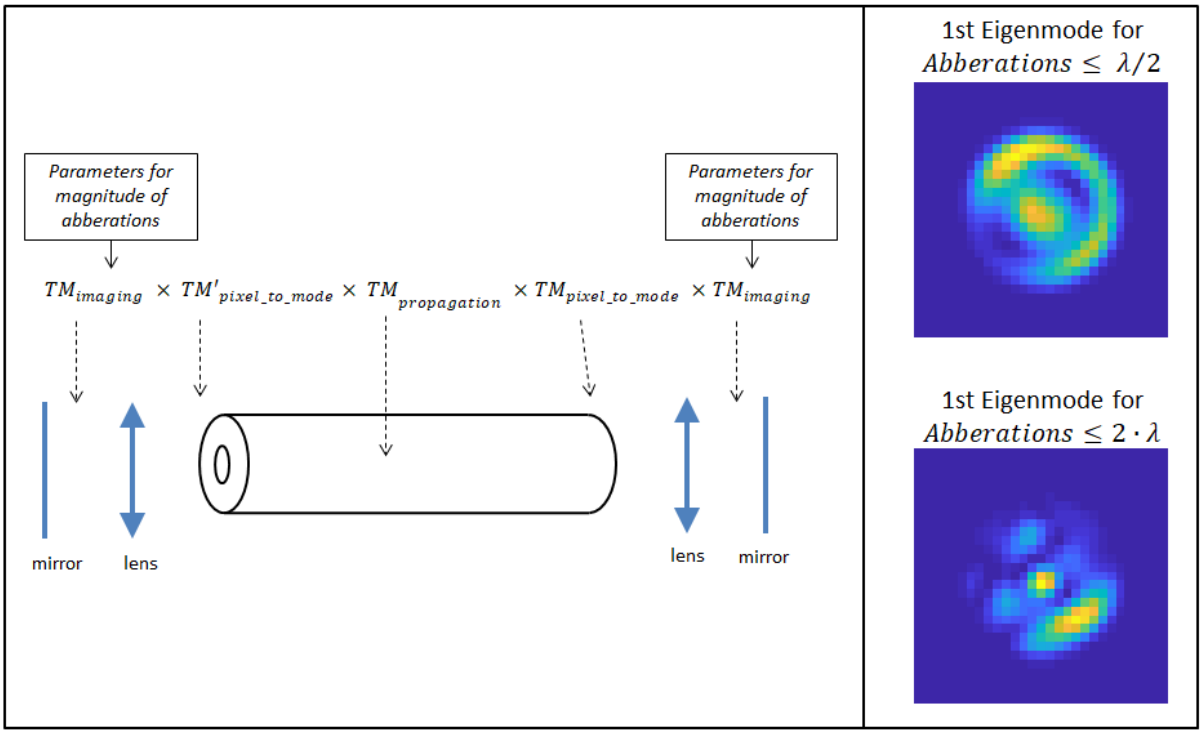

Figure C.1: Numerical simulation treating a round-trip in a cavity defined by external optics as a TM, with parameterized low-order aberrations representing imperfections in the imaging of the fiber output back into itself. The aberrations were expressed in units of the wavelength (e.g., a tilt of λ is a phase ramp of total 2π radian difference across the entire field). Left – conceptual illustration of the construction of the total TM by matrix concatenation. Right – examples of eigenmodes calculated from this TM, for minor aberrations (top), and for larger magnitude aberrations (bottom).

So far, the treatment has ignored the frequency domain: all the transmission matrices used in the model relate the complex amplitudes of the electromagnetic fields (i.e. the x,y,z dependencies) as if propagating in a single pass system, while dropping the wavelength-dependent interference arising from the circulation in the cavity. For this to be taken into account, we must remember that at some given wavelength, the cavity transmission *of a given discrete LP mode* varies according to the specific phase velocity assigned to this mode by the waveguide dispersion. Moreover, the relation is not linear in a straight-forward manner, because the circulation path in the cavity contains also the small free-space lengths where the travel time is independent of the modal dispersion. Formally stated: for a cavity with a length of fiber L_{fiber} and external optics of total length L_{FS} (for 'free space'), the phase term that determines whether a LP mode with indices l, m excited on a given optical frequency ν_0 experiences constructive or destructive interference after a full round trip of the cavity is the sum of these two expressions:

$$\phi_{l,m} = \beta_{l,m} \cdot 2L_{fiber} + \frac{2\pi\nu_0 \cdot L_{FS}}{c}$$

The consequence is that LP modes will experience differential attenuation factors due to the cavity-based interference. We may visualize this by plotting, separately for each LP mode, the 'Fabry-Perot comb' of transmission peaks it sees in the cavity; an example for three modes (over an arbitrary axis of frequency) is shown in figure C.2.

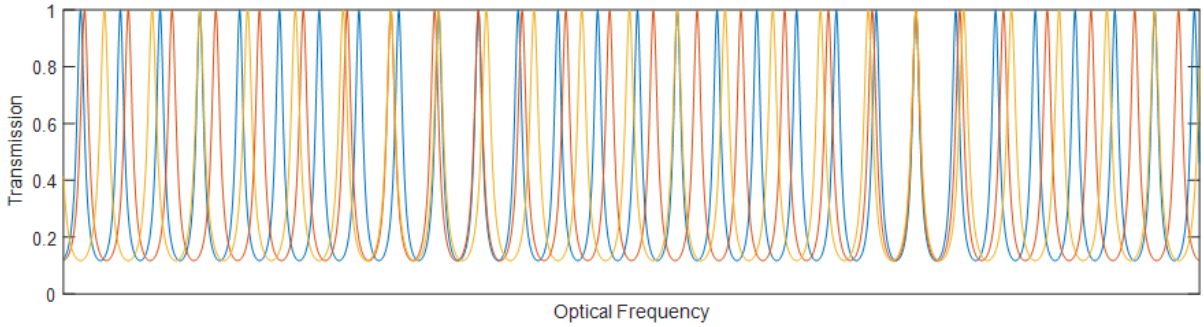

Figure C.2: Numerical example of 3 frequency combs with slightly different periodicities, representing the Fabry-Perot transmission function different LP modes would see in our MM fiber-based cavity. The combs are superposed on the same graph to demonstrate their 'beating', i.e. the slow period over which their mutual overlap fluctuates.

It should be therefore evident, that the numerical model presented above for finding the eigenmodes of the cavity is not complete; strictly speaking, a full model should repeat the construction of the TM at every relevant optical frequency, incorporating the differential loss coefficients the LP modes would have at the frequency as a result of the phase term presented above. One would obtain, in that case, different eigenmodes (different superpositions of LP modes) at different wavelengths. Although such modelization is beyond the scope of this work, an important qualitative conclusion may be drawn without full computation for a specific set of parameters: the simple periodicity of the resonances found in a SM Fabry-Perot cavity with small separations in frequency (corresponding to the inverse of the round-trip travel time) is removed in the MM fiber cavity with external optics. An eigenmode may be found (as a superposition of fiber modes) at some unique frequency, but a neighbouring resonance is not guaranteed to be found within some small separation, due to the very slow beating between the transmission combs of these discrete modes. Consequently, we may expect the requirement imposed by the free-space components, namely the formation of cavity eigenmodes as superposition of waveguide mode with different modal phase velocities, to entail a reduction in the number longitudinal modes supported by the cavity.